AD NUMBER

AD832496

NEW LIMITATION CHANGE

TO

Approved for public release, distribution unlimited

FROM

Distribution authorized to U.S. Gov't. agencies and their contractors; Critical Technology; JUN 1967. Other requests shall be referred to Naval Weapons Center, China Lake, CA 93555.

AUTHORITY

USNWC ltr dtd 14 Jul 1970

NOTS TP 4244

COMBUSTION OF SOLID PROPELLANTS AND LOW FREQUENCY COMBUSTION INSTABILITY

by

Aerothermochemistry Division

Research Department

ABSTRACT. This report summarizes studies of ammonium perchlorate deflagration, combustion of sandwiches of ammonium perchlorate crystals and binders, behavior of aluminum in the combustion zone of propellants, oscillatory combustion of propellants in several experiments, and experimental measurement of attenuation of axial mode oscillations in models of rocket motors.

U.S. NAVAL ORDNANCE TEST STATION
China Lake, California
June 1967

U. S. NAVAL ORD T STATION
AN ACTIVITY OF TH OMMAND
G. H. LOWE, CAPT., U N, PH.D.
Commander Technical Director

FOREWORD

This report summarizes progress on a program sponsored by the Office of Advanced Research and Technology of the National Aeronautics and Space Administration under Work Orders 11, 294; 3034, 3035 and 6030 during tne period June 1964 to March 1967. Other reports covering parts of this work include NAVWEPS Report 8971, NOTS TP 3932; and NOTS TP 4275.

The following persons contributed to this report: E. W. Price, J. D. Hightower, K. J. Kraeutle, J. E. Crump, M. W. Beckstead, H. B. Mathes, and F. G. Buffum.

This report is released at the working level for information purposes and does not represent the final judgement of the Station.

Released by
HUGH W. HUNTER, Head
Research Department
30 June 1967

Under authority of
WM. B. McLEAN
Technical Director

NOTS Technical Publication 4244

Published by.....Research Department
Collation.....Cover, 126 leaves, DD Form 1473, abstract cards
First printing.....240 unnumbered copies
Security classification.....UNCLASSIFIED

CONTENTS

NOMENCLATURE

A	Constant of integration (Section 2)
	$\frac{\mu}{R\ T_f\ C_d}$ (Section 5)
A_t	Throat area of the nozzle
B	Constant of integration
c	Specific heat
c_o	Average sonic velocity
c_{ob}	Sonic velocity of gas in combustion zone
c*	$1/C_d$, characteristic velocity for the combustion products
C	Coefficient in a steady-state burning rate law, $\bar{r} = C\bar{p}^n$
C_d	Isentropic discharge factor, $\left(\frac{\gamma\mu}{RT}\right)^{\frac{1}{2}} \left(\frac{2}{\gamma+1}\right)^{(\gamma+1)/2(\gamma-1)}$
E	Energy
$\dot{E}$	Rate of change of energy
f	Frequency of oscillations in cycles/sec
f_1	Frequency during growth of oscillations
f_2	Frequency during decay of oscillations
k	Reaction rate constant (Section 2, p. 34)
	Thermal Conductivity (Section 2, p. 56)
K	Ratio of propellant burning area to nozzle throat area
L	Burner chamber length

L^*	V/A_t, characteristic length of the chamber
M	Mass flow rate
M_a	Mass accumulation rate in burner
M_b	Mass burning rate
M_d	Mass discharge rate
M_o	Amplitude of oscillation in mass burning rate at arbitrary time zero
m	Mass burning rate per unit area of the solid
n	Pressure exponent in steady-state linear burning rate low, $\overline{r} = C\overline{p}^n$
P_o	Amplitude of pressure oscillation at arbitrary time zero
p	Pressure
r	Linear burning rate of the propellant
R	Gas constant in equation of state $p = \rho RT/\mu$
R	Ratio of amplitudes of mass flow perturbation and pressure perturbation
t	Time
T	Temperature
T_f	Adiabatic flame temperature of the propellant
T_m	Sample temperature at peak of exotherm
T_o	Temperature at $x = \infty$
T_s	Temperature at the surface of the solid
V	Volume of combustor (Section 5)
$V_{o,\ t}$	Volume of decomposed crystal at time 0 and t, respectively (Section 2)
x	Distance measured into the solid

α	Exponential rate constant for amplitude of oscillations (Sections 1, 5, and 6)
$\bar{\alpha}$	Percent relative weight loss (Section 2, p. 34)
$\underline{\alpha}$	Thermal diffusivity
γ	Ratio of specific heat capacities of the reaction product gas, C_p/C_v
λ	Latent heat of phase transition
μ	Molecular weight of reaction product gases (average)
ρ_s	Density of the solid
τ	Lead time of mass burning rate oscillations relative to pressure oscillations
τ_{ch}	Characteristic time of the chamber (i.e., flushing time), $\frac{\rho V}{M_b} = \frac{\mu L^*}{R\, T_f\, C_d}$
τ_ω	Period of oscillation, $\tau_\omega = \frac{2\pi}{\omega}$
τ_{tw}	Thermal wave relaxation time, $\alpha\tau/r^2$
ϕ	Heating rate
ω	Frequency of oscillations expressed in radians/sec
ω_o	Frequency at which the phase and time lead pass through zero
$(\frac{\sigma}{\epsilon})$	Density perturbation per unit pressure perturbation
$(\frac{\mu}{\epsilon})$	Propellant response function
	SUBSCRIPTS (Section 2)
tr	Refers to the phase transition
1	Refers to the cubic phase
2	Refers to the orthorhombic phase

SUBSCRIPTS (Section 6)

1	Refers to conditions during growth of pressure oscillations
2	Refers to conditions during decay of pressure oscillations
0	Refers to spacewise average conditions
0b	Refers to conditions in the combustion zone

1. INTRODUCTION

1.1. CONCEPT OF STUDIES

The problem of oscillatory combustion has recurred persistently through the history of development of rocket motors. Because of the penalties in both cost and time that have been imposed on development programs as a consequence of this phenomenon, it has received continuing and often intensive study both in development programs and research programs. At the time of the inception of the present program, relatively little attention had been given to the phenomenon of oscillatory combustion in the frequency range below 100 cps. Increased study in this low frequency domain was motivated by two concurrent trends in the development of solid propellant rocket motors. The first of these was the development of very large solid propellant booster rockets, whose dimensions were such as to permit oscillatory behavior in acoustic modes in frequencies down to about 10 cps. The second was the growing interest in motors for space applications which possessed very high volumetric loading density, and were designed to operate at relatively low pressures, both of these features being important for favorable mass ratios required for upper stage applications. Motors of this type were observed to exhibit oscillatory behavior in a low frequency, nonacoustic mode, particularly in the frequency range 10 to 200 cps (Ref. 1-3). At the outset of these investigations the nonacoustic oscillatory behavior had been observed in high mass ratio motors, and the low frequency acoustic type oscillatory behavior had been demonstrated in laboratory combustors designed specifically to explore the potential risk of instability in very large booster motors in sizes which had not yet been constructed and tested (Ref. 4-5). Both types of oscillatory behavior appeared on the basis of preliminary data to be more prevalent with the powdered metal-containing propellants which were coming into widespread use at that time.

In view of these considerations, the present program was initiated in order to gain some fundamental understanding of the processes involved in these two classes of low frequency combustion instability, before they emerged as major problems in oncoming rocket motor development programs. This seemed to be a particularly prudent course of action in view of the extremely high cost of individual firings of the very large rocket motors under development, and the absence of any significant opportunity for trial and error development of corrective measures in the event of an occurrence of low frequency combustion instability. The approach was to develop laboratory scale tests which would permit

qualitative evaluation of the susceptibility of propellants to low frequency combustion instability, and to determine those attributes of the combustion which were responsible for instability. At the outset it seemed clear that it would be necessary to carry out also studies of the steady-state combustion of the propellant, with particular reference to the combustion of the metal ingredient. This clarification of the qualitative nature of the steady-state combustion process appeared to be essential to any understanding of the perturbation behavior which was responsible for oscillatory combustion. The different major sections of this report reflect the different methods which were developed to study the steady-state and oscillatory combustion.

1.2. GENERAL CHARACTER OF SOLID PROPELLANT COMBUSTION

A solid propellant burns by propagation of a combustion wave inwards into the body of the material at the surface. Viewed as a one-dimensional wave (Fig. 1.1), the leading edge consists of a thermal wave moving into the body of the material as a consequence of heat transfer from exothermic reactions occurring further along in the combustion wave. At or near the surface of the propellant, the temperatures are sufficiently high to induce chemical reaction, as well as physical phase changes. In most cases the majority of the chemical energy released in the combustion occurs in a narrow layer in the gas phase very close to the propellant surface, although the variety of chemical systems and the status of our knowledge does not permit simple generalizations on this point. In steady-state burning, the heat supplied from the exothermic reactions to the unreacted propellant is exactly that required to maintain a steady supply of reactants to the reaction zone.

The idealized one-dimensional description of a combustion zone is strictly relevant only to a homogeneous propellant material which burns without surface irregularities or bubbles. In the case of heterogeneous propellants, the particulate ingredients from which the propellant is made differ so conspicuously in their chemical and physical properties that a one-dimensional description of the combustion zone neglects many of the more conspicuous aspects of the combustion. This is particularly so when the micro-structure of the propellant is comparable to or larger than the dimensions of the combustion wave itself (Fig. 1.2). Likewise, the homogeneous-monopropellant one-dimensional picture is inadequate to represent the behavior of a propellant in which one of its ingredients tends, by virtue of its high boiling point and low chemical reactivity, to accumulate on the burning surface to a much higher concentration than is present in the bulk of the propellant. In the case of most composite propellants comprised of granular oxidizer and polymeric fields, the heterogeneity does indeed lead under normal combustion conditions to a three dimensionally complicated combustion wave with lateral diffusion of heat and mass on a microscopic but important scale. The gasification characteristics and reactivity of the oxidizer and the binder differ sufficiently to lead typically to a non-planar surface whose

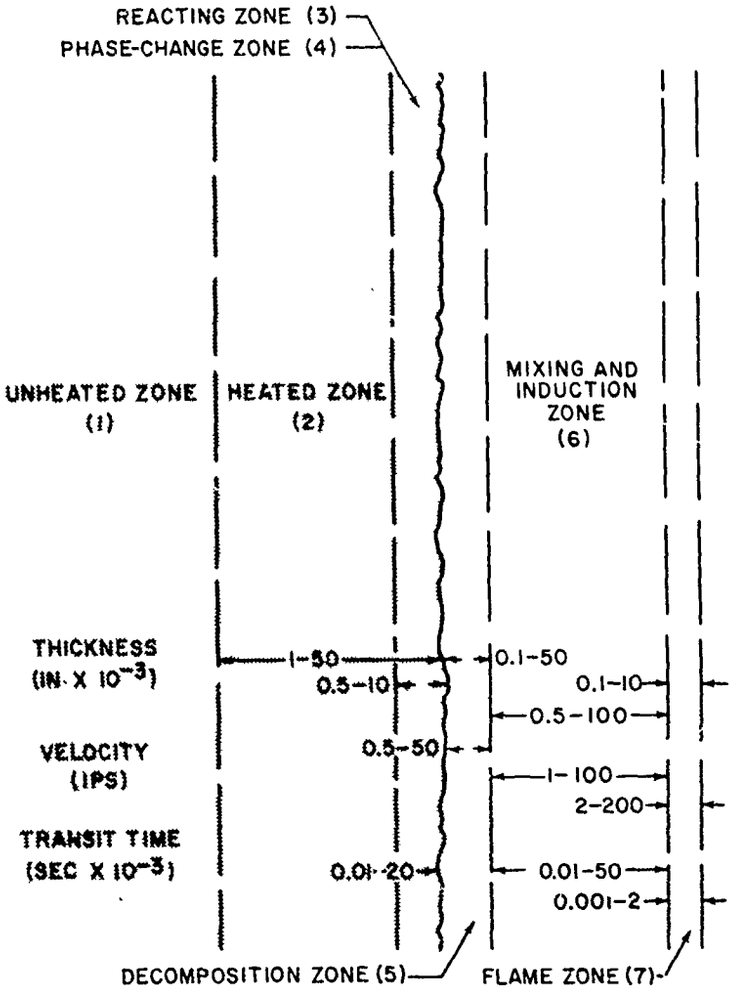

FIG. 1.1. One-Dimensional Representation of the Combustion Zone of a Solid Propellant.

characteristics depend upon the particle size of the oxidizer and the flow situation in the gas phase reaction region. When a powdered metal such as aluminum is used as a fuel ingredient in the propellant, its gasification characteristics and reactivity are conspicuously different from the other ingredients, with the result that the metal usually resides on the surface for an appreciable time before igniting or leaving the surface, and usually agglomerates into larger particles during its residence on the surface.

Although a detailed description of the microstructure of the combustion zone in a heterogeneous propellant will differ considerably, depending upon the characteristics of the particular ingredients of the propellant, and in fact is not presently known for many propellants, it is instructive to consider a description that can be made on the basis of existing information regarding the combustion of ammonium perchlorate (AP) propellants. Ammonium perchlorate is a material which will burn much as a solid monopropellant at pressures above about 400 psia. The

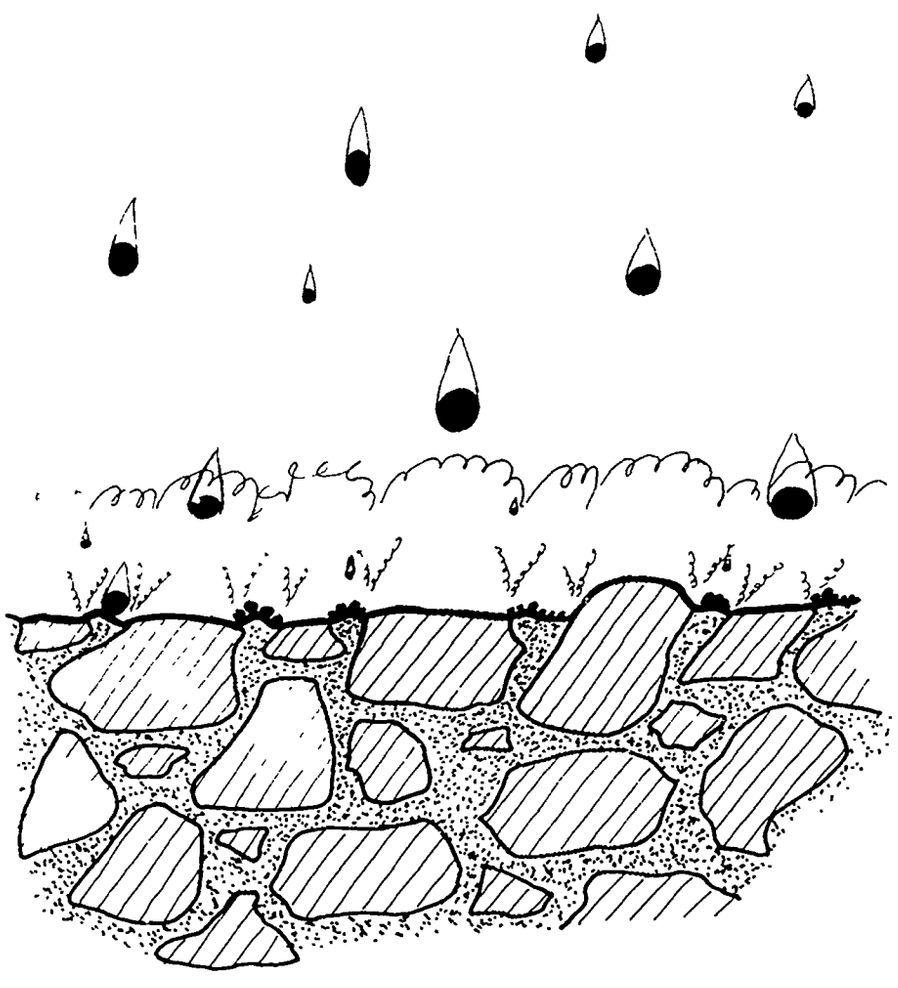

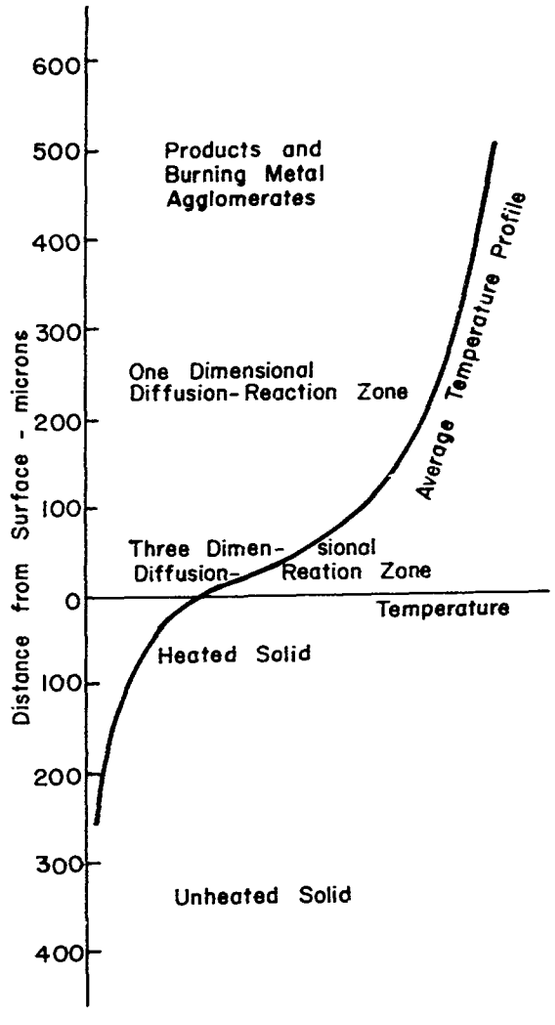

FIG. 1.2. Representation of the Combustion Zone With Three-Dimensional Microstructure: Typical Dimensions

resulting reaction products are highly oxidizer rich, and have a temperature in the vicinity of 1200°K (2160°R). Burning as a monopropellant, this oxidizer has a surface regression rate in the range 0.3 to 1.5 cm/sec (.12 - .59 in/sec), and burns with a surface temperature in the vicinity of 900°K (1620°R). Typical binders for composite propellants are hydrocarbon polymers such as polyurethane, which decomposes endothermally to produce a highly fuel-rich gas mixture. Decomposition of the binder in the combustion zone appears to be produced primarily by thermal activation of the molecules, although heterogeneous reaction is no doubt important in some cases. Surface temperatures of the binder are usually higher than are present at the surface of the AP. The decomposition products of the oxidizer and the binder mix in a geometrically complicated manner dependent upon the micro-structure of the propellant and flow conditions in the adjoining gaseous environment. At the mixing interfaces, the oxidizer and binder products react exothermally to products that are ultimately somewhat fuel-rich, with temperatures in the range of 2000 to 4000°K. The relative dimensions and transport times of ingredients in different parts of the combustion wave are depicted in Fig. 1.1 in an approximate manner, considering only the one-dimensional features of the wave.

When a powdered metal ingredient is included in the propellant as a fuel, it is initially present in a particle size much smaller than that of the oxidizer, and is distributed in a reasonably homogeneous fashion in the binder. During burning of the propellant, the metal emerges at the surface of the decomposing binder at temperatures that are not sufficient to produce gasification of the metal. Thus, the metal must either leave the surface as a condensed phase particle, and proceed outwards to a region where the conditions are favorable for its ignition, or the metal particle must remain for a period of time on the surface in a highly fuel-rich gaseous environment. In the former case, the droplet will ordinarily be ignited as it passes through the diffusion flame region and will burn to completion in a more or less rapid fashion depending upon such conditions as the size of the particle, the temperature of the reaction products of the diffusion flame, the oxidizer content of those products, and the prevailing pressure. In the case where the particle of metal resides on the burning surface, it is likely to encounter other particles already present or emerging at the same and adjoining points on the surface, and the material will eventually leave the surface in some state of agglomeration. The mechanistic details of this accumulation-agglomeration process are unknown at present, but may be expected to differ significantly as a function of propellant composition. Upon departing from the surface of the propellant, the agglomerate will ignite and burn in a fashion similar to one of the single original particles, but will of course burn more slowly than the corresponding mass of small particles because of its low specific surface. In practice, agglomerates are often observed to be of sufficiently great size to protrude into the diffusion reaction zone of the propellant before leaving the burning surface. Thus, ignition of the agglomerate may play a significant role in its detachment from the propellant surface,

whereas this appears to be less likely in the case of detachment of the original metal particles individually. Of course, the agglomeration-ignition-combustion history of the metal ingredient is highly dependent on the particular metal involved, since the ignition characteristics and phase change characteristics of metals differed conspicuously. The foregoing description appears to be particularly appropriate to the case of aluminum as the metal ingredient, this choice having been made because of the widespread use of aluminum as the metal fuel ingredient in propellants.

Because low frequency oscillatory combustion is more typical of combustors operating at relatively low mean pressure, it is appropriate to direct particular attention to the character of the combustion zone under these low pressure conditions. The conditions at low pressure are conducive to low chemical reaction rates and low diffusion rates, conditions which in turn lead to a slow regression of the propellant surface, thick thermal and reaction zones, and relatively long time constants for all of the constituent steps of the combustion wave. There are a number of important consequences of this trend in dimensions of the combustion wave, the importance of which have probably not yet been fully assessed. As an example, a heterogeneous propellant with a very fine particulate structure may begin to behave much as a homogeneous propellant, if the increasing thickness of the combustion zone causes it to become much larger than the dimensions of the particulate ingredient. As another example, the increasing dependence of the deflagration of the AP ingredient upon the diffusion flame region as pressure is reduced implies a shift in the direction of increasing dependence of the combustion zone on the diffusion flame as pressure is reduced. This implies further that at sufficiently low pressure the combustion zone may become dominated by the chemical kinetics of the reactions in the diffusion flame, since these kinetics become the slowest step in the process of sufficiently low pressure. While the full implications of this in terms of structural details of the combustion zone are not known, it is safe to assume that some accompanying effects on the transient behavior of the combustion zone will emerge and be important in the combustion instability studies.

Turning again to the question of the relative dimensions of the heterogeneity of the propellant on the one hand and the thickness of the combustion regions on the other hand, it must be anticipated that the behavior of powdered metal ingredients will be highly pressure dependent. In the case of a metal such as aluminum, which is not easily ignited at the surface, the remoteness of the diffusion flame from the surface under low pressure conditions implies a corresponding reluctance of the metal to ignite while residing on the surface. Thus, it may be anticipated that accumulation of the metal ingredient on the burning surface may proceed to a much higher degree at lower pressures, and the agglomerates leaving the surface may be correspondingly larger. Combustion of these larger agglomerates will naturally proceed over a longer time period simply because of their larger size, and the combustion rates will be further diminished by the less favorable conditions for combustion due

to low concentrations in the gas field. Under extremely unfavorable conditions, the combustion of the metal ingredients may not go to completion at all within the combustor, and it may even be difficult to induce the metal ingredient to leave the propellant surface at all. The actual details of the behavior will of course be highly dependent upon the type of metal, the type of oxidizing species present in the reaction products, and the concentration of oxidizing species. However, with propellants consisting of AP oxidizer, hydrocarbon binder, and aluminum as a metal ingredient, it is observed that the combustion of the metal occurs at low pressure in a cloud of oxide smoke and burning metal droplets which extends, in some cases, for several inches above the burning surface of the propellant. In the rocket motor situation it must be assumed that any cloud of burning metal droplets, which extends an appreciable distance away from the burning surface, becomes involved in the mean flow and turbulent mixing of the flow field which transports the reaction products from the burning surface to the nozzle of the rocket motor, and the combustion dynamics will be correspondingly affected by the enhanced mixing rates under these conditions of slow reaction rates.

Again, it would be inappropriate to assume that all propellants behaved in the manner described above or that any simple description can encompass all propellants and environmental conditions of interest. Likewise, it is not clear what significance the different details of the steady-state combustion have relative to unstable combustion. It is clear that a complete understanding or prediction of unstable behavior cannot be expected without knowledge of the steady-state combustion zone.

1.3. GENERAL CHARACTER OF OSCILLATORY COMBUSTION

Although the process of steady combustion is easier to visualize and describe in physical and mathematical terms than is transient combustion, there is no apriori reason to assume that the combustion will in any particular situation be steady. Aside from the obvious necessity to consider transient aspects of combustion in connection with the ignition of the propellant, it is observed in practice that the combustion in rocket motors often proceeds in an oscillatory way. Further, it is sometimes observed that the combustion, after proceeding in a reasonable steady fashion, will spontaneously extinguish. Likewise, considerable attention has been given to the possibility of a transition of an apparently steady deflagration to a pressure propagated detonation wave, although such occurrences apparently have not occurred with any ordinary well consolidated solid propellant materials.

In considering any of these transient combustion phenomena, it is important to recognize that the behavior may be an attribute not only of the combustion, but also of the dynamics of the overall combustor system. Thus, it may be that the combustion is capable of exhibiting some kind of oscillatory or non-steady behavior in its own right, even in a combustor which is unresponsive to these combustion perturbations. On the

other hand, in the majority of the instances of oscillatory combustion that concern us here, it is found that the oscillatory behavior is dependent upon an interaction between the dynamic combustion characteristics of the propellant itself and the dimensions or dynamic behavior of the combustor as a gas flow or acoustic system. In the former case, one is concerned with the aspects of the combustion process that lead to spontaneous perturbations from steady-state behavior. In the latter case, one is concerned with the nature of the interaction between the combustion behavior and the combustor dynamics, and inevitably also in the details of the combustion and the combustor flow that makes such interaction possible. In the present investigation we were concerned with both situations.

Figure 1.3 illustrates examples of four types of unstable combustion which are discussed in the present report. Figure 1.3a shows (see also Ref. 8-9) the periodic fluctuation in radiant energy from the combustion zone during the burning of a strand of solid propellant prepared by pressing a powdered mixture of AP and aluminum (Ref. 6-7). The strand was burned in a pressure vessel which was maintained at constant pressure so as to avoid any interaction between the combustor environment and the burning sample. The periodic fluctuation in radiation is seen in high speed motion pictures to be a consequence of intermittent ignition and burning of a surface accumulation of the aluminum component of the sample, illustrating an example of the spontaneous periodic combustion attributable to the combustion process alone.

Figure 1.3b shows the spontaneous development of pressure oscillations in a small combustor operating in the "rocket mode", that is, with the pressure in the combustor maintained by the generation of gases from the propellant combustion. The combustion and combustor pressure are mutually dependent upon each other. In this case the frequency of oscillation is several orders of magnitude lower than the lowest possible wave mode of the combustor, so that the pressure surges up and down in the combustor everywhere in phase, with each point on the burning surface of the propellant "seeing" at any given instant the same environmental state as every other point on the burning surface of the propellant. It is this type of instability, called L* or nonacoustic instability, that has been encountered in high mass fraction space motors at low operating pressures (Ref. 1-3).

Figure 1.3c shows low frequency pressure oscillations measured at the end of a 6-inch diameter pipe (Ref. 4-5) during oscillatory combustion involving longitudinal acoustic mode oscillations in the pipe. In this case the propellant is located at the ends of the pipe at positions corresponding to the pressure antinodes of the axial mode involved. The burning surface is so oriented that it experiences perpendicularly incident pressure waves, again with each point on the burning surface experiencing the same pressure oscillation as every other point. The propellant samples on opposite ends of the pipe experience similar oscillations except that they are 180° out of phase. While rocket motor

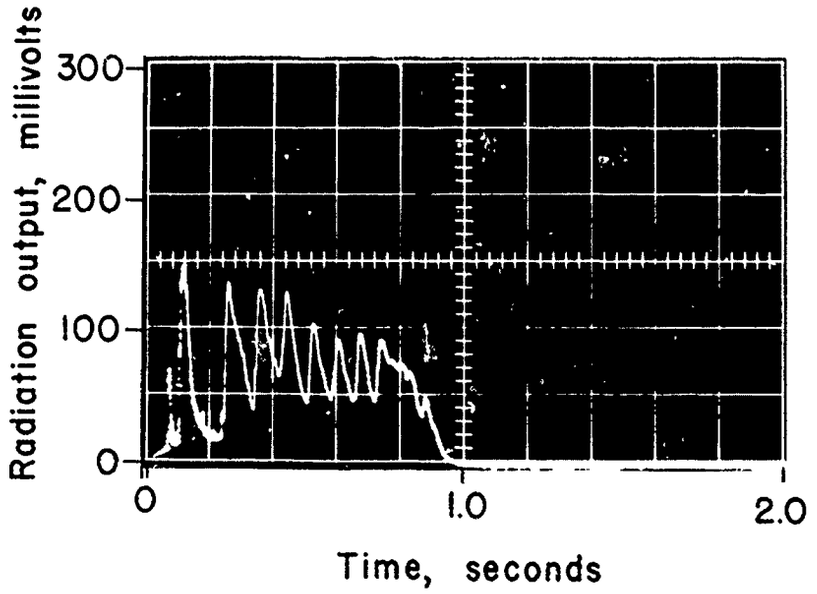

(a) Spontaneous combustion oscillations at constant pressure: Radiation output from a pellet dry-pressed from 8% Al, 92% AP mixture of AP, Al, and CuO at 800 psi.

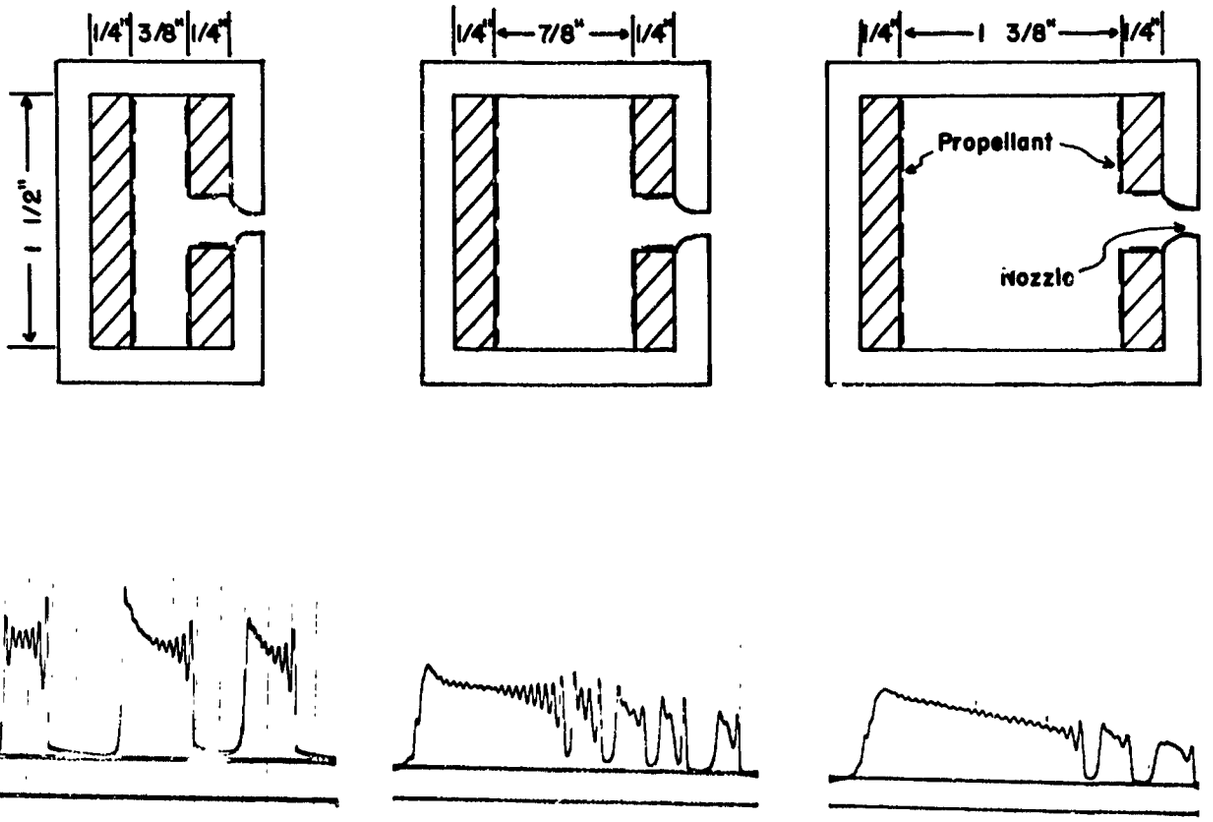

(b) Nonacoustic oscillation combustion: Pressure-time records from laboratory burners of different volumes, oscillating in a surging (non-wave) mode.

FIG. 1.3. Types of Oscillatory Combustion.

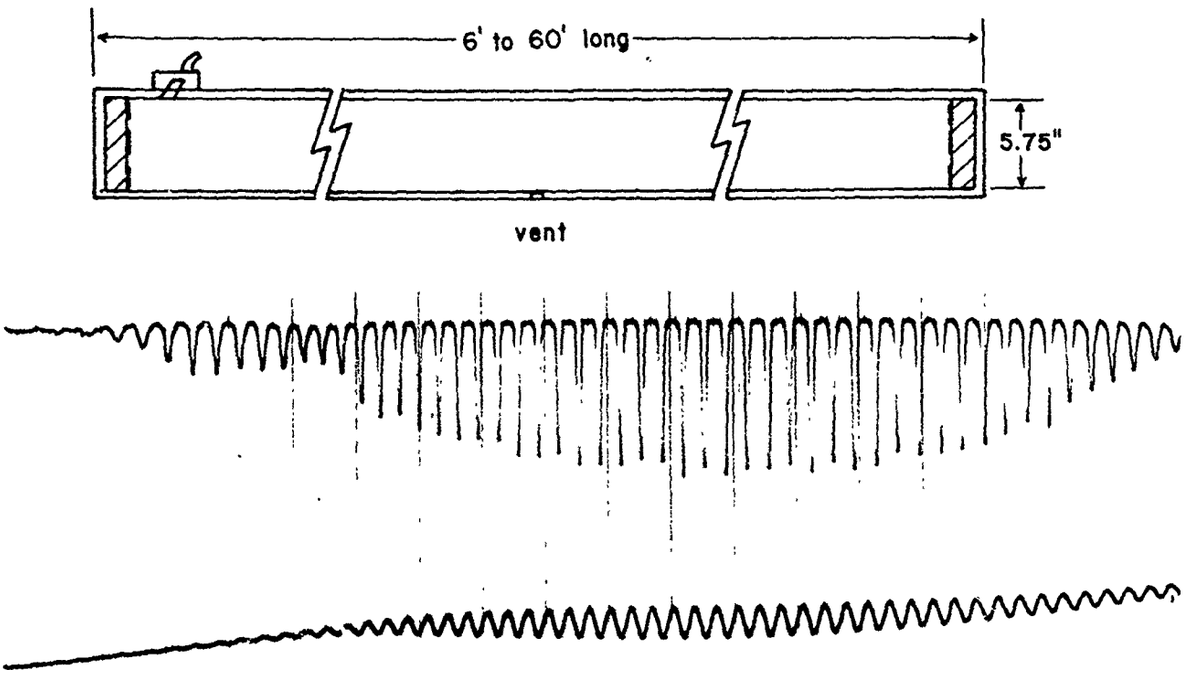

(c) Acoustic oscillatory combustion in a burner designed for pressure coupled, low frequency instability: Pressure-time history (bottom), combustion zone radiation (top).

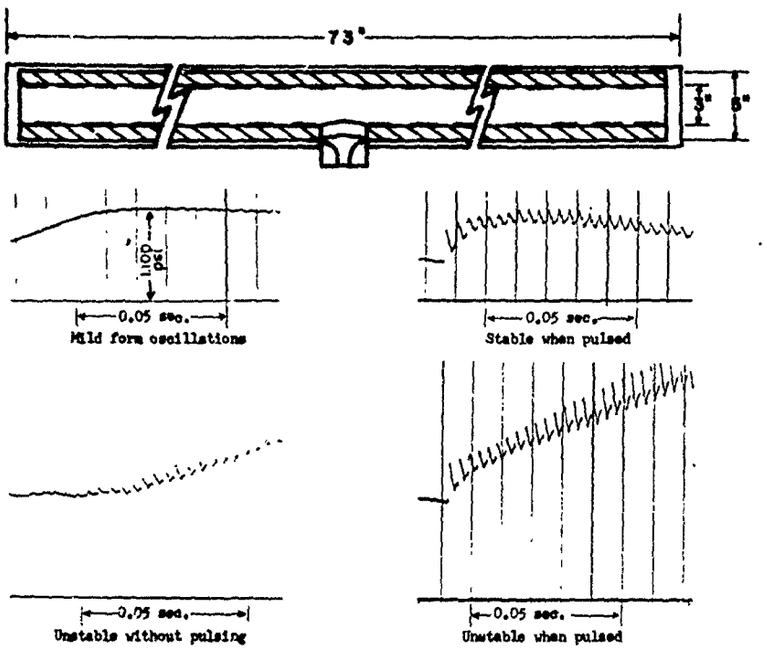

(d) Acoustic oscillatory combustion in a burner experiencing both pressure and velocity coupling: Pressure-time record.

FIG. 1.3. (Cont'd.)

geometries are too complicated to conform to such a simple combustion-flow interaction, the class of behavior involved is obviously possible in a motor.

Figure 1.3d shows the longitudinal mode oscillations in a combustor which has propellant burning surface along the entire longitudinal walls of the combustor. In this arrangement (see also Ref. 8, 10, and 11), the burning surface experiences a more complicated interaction with the motion of the adjoining gas field, including not only pressure disturbances but also shearing type interaction which may involve both mixing of the combustion zone and parallel stress at the surface. While obviously much more complicated to study and describe, this type of behavior is more typical of what may be expected in a rocket motor. Possibly because of the limited experience with rocket motors in sizes necessary to produce this type of instability in a low frequency range, this particular type of axial mode instability (as in Fig. 1.3d) has not been observed below frequencies of about 100 cps. However, the risk of occurrences of such instability in very large motors was considered serious enough in view of experience of low frequency instability in other modes, to merit a research effort in this area in preference to waiting for costly encounters with such behavior in very large solid rocket motors.

Reflecting on the different types of behavior that are exhibited in Fig. 1.3, there are certain key aspects of the instability phenomena exhibited which are essential to any orderly discussion of the problem area. The natural time constant of a combustion process is dramatically exhibited by the example in Fig. 1.3a. In those cases where the combustion is not spontaneously periodic in an otherwise steady-state environment, the combustion process nonetheless has inherent time characteristics such as the relaxation time of the thermal wave in the solid, the accumulation-agglomeration time of ingredients such as metals at the surface, and the transport time of materials through the gas phase combustion region. These time constants suggested in Fig. 1.1 will dictate the frequency range over which the phase relation between combustion and flow oscillations is conducive to combustor oscillations.

In most rocket motor situations, it is necessary to consider not only the time constants of the combustion process, but also the manner in which the oscillating environmental situation couples with the combustion process, since the propellants ordinarily do not burn in a periodic fashion without such interaction. As a matter of convenience, it has been customary to resolve the coupling processes in a slightly arbitrary way into four categories referred to as pressure coupling, velocity coupling, phase correlation and transport coupling. The first two of these can be visualized in terms of Fig. 1.3b, c and d. In Fig. 1.3b and Fig. 1.3c, the combustion is subjected primarily to fluctuations in the environmental pressure and associated fluctuations in temperature and density. This pressure coupled behavior can be viewed as the response of the combustion zone to a perpendicularly incident pressure

wave of wavelength long compared to the combustion zone thickness, and can be represented analytically in terms of one-dimensional models with the space coordinate perpendicular to the burning surface (the microscopic heterogeneity of the propellant must of course be ignored in such a model, or treated by introduction of some simplified mixing description). No physical effects or processes involving motion or transfer of energy or reactions parallel to the burning surface can be represented in such models.

In the case of Fig. 1.3d it is clear that the physical situation provides a possibility of interaction between the combustion zone and gas oscillations parallel to the burning surface, which would require an analytical model involving at least two space dimensions for representation of the phenomena. For the sake of simplicity, it has been assumed in small perturbation treatments of combustion instability that the complicated behavior in this situation can be resolved into two contributions, one consisting of the perpendicularly incident pressure wave-coupled behavior observable in the simpler combustor situations, and the other involving the contribution of pure velocity wave coupling, that is the response of the burning surface to a shearing type interaction with the adjoining flow. It is important to distinguish between these two types of interactions for two reasons; one is because the mechanistic and analytical aspects of the problem are quite different in the two cases, and the other because the conditions leading to combustor instability are quite different in the two cases. While considerable success has been realized in the conduct of controlled laboratory experiments on the pressure-coupled aspect of behavior, only very limited success has been experienced in the study of the velocity-coupled contributions in experiments which clearly resolve two types of interaction.

Returning now to the situation in which the propellant exhibits spontaneous combustion oscillations even in constant pressure vessels, the question must be posed as to whether or not such behavior will lead to organized oscillatory behavior of a combustor in which such a propellant is burning. Observations of such continuous oscillatory behavior have been made by burning small propellant samples in constant pressure test vessels. If one were to observe the combustion of such a propellant material using much larger samples with extensive burning surface, it must be presumed that the spontaneous oscillations in the combustion would not occur over the entire surface of the sample in a completely organized fashion unless there is present some process for bringing the oscillations at different points in the surface in phase with each other (at least in a statistical sense). In the absence of such a phase correlating process, the spontaneous oscillations in the combustion occurring locally at different points over the burning surface would not support any organized fluctuation in pressure in the combustor as a whole, and it would be impossible to experience combustor instability in the usual sense. Thus, one must direct attention not only to the details of the spontaneously oscillating behavior which can be observed with very small

samples of propellant, but also to the manner in which this local behavior at different points on a surface becomes organized to produce combustor oscillations. Such an organizing process could be accomplished either by a flame spreading process across the surface from local initiating sites, or by the responsiveness of the periodic combustion process to the usual pressure and velocity type coupling which may develop in the combustor environment. In the case of surface propagating processes, it is difficult to visualize effective phase correlation in the case of very large burning surfaces, simply because the surface propagative processes could not propagate rapidly enough over a very large surface to insure organized combustion oscillations occurring with the same periodicity as experienced in practice with combustors. However, such surface propagative processes could be important with small burners. On the other hand, the influence of pressure and velocity coupling can be transmitted over the region of the burning surface with the velocity of sound in the gas, and a spontaneously oscillating combustion surface which is also responsive to such acoustic disturbances thus may exhibit phase correlated behavior even over extremely large burning surfaces. This raises the important possibility that local spontaneously periodic combustion behavior can be made to support oscillatory combustor behavior and is responsive to coupling with the oscillations in the gas environment. It is also evident that the behavior of such a system would be different from that of a system in which the local combustion behavior is not spontaneously periodic in nature but instead becomes periodic only in the presence of oscillations in the flow environment. The case of spontaneously oscillating combustion has led to the concept of "preferred frequency" instability, in which combustor oscillations are observed to occur only over a very narrow range of frequencies at any given pressure, this range of frequencies being thought to be centered on a frequency at which the propellant has a tendency for local spontaneous oscillations.

It has been customary in combustion instability studies to assume that the thickness of the combustion zone is thin compared to the combustor dimensions and the wavelength of the gas oscillations. One advantage of this assumption arises from the implication that an interaction locally between the flow and the combustion leads to a combustion-generated flow perturbation at the same location. This concept is an integral part of representations of pressure and velocity coupling; however, the combustion zone is sometimes very thick. This may occur at low combustor pressure, or when the propellant charge is made up of sections of propellant of different compositions whose products are capable of further combustion upon mixing. Under such conditions, a disturbance in one step of the combustion process at one location may lead to disturbance of a later step in the combustion at a different location in the combustor, and it would be necessary to consider the transport and/or mixing field in the motor to relate the flow-perturbation of the combustion to the resulting combustion-generated flow disturbances. Because of the difficulty of observation or analytical representation of this type of transport coupling, little can be said about its practical

importance. However, it is difficult to believe that all "practical" instability problems are restricted to the thin-combustion zone situations, much as it would simplify analysis.

1.4. FACTORS DETERMINING STABILITY

The question of whether a given combustor will be unstable involves ultimately a consideration of the entire combustion-combustor-flow system, not just the transient combustion. Analytically, the appropriate conservation laws, equations of state, diffusion laws and chemical kinetic laws are combined and manipulated to see whether they predict a stable steady-state for the system or some kind of divergent behavior. The particular combination of laws applied in the analysis will usually differ depending upon a preconceived notion on the part of the investigator regarding the instability behavior to be expected. This is essentially an escape from considering the problem in full rigor, motivated by a rationalization weighing the importance of the problem against the effort that can be justified in its treatment. Since this rationalization has been made independently (and sometimes subconsciously) by the various investigators, the public is confronted with a rather bewildering array of theories with no overall rationale. This situation is not unique to the problem of combustion instability, and of course tends to be more visible in hindsight.

In its simplest form, a combustor stability analysis may be based simply on a conservation-of-mass argument (Ref. 12-15). In that case, the combustion is viewed as a source of mass in-flow to the combustor, responsive to the momentary state (e.g., pressure) in the combustor. The pressure in the combustor is a consequence of the balance (or imbalance) between mass in-flow, and mass outflow. Since no energy conservation is applied in this model, restrictive assumptions must be made regarding gas motion, energy dissipation, and entropy. The most conspicuous consequence of this is exclusion of wave-type phenomena, giving rise to the present body of theory of nonacoustic instability. In this theory, the bulk pressure in the combustor rises and falls, with the combustion rate (mass inflow) oscillating with sufficient phase lead so that the system overshoots equilibrium and sustains oscillations. Since only mass balance is considered for the combustor system in these models, there is no way to represent resistive or dissipative forces, and consideration of fluctuations in gas composition, temperature, energy or entropy cannot be included without reverting to energy considerations presently absent in the models. The adequacy of these mass-balance models for treatment of nonacoustic instability is not yet fully assessed, but the analytical and experimental work reported in Section 5 clarifies the significance of the approximations made in the models, and offers qualitative verification of the theory.

Oscillatory behavior in wave modes of the combustor cannot be described in terms of mass balance alone, and cannot be described without consideration of space variables. Thus, the analytical representation

is much more complicated than in the nonacoustic mode. Not only is the description of the gas motion more complicated, but the interaction between gas motion and combustion becomes correspondingly more complicated, and spacewise nonuniform. A stability analysis typically involves a spacewise integration of acoustic energy generation by the combustion, and by energy dissipation by various mechanisms. If the integral shows increasing net acoustic energy, the system is unstable. This analysis is normally carried out with respect to a particular acoustic mode of the combustor, for which the pressure oscillation is often seen (Fig. 1.3c) to conform to the relation

$$p = P_o e^{\alpha t} \cos \omega t \tag{1.1}$$

and oscillations are increasing (unstable) when $\alpha > 0$. Under certain ideal conditions, this representation is related in a simple way to the acoustic energy accumulation through the relation (Section 6).

$$2\alpha = \dot{E}/E \tag{1.2}$$

where $\dot{E}$ is the sum of energy gains and losses due to various mechanisms integrated over the combustor volume and surface, for example

$$\dot{E} = \dot{E}_p + \dot{E}_v + \dot{E}_n + \dot{E}_\omega + \dot{E}_b \tag{1.3}$$

Since the energy rates are additive, Eq. 1.2 may be written

$$2\alpha = 2(\alpha_p + \alpha_v + \alpha_n + \alpha_\omega + \alpha_b) = \frac{\dot{E}_p}{E} + \frac{\dot{E}_v}{E} + \frac{\dot{E}_n}{E} + \frac{\dot{E}_\omega}{E} + \frac{\dot{E}_b}{E}$$

and Eq. 1.1 may be written

$$p = P_o e^{(\alpha_p + \alpha_v + \alpha_n + \alpha_\omega + \alpha_b)t} \cos \omega t =$$

$$P_o e^{\alpha_p t} e^{\alpha_v t} e^{\alpha_n t} e^{\alpha_\omega t} e^{\alpha_b t} \cos \omega t \tag{1.4}$$

i.e., the individual amplification and attenuation processes and their energy rates affect the pressure oscillations independently through multiplicative exponentials in the corresponding gain α's.[1]

[1] In acoustics literature, the quantity α is called an "attenuation" constant, and a minus sign is used in the exponent so that positive attenuation will occur with positive α. Since we are concerned with unstable systems here, α is called a "gain" constant and the minus sign is dropped in the exponentials.

The concept of exponentially growing sinusoidal oscillations is intimately linked with a linearized representation of the oscillatory behavior. The pressure oscillation referred to in Eq. 1.1 and 1.4, and the energy fluxes in Eq. 1.2 and 1.3, may be viewed as representative of a particular acoustic mode of the system if the value of α is not so large as to invalidate the concept of orthogonal modes. Since the values of the $\dot{E}$'s will generally be different in each acoustic mode, the question of stability must be posed for each mode before stability is fully assessed.

In order to determine the values of the α's in Eq. 1.4 for a particular acoustic mode, one must turn to the detailed mechanism of gain or loss involved, and sum the contribution of that mechanism over the region of the combustor relative to the mode in question. Alternately, some of the α's may be determined by experimental observation of the pressure oscillation growth or decay rate under the influence of one mechanism at a time. As an example, the value of α_p may be estimated from tests in special burners in which α_v is zero and the loss α's are, by design, all small compared to α_p. Likewise, α_n may be evaluated by tests on simulated rocket motors in which all α's other than α_n are either small (pulsed cold flow systems) or equal to α_n and known (driven system with steady oscillations). The methods for making these determinations of α's are still in a relatively primitive state from the quantitative viewpoint, but it will become evident in the present report that the methods exist for semiquantitative determinations of the dominant α's.

In the case of nonacoustic instability, where only mass balance has been considered, the value of α has the same meaning in terms of Eq. 1.1, but is related to the conservation laws in terms of mass flow rate perturbations instead of perturbation energy (in this case the energy is transported with the mass, and perturbation energy equations are identical with perturbation mass equations except for a specific energy factor common to each term of the equation). Lacking wave behavior, the nonacoustic oscillator does not usually have harmonic modes of oscillation; hence, is characterized by only one α (although it will be seen that under certain conditions more than one frequency is permitted by the stability theory).

In the event that nonlinear physical processes are involved in the stability behavior, both the semantics and the analysis of the behavior become dislocated from conventional approaches. The concepts of modes, growth α's, and local characterization of acoustic environments become rigorously inapplicable. Linear concepts continue to be used for lack of nonlinear methods, but their relevance becomes less certain. In some instances the nature of the nonlinearities permits piecewise linear calculations, or permits cautious continued application of "linear semantics", but increasing reference appears to sharp fronted waves; initiation thresholds; spontaneous quenching; and finite wave amplification, reflection and attenuation.

1.5. PLAN OF THE REPORT

The purpose of this report is to summarize all significant work that has been done on the present program since the previous report of May, 1964. The report is divided into sections that stand fairly well by themselves, and in many cases represent work sufficiently complete for publication in the open literature. Such publications have been used where appropriate, but are augmented with additional material as needed to fill in, up-date, and relate different investigations to each other and to rocket motor problems.

Section 2 concerns investigations of decomposition and deflagration of large single ammonium perchlorate (AP) crystals, investigations motivated by the continuing ignorance of the behavior of this most extensively used propellant ingredient. The availability of large, high purity crystals from a companion program was also a factor in initiation of this work, plus a suspicion that current theories of AP deflagration were inadequate.

Section 2 also reports investigations of the edge-burning of laminates of AP sheets and propellant binders. This investigation was aimed at determining the relative importance of different classes of reactions in propagating the burning surface of propellants. Again the availability of high quality AP crystals was a factor in permitting the fabrication of suitable test samples, as earlier efforts with poor crystals failed because the crystal "sheets" fell apart in the deflagration wave.

Section 3 reports investigations of the condition of the burning surface of "real propellants" during burning, with particular reference to the behavior of powdered metal fuel ingredients. This study has been pursued primarily by photography of samples in a window bomb. The apparatus developed was also used for the studies reported in Section 2.

Section 4 reports studies of oscillatory combustion encountered with small propellant samples in window bombs. This behavior, exhibited most clearly during combustion of pellets pressed from powdered mixtures of AP-aluminum, is related to the accumulation-agglomeration-ignition sequence of metals on the burning surface. The resulting periodic combustion of the metal was studied by time-resolved radiation measurements, high speed photography, and sample variables. Studies were extended to "real propellants", and to the effect of externally induced pressure oscillations.

Section 5 covers work on low-frequency nonacoustic instability, including development of laboratory scale burner techniques, studies of the effect of propellant variables, and development of theory and analytical representation of nonacoustic instability.

Section 6 describes work on low frequency acoustic mode instability, including development of acoustic mode burners and technique for operation, and including studies of effects of propellant variables, oscillation frequency, and environmental pressure.

Section 7 describes experimental studies of acoustic attenuation in axial modes. These studies (using cold-flow simulation) were originally conceived on the thesis that the complicated geometries used in rocket motors would preclude the possibility of direct computation of acoustic losses from theory. Experimental apparatus was designed and built for cold-flow studies, and the apparatus was checked out and applied to both simple and complicated motor configurations.

Section 8 summarizes the highlights of the results and the status of current understanding.

2. AMMONIUM PERCHLORATE DECOMPOSITION AND DEFLAGRATION

2.1. INTRODUCTION

Ammonium perchlorate (AP) is the oxidizer and principal ingredient in most modern composite propellants, and its behavior in the combustion wave is an essential aspect of combustion as a whole. Ammonium perchlorate is a crystalline material which will deflagrate as a monopropellant at pressures above approximately 300 psia (Ref. 16). Its deflagration properties have been studied previously primarily with pressed powder test samples (see for example Ref. 17, 18 and 19), while studies of kinetics of decomposition have been carried out in isothermal tests at relatively low temperatures on granular material. Efforts to bridge the gap between low temperature decomposition studies (e.g., 200-350°C) and deflagration studies (surface temperature approximately 600°C) have been made by hot plate linear pyrolysis tests (Ref. 20 and 21). The low temperature studies possess the desirable attribute of relative ease of control of experimental variables and measurement of results, but leave unresolved the question of relevance of results to the deflagration process. This problem of relevance can be appreciated by noting the difference between the heating rates in, say, a differential thermal analysis (DTA) test, and a deflagration wave, a difference of four or five orders of magnitude. Unfortunately, it is extremely difficult to combine a well controlled, unambiguous experiment, with heating rates comparable to those in the deflagration wave, with the result that the deflagration process is poorly understood, and the relevance of low temperature decomposition work to deflagration remains uncertain.

Even in the low temperature work where relatively "clean" experiments are possible, the decomposition of AP is a remarkably complicated process that has escaped decisive elucidation. At temperatures below approximately 300°C, slow decomposition proceeds, but is observed to stop after about 30% of the AP is gone (Ref. 22 and 23). No chemical difference has been found between the original AP and the residual 70%. The AP crystals experience a crystal phase change from orthorhombic to cubic at about 240°C, with a net volume increase of approximately 10%. Russian investigators (Ref. 24) have reported that the decomposition rate below the phase transition temperature is slightly pressure dependent, but is relatively insensitive to pressure above this temperature. Shannon (Ref. 25), however, has found a large pressure effect using high pressure DTA. Activation energies from 22 kcal to 65 kcal have been reported for the low temperature AP decomposition process, based on various procedures for estimating decomposition rate versus temperature. No convincing explanation has been given for the limitation of

decomposition to 30% of the material, although it has been suggested that it might be related to a greater susceptibility to decomposition of AP molecules near the boundaries of the mosaic blocks of the crystal. It has been observed by the authors and others (e.g., Ref. 26) that the decomposition can be suppressed by testing in ammonia atmospheres, and that the 70% residue becomes "rejuvinated" in atmospheres containing water (or other AP solvent) so that further decomposition could occur. Aside from the "70% residue" mystery, the experimental results appeared to be explained by a mechanism involving a proton transfer reaction on crystal surfaces according to

$$NH_4^+ + ClO_4^- \underset{k_2}{\overset{k_1}{\rightleftharpoons}} NH_3 + HClO_4$$

followed by desorption of NH_3 and $HClO_4$. Presumably, the effect of an ammonia atmosphere was to increase the NH_3 concentration on the surface thereby limiting the net forward rate of the above reaction. The desorption is followed by decomposition of perchloric acid and oxidation of ammonia to give the final measurable gas products which are temperature dependent.

When the decomposition temperature of AP is increased to approximately 350°C (at one atmosphere), it is found that all of the material decomposes to gaseous products (Ref. 22). An ammonia atmosphere still retards the decomposition.[2] At this higher temperature, there is considerable NO in the product gases, which may offer a clue to the difference between the low and high temperature decomposition sequences. Considerable attention has been given to the question of stability of the $HClO_4$ molecule, because it was initially thought that it might be too short-lived to be present in appreciable concentration (Ref. 27). It is now believed (Ref. 28) that $HClO_4$ may decompose primarily in the gas phase, and slowly enough to permit high concentrations of $HClO_4$ (and hence NH_3) in the gas phase adjoining the surface. The decomposition in both the high and low temperature regimes is now believed (by some authors) to proceed by proton transfer on the surface to yield NH_3 and $HClO_4$, followed by desorption, decomposition of $HClO_4$, and oxidation of NH_3, with the proton transfer and desorption steps being reversible. The principal difference between the high and low temperature decomposition is thus the tendency at low temperature for decomposition to stop at about 30% with the reason for this being, as yet, unexplained.

[2]In recent experimental work on the phase transition of AP, we have successfully observed, on a macroscopic basis, the 240°C transition of single crystals. These tests were run in one atmosphere of NH_3 and during some of the runs temperatures as high as 350°C were made for several minutes without evidence of decomposition occurring.

The experimental work to date has unfortunately been rather disjointed. Efforts have been made to infer activation energies from experimental results, but it is not usually clear what reaction step is determining the apparent activation energy. This is illustrated by the use of differential thermal analysis records to measure activation energy, where determinations are made from exotherms on the DTA curve. Since the proton transfer reaction (which is really the AP decomposition reaction) is endothermic, its activation energy cannot be inferred from exotherms or other endotherms unless a careful analysis is made of the temperature dependence of subsequent processes (physical and chemical) leading to the exothermic reaction in the particular experiment. Only recently has attention been directed to experimental exploration of this question by varying the pressure (Ref. 29) used in the tests (where it is found that the exotherm disappears at lower pressures).

A further problem with experimental work has been its intermittency and corresponding indecisiveness. The appropriate range of test conditions is rarely covered, nor is the relevance to other experimental work. In the face of these attributes of the situation, a complete summary of the literature on slow decomposition of AP is a fairly courageous undertaking which is not attempted here. A recent survey by Pittman (Ref. 30) collects the references and presents a somewhat diagnostic review.

In order to study decomposition behavior at high temperature without problems of physical disruption of the sample, it is necessary to turn to surface heating experiments, in which the sample is no longer at uniform temperature and high reaction rates occur primarily at the surface. This complicated state of affairs seems to be essential to high rate studies, and explains the absence of reliable high rate data. However, experimental results with "hot plate", porous plug, and pressed AP deflagration experiments have characterized high temperature decomposition with qualitative accuracy and hold promise for future improvement. From such studies there has evolved an estimate of the surface temperature during deflagration of 600-700°C and estimates of a gas phase reaction zone thickness of the order of 1 micron at 1000 psi. The results of such experiments have not yet received a unified interpretation, nor correlation with results of low temperature decomposition studies.

A singularly obscure aspect of all of the work with AP is the role of crystal geometry and size in propagation of decomposition or deflagration. At the time of the present program, there became available a supply of large, chemically pure, physically "perfect" AP crystals, the use of which would permit less ambiguous study of decomposition and deflagration.

2.2. GROWTH AND PREPARATION OF AP SINGLE CRYSTALS[3]

The growth of single crystals of AP, large enough to be practical for combustion experiments, is a difficult process and has in the past been unsuccessfully attempted. Recently, in this laboratory,[4] large single crystals of AP have been successfully grown from aqueous solution utilizing a carefully controlled temperature-lowering technique. The water-jacketed apparatus shown in Fig. 2.1 was found to eliminate the major problems of crystal growth associated with temperature regulation and growth solution concentration gradients. Several crops of large single crystals have been grown from small seed crystals by utilizing the above apparatus. The essential details for this crystal growth equipment have been described previously by Torgesen, Horton and Saylor (Ref. 31).

Sustained growth for periods of several weeks or a month, without the veiling of mother liquor inclusions, which are produced by temperature fluctuations, has been fairly easy to accomplish with resulting specimen dimensions up to 1- by 1- by 1½-inch. Controlled growth for periods of several months, which is necessary for the complete growth of larger, essentially flawless crystals, has been achieved only with moderate difficulty. The material which has been utilized successfully for this work is "ammonium perchlorate, ultra high purity" from the American Potash and Chemical Corporation. The chemical analysis of this material supplied by the vendor is shown in Table 2.1. "Baker analyzed reagent" from J. T. Baker Chemical Company (a discontinued product) and reagent AP from Matheson, Coleman and Bell were not satisfactory for the present work.

The growth habit of the crystals in general followed that described by Tutton (Ref. 32). The large crystals taken from the bath solution were cleaved into smaller crystal segments of a size convenient to work with, typically 8-mm wide by 10 to 15-mm long and 2-mm thick. Cleaving the large crystals also allowed removal of portions of the crystal containing visible imperfections. The crystal segments used in this work were without visible internal flaws or inclusions. The clear, colorless crystals are transparent in the visible spectrum and display good cleavage along the (210) and (001)planes. The cleaved segments are parallelopipeds bounded by four *m* faces and two *c* faces with a rhomboid shaped cross section normal to the *c* axis. Figure 2.2 shows crystals typical of those used in the present work.

Ammonium perchlorate single crystals doped with the MnO_4^- ion were also grown with this equipment. Analysis of the doped crystals has

[3]This section contributed in part by Dr. W. R. McBride and E. J. Dibble.

[4]The authors wish to gratefully acknowledge Dr. W. R. McBride of the Research Department, Michelson Laboratories, NOTS, China Lake, California for the very excellent single crystals of AP used in this work.

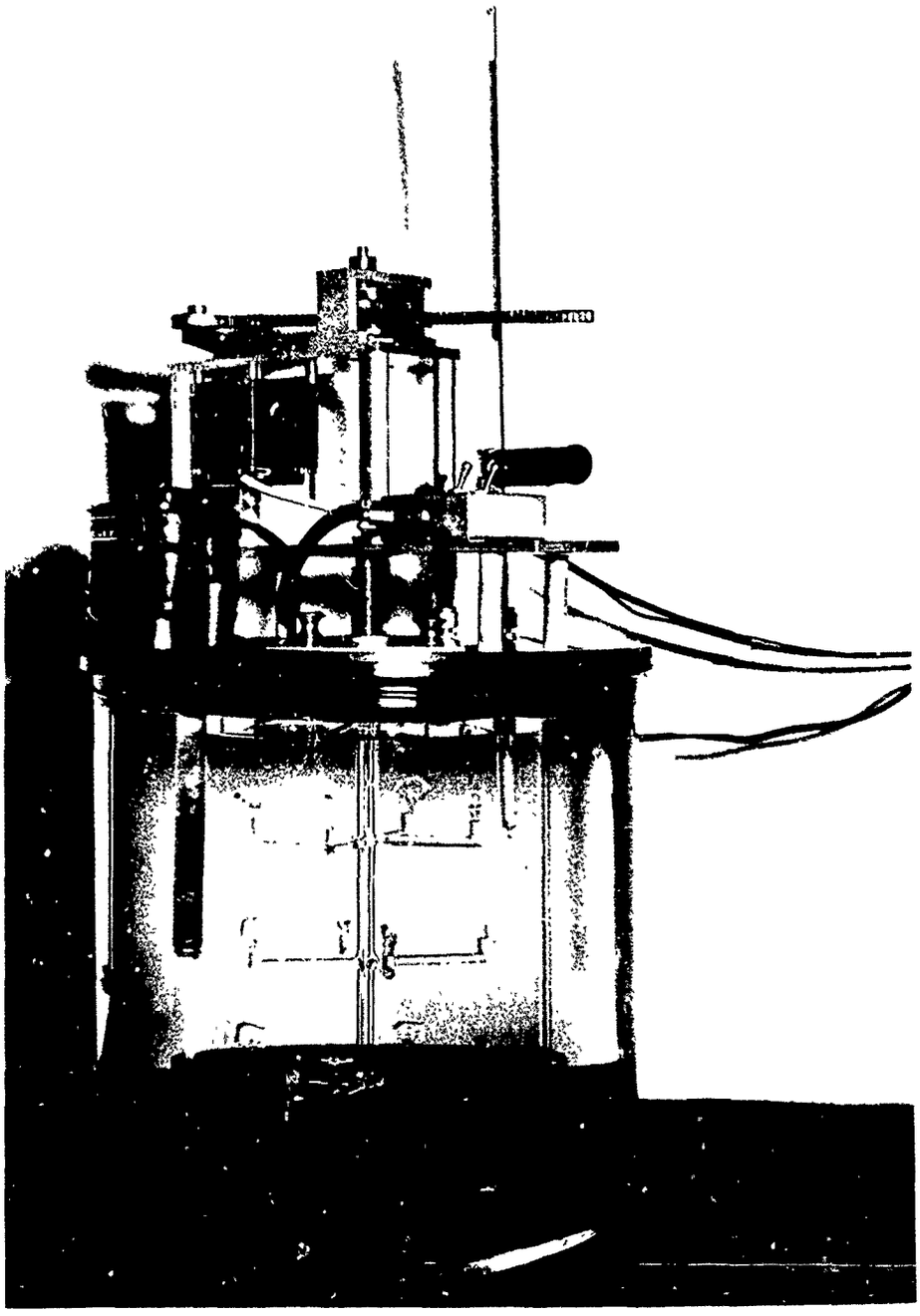

FIG. 2.1. Water Jacketed Crystal Growth Tank and Associated Equipment for the Growth of AP Single Crystals from Aqueous Solution. Note the single crystals growing on the glass "tree" inside the apparatus.

TABLE 2.1. Ammonium Perchlorate,
Ultra High Purity Analysis

Lot H-1093-22A

NH_4ClO_4	99.8%
NH_4Cl	0.02
$NaClO_3$	Trace
Moisture (surface)	0.008
Sulphated ash	Trace
$(NH_4)_2SO_4$	Trace
$NaBrO_3$	Trace
Insoluble	0.002
Metal oxide (non alkali)	0.001
pH	5.0
Moisture (total)	0.079
Na	5 PPM
K	4 PPM
Ca	N.D. (1 PPM max.)

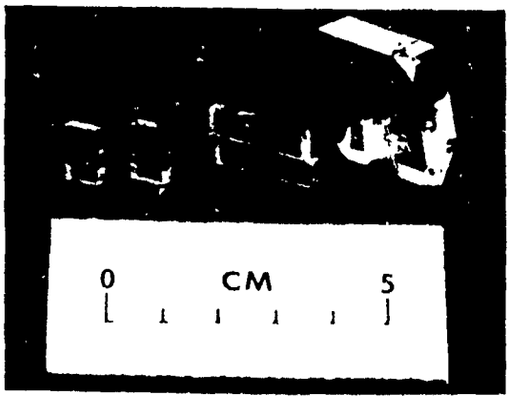

FIG. 2.2. Typical Ammonium Perchlorate Single Crystals. The large crystal on the right is typical of the crystals as they are removed from the bath. These large crystals are then cleaved into smaller segments such as those shown on the left. The visible flaws that can be seen on these crystals are surface defects such as cleavage steps or scratches.

indicated a concentration of the MnO_4^- ion of 0.0379% by weight. The doped crystals are also clear and free of visible imperfections and display a beautiful purple color characteristic of the permanganate ion. The addition of the MnO_4^- ion did not noticeably change the crystal habit. Other concentrations will be grown shortly, as well as crystals doped with other materials.

2.3. LOW TEMPERATURE DECOMPOSITION EXPERIMENTS

2.3.1. Isothermal Decomposition Below 240°C

The isothermal decomposition of AP has been studied below the phase transition temperature of 240°C. The experiments were carried out by utilizing the previously described single crystals which were cleaved to a minimum size necessary for convenient experimentation (approximately 4 x 3 x 2-mm weight between 45 mg and 50 mg). The cleaved crystals were carefully weighed and subsequently heated slowly to 200°C in a horizontally mounted (closed but not sealed) and resistively heated tube furnace. Heating to the final temperature was accomplished within five minutes after reaching 200°C. The temperature of the furnace was kept constant to $\pm$ 1/2°C. The decompositions were carried out at a chosen temperature for different periods of time. All runs were made under atmospheric pressure and a new crystal was used for each run.

The microscopic examination of the crystals has shown that the decomposition starts at nuclei on the surface. Three of the nuclei can be seen in Fig. 2.3 in an advanced state of development. The microstructure of the sites cannot be resolved with a normal light microscope because the individual points are smaller than 1 μ and excessive optical scattering occurs. On lowering the focal plane into the crystal one can see what appears to be limited decomposition in the bulk of the crystal in the direction of the crystallographic b-axis. This is shown in Fig. 2.4. The decomposition sites on the *m* faces grow in a disk-like shape whereas the spots on the c faces grow faster along the b-axis (in the same direction as the limited bulk decomposition) than along the a-axis. Thus, a streak-like pattern is formed (Fig. 2.5). This is in agreement with Ref. 33, 34 and 35. The formation of nuclei seems to be random on the surfaces of the average crystal, and was not affected by the presence of scratches scribed on the surface. In a few cases of especially well grown (or cleaved) crystals the opaque spots developed preferentially around corners and edges. The disk-like sites on the *m* faces and the streak-like sites on the c faces grow in size with time until they overlap and form a continuous, opaque, porous layer which envelopes the entire crystal. The thickness of this layer is initially very small, and the weight loss at the time the surface is first covered is still small.

The scanning electron microscope allowed detailed observation of the surface of the porous, partially decomposed AP layer. This

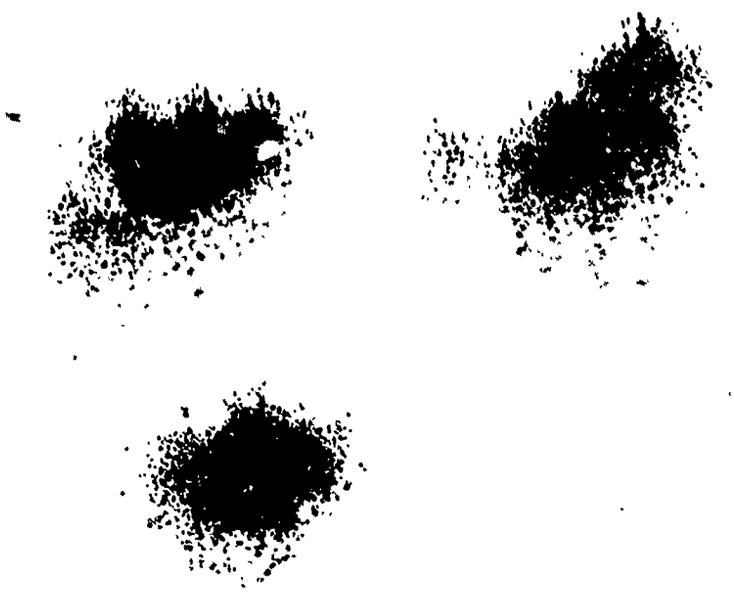

FIG. 2.3. Decomposition Centers on the Surface of an *m* face (210). Magnification approximately 140X.

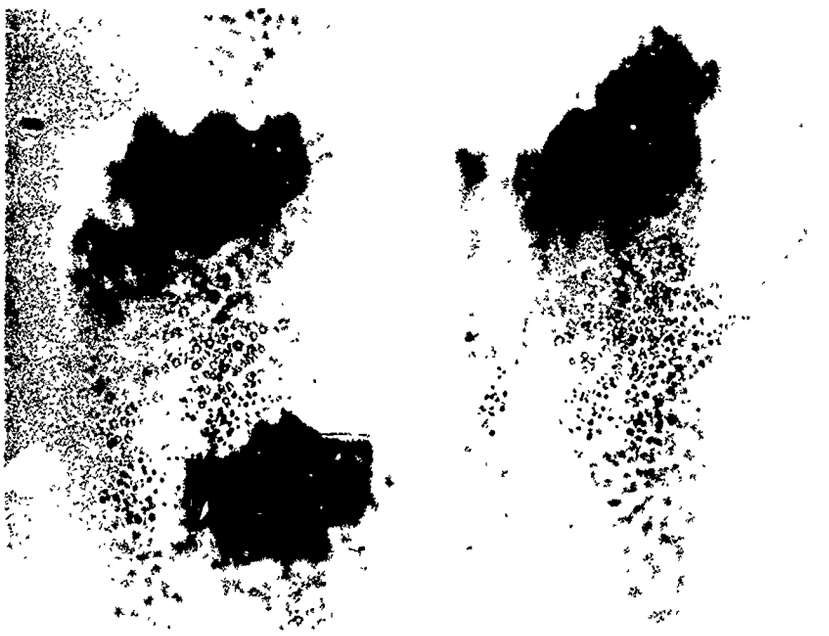

FIG. 2.4. Same Decomposition Centers as in Fig. 2.3 but with the Focus Slightly Below the Surface to Show the Limited Bulk Decomposition Streaks Along the b-axis.

FIG. 2.5. Streaklike Decomposition Sites Observed on the C faces (001) Due to Increased Rate of Nucleation Along the Crystallographic b-axis.

microscope has two great advantages over the light microscope, namely higher magnification and much greater depth of focus. Figure 2.6 shows the surface of an AP crystal after partial decomposition. Figure 2.6a, b and c show in different magnifications a rather homogeneous distribution of pores which have typical dimensions ranging from less than one micron to a few microns.

Once the decomposition has covered the crystal surface the reaction proceeds along the interface between transparent, undecomposed single crystal and the growing porous layer which consists of only 65% of the original weight. This partial weight loss has been observed by a number of investigators (Ref. 22, 23, 33 and 34), the only variation being minor differences in the amount of weight loss reported (usually around 30%).

The partially decomposed crystals could be easily cleaved and Fig. 2.7 shows a section through a sample with the porous layer, the interface, and the crystal core with its thin streaks of bulk decomposition. The bulk decomposition on a relative basis seems to be highly restricted, probably because of the difficulty for the escape of the decomposition products from the interior as compared to the crystal surface.

The above described experiments were repeated using $NH_4 MnO_4$-doped AP. The concentration of the permanganate ion MnO_4 was about 0.04 weight percent which gave the single crystals the characteristic purple color of this ion.

The experimental procedure as well as the microscopic examination were the same as for undoped crystals. The decomposition again started at nuclei which spread and coalesced to envelope the unreacted crystal in a porous continuous layer. From there on the reaction continued on

(a) 130X

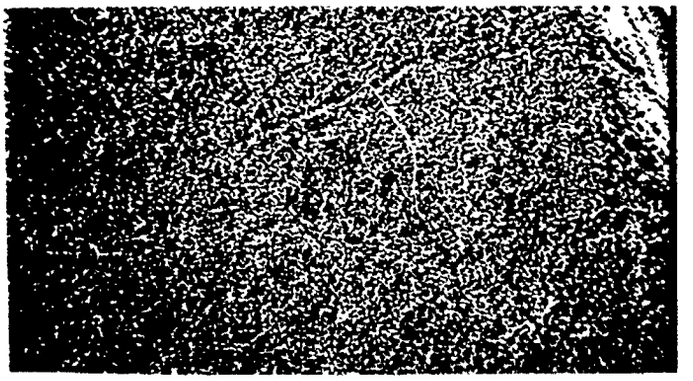

(b) 400X

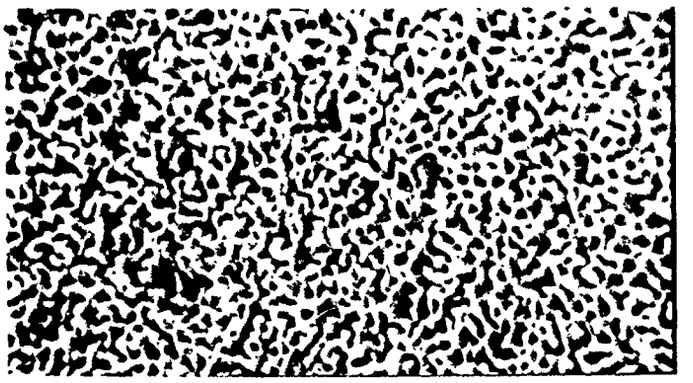

(c) 1300X

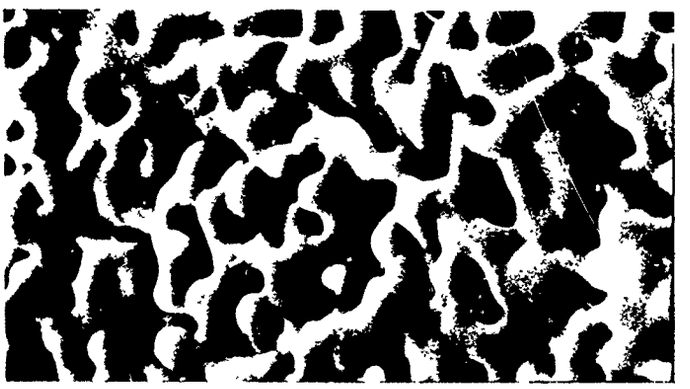

FIG. 2.6. Scanning Electron Microscope Photomicrograph of the Residue of the Partial Decomposition of AP (Weight Loss Approximately 35%). These photographs are of the c face (a) 130X, (b) 400X and (c) 1300X. Due to experimental difficulties these samples had to be exposed to atmospheric conditions in the laboratory before examination with the scanning microscope and may have suffered some degree of rejuvination.

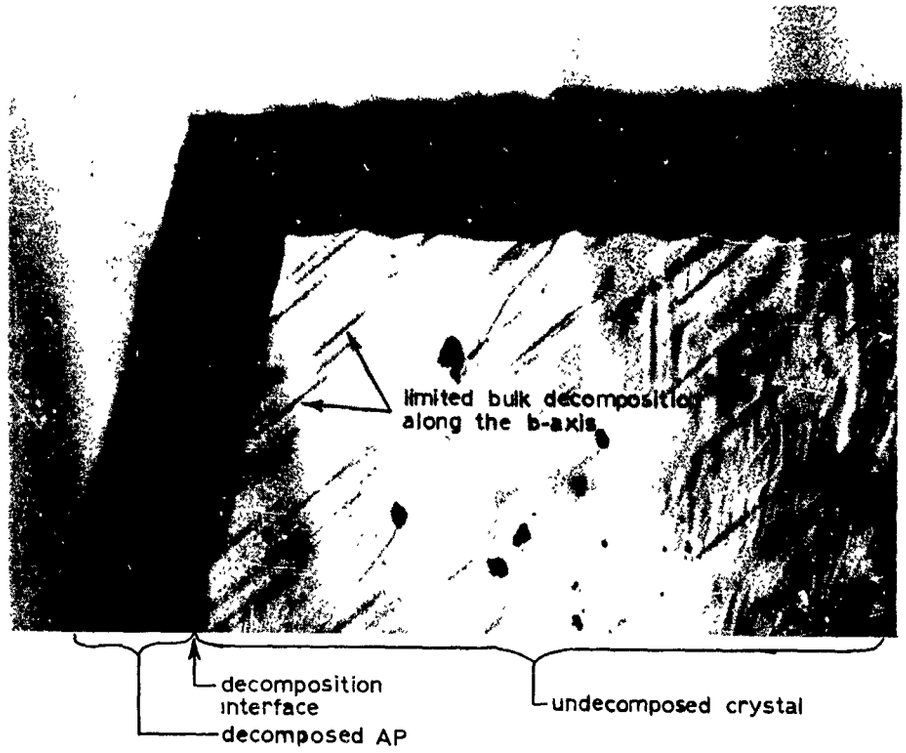

FIG. 2.7. Cross-Section Through Partially Decomposed AP Single Crystal. Viewed along the c axis at a magnification of approximately 50X.

the interface between porous layer and unreacted crystal. After completion of the partial decomposition, the porous residue retained about 60-65% of the original crystal weight. The characteristic difference between the decomposition of undoped and doped AP is the change in number of nuclei generated at the surface of doped and undoped crystals at constant temperature during equal periods of time. Because of experimental difficulties, only a rough estimate of the difference can be given. The number of nuclei appearing on the surface of a doped crystal under identical conditions is about 10^2 times greater than the corresponding number for undoped crystals. Consequently, covering of the surface with the porous layer is completed faster on a doped crystal than on an undoped crystal, not so much because the sites grow with a different velocity but because of the greater concentration of nuclei. The interface of a decomposing doped crystal is well defined (and becomes continuous more quickly than the undoped AP) by the greater number of intersecting half ellipses. Figure 2.8 gives a comparison of the growth of the porous layer on doped and undoped AP crystals. Measurements were made of the thickness of the layer of decomposed material as a function of time with

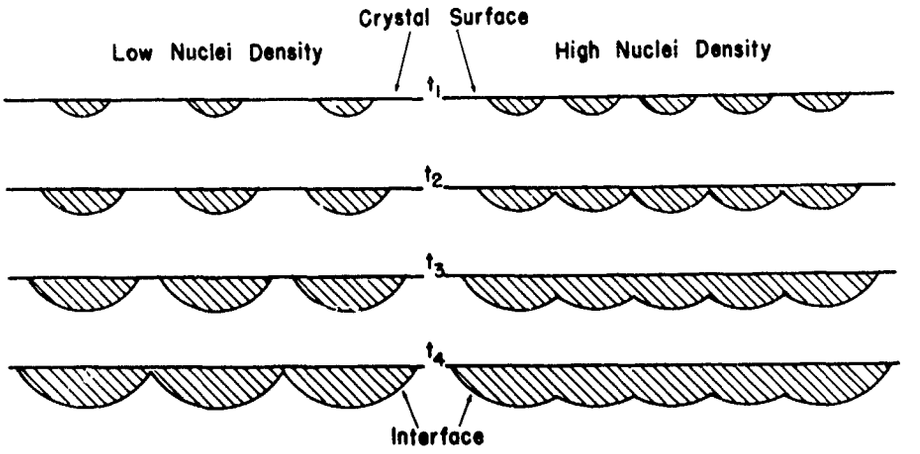

FIG. 2.8. Schematic Representation of the Development of the Interface of a Decomposing AP Crystal as a Function of Nuclei Density and Time.

temperature as the independent parameter. Because of the sharpness of the boundary between decomposed layer and crystal when doped crystals were used, it was possible to show that the thickness of the *m* face layers was 20% thicker than the c face layers. The same comparison could not be made with undoped AP because the interface between the porous layer and the crystal was not smooth enough.

The simple geometrical form of the samples and the possibility of cleaving the crystals and measuring the thickness of partially decomposed layers at different stages of decomposition provided an excellent opportunity to accurately determine the decomposition rates. Figure 2.9 shows plots of layer thickness versus time for pure AP at three different temperatures. Each data point represents an uninterrupted heating interval on a different sample. The thickness, d, of a porous layer increases linearly with time at a given temperature. Figures 2.10 and 2.11 show the difference of decomposition rates observed between *m* faces and c faces of MnO_4^--doped AP. The measured decomposition rates for pure and MnO_4^--doped AP are shown in Table 2.2. With the rate values, Arrhenius plots were drawn (Fig. 2.12 and 2.13) and pre-exponential factors and activation energies evaluated from the diagrams. The linear decomposition rate of pure and doped orthorhombic AP is given by the equations

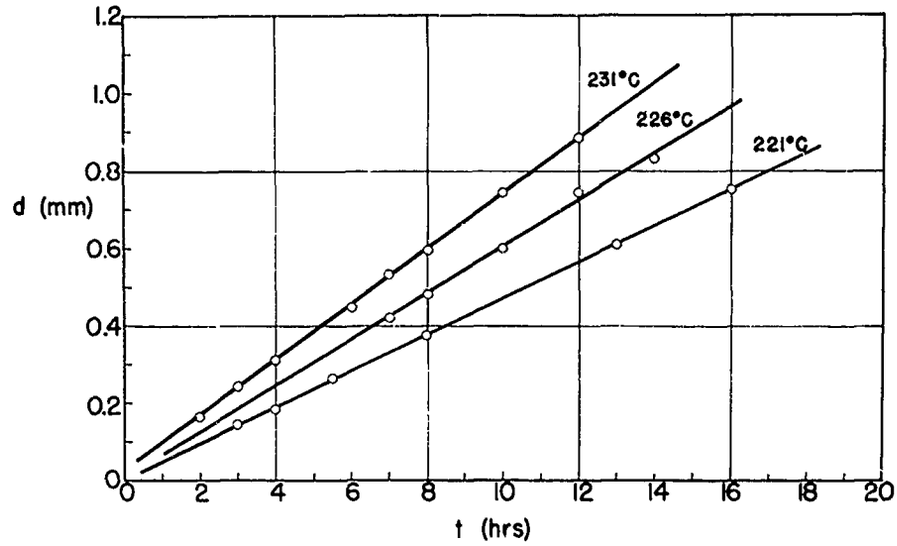

FIG. 2.9. Penetration of the Decomposition Interface Into an Ammonium Perchlorate Single Crystal as a Function of Time. d = distance from crystal surface to interface.

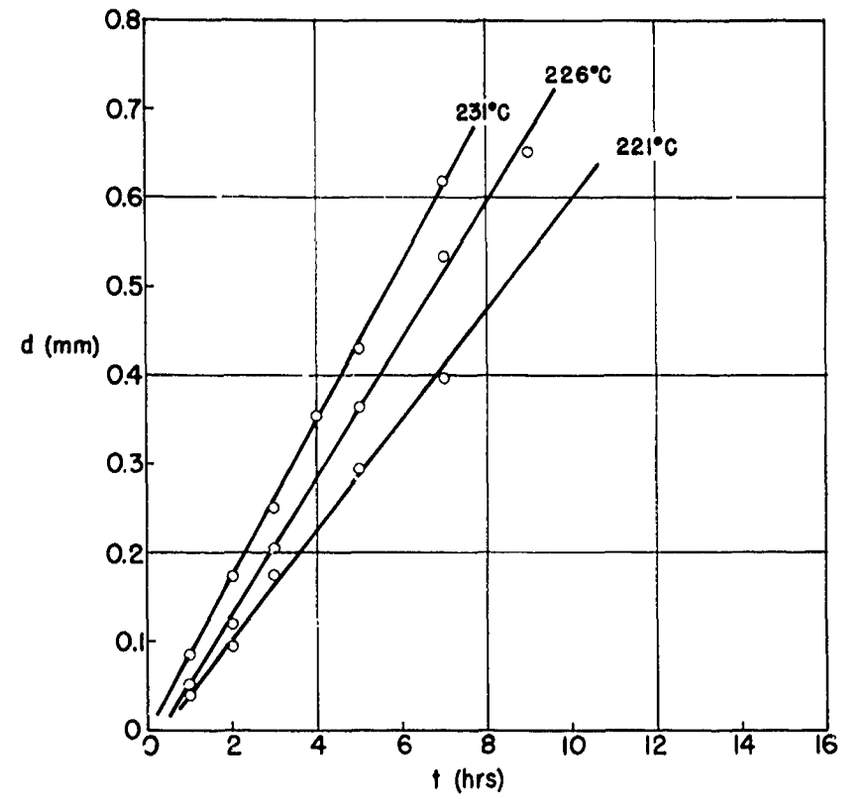

FIG. 2.10. *m*-Face Penetration of the Decomposition Interface Into a MnO_4^--Doped Ammonium Perchlorate Single Crystal as a Function of Time. d = distance from crystal surface to interface.

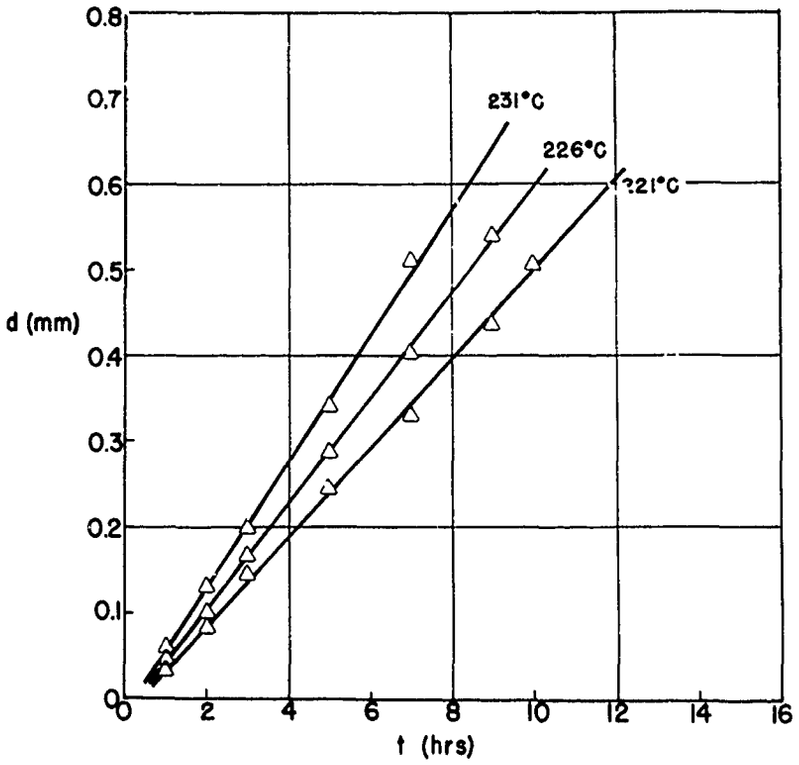

FIG. 2.11. c-Face Penetration of the Decomposition Interface Into a MnO_4^--Doped Ammonium Perchlorate Single Crystal as a Function of Time. d = distance from crystal surface to interface.

TABLE 2.2. Measured AP Decomposition Rates[a]

		Isothermal temperature		
Crystal		221 C	226 C	231 C
Pure AP		1.28×10^{-6}	1.67×10^{-6}	2.0×10^{-6}
MnO_4^--doped AP	*m* faces	1.73×10^{-6}	2.13×10^{-6}	2.44×10^{-6}
	c faces	1.44×10^{-6}	1.68×10^{-6}	2.02×10^{-6}

[a] All values are measured in cm sec^{-1}.

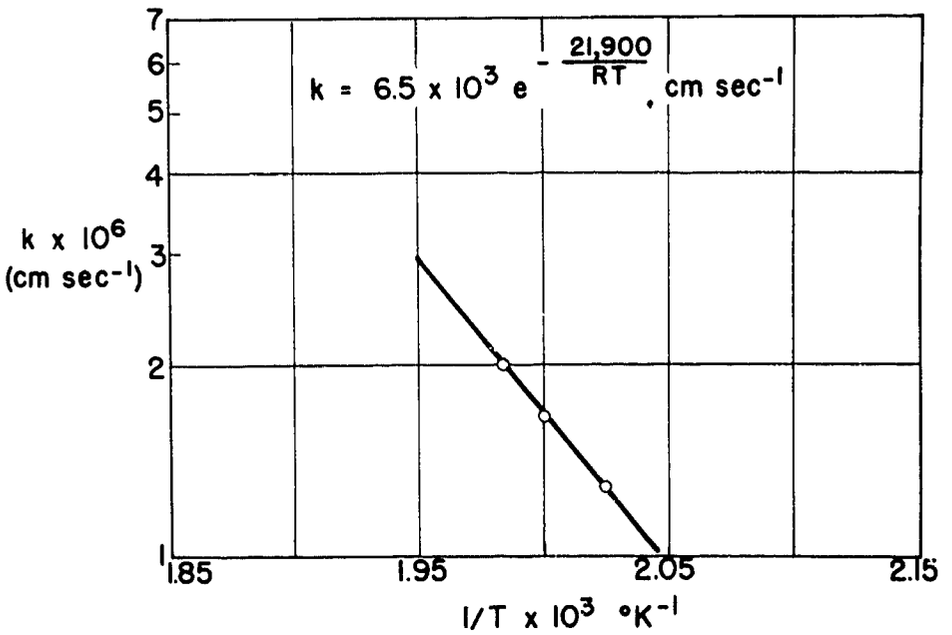

FIG. 2.12. Arrhenius Plot of the Rate of Decomposition of Orthorhombic Ammonium Perchlorate Single Crystals as a Function of Temperature.

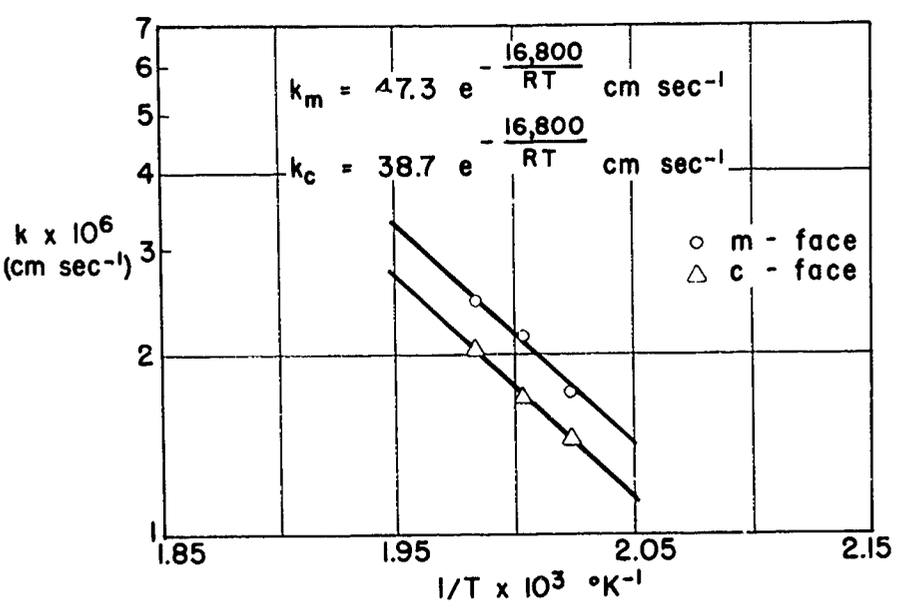

FIG. 2.13. Arrhenius Plot of the Rate of Decomposition of MnO_4^--Doped, Orthorhombic Ammonium Perchlorate Single Crystals as a Function of Temperature and Crystal Face.

$$k = 6.5 \times 10^3 \exp(-21{,}900/RT) \text{ cm/sec}$$

$$k_m = 47.3 \exp(-16{,}800/RT) \text{ cm/sec}$$

$$k_c = 38.7 \exp(-16{,}800/RT) \text{ cm/sec}$$

where k refers to pure AP, k_m to *m* face decomposition of MnO_4^--doped AP, and k_c to c face decomposition of MnO_4^--doped AP. The equations for the doped AP show that the frequency factor is direction dependent but not the activation energy E. An explanation of this result will not be attempted here but it may be noted that the specific ion conductivities of an anisotropic crystal indicate a similar behavior.

The weight loss of pure AP was measured immediately after decomposing and before cleaving the crystal. Figure 2.14 shows the relative weight loss, α, of AP versus time as determined at 221°C and 231°C. Corresponding weight loss versus time curves have been calculated using the formula

$$\bar{\alpha} = \frac{K \Delta V}{V_o} \times 100\%$$

where $\bar{\alpha}$ = relative weight loss in percent,

$\Delta V \equiv V_o - V_t$

V_o = volume of undecomposed crystal at time t = 0,

V_t = volume of undecomposed crystal at time t, and

K = maximum relative weight loss (0.35 x original weight for pure AP crystals determined by prolonged heating of crystals)

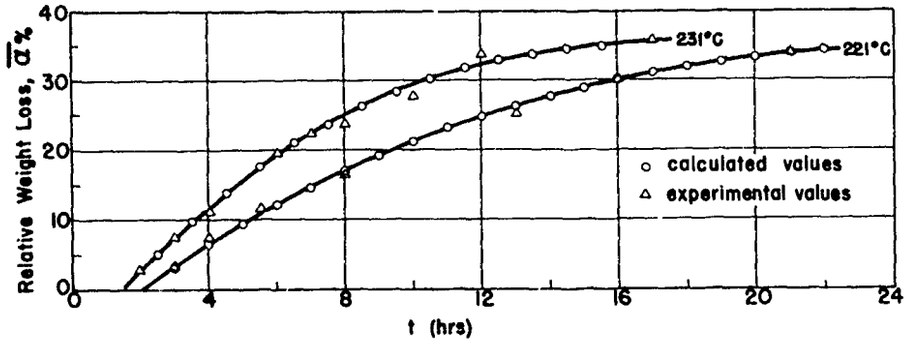

FIG. 2.14. Relative Weight Loss of Orthorhombic Ammonium Perchlorate Single Crystals as a Function of Time.

Comparison of observed weight losses with loss based on the above equation and observed thickness of the partially decomposed layer showed excellent agreement, indicating that the decomposed layer reaches its equilibrium density close behind the decomposition front. This result also highlights the importance of knowing how crystals decompose if one wishes to understand bulk decomposition measurements on granular material.

The measured and calculated weight loss curves shown here represent only the deceleratory part of the decomposition. It was not possible to evaluate the acceleratory period because the weight loss during this period was too small to be reliably measured as a function of time. The work described covers the low temperature decomposition of doped and undoped AP single crystals. Proceeding to higher temperatures not only involves a phase transition of AP from orthorhombic to cubic but makes it considerably more difficult to make an experimental investigation of the AP decomposition. An initial effort was made to use Differential Thermal Analysis in order to study the high temperature (T > 240°C) decomposition of AP. This will be described in the following section.

2.3.2. Decomposition of AP at Higher Temperatures[5]

Studies of AP decomposition can be pursued in detail over a range of temperatures up to 240°C because the sample decomposes slowly enough to permit effectively constant-temperature conditions, relatively easy observation of the progress of decomposition, and freedom from changes produced by the solid crystal phase transition. On the other hand, the conditions in the deflagration wave are very different. An element of AP passes through the wave and is completely consumed in one or two hundredths of a second, with most of the decomposition occurring in time intervals of about one millisecond, at temperatures in the range of 500-600°C. There is no way of knowing in advance whether the controlling decomposition reaction is the same over such a wide temperature range. Consequently, experimental studies at intermediate temperatures, even if they are less precise and definitive than at low temperature, are important for appropriate application of results of low temperature experiments.

A number of studies have been made of AP decomposition at temperatures above the phase transition temperature. Various methods of study have been employed, including isothermal decomposition (see for example Ref. 22, 23, 27, 33 and 34), differential thermal analysis (DTA) (Reference 35) and differential scanning calorimeter (DSC) (Ref. 29 and 36). The results of these studies have received a variety of interpretations based on a number of methods (see for example Ref. 37-42) for obtaining kinetic parameters. As a consequence of this diversity, the results are indecisive. In the present section most of the work reported was conducted with the differential thermal analysis (DTA)

[5]This research is supported by Naval Ordnance Systems Command ORD-33 129/200 1/R001-06-01, Problem #5.

method. However, some less refined experiments were also conducted which allowed visual observation of the AP decomposition and decomposition product reaction. These observations undoubtedly are important in interpreting DTA and related experiments and will be described first.

Loose granular AP was heated in an open test tube with a Bunsen flame. The first visible effect was the accumulation of water at the open (cool) end of the tube. As the temperature was raised, the water disappeared. The gaseous products from the tube were collected in an inverted beaker and were observed to explode when exposed to the burner flame. As the temperature was increased further, the AP turned chalky, and eventually an orange flame was observed to form above the AP in the tube. The flame disappeared when the burner was removed. Under conditions leading to the flame, the volume of AP was observed to decrease rapidly to final consumption, the rate being dependent on the degree of heating from the outside. From these observations it is clear that any proposed mechanism for AP decomposition should explain the presence of products from the surface of the solid that survive at low temperature to be collected, and support a deflagration[6] flame. One plausible mechanism would be dissociative sublimation of AP to give gaseous NH_3 and $HClO_4$, with decomposition of $HClO_4$ and oxidation of NH_3 providing the exothermic "flame" reactions. Whatever the sequence, it must be anticipated that the aspects of behavior described above may be important also in other decomposition experiments such as DTA and DSC.

In the present investigation two different DTA cells were used. One was a conventional type cell containing two wells for the sample and reference tubes and a third well close to the heater element for the heater feedback control thermocouple. The other cell was made of Inconel steel and provided with two slits which allowed visible observation of the reaction occurring in the sample tube. Heating rates were preprogrammed on a Research Incorporated Thermac Controller. Each of the DTA experiments was started at room temperature (approximately 25°C) and carried out with a constant heating rate (between 6 and 60°C/min.) to a temperature above the temperature of the last DTA peak. The sample temperature was recorded as a function of time on one channel of a two-pen recorder. The other channel was used to register the differential temperature between sample cell and reference cell. The differential temperature is an indication of an endo- or exothermic reaction in the sample. Heating rates as well as peak temperatures were evaluated from the DTA thermograms.

The samples were prepared by mixing 15 mg of AP material with 35 mg of 0.1 mm diameter glass beads which served as an inert component. The mixture was placed in the sample tube with the thermocouple inserted about 5 mm deep. The remaining space of the sample tube was filled with glass beads. The reference tube contained only the thermocouple completely embedded in glass beads.

[6]"Deflagration" meaning a flame without interdiffusion of oxidizer and fuel.

The majority of the granular AP used was obtained from the American Chemical and Potash Company. The as received material was sieved into three size fractions with particle diameters 75μ ≤ dia ≤ 105μ, 150μ ≤ dia ≤ 250μ, and 495μ ≤ dia ≤ 700μ. Other sample material was obtained in ungraded particle size by crushing large AP crystals, including high purity AP, and large AP crystals doped with MnO_4 (approximately 0.04 weight percent). Runs were also made with recrystallized AP doped with $KMnO_4$ (approximately 0.05 weight percent).

Figure 2.15 shows a typical DTA record for AP. The first peak or endotherm typically appears at 238°C-241°C with either doped or pure material and is independent of particle size or heating rate. This endotherm is identified as the solid phase transition from orthorhombic to cubic crystal phase. When observed with the slit cell, the sample is seen to remain translucent (unchanged in optical appearance) while undergoing this transition. The second peak, which is the first exotherm, normally occurs between 300°C and 400°C. The third peak, or second exotherm, occurs between 450°C and 550°C. Both exotherm peaks are dependent on particle size and heating rate as shown in Table 2.3.

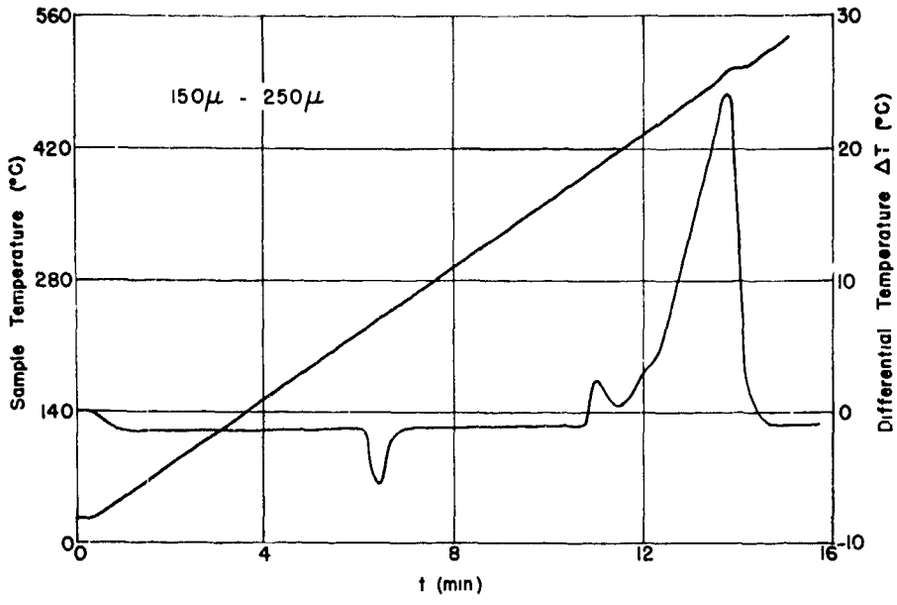

FIG. 2.15. Thermogram of Pure AP. Heating Rate 35°C/min.

The area under the thermogram curve representing the first exotherm is much smaller than the corresponding area for the second or higher temperature exotherm. In a typical case (see Fig. 2.15, for example) the area ratio is on the order of 20 to 1. We have observed, however, that if the heating is interrupted after passing the first exotherm the

TABLE 2.3. Peak Temperatures of DTA Exotherms as a Function of AP Particle Size and Heating Rate

Sample	Heating rate ϕ °C/minute	Peak temperature of first exotherm °C	Peak temperature of second exotherm °C
75μ-105μ pure AP	6.25	351	452
	15.75	381	485
	20.00	380	592
	30.50	386	508
	43.50	398	529
	61.40	398	555
150μ-250μ pure AP	16.35	381	481
	21.25	390	488
	33.00	399	506
	42.00	404	515
	63.25	413	533
495μ-700μ pure AP	10.90	310	449
	16.45	314	464
	22.00	325	479
	32.90	333	487
	44.00	341	506
	66.20	351	510
NH_4MnO_4-doped AP (0.04 by weight)	16.40	285	360
	21.80	293	369
	32.20	305	381
	43.00	312	395
	64.60	320	408
$KMnO_4$ - doped AP (≈ 0.05% by weight)	16.20	283	352
	22.50	291	360
	32.20	298	371
	42.40	309	382
	64.80	317	396

sample has suffered a weight loss of 30 to 35%. Utilizing the slit cell the sample is observed to become chalky white during this first exotherm. Further, a sample which was heated past the first exotherm, cooled and heated again, did not exhibit this first exotherm. Although the repeated sample did not exhibit the first exotherm, some additional weight loss occurred (approximately 10% based on the original sample weight).

When heating is continued to higher temperatures, the second and larger exotherm occurs. The thermogram curve for this second exotherm was usually observed to be smooth and continuous, similar to that shown in Fig. 2.15. With a higher heating rate and/or sample concentration, however, the second exotherm can be made to terminate with a violent reaction of the sample which may be accompanied by spontaneous expulsion of the sample tube contents. When the violent reaction occurs, an orange flame is visible above the sample in the slit cell (provided the sample tube contents are not expelled). Figure 2.16 shows a thermogram typical of a run displaying this rather abrubt deflagration reaction. Notice that the sample temperature trace begins to deviate from the programmed heating rate at about 450°C. At about 570°C, a sharp spike appears on the sample temperature trace coincident with the appearance of the orange flame above the sample.

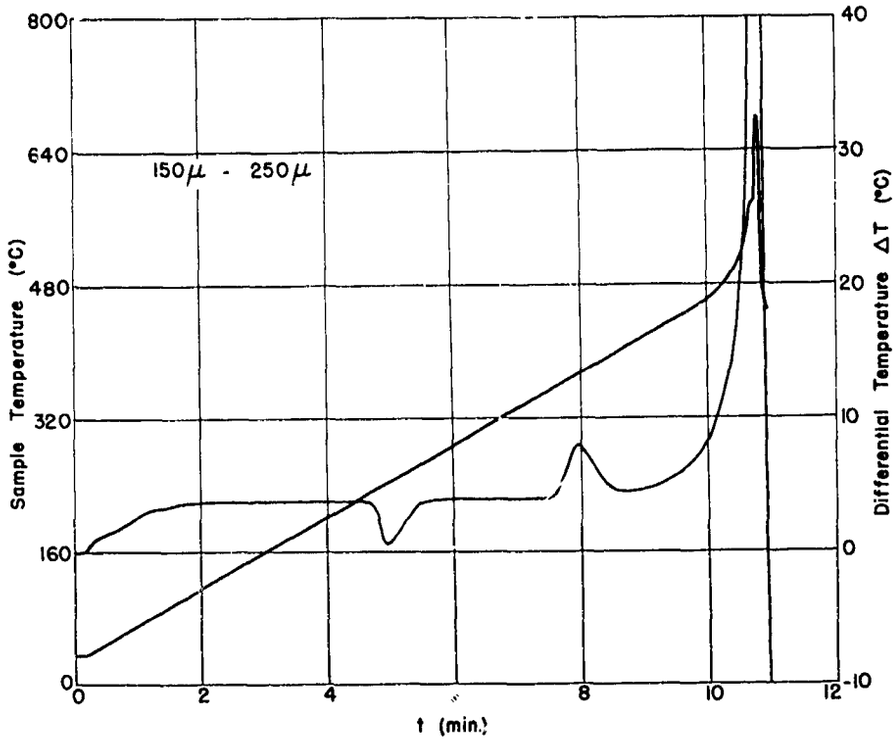

FIG. 2.16. Thermogram of Pure Ammonium Perchlorate. Heating rate 43°C/min. AP concentrated at bottom of sample tube.

From the results of the open test tube experiments, it seems probable that reactive gas species are evolved during a major portion of the DTA heating period. At lower temperature or heating rate these gases can diffuse away from the sample volume (at least away from the

temperature sensing element) with only a very limited amount of further reaction. Under sufficient conditions of high heating rate, high temperature and high reactive species concentration, ignition can occur and produce the observed sample temperature "spike". With this line of reasoning, it is significant that the second exotherm is typically ten or more times as large in area as the first exotherm, even though the weight loss during the second exotherm is only about twice the weight loss in the first exotherm. This indicates a higher degree of confinement of the gas phase exothermic reaction to the sample volume at high temperature, culminating ultimately in ignition when test conditions provide for sufficient residual AP at high temperature. In this context, it is appropriate to note that other investigators (Ref. 29) find that the second exotherm becomes an endotherm when the pressure is reduced to 250 mm Hg, further supporting the view that the initial decomposition of the AP is endothermic and the exothermic reaction is primarily in the gas phase and remote from the sample thermocouple.

Quantitative evaluation of the DTA records was carried out by measuring the peak temperatures of the exotherms, and by determination of the apparent activation energy using Kissinger's method (Ref. 41). The peak temperatures were given in Table 2.3 with the apparent activation energies and pre-exponential factors are summarized in Tables 2.4 and 2.5 respectively. According to Kissinger's method, the activation energies may be calculated from

$$\frac{d\ (\log\ \phi/T_m^2)}{d\ (1/T)} = -\frac{E}{2.302\ R}$$

by plotting $\log\ (\phi/T_m^2)$ versus $1/T$ and evaluating E from the slope (see Fig. 2.17-2.20). In these graphs ϕ is the heating rate in °C/min, and T_m is the sample temperature at the peak of the exotherm. The apparent reaction orders were also calculated according to the Kissinger method and are shown in Table 2.6.

Examining the results in Table 2.4, it is clear that the doped AP behaves differently from the pure AP, with lower activation energies for the doped material. Interpretation of this is risky in view of the apparent involvement of gas phase reactions, but the low activation energy may reflect a greater contribution of the desorption step for doped materials. These materials were observed in isothermal decomposition work to have very high nucleation rates and might thus be relatively more desorption-limited in the DTA, with correspondingly lower activation energy. Again, this or any quantitative interpretation is highly dependent on a better knowledge or control of the experiment than is currently available. In the meantime, the qualitative observations to date are consistent with the view that the AP decomposes and gassifies endothermally, probably yielding gaseous NH_3 and $HClO_4$, which react further exothermally. This latter reaction presumably proceeds appreciably within the volume of the sample tube, but primarily external to the sample itself.

TABLE 2.4. Activation Energies of the Thermal Decomposition of AP

Sample	Activation energy K cal/mole	
	First exotherm reaction	Second exotherm reaction
75μ-105μ	33.9	28.9
150μ-250μ.	36.6	28.1
495μ-700μ.	27.7	26.7
$NH_4MnO_4^-$-doped AP (0.04 weight %). . .	23.9	21.8
$KMnO_4$-doped AP (0.05 weight %). . .	24.3	22.9

TABLE 2.5. Pre-Exponential Factors for the Thermal Decomposition of AP

Sample	Pre-exponential factor (sec^{-1})	
	First exotherm reaction	Second exotherm reaction
75μ-105μ	1.7×10^{11}	9.2×10^{7}
150μ-250μ	1.0×10^{12}	6.0×10^{7}
495μ-700μ	1.1×10^{10}	3.5×10^{7}
NH_4MnO_4-doped AP (0.04 weight %). . .	1.2×10^{9}	1.5×10^{7}
$KMnO_4$-doped AP (≃ 0.05 weight %). .	2.1×10^{9}	5.3×10^{7}

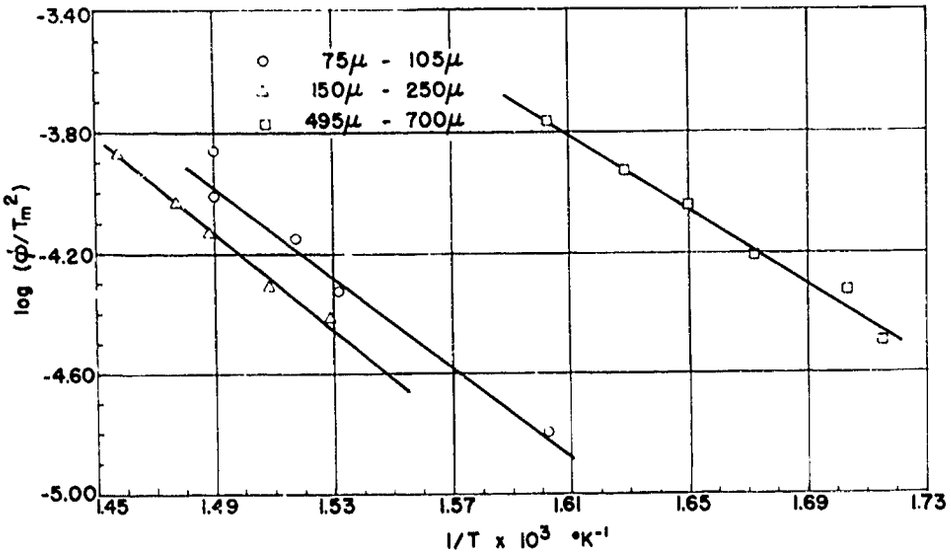

FIG. 2.17. Plot of Log (ϕ/T_m^2) Versus 1/T for the Decomposition of Pure AP: Reaction of the first DTA exotherm. Particle sizes 75 μ - 105 μ, 150 μ - 250 μ, and 495 μ - 700 μ.

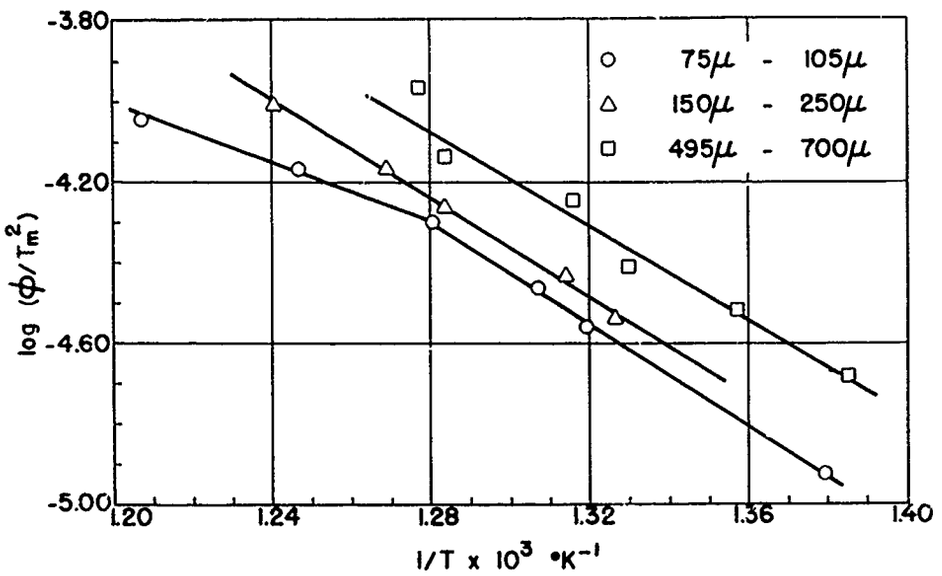

FIG. 2.18. Plot of Log (ϕ/T_m^2) Versus 1/T for the Decomposition of Pure AP: Reaction of the second DTA exotherm. Particle sizes 75 μ - 105 μ, 150 μ - 250 μ, and 495 μ - 700μ.

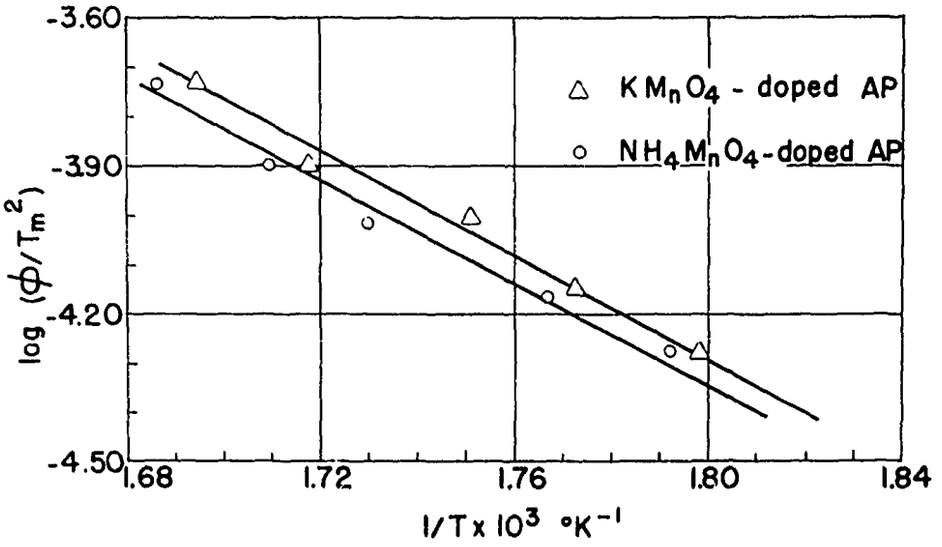

FIG. 2.19. Plot of Log (ϕ/T^2) Versus 1/T for the Decomposition of $KMnO_4$-Doped AP and NH_4MnO_4-Doped AP: Reaction of the first DTA exotherm.

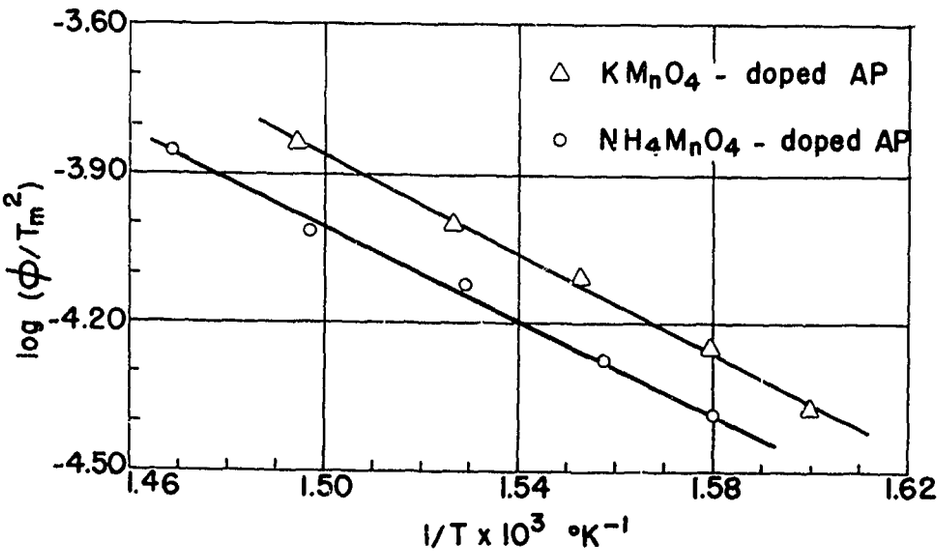

FIG. 2.20. Plot of Log (ϕ/T_m^2) Versus 1/T for the Decomposition of $KMnO_4$-Doped AP and NH_4MnO_4-Doped AP: Reaction of the second DTA exotherm.

TABLE 2.6. Reaction Orders for the Thermal Decomposition of AP

Sample	Heating rate ϕ °C/minute	Reaction Order	
		First exotherm reaction	Second exotherm reaction
75μ - 105μ	15.7	2.46	0.69
	20.0	2.75	0.67
	30.5	2.90	0.55
	43.5	2.30	0.70
150μ - 250μ	7.3	1.83	0.60
	9.4	2.20	0.80
	16.4	1.90	0.59
	21.3	2.35	0.86
	33.0	2.52	1.00
	42.0	2.18	0.73
	43.0	2.14	0.78
	63.2	2.70	0.94
	65.6	2.50	1.12
	65.0	2.80	0.82
495μ - 700μ	10.9	1.81	0.73
	22.0	1.75	0.74
	32.9	1.51	0.63
	44.2	1.81	0.80
	66.0	1.77	0.81
NH_4MnO_4-doped AP (1.2 weight %)	21.8	2.04	0.87
	32.2	2.04	0.98
	43.0	1.67	0.93
	64.6	1.94	0.99
$KMnO_4$-doped AP (≈ 1 weight %)	22.5	1.70	1.00
	32.2	1.60	1.13
	42.4	1.80	1.08
	64.8	1.70	1.21

2.4. SINGLE CRYSTAL DEFLAGRATION STUDIES[7]

2.4.1. Experimental Description

Combustion experiments with both pure and doped AP single crystals were carried out in a small combustion bomb equipped with windows and an automatic pressure release vent for extinguishment of burning samples.

[7] A major portion of this section was presented at the 11th Symposium (International) on Combustion, Berkeley, Calif., 1966, in a paper entitled "Combustion of Ammonium Perchlorate," by J. D. Hightower and E. W. Price.

The bomb was pressurized with dry nitrogen and ignition of the crystals along the top edge was accomplished with an electrically heated 10 mil nichrome wire (or wires). A small quantity of an energetic igniter paste or a small droplet of MAPO[8] applied to the top edge of the crystal proved to be effective in producing a more uniform ignition along the entire top edge of the crystal, especially at pressures below 500 psia. A surge tank connected to the combustion bomb served to limit the pressure increase during burning to the range of 4 to 8 psi. Combustion pressure was monitored visually on a 0 to 2500 psi Heise gauge. For purposes of high speed motion picture photography, a 2500 watt xenon lamp was used for illumination. A heat absorbing filter was used to remove that portion of the xenon beam spectrum that was not useful for photography. A slow nitrogen flush past the sample was used to remove the products of combustion from the field of view. An overall view of the experimental apparatus is shown in Fig. 3.3.

Burning rates were determined from motion picture photography taken at 400 frames per second and a magnification of 0.5 to 1 with a Milliken camera. A small scale placed directly behind and approximately 1 mm away from the crystal (Fig. 2.21) was used in conjunction with a Vangard motion analyzer to measure the regression distance. Time base measurements were made using an Adtrol Electronics timing light generator at 100 cps. For more detailed observation of the burning surface motion pictures were also taken on color film at a magnification of 2 to 1 and a framing rate of approximately 3000 frames per second. Following a short ignition transient the pure AP crystals usually burned smoothly, although some crystals tended to burn with a slightly tilted surface and occasional fracturing was noted. The condensible products of combustion were observed to form a dense fog as they mixed with the cool nitrogen flow. There was no observed tendency for the development of a conical burning surface and no inhibitor on the crystal edges was used. When observed in a darkened room, a pink-orange visible reaction was seen at or near the regressing surface.

Attempts to burn the MnO_4-doped AP were made over a wide pressure range; 200 to 1500 psia. These crystals would not sustain self-deflagration in nitrogen. A few tests were made to photograph the ignition attempts with motion pictures. In these tests the external xenon illumination was employed and some of the crystals were observed to ignite and burn in a very irregular manner. The burning in these cases was so irregular that rate measurements could not be made. It is tentatively concluded that the darker color (purple) of the doped crystals allowed absorption of sufficient external radiant energy to allow marginal combustion to occur. A small quantity of the doped AP was ground and mixed with a PBAA binder. This uncured propellant was observed to burn smoothly at atmospheric pressure in air. Two of the doped crystals were observed to burn at 2500 psia in air without the xenon. Work is being continued at these higher pressures to establish the deflagration rate and low pressure deflagration limit.

[8] Tris (2-methyl - 1-aziridinyl) phosphine oxide.

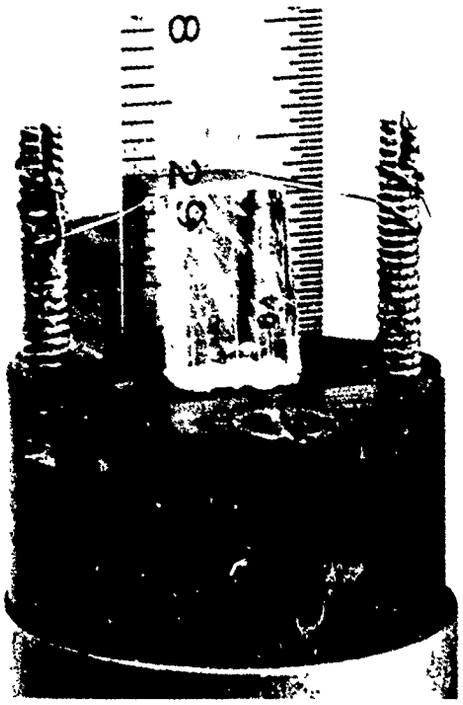

FIG. 2.21. Ammonium Perchlorate Single Crystal Mounted on the Sample Holder Showing the Ignition Wire and Machinist Scale Used to Measure Regression Distances. Note the nitrogen flushing slits located immediately in front of and behind the sample.

Partially burned samples of the pure AP crystals suitable for microscopic examination were obtained by a rapid depressurization of the combustion bomb during burning. Depressurization was accomplished with the pressure release vent which was automatically coordinated with ignition of the samples through a multi-channel, electro-mechanical timer. Depressurization rates have been measured (Ref. 43) and are of the order of 10^{-4} to 10^{-6} psi/sec for the range of pressures investigated. High speed motion pictures of the quenching event, taken with a Fastax camera at 3000 frames per second, indicated that the quench was complete in less than 10^{-3} sec. Microscopic examination and photomicrographs of the surface and subsurface details of the quenched samples were made using a Zeiss Photomicroscope. Various types of illumination were employed to reveal the details of the surface and subsurface regions of the samples. Microscopic measurements of characteristic details were made with a K8X, Zeiss eyepiece screw-micrometer with a resolution of 0.25 microns at a total magnification of 512X. Tests were run over a pressure range of 275 to 2050 psia.

2.4.2. Results of Single Crystal Deflagration

Observation of the surface of the crystal by high speed motion pictures during burning revealed a very intricate, pressure dependent structure of ridges, troughs and depressions. The pattern on any one sample remained substantially unchanged as the surface receded, indicating that a stable three-dimensional combustion zone structure prevailed. The character of this pattern was revealed in greater detail by microscopic examination of quenched specimens. Figure 2.22 shows photomicrographs of quenched samples which were burned at different pressures. Numerous samples of this type, burned and quenched over a wide pressure range, were subjected to careful microscopic examination using different types of illumination at various angles to reveal the surface details. The photomicrographs serve as an excellent aid in helping the reader visualize the general surface features. The description of observations, however, is made on the basis of much more revealing and detailed microscopic examination of large numbers of samples. From samples burned at 275 to 600 psia it was observed that the quenched surface consisted of an array of craters roughly 150 microns in diameter ringed with translucent protrusions which proved to be hollow bubbles approximately 70 microns in diameter (Fig. 2.22a). At pressures around 800 psia (Fig. 2.22b), the crystal surface was apparently flat, with the quenched samples still showing numerous bubbles somewhat smaller than those formed at lower pressure. Samples quenched from burning at higher pressure, around 1000 psia, showed a "fingerprint like" surface pattern of ridges and troughs (Fig. 2.22c) of somewhat finer spacing than the craters seen at low pressure. Bubbles were still evident, but were smaller than at lower pressure, and tended to be concentrated on the sloping sides of the ridges. The tops of the ridges at the higher pressures were glossy and smooth and when viewed with transmitted illumination appear to have undergone no visible subsurface decomposition.

The use of an electronic scanning microscope allowed a more detailed observation of the quenched sample surfaces. Figure 2.23 shows photomicrographs obtained by this method of a crystal burned and quenched at 800 psia. The surface is seen in general to consist of a frothy layer which indicates that a decomposing melt was present before quenching occurred. Figure 2.23b shows a close-up view of a bubble approximately 60 microns in diameter with a section broken out indicating its hollow nature. Around the base of the bubble in the frothy surface layer a continuous wavelet pattern can be seen indicating the mobility of the melt when the bubble formed. A more dramatic view of a bubble is shown in Fig. 2.24. This is a low-angle photomicrograph of an approximate 85 micron diameter bubble on a surface burned and quenched at 300 psia. Note the extremely frothy nature of the surface material to the right of the bubble and the jagged break in the bubble wall where the subsurface crack runs under the bubble. From other microscopic examinations of broken bubbles, the bubble wall thickness for large well developed bubbles is estimated to be on the order of 2 microns. Several crystals

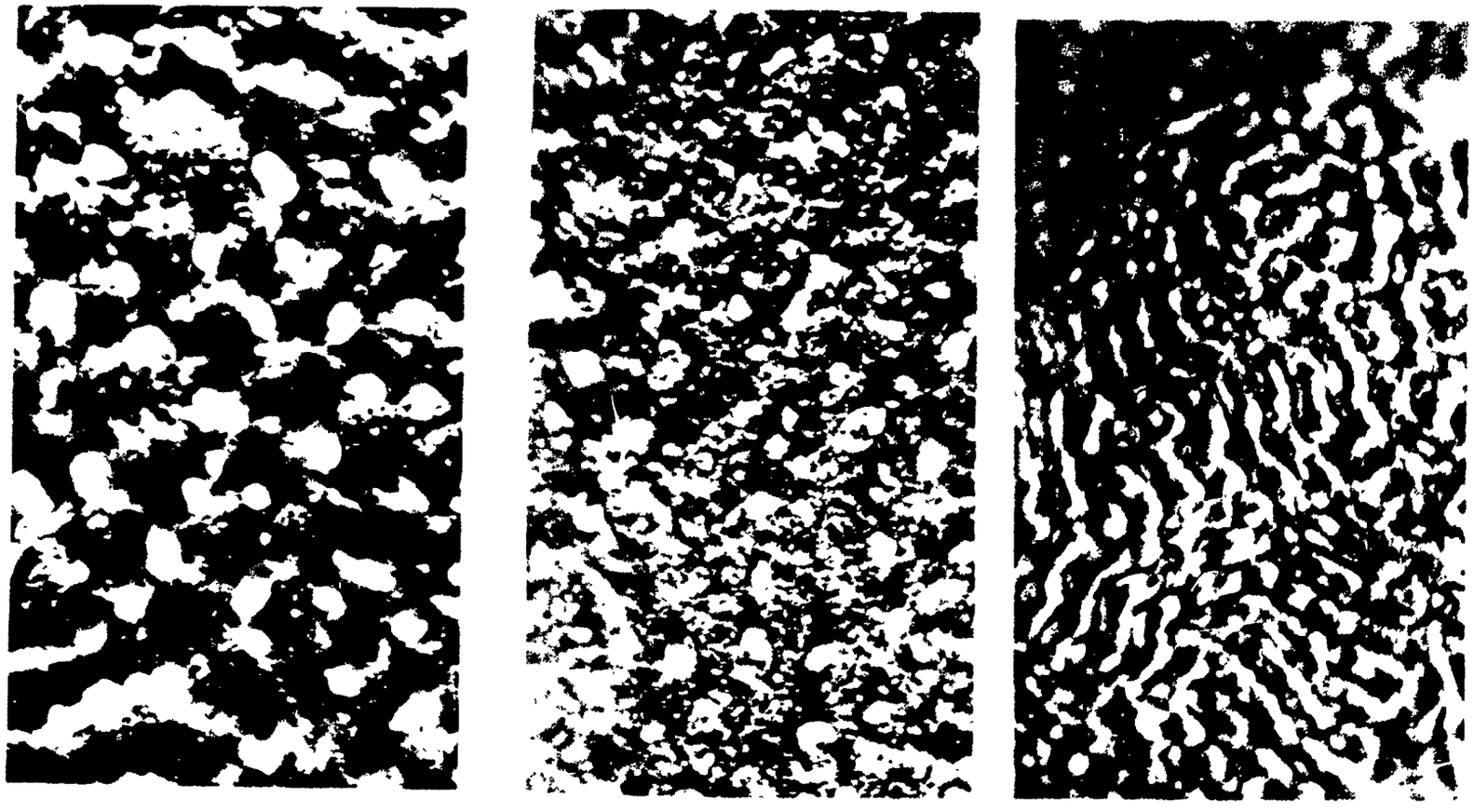

FIG. 2.22. Surface Pattern on Ammonium Perchlorate Single Crystals Burned and Quenched at Different Pressures; (a) 400 psia, (b) 800 psia and (c) 1200 psia. Illumination at a low angle from the left. Magnification is the same on all samples.

(a)

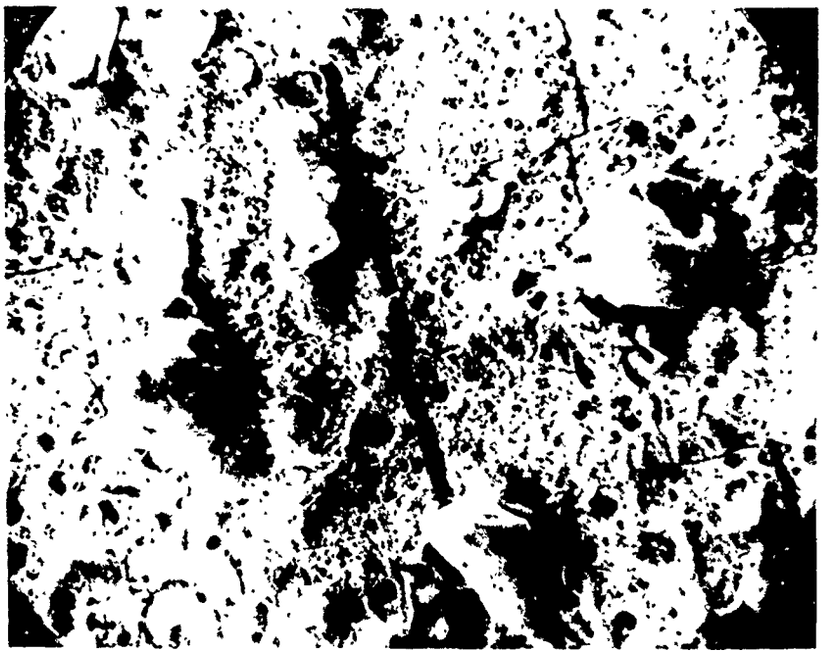

(b)

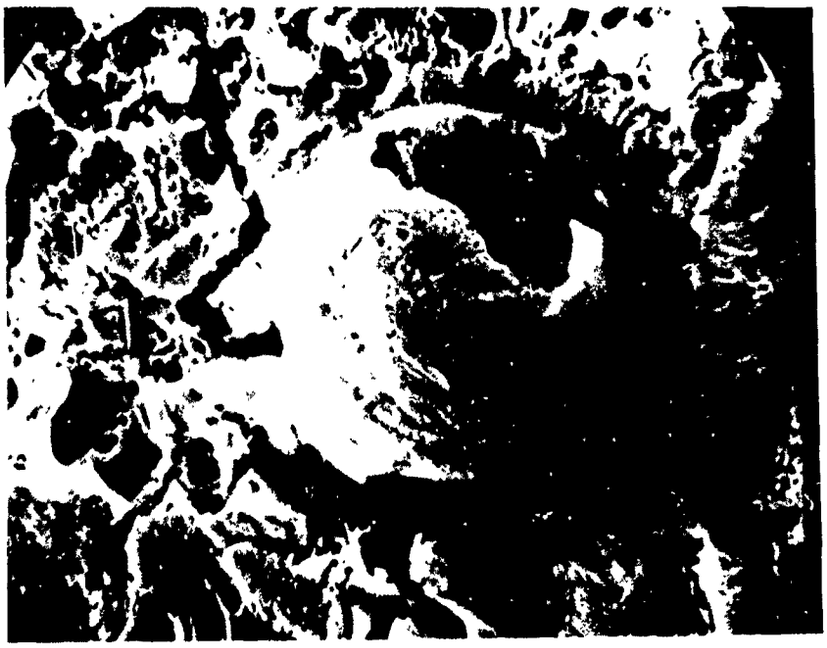

FIG. 2.23. Scanning Electron Microscope Photomicrographs of the Surface of an AP Single Crystal Burned and Quenched at 800 psia. Note the general "frothy" appearance of the surface in (a) and the rectangular-like blocks that are defined by the subsurface cracks associated with the quench transient. (b) Close-up large bubble and surface froth. Note wavelet pattern around base of bubble.

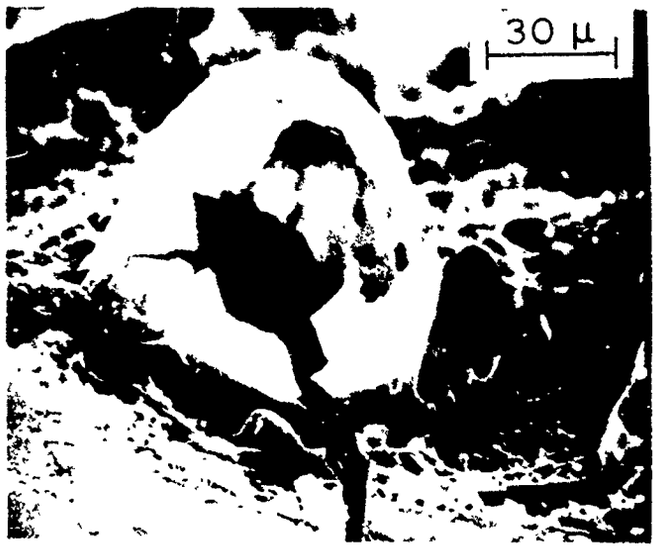

FIG. 2.24. Scanning Electron Microscope Photomicrograph of an Ammonium Perchlorate Bubble on the Surface of a Single Crystal Burned and Quenched at 300 psia. The bubble wall thickness is approximately 1 micron.

were quenched and a quantity of the bubbles were carefully removed with a small microspatula. These were crushed and X-ray powder patterns of this material indicated that it was ammonium perchlorate.

Also evident on the surface of quenched samples was a rectangular block-like pattern of cracks in the crystal. High speed motion-pictures taken during the quench showed these cracks forming during and immediately after quenching. The spacing of the cracks and their depth of propagation were pressure dependent, becoming smaller at higher pressure, but the patterns showed no simple relation to the surface pattern described above. These subsurface cracks are presumed to be a stress relieving mechanism associated with the steep temperature gradient at the surface and the volume change of the crystallographic phase change. In numerous places the frothy surface layer and bubbles were visibly "torn" where they extended over the cracks, indicating the continuous nature of the surface melt prior to quench and crack formation.

In addition to the obvious subsurface cracks formed during quenching, there is a thin layer immediately below the surface which is plainly visible under polarized illumination and apparently corresponds to the layer that has experienced the crystallographic phase transition at 240°C. Below the phase transition temperature of approximately 240°C, AP has an anisotropic orthorhombic structure with the isotropic cubic structure

occurring at higher temperature. The regressing surface of an AP crystal undergoing steady deflagration is preceded by a thermal wave that heats a thin layer of the AP to a temperature above the transition point. Following extinguishment, this thin layer inverts back to the orthorhombic phase but in so doing suffers a slight lattice disorientation with respect to the original crystal. When suitably viewed with polarized illumination this layer is easily distinguished from the undisturbed crystal as a result of a different optical extinction position. McGurk (Ref. 44) has observed this optical discontinuity in thin microtomed sections of extinguished AP propellants and interpreted it as being the 240°C isotherm corresponding to the phase transition temperature.

Typical examples of the phase transition layer of crystals burned and extinguished at different pressures are shown in Fig. 2.25a and b. It can be seen in this figure that the phase transition thickness is a function of the burning rate, being thicker at lower rates and thinner at higher rates. Measurements of the phase transition thickness as a function of pressure were made over a pressure range of 300 to 1100 psia using the apparatus described earlier. The 400 psia sample in Fig. 2.25a clearly shows the undulating nature of the surface profile; a result of the pressure dependent surface pattern discussed previously. It is also evident in this figure that the minimum phase transition thickness occurs at the bottom of the depression. The transition thickness measurements reported here were made at the minimum point. It was felt that the gentle contour at the bottom of the depression most nearly simulated a one-dimensional heating situation which allowed the data to be used with a one-dimensional mathematical heat transfer analysis to calculate surface temperatures.

The phase transition data is shown in Fig. 2.26 as a function of the burning rate. Each datum point is the average of at least 10 independent measurements made from several thin sections which were cleaved from different parts of an individually burned and quenched sample. The error bars indicate the extremes of the data scatter with better than 85% of all measurements being within $\pm$10% of the average points. These measurements did not include the thickness of the thin frothy layer on the surface but were made only of the solid phase transition layer. The optical details of the phase transition layer were observed to be fairly independent of the distance from the burned surface suggesting that very little decomposition, if any, occurred in this layer. If appreciable decomposition had occurred it seems reasonable that an optical gradient would exist corresponding to the temperature gradient through the altered layer. This layer is generally quite transparent and although it can in some cases be detected with plain transmitted illumination, it does not display an optical opacity as contrasted to those crystals that have undergone prolonged low temperature decomposition.

The burning rate measurements of pure single crystals made from approximately 275 to 2050 psia are shown in Fig. 2.27. Burning rates were determined normal to both the *m* face, (210) plane, and the c face,

(a) Combustion pressure 400 psia

(b) Combustion pressure 1000 psia

FIG. 2.25. Typical Examples of the Phase Transition Layer at the Surface of AP Crystals Burned and Quenched at Different Pressures. Photographed with crossed polars.

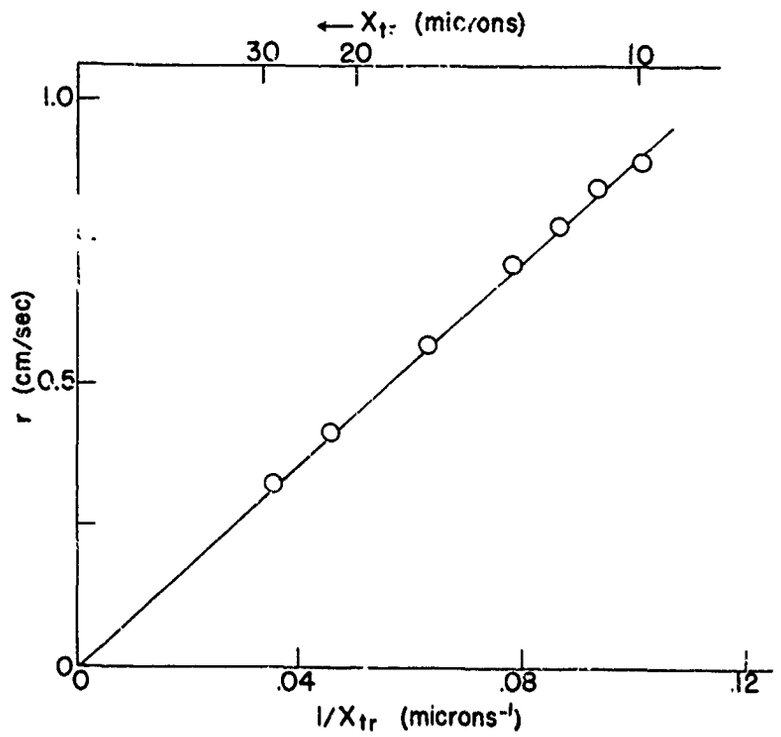

FIG. 2.26. The Phase Transition Thickness as a Function of Burning Rate. The product r x_{tr} is a constant.

(001) plane. Within the data scatter no observed difference was noted. This is essentially in keeping with similar observations of Whittaker and Barham (Ref. 45). However, the burning rates obtained in the present work are appreciably higher than the limited data of Whittaker and Barham, possibly because they modified the crystal habit with the addition of a small amount of polygalacturonic acid and inhibited the edges with Lucite. The pressed pellet burning rate data of Levy and Friedman (Ref. 18) and Adams, Newman and Robins (Ref. 46) are shown for comparison in Fig. 2.27. The data of Levy and Friedman are seen to be slightly lower but in close agreement from 750 to 1400 psia. Levy and Friedman reported a low pressure deflagration limit of approximately 325 psia for the pressed material. In the present investigation the single crystal limit was found to be in close agreement at approximately 275 psia. The burning rates in the present work are appreciably higher than the results of Adams, Newman and Robins but are in reasonable agreement considering the particle size effect if the single crystal is presumed to be comparable to a "zero particle size" material. Shannon and Petersen (Ref.19) reported a systematic study of the particle size effect on burning rate and extrapolation of average values of their data to zero particle size are shown in Fig. 2.28 to be in close agreement with the single crystal

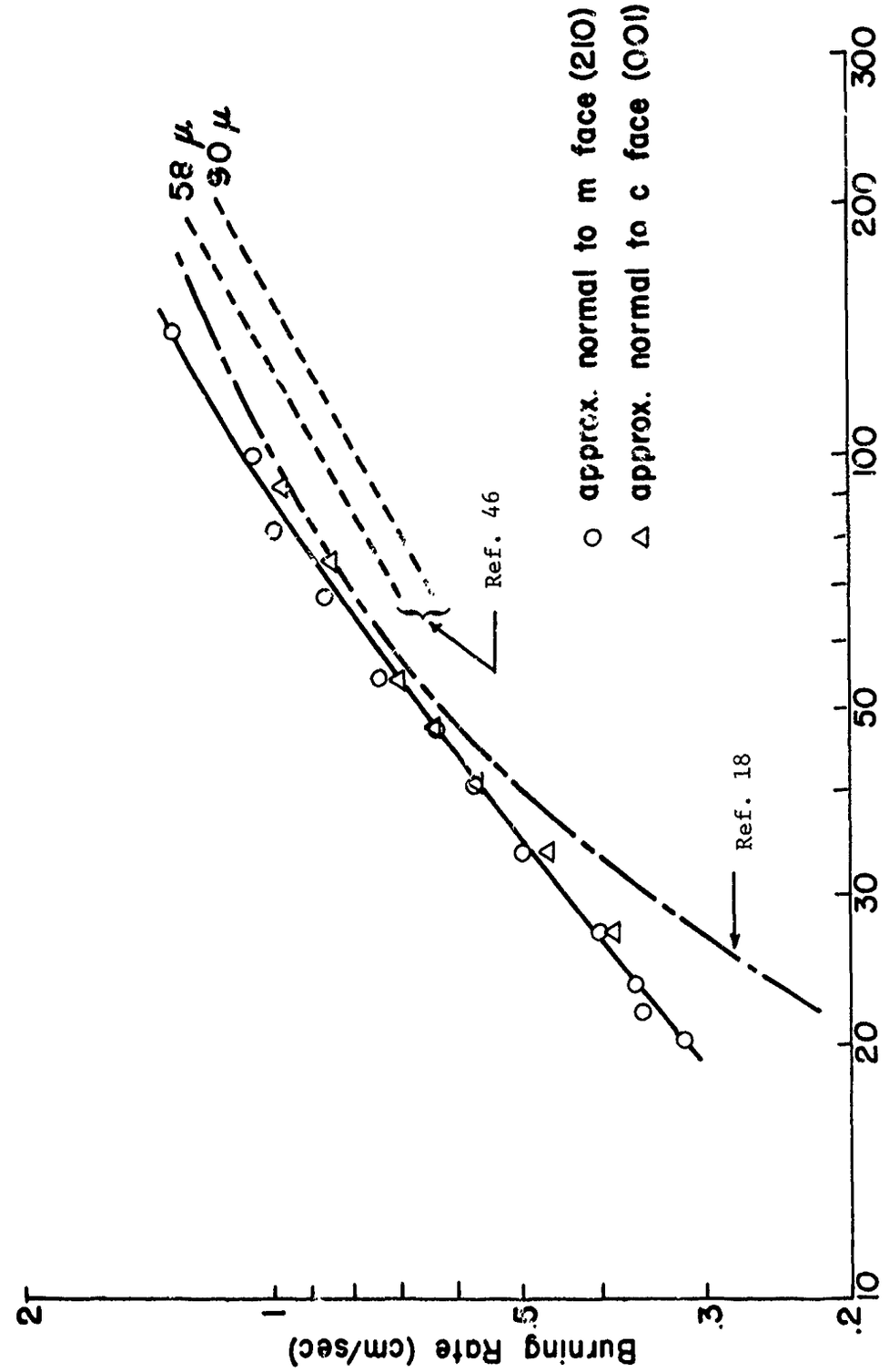

FIG. 2.27. Rate of Deflagration of Ammonium Perchlorate Single Crystals With Comparative Data on Pressed Pellets. Data points refer to single crystals.

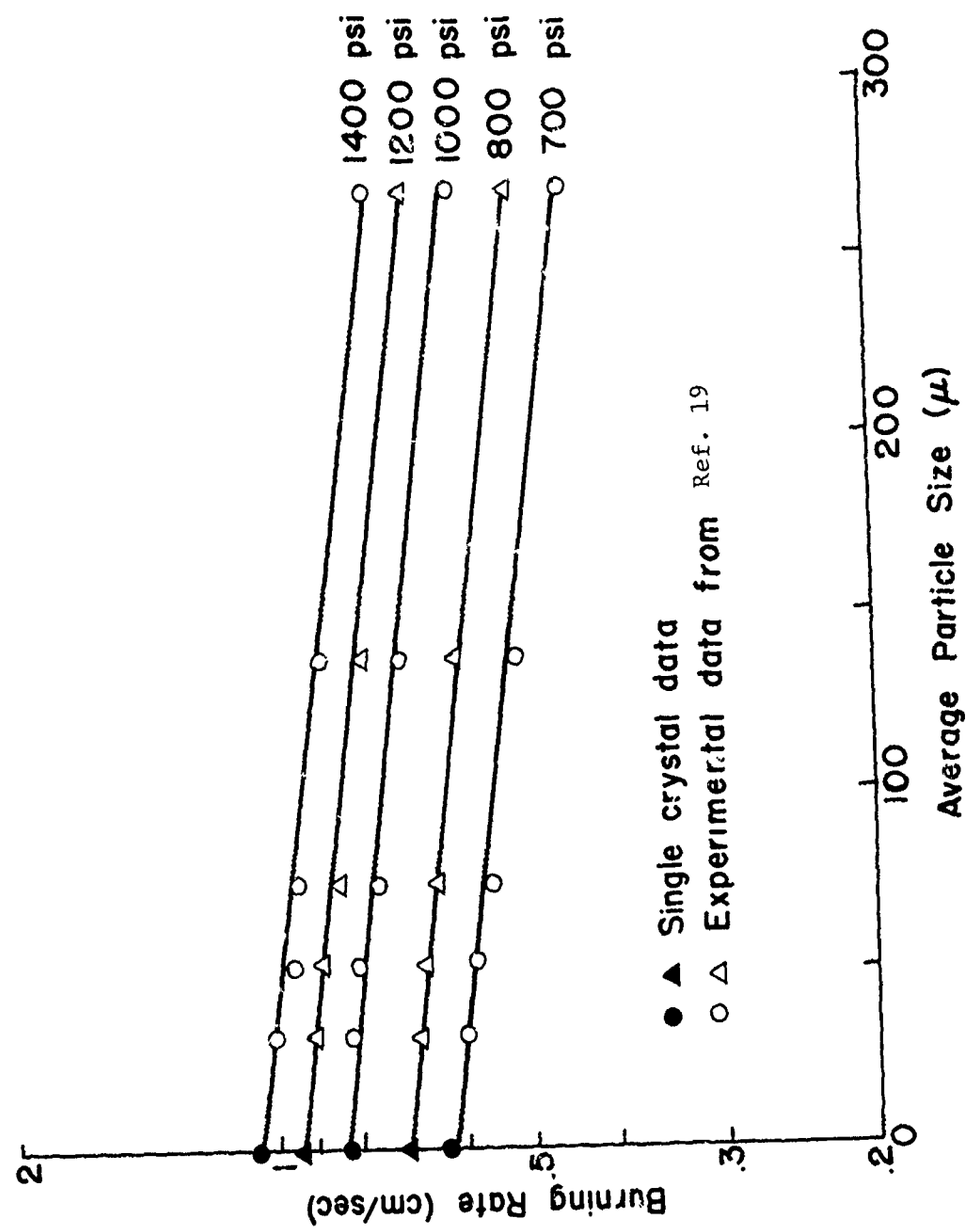

FIG. 2.28. Comparison of Single Crystal Deflagration Rate With Deflagration Rate of Pressed Pellets as a Function of Particle Size. Data points shown for pressed pellets are average values from the data of Ref. 19.

data. This data suggests that very fine particle pressed material should exhibit burning rate characteristics that would be approximately the same as single crystals.

The well defined phase transition isotherm and the regression rate as a function of pressure allows a surface temperature calculation to be made that affords some insight regarding the magnitude of the burning surface temperature as well as the physicochemical processes occurring on the surface.[9] The idealized temperature profile in a burning solid propellant is usually considered as being continuous. However, in the case of AP, there is a discontinuity in the profile at the phase transition temperature similar to that indicated in Fig. 2.29. In this figure, the temperature has been taken as the ordinate; the distance into the burning crystal is the abscissa; and the origin is taken at the surface of the burning AP with the crystal traveling into the coordinate system at a velocity equal to the linear burning rate. Assuming that one-dimensional, steady-state conditions exist, the conservation of energy at the point of the phase transition can be written as

Energy Input		Energy Output		Energy Absorbed	
$-k_1 H_1 + r \rho_2 c_2 T_{tr}$	$-$	$[-k_2 H_2 + r \rho_1 c_1 T_{tr}]$	$=$	$\rho_2 r \lambda$	(2.1)

where H is the temperature gradient at the phase transition point and other symbols are defined in the nomenclature. Assuming constant coefficients, the temperature gradient terms can be evaluated by solving the steady-state heat conduction equation with the appropriate boundary conditions. This equation is

$$\frac{\alpha}{} \frac{d^2T}{dx^2} + r \frac{dT}{dx} = 0 \qquad (2.2)$$

The general solution to this equation is

$$T = A + Be^{-\frac{r}{\alpha} x} \qquad (2.3)$$

[9] The surface temperature calculation technique has also been reported separately by Beckstead and Hightower in a paper entitled "On the Surface Temperature of Deflagrating Ammonium Perchlorate Crystals". This paper has been presented at the 3rd ICRPG Combustion Conference, Cape Kennedy, Fla. and the 5th AIAA Aerospace Science Meeting (AIAA Preprint #67-68), New York, and has been accepted for publication in the AIAA Journal.

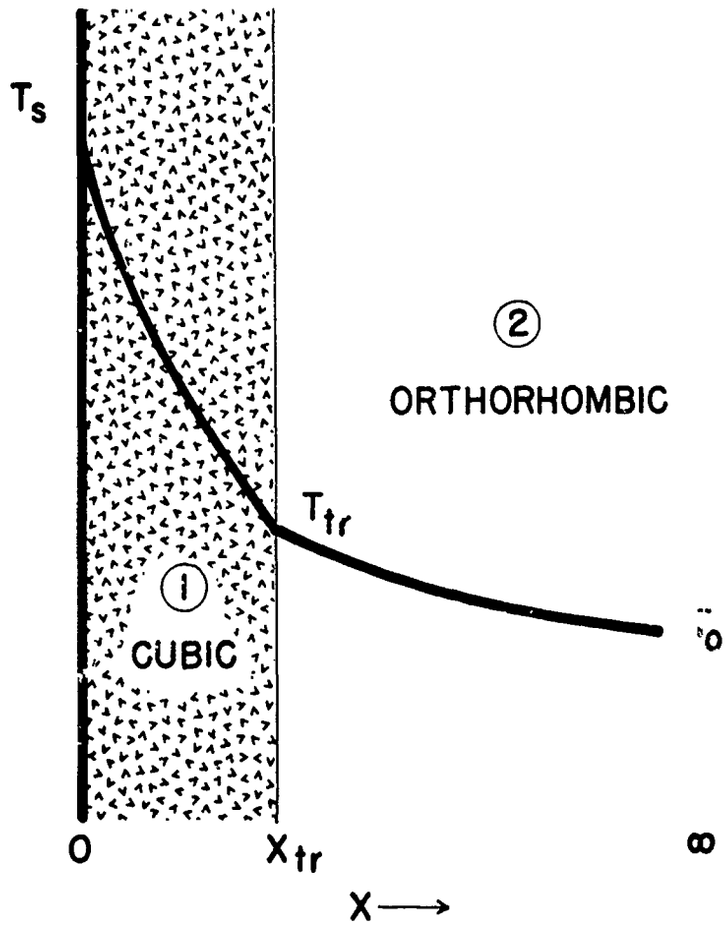

FIG. 2.29. Idealized Temperature Profile for Burning Ammonium Perchlorate.

The boundary conditions that apply in the orthorhombic phase are

$$\text{at } x = \infty,\ T = T_o$$
$$\text{and at } x = x_{tr},\ T = T_{tr} \tag{2.4}$$

Applying the boundary conditions and differentiating the solution, the temperature gradient on the orthorhombic side of the phase transition point can be written

$$H_2 = -\frac{r}{\alpha_2}(T_{tr} - T_o) \tag{2.5}$$

The boundary conditions in the cubic part of the crystal are

$$\begin{aligned} &\text{at } x = 0, && T = T_s \\ &\text{and at } x = x_{tr}, && T = T_{tr} \end{aligned} \tag{2.6}$$

Applying these boundary conditions, the temperature gradient on the cubic side of the phase transition point is

$$H_1 = -\frac{r}{\alpha_1}\left[\frac{T_s - T_{tr}}{e^{\frac{r}{\alpha_1}x_{tr}} - 1}\right] \tag{2.7}$$

Substituting Eq. 2.5 and 2.7 into Eq. 2.1 and solving for the temperature at the solid surface yields

$$T_s = T_{tr} + \left(e^{\frac{r}{\alpha_1}x_{tr}} - 1\right)\left[T_{tr} - \frac{\rho_2 c_2}{\rho_1 c_1}T_o + \frac{\rho_2 \lambda}{\rho_1 c_1}\right] \tag{2.8}$$

The transition temperature, the latent heat of phase transition, and values of the specific heat for both phases (averaged with temperature) may be obtained from the JANAF Tables (Ref. 47). The initial temperature and the density of the orthorhombic phase (Ref. 48) are known. The density of the cubic phase has been calculated by Markowitz (Ref. 49) using data published on the structural parameters for the two different forms of the crystal. In order to evaluate the temperature by using Eq. 2.8, the thermal conductivity of the cubic phase must also be determined or approximated. It has been noted (Ref. 50) that the thermal conductivity of crystalline solids is inversely proportional to the temperature at high temperatures. Therefore, it should be possible to approximate the high temperature cubic phase thermal conductivity by extrapolating from low temperature data. Figure 2.30 shows the data of Rosser, Inami, and

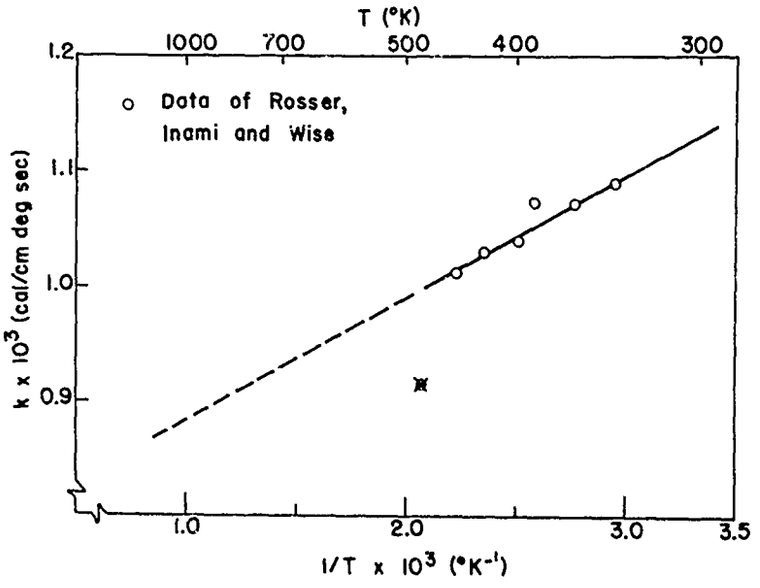

FIG. 2.30. The Relationship Between Thermal Conductivity and Temperature Determined by Extrapolating the Data of Rosser, Inami and Wise (Ref. 51).

Wise (Ref. 51) for the thermal conductivity of pressed AP pellets plotted versus the reciprocal of the absolute temperature. With the exception of the datum point at the highest temperature, the data do indeed exhibit an inverse proportionality with temperature. A least squares fit of the data, excluding the one datum point, was thus extrapolated to the higher temperatures of interest. Although there is probably a discontinuity in the thermal conductivity at the transition point, present knowledge does not warrant including this in the extrapolation.

Rosser, Inami and Wise also studied the effect of the porosity of the pressed AP on the thermal conductivity. Their data indicate that for AP with zero porosity (which would correspond to single crystals such as those used in the present study) the value of the conductivity would be approximately 4% greater than the values reported in Fig. 2.30. Taking this into account, and averaging the values of the resultant thermal diffusivity for the temperatures at the transition point and the surface, yields an average value of 1.27×10^{-3} cm^2/sec. Combining this with the results of Fig. 2.26, Eq. 2.8 can be employed to estimate the value of the surface temperature as a function of the burning rate or pressure. The data from Fig. 2.26 have been used in these calculations and the results are presented in Fig. 2.31 plotted against the pressure as well as the mass burning rate (in order to compare with the data of Powling (Ref. 52)). It is observed that the temperature is a constant with a value of approximately 560°C.

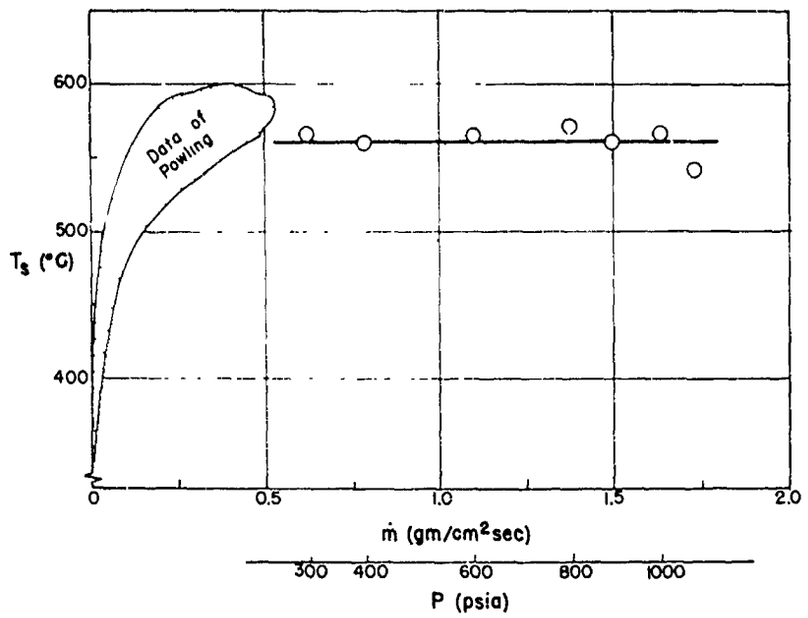

FIG. 2.31. Calculated Temperature of the Solid Surface as a Function of Pressure and Mass Burning Rate (Compared with the Data of Powling (Ref. 52).

It should be kept in mind that both the specific heat and the thermal conductivity for the cubic phase were determined by extrapolating from values determined for the orthorhombic phase at low temperatures. Also, in solving the heat conduction equation, it was assumed that the thermal diffusivity is a constant which, of course, it is not. However, present knowledge of the temperature dependence of the diffusivity does not warrant an analytical solution to the nonlinear equation that would result from including this dependence. The uncertainties in the extrapolations and averages of the thermal properties only affect the magnitude of the calculated temperature so that different techniques in determining these properties could cause either positive or negative fluctuations in the calculated value of the temperature, but would have no affect on the pressure dependence. For example, a 10% change in the value of the thermal diffusivity would cause a 6-7% change in the calculated magnitude of the surface temperature, but this value would be constant over the pressure range. Considering this and the scatter of the data in Fig. 2.26, it appears reasonable to conclude that the temperature of the solid surface is between 525 and 600°C, which is in good agreement with the work of previous investigators.

2.5. PROPELLANT SANDWICH DEFLAGRATION

2.5.1. Experimental Procedure

Propellant sandwiches were prepared from matched crystal pairs by laminating the crystals together with a thin layer of typical non-explosive propellant binder containing various ballistic modifiers. The crystals were laminated together by placing a drop of binder between the crystals and applying a gentle pressure to spread the binder uniformly over the crystal faces. The thickness of the binder was varied over the range of approximately 30 to 200 microns and was controlled by visual observation with a stereo-microscope during the laminating procedure. The sandwiches were placed on a glass slide and cured in a small oven. Special care was exercised to keep the crystal faces clean to promote the wetting action of the binder and, hence, the bonding between binder and AP. Peel tests made on several of the cured samples indicated that good bonding had occurred. Polybutadiene acrylic acid acrylonitryle (PBAN) has been the principle binder used to date with a limited number of tests run with carboxy terminated polybutadiene (CTPB) and polyurethane. Ballistic modifiers that have been used include copper chromite (Harshaw Chemical Cu0202), lithium fluoride (LiF), and carbon (C). A typical sandwich mounted on the sample holder is shown in Fig. 2.32.

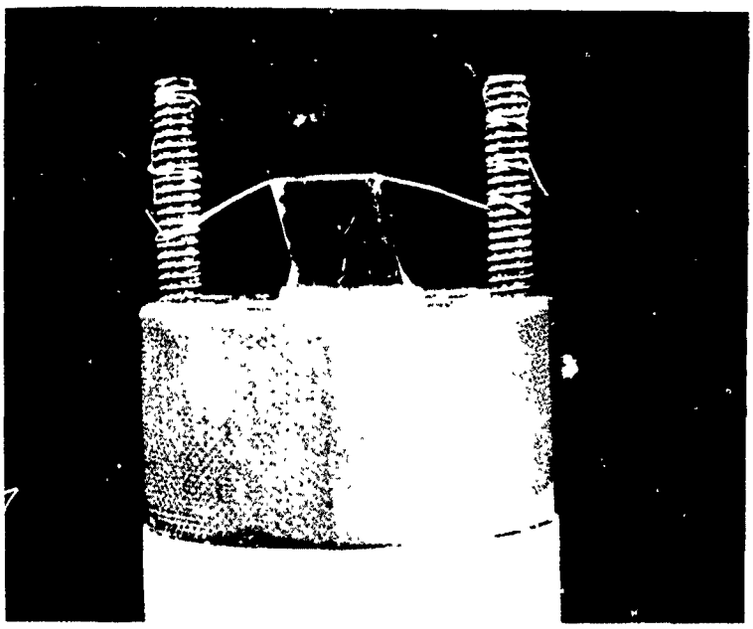

FIG. 2.32. Typical "Sandwich" Mounted on Specimen Holder. Nichrome ignition wire is shown positioned along the top edge of the specimen.

Ignition of the sandwiches was accomplished with a hot 10 mil nichrome wire laid along the top edge of the sandwich (Fig. 2.32). Propagation of the burning surface was in a downward direction. Most sandwiches were prepared as shown in Fig. 2.32 with the direction of burning occurring normal to the *m* face. Combustion of the sandwiches was studied utilizing the experimental apparatus described earlier. Quenched samples were again obtained by a rapid depressurization during burning.

The quenched samples were microscopically studied with various types of illumination to reveal the character of the burned and quenched surface. The burned surface profiles of the quenched samples were studied by sectioning thin slices normal to the burned surface and examining these "edge on" with a microscope. Tests were run over a pressure range of 100 to 1200 psig.

2.5.2. Results of Sandwich Burning

The quenched surfaces of the AP crystals burned in sandwich configuration have displayed the same general pressure dependent surface pattern as the single crystals deflagrating as a monopropellant. The only exception to this occurred when lithium fluoride was used as burning rate catalist. Figure 2.33 shows examples of the burned and quenched surfaces of sandwich with a PBAN binder containing carbon or copper chromite as ballistic modifiers. By comparing these examples with Fig. 2.22 it is readily seen that the general surface features are the same at corresponding pressures, as single crystals burned without a fuel present. High speed motion pictures have shown that all of the surfaces have the common characteristic found with the single crystals, i.e., the surface pattern, once formed, is stable.

In contrast to this, Fig. 2.34 shows examples of burned and quenched sandwiches that contained lithium fluoride as a ballistic modifier in the PBAN binder. The depressions in the surface appear to be slightly larger and the entire surface is glossy in appearance. The thin frothy layer and large bubbles that were observed on the other samples were not observed on the samples burned with lithium fluoride in the binder. As the pressure was increased the depressions became smaller but persisted to the upper pressure limit of the depressurization mechanism (approximately 1200 psig) and did not develop into the ridge pattern observed with the other samples. Conspicuous bubbles were not observed at any pressure. A crystal was coated with a thin layer of cellulose nitrate dissolved in acetone and containing approximately 2% lithium perchlorate and burned at 500 psig for comparison. The quenched surface was observed to be of the same general character as those burned with lithium fluoride in the binder, i.e., a glossy surface with depressions and no bubbles.

Following a careful examination and documentation of the surface characteristics, the quenched samples were sectioned approximately perpendicular to the burned surface to allow microscopic examination of the burned and quenched profile. Figure 2.35 shows samples of such "edge on"

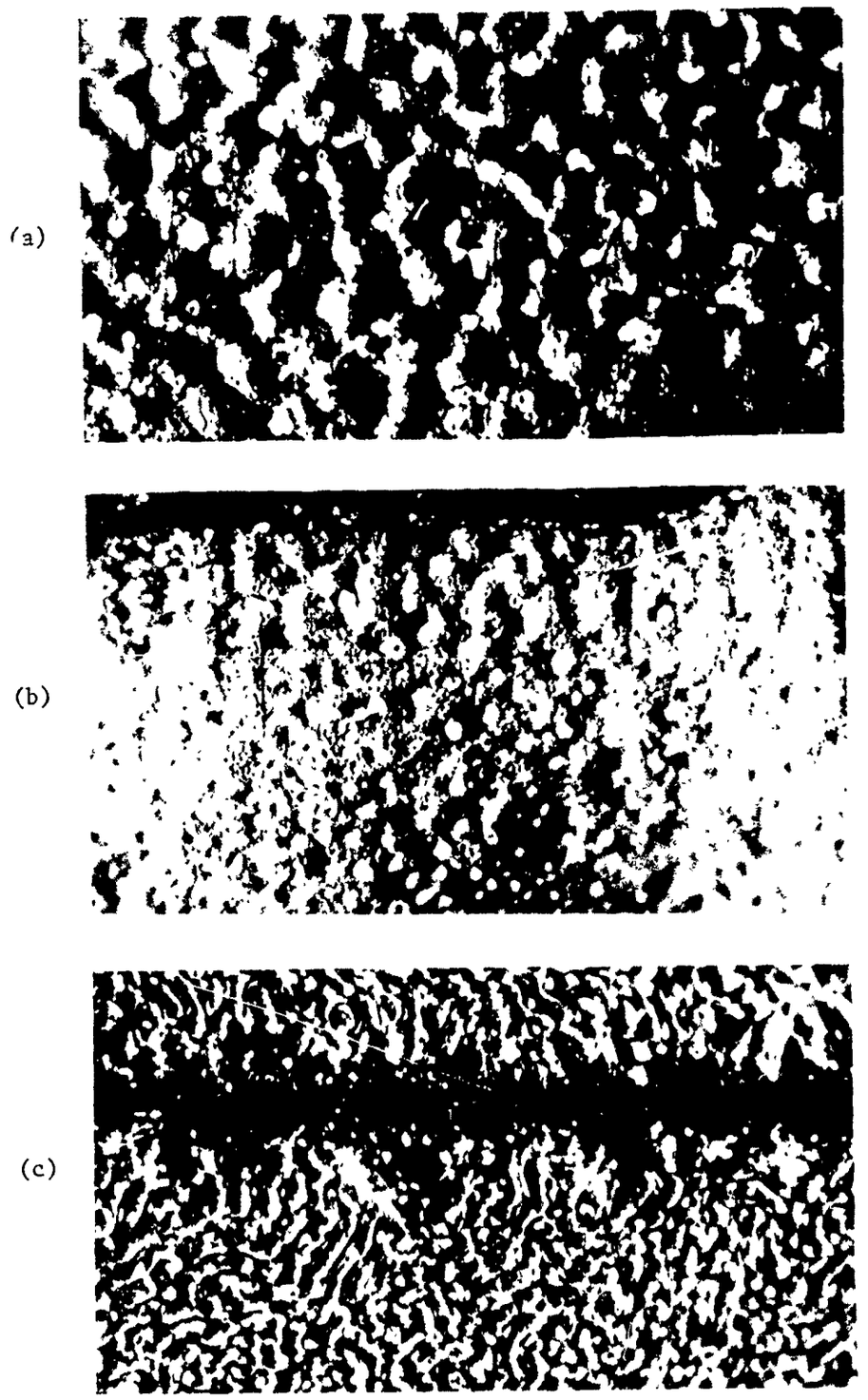

FIG. 2.33. Burned and Quenched Ammonium Perchlorate Surfaces Burned in Sandwich Configuration with PBAA Binder. (a) 300 psig with 1% Cu 0202 in binder. (b) 700 psig with 1% carbon in binder. (c) 1200 psig with 1% Cu 0202 in binder. Magnification approximately 35X.

(a)

(b)

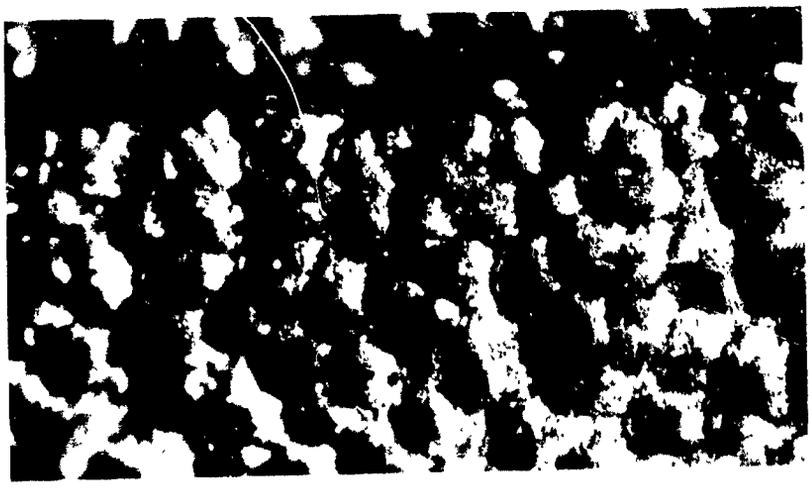

(c)

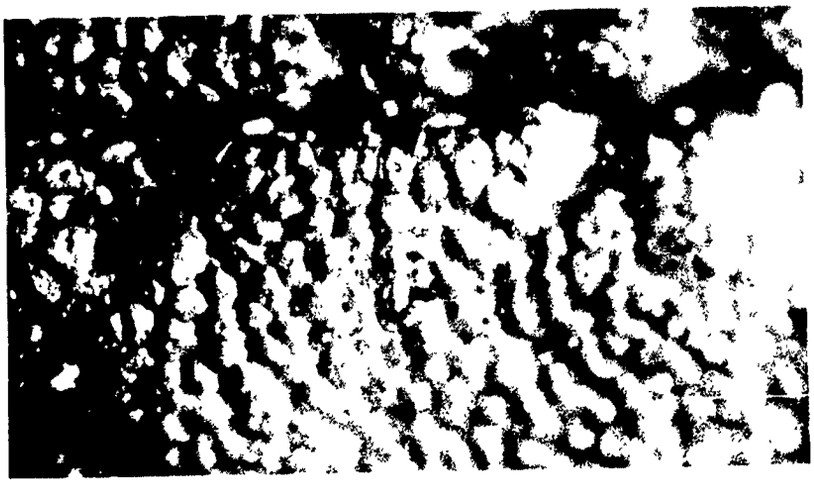

FIG. 2.34. Burned and Quenched Ammonium Perchlorate Surfaces Burned in Sandwich Configuration with PBAA Binder Containing Lithium Fluoride. (a) 300 psig with 1% L.F. (b) 700 psig with 1% L.F. (c) 1000 psig with 2% L.F. Magnification approximately 35X.

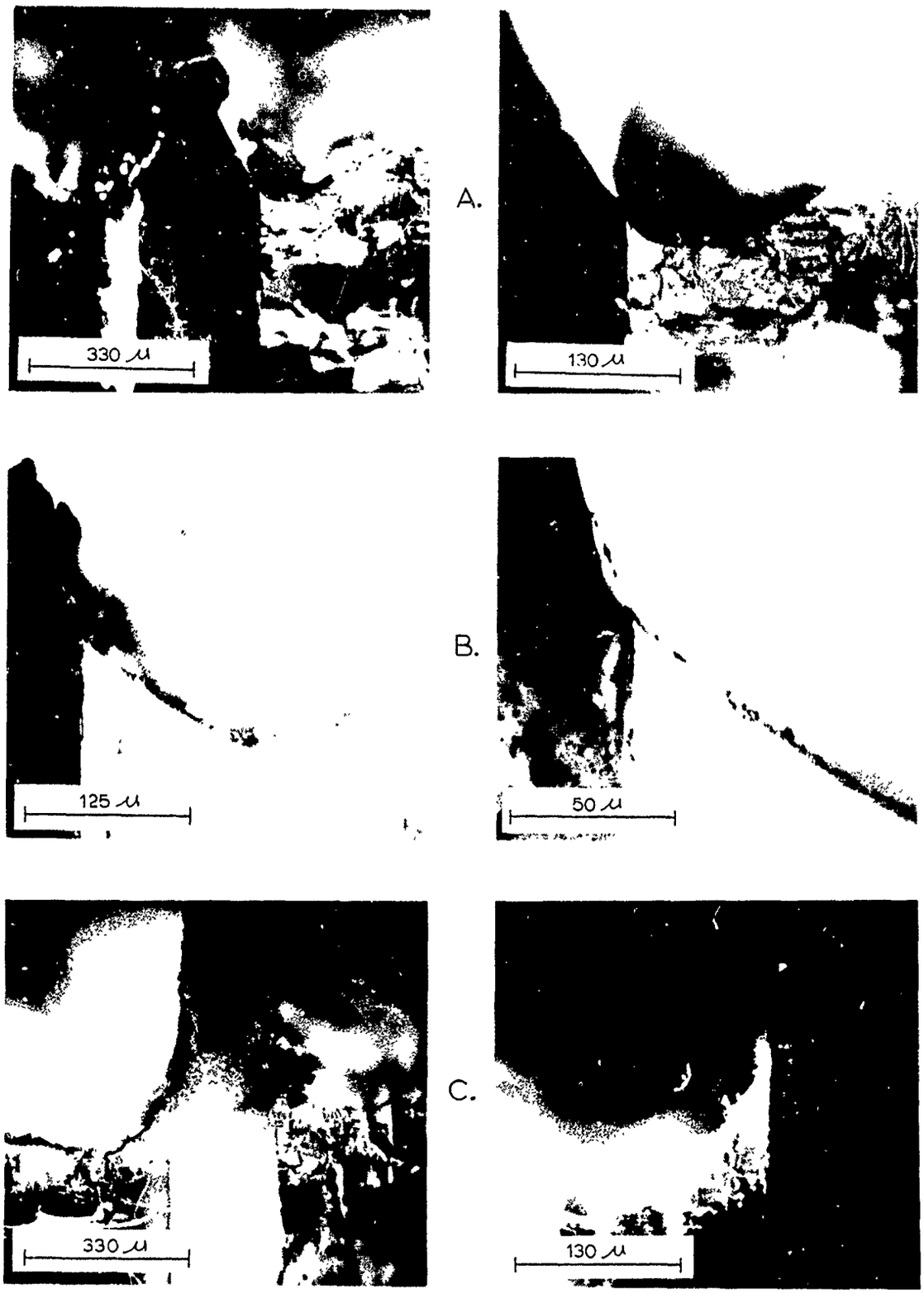

FIG. 2.35. Profiles of the Burned and Quenched Surfaces of AP-PBAA Binder Sandwiches. (a) 200 psig plain PBAA. (b) 700 psig 1% Cu 0202. (c) 1000 psig 1% L.F.

profiles of the combustion surface obtained at several different burning pressures with sandwiches having a binder layer with a thickness on the order of 100 to 150 microns. This figure shows several general characteristics that have been observed in these sandwiches over the entire pressure range investigated. First, the point of maximum regression was always observed to occur in the AP a short distance from the oxidizer-binder interface. Second, the AP appeared to be regressing at a lesser rate adjacent to the binder, producing a "trailing edge" effect with the surface of the AP blending smoothly into the binder surface forming a continuous regressing surface at the interface (Fig. 2.35b). At higher burning pressures (above the deflagration limit of AP) the AP will burn as a monopropellant and that part of the burning surface that was well removed from the binder layer was observed to regress as a plane wave. This surface was usually inclined at a slight angle, presumably to allow the regressing surface to maintain a steady-state configuration with the point of maximum regression rate (See Fig. 2.36a). At lower pressures (below the deflagration limit of AP) the AP will not undergo sustained steady deflagration unless some additional external energy is supplied to the burning surface. Under these conditions it was observed that regression of the AP occurred only in close proximity to the binder layer where the presence of an oxidizer-fuel flame (apparently a diffusion flame) could assist the AP deflagration process. This produced a burned sandwich with the outside crystal faces virtually undisturbed and a deep groove burned into the sample centered around the binder layer (See Fig. 2.36b). Even under these conditions, however, the maximum regression of the surface was observed to occur in the AP a short distance from the binder interface. Although the addition of lithium fluoride to the binder produced a distinct change in burned surface pattern of the sandwiches it did not alter the general features of the burned profile near the oxidizer-binder interface region (Fig. 2.35c).

The profiles of sandwiches burned with a thinner binder layer (on the order of 30 microns) were observed to be significantly different from those with thick binder layers. Figure 2.37 shows the profile of a sandwich with a plain PBAA binder layer approximately 30 microns thick that was burned and quenched at 500 psig. As can be seen from Fig. 2.37a there is an assymmetry about the binder layer that was not observed in the sandwiches with thicker binder layers. Examination of this sample with the higher magnification revealed a curious dip in the binder (Fig. 2.37b) but with the contour of the burned surface remaining very smooth across the interface. The large hump of AP to the right of the binder layer was observed to have a very thin binder layer on its surface. High speed motion pictures have shown this hump to be present during burning with a visible flame distributed above this region. The general nature of the flame structure can best be described as unstable and was observed to move back and forth across the binder layer. With sandwiches containing thicker binder layers the flame zone appeared to be of a much more stable nature although it was observed to consist of a series of "finger-like" flamelets instead of a continuous flame sheet.

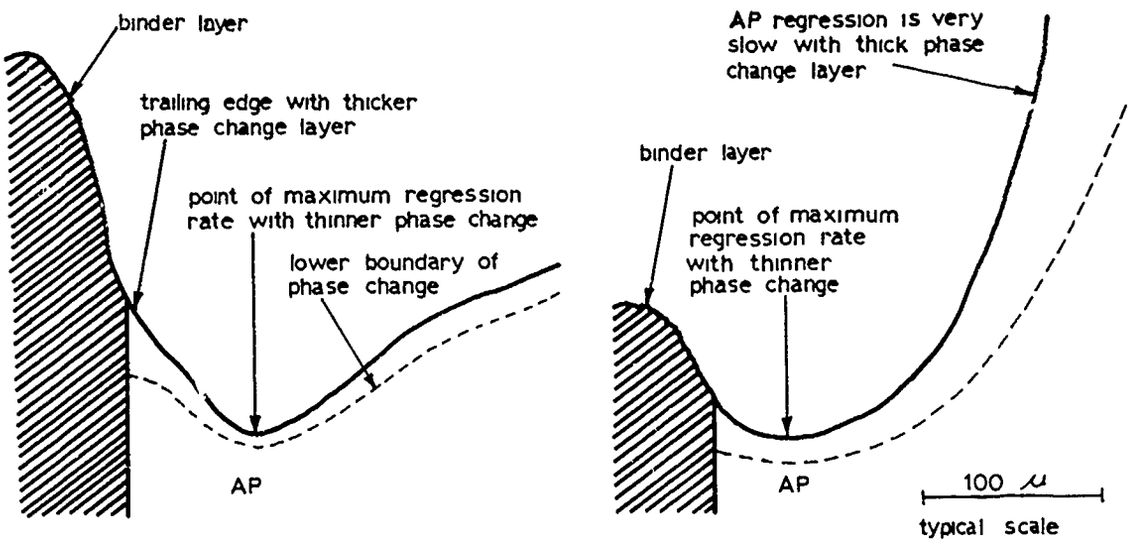

FIG. 2.36. Freehand Sketch of Profiles Typical of Those Examined with the Microscope. (a) Above the AP deflagration limit. (b) Below the AP deflagration limit.

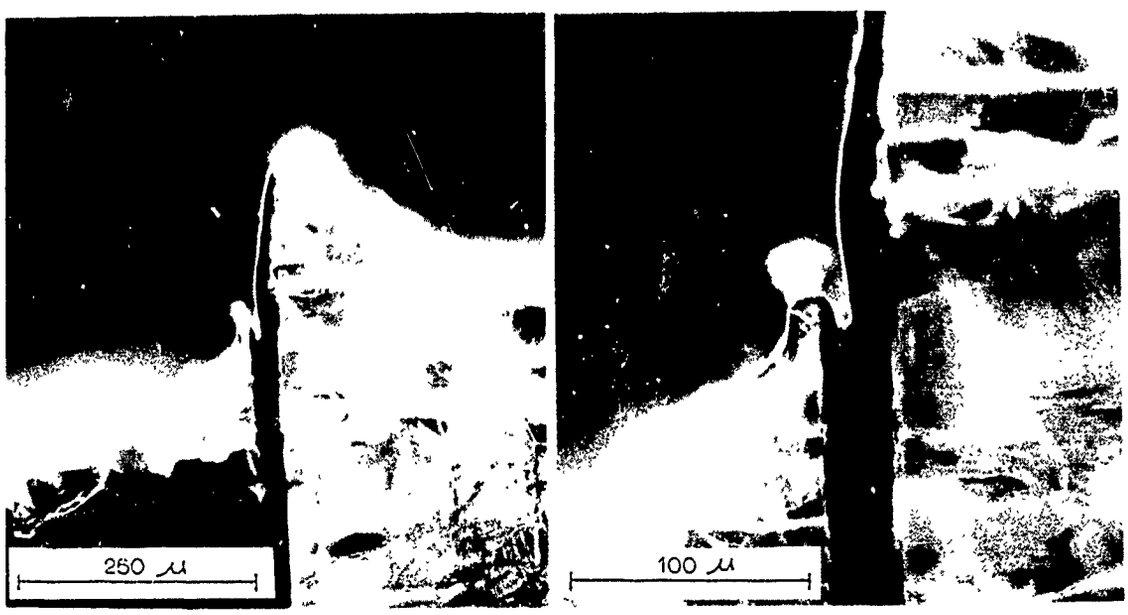

FIG. 2.37. Profiles of Sandwich with Thin PBAA Binder Layer Burned and Quenched at 500 psig.

That portion of the crystal that had undergone the 240°C phase transition was also observed in the "edge on" quenched sandwich sections. As with the single crystal samples described previously, the thickness of this layer was observed to be sensitive to the burning rate, being thicker at lower pressure (lower burning rate) and thinner at higher pressure (higher burning rate). For samples burning above the low pressure deflagration limit of AP the phase change thickness was observed to be approximately constant from the region near the point of maximum regression to the outer crystal edge (Fig. 2.36a). In this region for a crystal burning at 10 0 psig typical dimensions of the phase change thickness would be on the order of 10 to 12 microns. Near the binder layer, where the AP exhibits the "trailing edge" effect, the phase change layer is observed to vary in thickness, being thinest at the bottom of the dip, or maximum regression point, and becoming appreciably thicker at the interface.

2.6. DISCUSSION AND INTERPRETATION

It is generally conceded that the objective of propellant combustion research is to arrive at an understanding that will allow the prediction or modification of the burning rate and other ballistic properties of a propellant. This thesis has been used as a guiding philosophy in the present work. The complexities involved in propellant combustion are undeniable and it may be impossible to ever fully attain the stated objective. In the present work our attack has been to observe the physical nature of the combustion and decomposition behavior of major propellant ingredients in as much detail as possible, under the simplest conditions possible; any mechanistic description then must include those features that are of unquestionable importance.

More than anything else, so far, the results of the present investigation indicate that previous, and often widely accepted, views of the decomposition and deflagration of AP and AP propellants are incorrect and need to be re-examined in light of new evidence. In the following discussion we advance a new hypothesis for the deflagration of AP which incorporates several of the recent unreported or little known observations. At the present time there are many issues that must be considered as speculative, but in general we feel the new concept achieves a rationalization of both new observations and old ones that have thus far resisted explanation.

First, let us consider the evidence concerning the decomposition and deflagration of AP. It is widely (but not universally) believed that the AP decomposes to NH_3 and $HClO_4$ at the surface followed by desorption (endothermic), and that the exothermic reaction that sustains burning occurs in the gas phase. The importance of such a gas phase reaction is supported by recent tests by the authors. It was observed that granular AP would deflagrate in an open test tube under atmospheric pressure after heating to a temperature close to the second exothermic peak of a

corresponding DTA experiment. If the external heat source is removed, the deflagration ceases in a few seconds. On sustained heating, the deflagration continues to complete consumption of the AP. The gas phase reaction is visible with a weak, orange colored flame. This same orange colored flame was also observed at the surface of AP single crystals undergoing self-deflagration above 300 psia in nitrogen. Ammonium perchlorate grains heated more slowly decompose completely also, but without deflagrating. The initial decomposition products under non-deflagration conditions are observed to be both condensible, which form a liquid on the cooler portion of the tube, and reactive gas species which can be collected and ignited in an inverted beaker.

A similar behavior of AP can be shown in DTA experiments. The general features seen on a DTA trace depends primarily on the concentration (amount) of AP in the sample tube and the heating rate. As long as the sample is diluted with inert material and the heating rate is relatively low, the DTA curve shows the familiar pattern of one endotherm (crystal phase transition) and two exotherms. The first exotherm apparently corresponds to the partial decomposition of AP, which can be observed (to the same extent) at temperatures below the phase transition under isothermal decomposition tests. The second exotherm covers the complete reaction and shows a smooth peak under the above mentioned conditions. However, if the heating rate and/or concentration of the AP or environmental pressure are increased, an ignition of the decomposition products can occur (visible in the DTA cell with observation slits), which may be so violent as to expel the thermocouple and inert material. The ignition occurs shortly after passing the peak temperature of the second exotherm.

The experiments show that reactive and non-reactive species evolve from decomposing AP samples. The concentration and temperature of the species can cause their self-ignition. If the supply of reactive species is sustained by externally heating at a sufficient rate, deflagration can be obtained at atmospheric pressure. As in most experiments, these results do not establish unequivocally the details of the decomposition-deflagration process, but the total evidence strongly supports the scheme involving surface dissociative sublimation of AP followed by gas phase decomposition of $HClO_4$ and oxidation of NH_3. Some surface decomposition of $HClO_4$ is not excluded by these observations.

In the case of self-deflagration of room temperature single crystals in inert atmospheres at elevated pressure, the results suggest a property of AP deflagration that is important but only recently observed. That is the observation that the burning surface is a <u>liquid</u>. The presence of a surface melt is in contrast to views expressed often to the contrary in the literature. However, the supporting evidence is about as decisive as nature permits in so complex a phenomenon, and in hindsight is not surprising. In summary, the evidence includes (a) observations and photomicrographs of a frothy-appearing layer on large portions of the surface of quenched samples, (b) "tears" in this layer where cracks developed in

the underlying crystal during quench, (c) the observation of many bubbles in the frothy layers, some of which are seen in motion-pictures to form on the surface during quench, (d) photomicrographs showing large bubbles with portions broken out to show their hollow character, (e) x-ray analysis of fragments from a number of bubbles showing the material to be AP. The presence of a surface melt implies that the gasification step is not controlled by desorption from a crystal surface, a fact that may have profound significance in terms of concepts of kinetic control of deflagration. What seems even more important, the liquid surface would be expected at some pressures at least to be full of bubbles since the AP is decomposing. The available observations do indeed indicate the melt to be frothy. Since the bubbles in the froth consist of an exothermally reacting gas, the froth is self-heating, and heats the underlying solid. If the process is also significantly dependent on surface reactions, the froth provides a very large surface for such reactions.

It seems to be a point of some fundamental importance that a material which decomposes without melting in laboratory experiments at, say, 400°C, may still have a liquid state at some higher temperature such as those present in a deflagration wave. Since the decomposition rate is governed by relatively improbable molecular collisions at the extreme high energy end of the molecular energy distribution, the mean energy may be pushed to fairly high values before complete decomposition, if the heating rate is very high. As a result, a liquid state may be reached which would not be observed at lower heating rates where the sample decomposes before reaching the "melting" point.

From a knowledge of the regression rate and the depth of the 242°C isotherm it is possible to estimate a conservative heating rate typical of conditions experienced near the burning surface of AP. At a combustion pressure of 1000 psia, for example, it is estimated that the heating rate is on the order of 10^5°C/sec. This is roughly five orders of magnitude higher than a fast DTA heating rate (80°C/min). This may explain the observed absence of conspicuous decomposition below the first few microns on the burning surface, since the induction time for condensed phase decomposition, observed in isothermal decomposition tests, have been explained previously in terms of propagation laws for relatively slow moving decomposition fronts from active sites. In the frothy liquid surface layer, such propagation laws would not be expected to hold, nor would the decomposition necessarily depend upon the same active sites or reaction steps.

Many investigators have speculated on the importance of the low temperature decomposition process in the deflagration wave. There is an intrinsic appeal to this approach in that it is much easier to obtain "accurate" data in the low temperature, low rate region. It has never been demonstrated, with any authority, however, that low temperature decomposition or, for that matter, high temperature thermal decomposition in the solid phase, significantly contributes to the exothermic heat release in a deflagration wave. In order to compare observed low temperature

decomposition rates to actual deflagration data it is necessary to extrapolate the low temperature data, sometimes over several orders of magnitude, which is always risky at best. The temperature of the deflagrating surface is a key factor in any such extrapolation. The thermal decomposition rate is exponentially dependent on temperature and any comparison to deflagration rates is dependent on an accurate knowledge of the surface temperature during deflagration.

It is important to pursue elucidation of the relationship of thermal decomposition to deflagration. It is instructive in this respect to extrapolate low temperature data to rates comparable to deflagration rates. It is assumed that the majority of decomposition (in a deflagration wave) will occur at a temperature corresponding to the surface temperature. The most conservative rate calculation (in favor of low temperature decomposition) is obtained using the Arrhenius expression. Accordingly, if one uses the kinetic parameters discussed earlier in this section (activation energy of 21.9 Kcal/mole and pre-exponential factor of 6.5×10^5 cm/sec) the following values can be calculated: (1) for an assumed surface temperature of 600°C the low temperature decomposition interface would have a rate of 0.023 cm/sec; as compared to a rate of 0.3 cm/sec at the low pressure deflagration limit; (2) for the same kinetic parameters but assuming a decomposition rate comparable to the minimum deflagration rate (0.3 cm/sec) the surface temperature must be approximately 850°C. Similar results can be obtained by using the kinetic data of other investigators.

In addition to the uncertainties surrounding the parameters employed in making a somewhat tenuous extrapolation, it is difficult to reconcile the observed deflagration rates in terms of a low temperature decomposition mechanism. The reconciliation becomes even more difficult in view of the fact that a surface melt exists during normal self-deflagration while the non-deflagration thermal decomposition studies (both "low" and "high" temperature) are conceded to involve solid phase processes.

A knowledge of the surface temperature is fundamental, also, in resolving the nature of the processes occurring at the burning surface-equilibrium, vaporization of kinetic limited. In the present work the calculated temperature is for the solid surface. The fact that it is constant with pressure is believed due to the presence of the melt. As such these calculations do not give direct information on the temperature-pressure relationship at the melt-gas interface. The present results do support the concept of a surface melt and do give an idea of the magnitude of the burning surface temperatures. Work is now in progress to measure "surface temperature" with thin film thermocouples laid directly on an AP substrate. This method may provide the resolution necessary to answer the question surrounding the surface processes.

The results of the present studies suggest the following description of the deflagration wave in the AP crystal. The leading edge is a thermal wave in which the temperature rises until the crystallographic phase change occurs, presumably at 242°C. This point occurs at from 10 to 35 microns

from the surface, depending on the pressure (1200 to 275 psia respectively). Closer to the surface, the temperature increases to within roughly 2 to 5 microns of the surface without evidence of progressive decomposition. Although the phase transition layer was observed to be optically different from the original crystal structure, it was uniform in optical density. In a layer about 5 microns thick (depending on the pressure), the details are not resolvable, although a major portion if not all of the layer has apparently been in a liquid phase. The liquid layer appears to have been frothy as judged from quenched samples, and similar details are often visible also in motion pictures during burning (resolution in motion pictures is much poorer than in photomicrographs of quenched samples). Assuming that the usual temperature dependence of reaction rates holds, the present results indicate that the majority of the decomposition of the condensed phase occurs in a (non-crystalline) melt rather than in or on the crystal.

From these results we hypothesize that when AP undergoes self-deflagration the energy release necessary to sustain steady-state regression occurs in two phases; in the gas phase above the condensed surface and in a psuedo-condensed phase which is primarily gas phase in nature, but confined within bubbles which nucleate and grow in the melt layer. The energy transfer from the gas phase to the regressing surface is by conduction in the gas phase with the driving potential being the temperature gradient between the gas phase temperature and the surface temperature.

That portion of the energy release which is confined within bubbles (or froth), however, is more effectively transferred to the condensed phase since by the nature of its confinement the energy gradient is much larger and the energy transfer is essentially three-dimensional (large surface area). Both energy feedback mechanisms are effectively coupled to provide the total energy feedback necessary to sustain a surface heating rate high enough to maintain the melt and evolution of reactive species. It can be anticipated that the gas phase reaction above the surface will become the dominate heat release mechanism at higher pressures since under these conditions the gas phase flame and melt thickness will become very thin with less chance of "exothermic froth" being present.

While direct proof of the foregoing hypotheses is no better than the proof of competitive "theories", it appears to provide better rationalization of the known facts. Consider for example the abrupt low pressure deflagration limit. It is known that a melt is not observed during laboratory decomposition tests, where the heating rates are usually only a few ^{o}C/sec and the sample decomposes completely before temperatures comparable to those at the deflagrating surface are reached. We postulate then that a critical heating rate (critical regression rate) is necessary to produce a melt of AP.[10] We expect the phase change from crystalline to

[10] The "melt" is very likely a solution containing also NH_3 and $HClO_4$, and possibly other species which are being formed in the melt.

melt and vice versa to occur suddenly so that just above a critical rate a melt is present; just below a critical rate the melt is not present. Below this rate all of the energy feedback has to be supplied by a relatively weak distributed gas phase flame. This energy flow cannot maintain the necessary supply of reactants from the solid surface and the deflagration ceases abrubtly just below the critical rate necessary to maintain the melt.

It is, of course, well known that relatively small amounts of catalysts such as copper chromite when mixed with granular AP, produce a dramatic increase in the deflagration rate. Explanations for this assuming a "dry" surface are very tenuous. The presence of a melt, however, allows a very high degree of surface contact and hence catalytic action to occur.

The concept of surface heating by the exothermic froth is further supported by the results obtained with doped crystals. With the high surface nucleation rate observed with the doped crystals at low temperature, one might expect that a much higher heating rate (attainable only at higher pressure in deflagration) would be required to reach the "melting" point, with a significant amount of undecomposed material remaining to form the melt. Thus, the low pressure deflagration limit would be much higher, as was indeed observed with the doped crystals. Relative to this, it is interesting to note that a similar effect on deflagration limit was obtained by Friedman (Ref. 17) using pressed pellets of AP with added MnO_2 and $NoMnO_4 \cdot 3H_2O$.

The exact character of the surface melt during deflagration is unknown. The formation of surface lithium perchlorate in the sandwich burning tests indicates the possibility of solutions, but there is evidently no decomposition product remaining in the post-quench layer of single AP deflagration. On the other hand, AP crystals placed in an atmosphere of gaseous ammonia at 2 to 4 atmospheres pressure quickly dissolve to a liquid. Since ammonia is being formed in the melt on the burning surface, it is probably in solution with the AP and may affect the state of the melt.

Thus far the discussion has centered around the decomposition and deflagration of AP, the major constituent in most modern solid propellants. Although the study of this one constituent has proven to be remarkably complex, the situation with true propellants is even more formidable. The physicochemical process of propellant combustion is so complex that mathematically tractable models are generally found to be of only restricted relevance. In the case of propellants composed of granular oxidizers and plastic fuel-binders, the three-dimensional microstructure greatly complicates any attempts at analytical representation or experimental investigation of the combustion. On the other hand, none of the propellant ingredients is individually dominant in governing the combustion of composite propellants, so that the complexity of the

microstructure can hardly be ignored in elucidation of the combustion mechanism. As a compromise between the complexity of the three-dimensional "combustion zone" and the naivety of a one-dimensional approximation, it was decided to explore the potentialities of experimental studies of two-dimensional propellant structures prepared by laminating a binder layer between thin oxidizer single crystals. By the use of a suitable technique, the dimensional relations of a conventional propellant microstructure could be duplicated while preserving the relative simplicity of a two-dimensional configuration. Initial efforts using AP oxidizer crystals grown under poorly controlled conditions proved disappointing in that the crystals fractured ahead of the combustion wave and obscured the normal surface regression. In the present work the use of high quality AP single crystals allowed us to prepare sandwiches which burned smoothly in a manner considered typical of the behavior of the small AP particles in a composite propellant.

In composite propellants containing AP the possibility exists that regression of the surface is dominated by decomposition characteristics of the AP, by subsurface interface reactions between binder and oxidizer, oxidation attack on the binder surface, or an exothermic gas phase reaction feeding heat back to the condensed phase. These issues have been partially resolved by examination of the burned profiles in the region near the oxidizer-binder interface. The profile examples shown in Fig. 2.35 are typical of the observations made on numerous samples with the thicker binder layers over the entire pressure range investigated. The absence of significant interface reactions is indicated by the smooth burning contour at the interface. If significant interface reactions had occurred it would seem reasonable that evidence of this would have manifested itself in an increase of the regression rate at the interface. Instead, there is a decided reduction in the regression rate as evidenced by the "trailing edge" of AP at the interface. The deflagration rate of AP seems to be fairly sensitive to various heat loss mechanisms as indicated by the effect of convective losses to the high pressure environmental nitrogen gas in the pressed pellet deflagration studies of Friedman, et al (Ref. 17). They observed an upper maximum deflagration rate at approximately 2200 psi which was subsequently shown to be due to convective losses (Ref. 18). The present results suggest that a conduction heat loss mechanism may be operative where the AP is in good thermal contact with non-reactive binder.

At pressures above the AP deflagration limit, and relatively far from the binder (where conduction losses to the binder are negligible), the AP burns as a monopropellant. Moving closer to the binder a position is reached where heat loss to the binder is still relatively low, but where the proximity of the fuel-oxidizer diffusion flame can supply additional heat feedback above that normally supplied by the AP monopropellant gas phase reaction. The characteristic "dip" or point of maximum regression is reached in the AP where the net energy feedback to the surface is a maximum (Fig. 2.36a). Moving closer to the binder layer the heat loss to the binder begins to dominate with a decrease in the

regression rate and the resultant "trailing edge" effect. The increase in thickness of the phase change layer adjacent to the binder gives further insight into the influence of the binder layer on the behavior of the thermal wave in the AP and indicates the importance of the two-dimensional heat transfer that is occurring in this region. At pressures well below the deflagration limit the AP was still observed to lead the regressing surface a short distance away from the binder interface where the gas phase diffusion flame could supply the necessary energy feedback to allow the AP to sustain steady deflagration. Further from the binder the AP regresses more slowly (or not at all, depending on the pressure) since the diffusion flame is too far removed to supply the necessary energy feedback (Fig. 2.36b).

As noted previously, the surface pattern on the AP burned in sandwich configurations was in general the same as on the AP single crystals burned without a fuel binder present. The same evidence for a surface melt was also observed on the sandwiches and is undoubtedly a significant factor in propellant combustion. Although the presence of a melt on the surface of deflagrating AP is contrary to most speculations on the subject, it is not obvious that there has ever been strong experimental evidence to indicate the presence of a completely "dry" surface under conditions prevailing in a deflagration wave. The heating rate near the burning surface is estimated to be several orders of magnitude higher than the heating rates normally employed for laboratory decomposition studies and is apparently the significant factor responsible for the occurrence of a surface melt. While there is no decisive evidence that the presence of a surface melt is an important factor in the combustion characteristics of the propellant, it seems unlikely that it would not have an influence. Oxidizer decomposition in a frothy melt is not likely to follow the same laws of propagation as in crystalline materials, and activity of ballistic modifiers might well be different in a melt, as suggested by the results with lithium fluoride. The larger surface area of a frothy melt provides an opportunity for increased importance of surface reactions. The vulnerability of a frothy melt to disturbance by flow oscillations in the adjoining gas flow field may explain the relatively high susceptibility of AP propellants to oscillatory combustion. The possibility exists that there is some mixing of molten fuel and oxidizer near the interface, a condition which would be increasingly important as oxidizer particle size is reduced. Thus, it appears that future work should include serious consideration of the presence and effect of a frothy melt layer.

The distinct change in the appearance of the burned surface that resulted with the addition of lithium fluoride to the binder was one of the more puzzling observations made in the present investigation. The fact that AP will form a liquid solution with lithium perchlorate (Ref. 53), suggested that a similar mechanism might be operative on the burning surface of sandwiches containing the necessary species for such a reaction. Single crystals coated with a thin layer of cellulose

nitrate dissolved in acetone and containing approximately 2% powdered lithium perchlorate exhibited a burned surface pattern very similar to the burned surface of sandwiches with lithium fluoride in the binder. In another rather crude experiment, a small quantity (approximately 200 mg) of a mixture of powdered propellant grade AP and lithium fluoride was heated in a small pyrex test tube with an oxy-acelylene flame. For the first second or two after heating was started, the mixture visibly decreased in volume with a white condensate forming on the upper cooler portion of the tube. Quite suddenly the remaining mixture melted and rapidly climbed to the top of the tube and solidified. Analysis of the solidified residue by x-ray powder pattern indicated the material to be a mixture of AP and lithium perchlorate. This evidence suggests the possibility that a melt of lithium perchlorate-ammonium perchlorate could be present on the sandwiches burned with lithium fluoride in the binder.

The sandwich deflagration studies have provided us with the unique opportunity to study the behavior of the interaction between the major propellant constituents in a system of relative simplicity, but in a configuration that must surely have a bearing on true propellant combustion. The most significant results are found in the detailed study of the burned and quenched profiles. In the study of these profiles it is noteworthy that in no case was the regression led by the oxidizer-binder interface, indicating the relative unimportance of interfacial reaction. Additionally, in no case was the regression led by the binder, indicating the relative unimportance of oxidative heterogeneous attack on the binder. This, of course, does not completely eliminate such reactions as important factors in propellant burning, where part of the surface regression involves pyrolysis of the binder layer separating successive oxidizer particles.

2.7. CONCLUSIONS

The work reported in this section is still being pursued. The results to date indicate the following important conclusions:

(1) Under self-deflagration conditions AP has a thin melt layer on the surface, which is the site of some exothermic reactions and provides improved heat transfer from these reactions to the solid.

(2) The presence of a stable surface pattern indicates the importance of gas phase exothermic reactions in the deflagration of AP. The general character of the surface pattern is influenced by some catalysts while being virtually unchanged by others offering a clue to the mechanism of catalysis.

(3) The addition of small amounts (0.04%) of doping ingredients produces a significant change in the decomposition and deflagration behavior of AP.

(4) The use of single crystals has allowed an unambiguous definition of the partial decomposition interface in AP and allowed for precise measurement of its rate of propagation.

(5) Ammonium perchlorate-binder sandwiches burn with the leading edge of the burning front located in the oxidizer, near the diffusion flame. The surface is continuous over the interface between oxidizer and fuel indicating that exothermic reactions at the interface do not dominate the burning rate.

(6) The deflagration characteristics of AP manifest themselves in further detail in the sandwich burning tests, e.g., the crystallographic phase change layer is evident in the AP, and the AP far removed from the diffusion flame burns very slowly at pressures below the normal low pressure deflagration limit of AP.

(7) The diffusion flame is seen to fluctuate in location and intensity when the binder layer is thin, and the interface details on the quenched samples become more complicated and less reproducible.

(8) The general character of the results is not sensitive to the type of hydrocarbon binder used.

(9) The experimental technique offers a unique opportunity to study combustion mechanisms.

3. BEHAVIOR OF ALUMINUM IN COMPOSITE PROPELLANTS

This section is devoted to the investigation of the steady-state combustion of solid propellants with particular emphasis on the behavior of aluminum as it passes from the non-burning portion of the propellant outward through the surface and combustion zone and into the gas phase. The continuing work (Ref. 54, 55 and 56) is being done with the hope that an understanding of the steady-state combustion of aluminized solid propellants will contribute significantly to the understanding of various aspects of propellant burning and combustion instability. A color/sound movie (Ref. 57) has been produced which summarizes the major portions of this section.

3.1. GENERAL OBSERVATIONS

The studies have been concentrated almost exclusively on composite propellants and it is important to again stress the heterogeneous nature of the propellant. The original propellant is a composite structure consisting of ammonium perchlorate (AP) particles (ranging in diameter from 15 to 600 microns), and aluminum particles (ranging in diameter from 5 to 40 microns) held together by a rubber-like plastic. Thus, on a microscopic scale, the original propellant structure is quite non-homogeneous, and during combustion one should expect to encounter manifestations of this heterogeneity.

Indeed, this is the case as seen in Fig. 3.1 and as pointed out in Ref. 54. The gross irregularity of the quenched burning surface shown in Fig. 3.1 is demonstrated by the portions of the picture that are out of focus (the bottom of a hole near the upper edge and the top of a ridge of pinnacles on the left side). The dimensions of these gross irregularities are on the order of twice the diameter of the original AP size. Smaller irregularities are produced by the AP particles themselves; from quenched propellant samples tested at 100 and 400 psi, the AP was observed to protrude above the surrounding surface. The AP particles appear in Fig. 3.1 as dark areas with approximately 200-micron diameters.

Perhaps the most interesting feature on the quenched surface is the aluminum; the propellant surface is almost entirely covered with aluminum. In fact, as seen in the center of Fig. 3.1, there is even aluminum on the surface of the AP. On the basis of the 10% volumetric concentration of aluminum in this particular propellant, one would expect a very small percentage of the surface to be covered by aluminum if there had been no accumulation. But from the figure, it is evident that there was a great

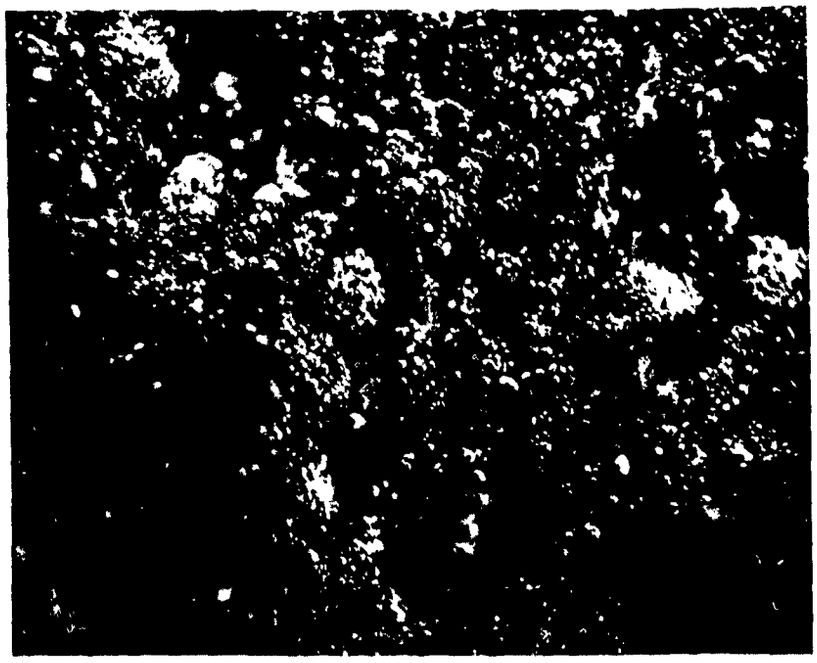

FIG. 3.1. Photomicrograph of a Quenched Aluminized Propellant Sample.

deal of aluminum accumulation. Thus, the heterogeneity originally present in the propellant structure is seen to become even more pronounced at the surface as the combustion wave proceeds through the propellant.

In addition to the studies of the surface of quenched aluminized propellants, high speed motion pictures have also shown not only that the original aluminum particles in the propellant accumulate at the burning surface but that subsequently they form large agglomerates of molten aluminum which burn in the gas phase above the propellant surface with a vigorous detached flame. The entire sequence of events occurring with the aluminum can be described, in general, as follows. During the steady-state combustion of aluminized solid propellants, the AP and the binder pyrolyze and the original aluminum, protected from ignition by its own oxide coating, is left behind and accumulates on the surface of the propellant. After the accumulation period, the aluminum behaves in one of two ways:

(1) If conditions are favorable for aluminum combustion, e.g., sufficient oxidizer available, sufficiently high pressure and/or temperature, etc., a small portion of the accumulated aluminum, perhaps only one or two of the original particles ignites. This event is most likely to occur at a time when the accumulate is most effectively exposed to the

oxidizer-binder diffusion flame and/or the decomposition products of the oxidizer. The heat from this small zone of burning aluminum generates a thermal wave which passes through the remaining portion of the accumulated aluminum and melts the rest of the accumulate. The entire mass then draws up into a spherical ball of molten aluminum and leaves the surface of the propellant burning vigorously.

(2) If conditions are unfavorable for aluminum combustion, the accumulated aluminum will not ignite locally; instead, it will remain on the surface of the propellant until it is undermined sufficiently by the regression of the AP and binder so that it is released (unignited) into the gas phase. Under some conditions, the accumulate is heated enough to "sinter" the accumulate into an irregularly shaped mass which exhibits a red glow and apparently undergoes surface oxidation without complete melting of the Al_2O_3 present.

In addition to the large spherical agglomerate and the large irregular accumulated mass of aluminum, a third type of aluminum behavior has been observed. The third type is the ignition and combustion of a single original aluminum particle. This type of aluminum combustion has been observed to a greater or lesser extent in all the propellants that have been photographed. It is obvious that this is the most efficient way to burn aluminum in solid propellants and efforts should be expended to eliminate the aluminum accumulation and agglomeration processes and produce only single particle ignition and combustion. The three types of aluminum behavior are sketched in Fig. 3.2.

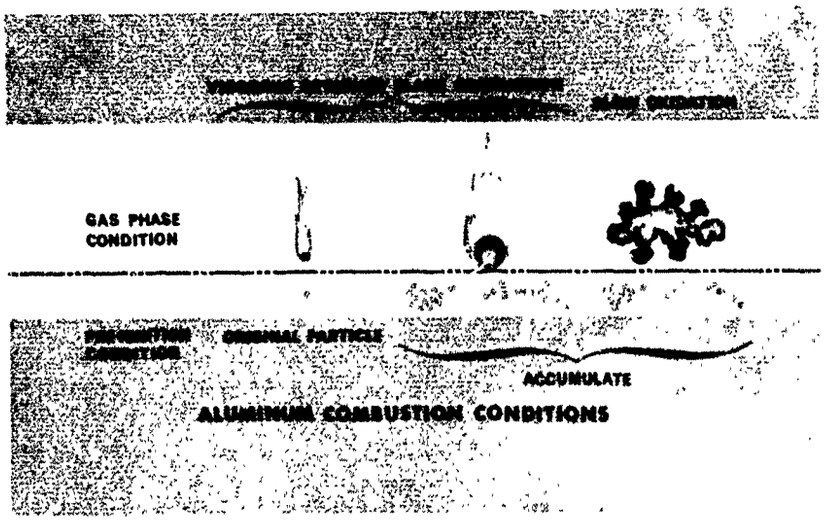

FIG. 3.2. The Three Types of Aluminum Behavior

3.2. CINEPHOTOMICROGRAPHY

The principal tool used in this study has been high speed motion picture photography using magnification. Single frame reproductions of some of the best movie footage are shown in Fig. 3.3. However, with most of the movie footage such reproductions are quite unsatisfactory in representing the dynamic behavior of the aluminum. Because of this, a sound/color movie has been prepared.[11]

An overall view of the photographic set-up is shown in Fig. 3.4. On the left is a Fastax camera with a lens extension tube. On the right is the photographic burner. The burner itself is rather small; the internal dimensions are 2 x 2 x 2 inches. It has three fused quartz windows, two of which are used in this experiment. In the background to the left is a 2500 watt xenon arc lamp which is used to externally illuminate the propellant sample at an oblique angle. A shutter and an infrared absorbing filter are placed between the xenon lamp and the burner in order to minimize the amount of radiation that does not contribute to the photographic illumination. The xenon lamp is focused on the propellant sample and adjusted to give an incident flux of 3 cal/cm^2 sec. All the movies are taken under the same photographic conditions. Those conditions are a Fastax camera running at approximately 4000 frames per second using Anscochrome 2290 film, a magnification of four, and f/stop of f/11 and oblique lighting by the xenon arc lamp.

The propellant sample arrangement is shown in Fig. 3.5. The propellant is mounted in the center of the holder and is uninhibited. Ignition is accomplished by a hot wire. The propellant sample itself is quite small and the actual field of view of the camera is one-tenth of an inch in width. The burner is pressurized and continually flushed by a small flow of nitrogen. The nitrogen comes through the sample holder and out the opening in front of the propellant sample. The purpose of the nitrogen flow is to minimize smoke in the optical path. While the cold gas no doubt interacts extensively with the combustion in the region a short distance above the surface (outside the field of view of the camera), the effect in the camera field of view appears to be restricted to some retardation of aluminum ignition at the front edge of the burning surface. While the importance of this effect could be further reduced by going to larger propellant samples, the depth of focus available with this optical magnification is too shallow to view a thicker combustion region clearly. Since the surface activity of the aluminum was of primary concern in this study, the present arrangement was selected as a suitable compromise between sample size effects and photographic requirements.

---

[11] Copies of the movie "Aluminum Combustion in Composite Propellants," (Ref. 57) are available for short term loan. Send request to Commander, U. S. Naval Ordnance Test Station, Code 508, China Lake, Calif., 93555.

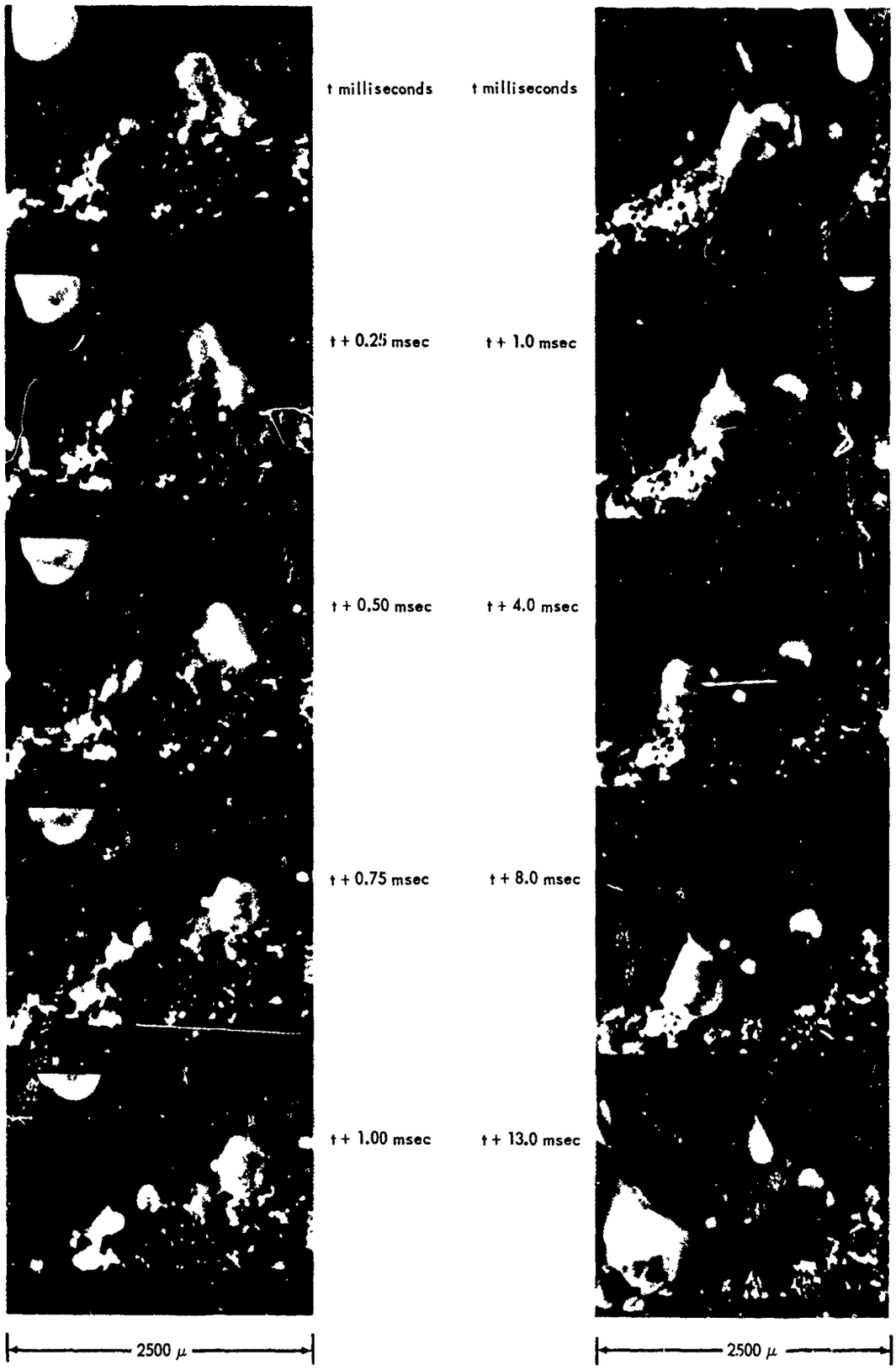

a. Sequential frames from 16-mm movie of propellant burning at 100 psi.

b. Selected frames from same movie showing formation of a burning aluminum agglomerate.

FIG. 3.3. Portions of 16-mm Movie of Burning Composite Propellant (P-5 Propellant in Table 4.2).

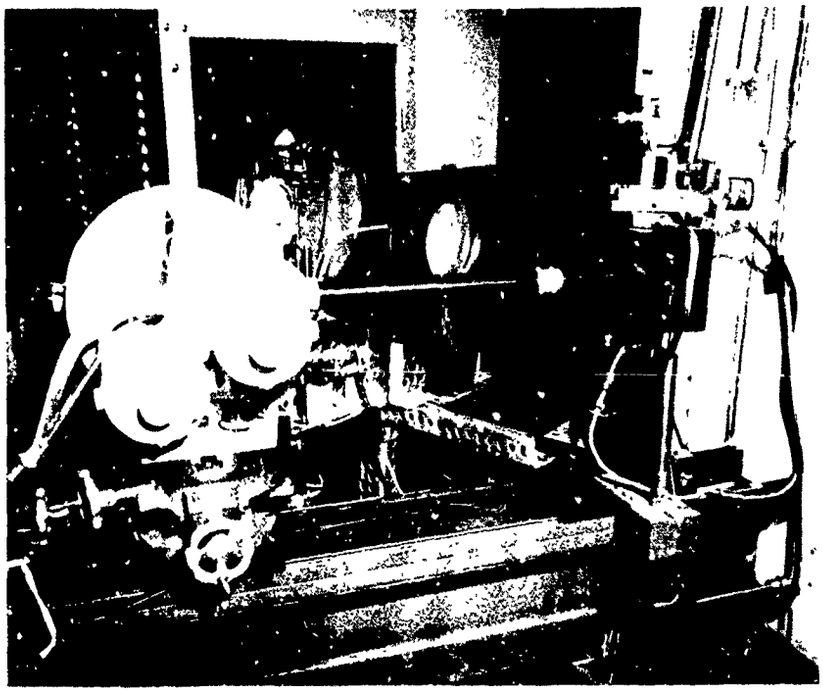

FIG. 3.4. Photographic Arrangement.

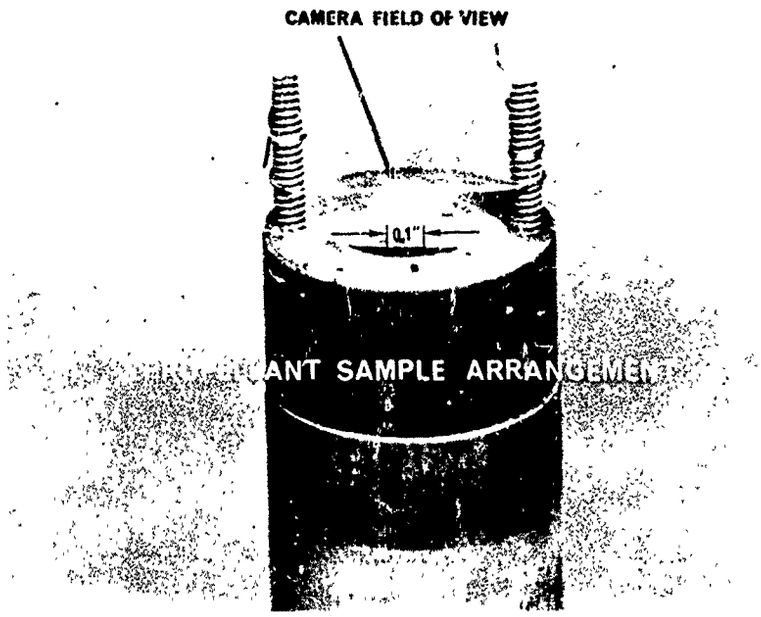

FIG. 3.5. Propellant Sample Holder.

3.3. EXPERIMENTAL PROCEDURE

To investigate the various aspects of the aluminum activity in composite propellants, an extensive systematic series of propellants were formulated and photographed. The propellant variables studied were the AP particle size, the aluminum particle size, the aluminum concentration, and the binder type. The basic formulation was 59% AP, 16% aluminum, and 25% binder. For the aluminum concentration series, the binder percentage was held constant at 25%. This rather high concentration of binder was chosen so as to circumvent mixing difficulties as the unimodal ammonium perchlorate particle size was varied over a wide range of values. Table 3.1 gives the particle sizes and aluminum concentrations investigated.

These formulations were burned and photographed in general at 100, 200, 400 and 800 psi. In addition, several propellants from development programs were burned and photographed to determine if there were any basic differences between practical propellants and the systematic ones. To date, no basic differences have been discovered.

3.4. SUMMARY OF COMBUSTION TRENDS

From a detailed study of the combustion movies a qualitative picture of how the aluminum behaves in composite propellants has emerged. The first clue to the qualitative model came from the data shown in Fig. 3.6. The graph shows the results of measurements of the apparent size of the aluminum agglomerates in the gas phase above the surface for a series of three propellants. The three propellants had the same formulation except for the aluminum particle size; the three particle sizes were 7, 21 and 41 microns. Measurements were made of the diameter of all the aluminum agglomerates in one frame in the volume above the burning surface for a height of 2500 microns. Measurements were made on a total of 25 frames for each propellant; every one-hundredth frame of each film was measured to avoid measuring the large, slow moving agglomerates more than once. The ordinate, n, is the average number of particles that are in the specified volume above the surface at any instant. This number was obtained by lumping the measured diameters into 25-micron intervals and dividing the number of particles in each interval by the number of frames measured. The abscissa is the particle diameter of the agglomerates.

This graph indicates that, regardless of the size of the original aluminum particles, the greatest number of aluminum agglomerates have a diameter of approximately 100 microns. This immediately leads to the question, "what do the original aluminum particles of different sizes have in common which would cause them to form agglomerates of the same size?". One answer is that all the original aluminum is originally contained in the binder; in particular, the majority of the original aluminum is contained in the spaces between the AP particles, i.e., the binder "pockets". This realization leads to the formulation of the "pocket model" of aluminum accumulation and agglomeration described in the following section.

TABLE 3.1. Summary of Aluminum Behavior in Composite Propellants at 400 psi (Nitrogen)

Oxidizer Size			15μ			90μ			200μ			600μ		
Aluminum Size			5μ	15μ	30μ	5μ	15μ	30μ	5μ	15μ	30μ	5μ	15μ	30μ
Polyurethane Binder	Aluminum Concentration	1%				A-93 M!				A-113 S! Fs0				
		2%				A-92 M!, Fs0								
		4%	A-82 M!, Fs0			A-83 Ss0 S!		A-38 Ss0, S!		A-60 Mm0, F!				
		8%	A-139 M! Fs0			A-91 Ss0, S!	A-140 Ss0, S!					A-142 Sℓℓ0		
		16%		A-51 M!, FsI		A-52 Mm0, F!	A-50 Mm0, F!	A-40 Sm0, MnI	A-117 Mℓ0, F!	A-49 Mℓ0, F!			A-107 Mℓℓ0, F!	
PBAA Binder	Aluminum Concentration	1%												
		2%												
		4%						A-73 Ssl, S!						

Notation: A - number is the propellant designation
! - original particle (burning)
I - irregular accumulate (non-burning)
0 - agglomerate (burning)

F - a few
S - some
M - many

s - small
m - medium
ℓ - large

TABLE 3.1. (Cont'd.)

Oxidizer Size			15μ			90μ			200μ			600μ		
Aluminum Size			5μ	15μ	30μ	5μ	15μ	30μ	5μ	15μ	30μ	5μ	15μ	30μ
PBAA Binder	Alumunum Concentration	8%												
		16%		A-55 M!, Fs0			A-54 Sm0, SmI,S!	A-47 MmI, F!		A-53 SℓI, S!				
Polysulfide Binder	Aluminum Concentration	1%		A-89 M!										
		2%												
		4%												
		8%												
		16%		A-88 M!, Ss0			A-57 Mm0, F!	A-45 Mm0, F!		A-64 Mℓ0				

Notation: A - number is the propellant designation
! - original particle (burning)
I - irregular accumulate (non-burning)
0 - agglomerate (burning)

F - a few
S - some
M - many

s - small
m - medium
ℓ - large

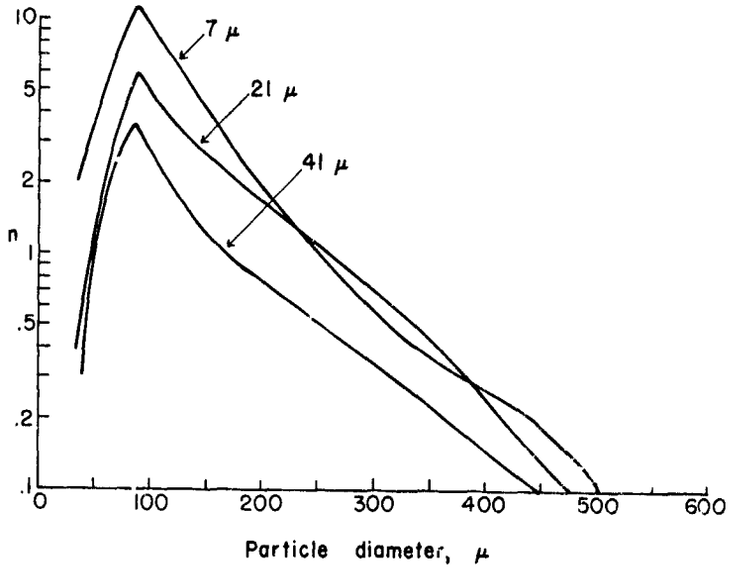

FIG. 3.6. Size Distribution of Aluminum Agglomerates for Three Propellants with Different Original Aluminum Particle Sizes.

3.4.1. Pocket Model

The essence of the pocket model is that for a propellant with a unimodal oxidizer blend, the size of an aluminum agglomerate is determined by the amount of the aluminum in the binder pocket.

The pocket model is depicted diagrammatically in Fig. 3.7. The left-hand portion of this figure shows the propellant at any particular time during burning. The pocket referred to is that large portion of the binder between the AP particles where the majority of aluminum is situated. As the oxidizer and the binder pyrolyze, the original aluminum is left behind and accumulates in the disappearing pocket, protected from ignition by its own oxide coating. This accumulation phase is shown in the center portion of the figure. The aluminum that accumulates is not laying loosely on the propellant surface. It is held reasonably well, perhaps by remnants of the decomposed binder or perhaps the particles are partially sintered together. The fact that it is held at the surface has been confirmed by photographing samples which were burned in the inverted position. After the accumulation period, if conditions are favorable for aluminum ignition, as mentioned in Section 3.1, a small portion of the aluminum, perhaps only one

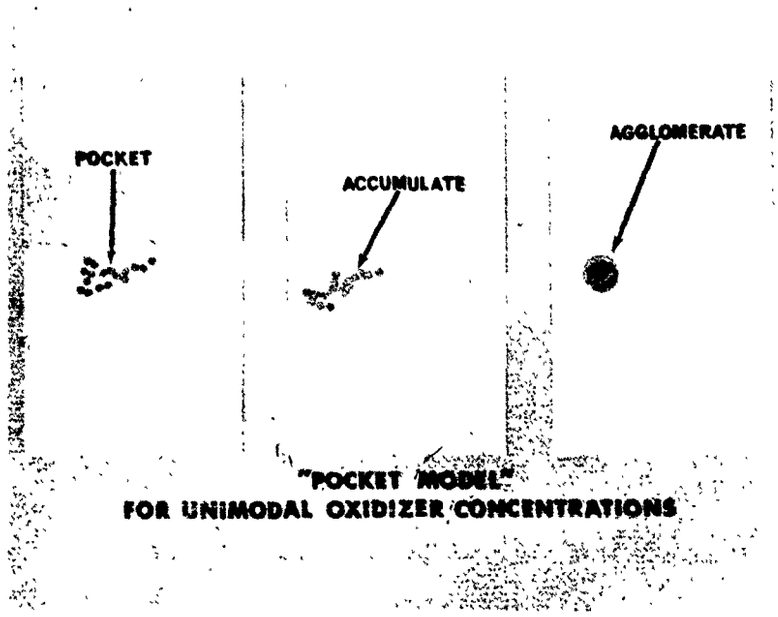

FIG. 3.7. Generalized Picture of the Cross-Section of Burning Composite Propellant.

or two of the original aluminum particles, ignites. This event is most likely to occur at a time when the underlying binder in the pocket is largely consumed and the accumulate is exposed more effectively to oxidizing gases. The heat from this small zone of burning aluminum generates a thermal wave which passes through the remaining portion of the accumulated aluminum and melts the rest of the accumulate. As shown on the right side of the figure, the entire mass then draws up into a spherical ball of molten aluminum which is burning vigorously and leaves the surface of the propellant.

If conditions are unfavorable for aluminum ignition, e.g., low pressure, low temperature and/or a deficiency of oxidizer, the accumulated aluminum will remain on the burning surface until it is undermined sufficiently due to the regression of the AP and binder. It will then leave the surface as an irregularly shaped accumulation of the original particles.

The appropriateness of the pocket model for describing the behavior of aluminum in composite propellants was investigated by formulating a systematic series of propellants and photographing them in a window bomb. The observations from the film on the aluminum behavior at 400 psi are summarized in Table 3.1. The pressure of 400 psi was felt to be a good compromise; it is high enough to be meaningful to rocket motor applications, yet it is low enough, in most cases, so that the combustion zone was far

enough away from the propellant surface so that many surface details could be seen. The trend of the aluminum behavior with pressure is described in Section 3.4.2.

In Table 3.1 the value of the propellant variables is listed for the propellant ingredients studied-AP particle size, aluminum particle size, aluminum concentration and binder type. Table 3.2 lists the sources of the ingredients. The binder level in all the propellants was 25% (which includes curing agent, stabilizer, etc.). The trends of aluminum behavior are recognizable in the table and are summarized below. The supporting evidence (the individual film clips) from which the observations were made are listed in Table 3.3 at the end of this chapter.

3.4.1.1. Effect of Ammonium Perchlorate Particle Size. In the framework of the pocket model, as the AP particle size is decreased, the volume of the binder pocket is decreased and the amount of aluminum in the pocket is decreased; hence, the size of the aluminum agglomerate is decreased. This is the trend of behavior that has been observed experimentally and noted in Table 3.1. As the AP size is decreased, the aluminum agglomerate size is decreased.

3.4.1.2. Effect of Original Aluminum Size. From the pocket model, changing the size of the original aluminum particles should not affect the size of the aluminum agglomerates because the agglomerate size depends only on the amount of aluminum in the pocket. This is the behavior that was observed experimentally; the size of the agglomerate is independent of the size of the original aluminum particles. However, an interesting aspect was quite evident from this series of tests. With the propellants in which the original aluminum particles were quite small, the ignition of the agglomerates occurred much more readily and closer to the propellant surface than those with larger original aluminum particle sizes. In fact, with the larger aluminum particle sizes, it is evident that a great number of the aluminum accumulates left the burning surface without igniting and forming the burning agglomerates within the camera field of view. Similar observations have been reported by Wood in Ref. 58.

3.4.1.3. Effect of Aluminum Concentration. According to the pocket model, as the aluminum concentration is decreased, the amount of aluminum in the binder pocket decreases and, hence, the size of the aluminum agglomerate decreases. This behavior was also qualitatively confirmed by the high speed motion pictures.

3.4.1.4. Effect of Binder Type. Since the pocket model is based only on geometry for the determination of the aluminum agglomerate size, the type of binder should have no affect on the agglomeration. With the three binders tested,[12] a polysulfide, a polyurethane, and a PBAN, there

[12] In this extensive series of systematically varied propellant compositions, the binder cencentration was held constant at the 25% level.

TABLE 3.2. Source of Propellant Ingredients

Ingredient	Source	Note
NH_4ClO_4, 600μ	American Potash & Chemical Corp.	
NH_4ClO_4, 200μ	"	Screened-60+100 mesh
NH_4ClO_4, 90μ.	"	
NH_4ClO_4, 15μ.	"	
Al, 30μ	Valley Metalurgical Processing Co.	H-30
Al, 15μ	"	H-15
Al, 5μ.	"	H-5
Al (dichromated), 5μ . .	"	H-5 (dichromated)
Al (dichromated), 15μ . .	"	H-15 (dichromated)
Copper Chromite	Harshaw Chemical Co.	Cu0202
Polyurethane Binder		
Estane	B. F. Goodrich Chemical Co.	
TMP.	Celanese Corp.	
1,4BD.	General Aniline & Film Corp.	
TEA.	Allied Chemical Corp.	
PBAN Binder		
PBAA-TER	American Synthetic Rubber Co.	
EPON 828	Shell Chemical Co.	
Polysulfide Binder		
LP-3	Thiokol Chemical Corp.	
GMF.	U. S. Rubber Corp.	
S.	(Reagent grade)	
Polybutadiene (CT) Binder		
Butarex CTLII	Phillips Petroleum Co.	
HX-868	Minnesota Mining & Mfg. Co.	
MAPO	Interchemical Corp.	
Fluorocarbon Binder		
Viton A	E. I. du Pont de Nemours & Co.	
Teflon	"	

was no significant difference in the aluminum accumulation. After the accumulation period, the usual spherical agglomerates were formed with the polysulfide and polyurethane binders; however, with the PBAN binder, the majority of the accumulates left the surface without igniting. The few spherical agglomerates that were formed from the accumulates, however, were the size that were consistent with the pocket model.

More recently, another series of systematically formulated propellants was initiated to investigate the details of the accumulation-shedding sequence. With the information gained from the extensive series (with 25% binder) and with the guidance of the pocket model, it was anticipated that this investigation of the detailed accumulation-shedding process could be accomplished without resorting to propellant formulations where mixing and casting might be a problem. Thus, the binder level was reduced to a more conventional 20%. This series was initiated by formulating five propellants containing 64% AP (200 μ), 16% aluminum 15 μ), and 20% of five different binders - a polyurethane, a PBAN, two carboxy-terminated polybutadiene binders with different cross linking agents, and a fluorocarbon binder.

The propellant with polyurethane binder[13] behaved in the typical pocket model manner; the combustion of a few original aluminum particles was observed along with the formation of many large spherical agglomerates. The aluminum agglomerate combustion appeared to be a little more vigorous than with 25% binder. The PBAN propellant[13] behaved in the typical PBAN fashion; only a few spherical agglomerates were formed and many irregular accumulates left the propellant surface unignited. Again, the aluminum combustion appeared more vigorous and a few more spherical agglomerates were formed than with 25% binder.

A very interesting effect was observed with the two carboxy-terminated polybutadiene binders[13] using different cross-linking agents. The propellant utilizing HX-868 was very similar to the PBAN propellant (above) a few spherical agglomerates, many irregular accumulates, and many original aluminum particles were observed. The propellant utilizing MAPO was very similar to the polyurethane propellant (above). Thus, very notable differences were observed in the aluminum behavior when only the binder cross-linking agent was changed. This raises the possibility that the aluminum accumulation-shedding process can be modified beneficially by appropriate manipulation of the binder.

The fifth binder in this series was a fluorocarbon.[13] The aluminum agglomerate size in this situation was less than half the size that would have been produced according to the pocket model. The different decomposition products from this binder system undoubtedly account for the deviation of the agglomerate size from the pocket model. This

[13]The propellant designations and representative film clips are tabulated in Table 3.3.

result again emphasizes the role the binder chemistry can play in the behavior of the aluminum.

3.4.2. Pressure Effect

It has been experimentally observed that with all the polysulfide and polyurethane propellants and with the majority of PBAN propellants, the aluminum agglomerates conform in size to the pocket model at pressures above 100 psi, i.e., pressure has no significant effect on determining the size of the agglomerate.

At lower pressures with the polysulfide[13] and polyurethane[13] propellants and the majority of the PBAN propellants,[13] the aluminum is more reluctant to ignite. Since the ignition of the aluminum accumulate can play a significant role in the aluminum shedding process and since the aluminum ignition does not occur readily, the aluminum accumulates to a greater extent on the surface than at higher pressures. The accumulate can consist of aluminum from several binder pockets and if it does manage to ignite, it will form a large agglomerate. The more likely situation is that it will not ignite at the surface and will leave as a non-burning irregular mass when it is sufficiently undermined by the regression of the AP and binder. Ignition may or may not occur in the combustion volume, depending on stay time, temperature and oxidizer concentration.

3.4.3. Other Effects

It was noted in Section 3.1 that with the PBAN binder propellants, the aluminum accumulates formed according to the pocket model but the majority of them did not ignite even at the higher pressures. This lack of ignition is believed to be due to an extra deficiency of oxygen in this propellant system as compared to the polyurethane. For propellants in this series (25% binder), the PBAN system has approximately one-third less oxygen in the binder than the polyurethane system. This point of oxygen deficiency as the cause of non-ignition of the aluminum accumulates has not been definitely established; however, a comparable PBAN propellant[13] with only 20% binder showed a noticeable increase in aluminum accumulate ignition.

Another interesting effect was noticed with the PBAN propellants under rather restricted conditions[13] of propellant composition and pressure. At 200 psi and below and when the aluminum particle size and AP particle size were near the same size (15μ aluminum and 15μ and 80μ AP), the aluminum accumulated to a larger extent than was consistent with the pocket model and as described under paragraph 3.4.2. In addition to this large accumulation, the accumulate, in general, would start to glow red

in a localized spot when a portion of it extended significantly out into the gas. The localized red glow spread throughout the remaining accumulate and the accumulated mass would "float" away from the burning surface. The irregularly-shaped mass in general did not draw up into the usual spherical, molten agglomerate but its luminosity indicated that it was being oxidized. It should be emphasized that this sequence of events occurred only under specific combinations of pressure and aluminum and AP particle sizes with PBAN binder. The behavior appeared to be a limiting situation where self-heating of the accumulate was at a rate insufficient to produce melting of the accumulate.

From some scattered results on propellants from development programs, there was an indication that the addition of copper chromite might greatly reduce the accumulation of aluminum and size of the resulting aluminum agglomerate. To pursue this point, six propellants were formulated and burned. The propellants were variations of members of the original systematic family; one set was with the polyurethane binder with 0.50%, 1% and 2% copper chromite, and the other was with PBAN binder with the same copper chromite percentages. The results[13] with the polyurethane propellants were that the copper chromite at all three concentrations had no noticeable effect on the aluminum accumulation and agglomeration. With the PBAN propellants, as the copper chromite concentration was increased, the number of original aluminum particles that ignited was decreased and the number of aluminum accumulates that ignited and formed spherical agglomerates increased. The most significant change was that many of the aluminum accumulates which formerly left the surface unignited made the transition to the spherical burning agglomerate when copper chromite was added.

From the favorable results with the fluorocarbon binder in Section 3.4.1.4, it appeared desirable to test what effect a fluorocarbon coating on the original aluminum particles would have on the aluminum agglomeration. A propellant was formulated which had five micron aluminum particles coated with 0.9% Viton A. A comparison of the photographic results[13] of the coated versus uncoated aluminum showed that the resulting aluminum agglomerates were essentially the same size regardless of coating; the only noticeable difference was that with the original fluorocarbon coated aluminized propellant, the aluminum agglomerates appeared to be surrounded by a brighter, more vigorous diffusion flame than were the agglomerates from the uncoated aluminum.

Because the ignition of aluminum is retarded by the aluminum oxide coating on the aluminum particles, the effect of changing the oxide coating was investigated by using dichromated aluminum particles. A comparison of the photographic results[13] of the dichromated versus the untreated aluminum particles showed that the aluminum agglomerates from the dichromated aluminum were approximately three-quarters of the size

of those arising from the untreated aluminum. Also, the ignition of the agglomerates occurred closer to the propellant surface with the dichromated aluminum. A more extensive study of the effect of dichromated aluminum in double-base propellants has been made in Ref. 59. Their results indicated a definite decrease in aluminum agglomerate size as the amount of coating was increased.

3.4.4. Results with Polymodal Oxidizer Propellants

Tests have also been made on 24 composite propellants from motor development programs or service motors. These propellants had bi-, tri-, or tetramodal oxidizer blends and high solids loading. The aluminum in these propellants[13] behaved in a very similar way to that described above; the aluminum accumulated on the surface and agglomerate sizes on the order of 100 to 300 microns in diameter were formed. These sizes are of the same order as those observed with the unimodal oxidizer propellants; however, since the binder pockets are not well defined with the polymodal oxidizer distributions, the agglomerate size cannot be correlated by the pocket model.

3.4.5. Results with Double-Base Propellants

A limited number of photographic tests have been made with aluminized double-base propellants. In tests with extruded double-base propellants, aluminum agglomerates in the range of 100 to 300 microns in diameter have been observed. The aluminum accumulates on the burning surface and at 800 psi the aluminum ignites and forms spherical burning agglomerates at the burning surface. At lower pressures, the aluminum accumulates leave the surface unignited; they generally ignite in the gas phase above the surface; the resulting agglomerate is larger than that observed at higher pressures. Similar observations have been made with composite-modified double-base propellants.[13]

3.5. SUMMARY AND CONCLUSIONS

The general picture of the behavior of aluminum in solid propellants that has emerged from these studies is that the aluminum is very reluctant to ignite as the propellant combustion wave passes through the aluminum-containing regions. In general, the aluminum is left behind and accumulates on the surface of the propellant as the AP and binder pyrolize. After the accumulation period, the aluminum ignites and forms large, vigorously burning spherical balls if conditions are favorable. If conditions are unfavorable, e.g., insufficient oxidizer, low pressure and/or low temperature, the aluminum will remain on the surface until it is sufficiently undermined; then it will be released into the gas phase as an irregularly-shaped, unignited mass.

For the case of composite propellants with unimodal oxidizer distributions and conventional hydrocarbon binders, the aluminum accumulation and shedding processes can be correlated by the pocket model. The main thesis of the pocket model is that the size of the aluminum agglomerate formed from the accumulate is determined by the amount of aluminum that is contained in the binder pocket. The experimental observations which have been correlated by the model are:

1. The agglomerate size is determined by the pocket size, and hence by the AP size.

2. The agglomerate size is independent of the size of the original aluminum particles.

3. The agglomerate size decreases as the aluminum concentration decreases.

4. The aluminum accumulation is essentially unchanged by the polyurethane, PBAN, and polysulfide binders; however, there are indications that other binders (such as a fluorocarbon) may greatly reduce aluminum accumulation.

The process of aluminum accumulation is perhaps the most important aspect of the steady-state combustion of aluminized propellants that has been encountered in this investigation. The size and the state that the agglomerate is in when it is released into the gas phase is determined by the geometry of the matrix in which it is originally held. The preignition environment of the aluminum predetermines the state in which the aluminum will enter the gas phase. It appears that any attempts to improve the efficiency of aluminum combustion in rocket motors should be concentrated first on understanding the details of the accumulation process and, secondly, on devising means to reduce the accumulation tendency or to cause the original aluminum particles to ignite during the very early stages of accumulation. Once the accumulate has ignited and formed the agglomerate, there is very little that can be done to influence the subsequent combustion of the large aluminum droplets.

TABLE 3.3. Photographic Supporting Evidence

Aspect of behavior	Location	Propellant	(Note)	Film Designation
Pocket model	Table 3.1	A-38	400 psi	21 Dec 1966 #1
		A-40		15 Mar 1966 #5
		A-45		21 Dec 1966 #2
		A-47		11 Aug 1966 #6
		A-49		12 May 1966 #1
		A-50		18 Aug 1966 #6
		A-51		31 Aug 1966 #5
		A-52		19 Aug 1966 #2
		A-53		2 Sep 1966 #5
		A-54		16 Apr 1966 #11
		A-55		23 Dec 1964 #2
		A-57		4 Aug 1966 #2
		A-60		10 Sep 1966 #3
		A-64		19 Aug 1966 #4
		A-73		21 Dec 1966 #3
		A-82		21 Sep 1966 #10
		A-83		8 Apr 1965 #8
		A-88		10 Sep 1965 #10
		A-89		12 Jan 1965 #5
		A-91		8 Mar 1966 #6
		A-92		8 Apr 1965 #10
		A-93		24 Aug 1965 #12
		A-107		12 Jan 1966 #4
		A-113		10 Sep 1965 #6
		A-117		11 Aug 1966 #2
		A-139		26 Aug 1966 #9
		A-140		26 Aug 1966 #13
		A-142		31 Aug 1966 #1
Binder type (20%)	Sect. 3.4.1.4	A-123	Polyurethane	24 Jan 1966 #5
		A-124	PBAN	21 Jan 1966 #9
		A-134	CT-PB W/HX-868	1 Jun 1966 #5
		A-137	CT-PB W/MAPO	26 Aug 1966 #3
		PL-6866	Fluorocarbon	17 Aug 1966 #10

Low pressure effect	Sect. 3.4.2	A-107	400 psi, polyurethane	23 Feb 1966 #10
		A-107	100 psi, polyurethane	8 Feb 1966 #1
		A-49	400 psi, polyurethane	6 Dec 1965 #2
		A-49	100 psi, polyurethane	6 Dec 1965 #1
		A-53	400 psi, PBAN	6 Dec 1965 #5
		A-53	100 psi, PBAN	6 Dec 1965 #4
		A-64	400 psi, polysulfide	19 Aug 1966 #4
		A-64	100 psi, polysulfide	16 Apr 1965 #8
PBAN binder (oxygen effect)	Sect. 3.4.3	A-53	25% binder	2 Sep 1966 #5
		A-124	20% binder	21 Jan 1966 #9
PBAN binder (small particles)	Sect. 3.4.3	A-55	100 psi	10 Sep 1965 #12
		A-55	200 psi	10 Sep 1965 #13
		A-54	100 psi	16 Apr 1965 #9
Copper chromite effect	Sect. 3.4.3	A-125	1/2% CuO 202, PU	1 Mar 1966 #9
		A-126	1% CuO 202, PU	1 Mar 1966 #11
		A-127	2% CuO 202, PU	1 Mar 1966 #13
		A-128	1/2% CuO 202, PBAN	1 Mar 1966 #15
		A-129	1% CuO 202, PBAN	1 Mar 1966 #17
		A-130	2% CuO 202, PBAN	1 Mar 1966 #19
Fluorocarbon-coated Al	Sect. 3.4.3	A-117	Uncoated Al	11 Aug 1966 #2
		A-143	Viton-coated Al	16 Aug 1966 #14
Dichromated Al	Sect. 3.4.3	A-49	Untreated Al	5 Nov 1964 #4 (split frame)
		A-85	Dichromated Al	5 Nov 1964 #4 (split frame)
Polymodal oxidizer	Sect. 3.4.4	-	Aerojet	19 Jan 1966 #2
		-	Rocketdyne	9 Jul 1965 #2
		-	Thiokol	16 Mar 1965 #12
Double-base propellants	Sect. 3.4.5	-	NOTS DB, 5% Al	19 Aug 1966 #9
		-	NOTS DB, 10% Al	19 Aug 1966 #11
		-	Hercules CMDB	21 Sep 1966 #2
		-	Hercules CMDB	11 Oct 1965 #1

4. COMBUSTION OSCILLATIONS

The principal motivation of the present combustion research program was the problem of oscillatory combustion, with particular emphasis on low frequency oscillations. The balance of this report is concerned primarily with this problem. The present section is devoted to a discussion of observed combustion oscillations, while subsequent sections are devoted to considerations of combustor stability, experimental studies of stability, and propellant variables affecting stability.

4.1. TRANSIENT COMBUSTION

While the status of analytical models of transient combustion of solid propellants is very unsatisfactory insofar as accuracy of representation of the physio-chemical processes is concerned, the qualitative nature of such combustion can be inferred with reasonable certainty. Before the present work began, it was generally recognized that the accommodation of the thermal wave in the solid would be a major factor in determining the low frequency transient combustion behavior, but it was suspected (Ref. 5) that the accumulation-agglomeration-ignition-combustion sequence of powdered metal ingredients would also be important at low frequency. It was for this reason that the work in Section 3 was pursued in such detail.

Considerable effort has been devoted by various investigators to the analytical representation of transient combustion (Ref. 60-64). The result of these efforts is a somewhat bewildering array of analytical models that are, (1) very complicated, and (2) unrealistic representations of the real physical phenomena. The principal value of these analyses is their contribution to physical insight and to determination of what future improvement in analytical models and experiments is most appropriate. On the present program, a critical review of all analytical models has been made, with the objective of reducing all analyses to the same notation, classification of the models according to their assumptions, comparing the predictions and validity of the different models, and establishing a more general model in which the existing ones are special cases. This permits a more methodical development of the body of theory in the future, as well as increasing the usefulness of present theory. This theoretical work is reported in Appendix A (See also Ref. 65 and 66), and shows that the various published theories are not conspicuously different when reduced to the same notation, and the differences are generally identifiable with the nature of the assumptions in the models. In the low frequency range, it is seen that the thermal wave accommodation dominates

the frequency dependence of the combustion response to pressure perturbations, with the site of the exothermic reaction being important in determining the magnitude of the combustion response. In general, it can be said that analytical models provide a useful framework in which to discuss the role of thermal wave accommodation in low frequency oscillatory combustion, but provide no basis whatsoever for treatment of the metal combustion sequence, more generally, or for the contributions of any process arising from chemical or physical heterogeneity of the propellant. Much of the following discussion will be concerned with phenomena which are a consequence of heterogeneity.

4.1.1. Character of the Combustion Zone

Figure 1.2 shows a somewhat idealized representation of the character of the combustion zone, showing the relative dimensions of heterogeneities and the thermal wave under rocket motor conditions. The details are known to be dependent on environmental conditions, propellant composition, and particle sizes in a very complicated way, so that generalizations are risky. With composite ammonium perchlorate-aluminum propellants, the accumulated metal is known to be loosely attached to the propellant surface, and is less in evidence when gas flow parallel to the burning surface ("erosive" flow) is present. Likewise, the surface tends to be smoother in the presence of parallel flow. It is also known that more extensive accumulation of aluminum occurs at low pressure with accumulation involving interconnection of the "pocket" accumulates described in the last section. It is seen in photography of quenching by rapid depressurization that a substantial portion of the accumulated aluminum is removed by the pressure transient, indicating the responsiveness to perturbations.

Combustion of the metal is an extremely complicated process in itself. In the case of aluminum, the original particles are coated with a layer, probably mostly Al_2O_3, which tends to impede ignition of the particle. An accumulated mass of such particles apparently continues to oxidize slowly on the surface of the propellant, but it is not known under what conditions this oxidation is a competitive source of heat. The propellant surface temperature is usually slightly below the melting point of aluminum, but the heat flux from the diffusion flame (and possibly from aluminum oxidation) eventually breaks down the irregular accumulate to produce a spherical droplet. The oxide on the surface of the droplet draws up into a "cap" (Fig. 4.1) on the droplet, and the exposed aluminum evaporates to react in a flame envelope around the exposed part of the droplet. The time sequence of events is not resolved, in that visible melting, ignition, and detachment from the surface all occur together.

When an aluminum droplet leaves the surface, it burns for an appreciable time as it moves away from the surface (Fig. 4.2). Thus, the region above the surface contains a cloud of burning droplets which is

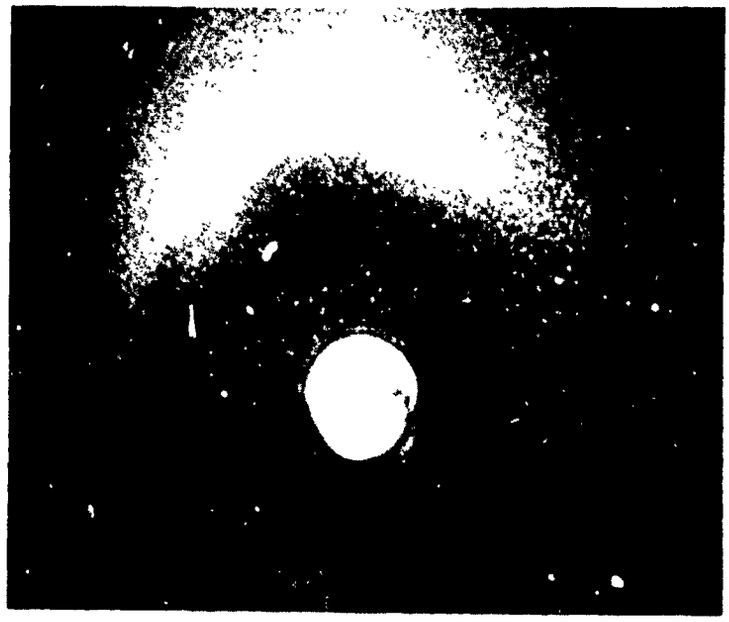

FIG. 4.1. Quenched Aluminum Particle Showing Oxide "Cap".

FIG. 4.2. Cloud of Burning Aluminum Droplets Above Surface of Propellant; Average Droplet Diameter is Approximately 200 Microns.

much thicker than the normal binder-AP diffusion flame region. It is difficult to clearly observe this cloud because it consists also of extremely fine (e.g., 1 micron) droplets of Al_2O_3 smoke. However, the available evidence is quite decisive in establishing that this aluminum combustion field is typically on the order of one-inch in thickness, being greater at low pressure (see, for example, Section 6.4). The reaction rate is presumably dependent on oxidizer concentration, temperature of the surrounding field, and especially on the number and size of the droplets present.

4.1.2. Meaning of Combustion Rate

In steady-state burning of solid propellants the "burning rate" is the linear regression rate of the burning surface, or the corresponding mass burning rate per unit surface area. All ingredients are consumed at a rate proportional to the product of the linear burning rate and the weight fraction of the ingredient in the propellant. Since the decomposition-combustion characteristics of the ingredients differ widely, the burning surface is characterized by higher than average concentrations of ingredients that are not readily vaporized - this higher concentration being necessary to support the steady-state rate in the face of low susceptibility to vaporization. Such ingredients also tend to acquire relatively high temperatures at the surface. These accommodations, essential to existence of steady-state burning, assure that the combustion rates of ingredients will be in ratio to their concentration in the propellant.

This situation does not apply in transient combustion, where the relative combustion rates of the ingredients may oscillate in response to environmental oscillations. In such a situation, what is meant by oscillations in combustion rate? The answer surely depends upon the problem, or the method of observation. Even in the case where the problem is chosen, there is no unequivocal choice of a definition of combustion rate. Physically, the concern is with the fluctuation in work done on the propellant product gas field when the propellant expands from a solid to hot gaseous products. The expansion occurs first with gasification, and further as temperatures rise with further reaction. The complexity of this is particularly notable in connection with aluminum combustion, where the aluminum liquid proceeds to a reaction with gaseous oxidizing species to form a liquid product (Al_2O_3). The expansion results from the temperature rise in the remaining gas. With these and other combustion processes all going on at once, it seems clear that they will not all oscillate in the same way under any given oscillating environmental conditions. Insofar as expansion work on the flow field is concerned, "combustion oscillations" may sometimes be due primarily to the fluctuation in only one aspect of the combustion, and the concept of combustion rate might consequently be applied to that aspect. In any case, the fluctuation in rate of different steps in the combustion may proceed in

differing degree and phase, and care must be exercised in describing combustion rate or relating it to any given type of experimental observation.

4.1.3. Time Constants of Reactions

The amplitude and phase of the oscillation of the unit processes of combustion relative to incident environmental oscillations are determined by the vulnerability of the unit process to the environmental oscillations and by compatibility of their own rate processes with the rates of change involved in the environmental oscillations. Fast reactions such as gas phase flames will be in equilibrium except at high frequency, and will oscillate only because slower reactions supplying reactants to the flame are oscillating. For example, the mass combustion rate of aluminum in propellants will oscillate at low frequency according to the slowly responding process of surface accumulation and shedding of aluminum droplets that control the population of the droplet cloud. At high frequency the population of the cloud is not able to respond because of the slowness of the consumption and replacement of droplets. On the other hand, the "fast response" flame region around individual aluminum droplets may respond significantly at high frequency because response is possible without dependence on replenishment of the supply of droplets between cycles of oscillation.

As suggested above, there are two aspects of the combustion wave that have time responses of the same order as the period of oscillation at low frequency. One is the metal accumulation-combustion sequence discussed above and in Section 3, and the other is the thermal wave in the solid. The latter is fairly well represented in some one-dimensional transient combustion models (Appendix A), which leaves no room for doubt about the role of thermal wave accommodation to flame and environmental oscillations as a major factor in combustion response at low frequency. This is reflected in the calculated dependence of the response of combustion rate on frequency of incident pressure oscillations, illustrated in Fig. 4.3. The curve was calculated using the model of Denison and Baum. The quantity on the left ordinate represents the real part of the response of the burning rate oscillations relative to the pressure oscillations, and the quantity $\omega\tau$ is the phase between these two. The maximum response occurs at a period of oscillation approximately equal to the characteristic time of the thermal wave,

$$T \simeq (2\pi/9)\tau_{t\omega} = (2\pi/9)(\lambda/\rho C r^2)$$

$$\simeq 2 \times 10^{-4}/r^2$$

where the last expression is for $\lambda/\rho C = 3 \times 10^{-4}$ in.^{2}/sec and r is in inches per second, typically 0.2 in/sec. Thus, the most unstable domain

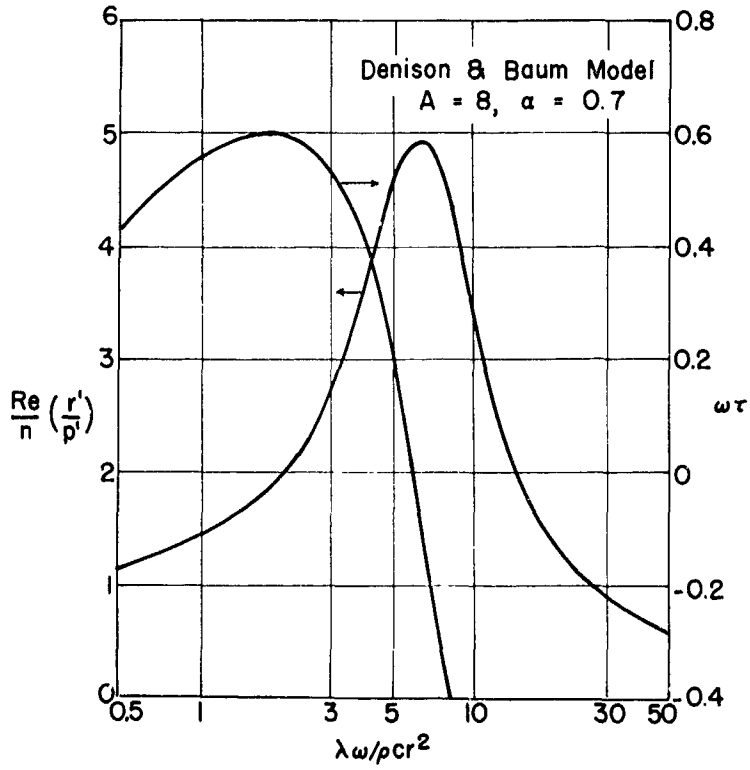

FIG. 4.3. Response and Phase of Combustion Relative to Pressure.

is at a frequency in the vicinity 200 cps. This is attributed to thermal wave accommodation because the Denison and Baum model used here assumes all other combustion steps are in quasi steady-state.

4.1.4. Spontaneous and Phase Coupled Oscillations

Published theories of combustion dynamics are generally concerned with the nature of combustion perturbations resulting from incident environmental perturbations, i.e., concerned with coupled oscillations. The implication is that no combustion oscillations occur when the environment is steady. The coupled oscillations are typically described by the response function (Sections 5 and 6; Appendix A).

It has been suggested (Ref. 5) that under some conditions, combustion will oscillate even in a stagnant atmosphere. Such behavior is described later in this section and it is clearly evident in combustion of solid pellets made by pressing powdered mixes of AP and aluminum. The periodicity arises from the tendency of the aluminum to accumulate without igniting, and then ignite, detach from the surface, and burn. This sequence repeats with a frequency that is dependent on the burning

rate of the solid. One might assume that a combustion chamber containing such a "propellant" would surely be unstable, especially if the frequency of the spontaneous oscillation matched the natural frequency of a suitably oriented acoustic mode of the combustor. However, the usual stability analysis based on coupled oscillations is inapplicable to the situation where spontaneous oscillations of finite amplitude occur without coupling, and the concept of a response function is inapplicable. Thus, a different approach to the question of stability must be pursued.

In trying to describe the behavior of combustors with spontaneously oscillating propellants, it is necessary to consider the question of whether the spontaneous oscillations will be substantially in phase over large areas of the propellant. If such a "phase correlation" does not occur, no organized combustor oscillations will occur even if the combustion and combustor mode frequencies match. Instead, different locations on the burning surface will oscillate with the same frequency but randomly related phase, with no net effect on acoustic mode oscillations. Such a situation is actually hard to visualize, because it seems likely that there would be some interaction among the sites of combustion oscillation that could, at least in a statistical sense, produce some phase correlation. Indeed, it seems likely that the spontaneous combustion oscillations are always in some measure responsive to acoustic disturbances, even though not completely dependent on such coupling. If such is the case, there would be a tendency for spontaneous oscillations at various locations on the burning surface to be drawn into phase by coupling with the acoustic oscillations - leading to growing gas oscillations somewhat similar to the more conventional amplitude-coupled oscillations. The most distinctive attribute of such phase-coupled instability would be its tendency to occur only over a narrow frequency range centering on the frequency of the uncoupled spontaneous oscillations. This "preferred frequency" attribute is indeed observed in combustor tests using "propellants" made from AP-aluminum powder mixes. What is more significant, this "preferred-frequency" attribute is also evident in combustor tests with conventional propellants having significant aluminum content, suggesting that the aluminum accumulation-combustion sequence is locally periodic and sufficiently coupled to produce phase correlation in propellant-combustion - at least in a statistical sense. Because of the difficulty of making direct observations of such a combustion behavior, it has to date been established only on a speculative basis supported by the instability behavior of combustors, the decisively demonstrated oscillatory behavior of AP-Al pellets, and supporting mechanistic arguments.

The important points of the foregoing arguments are not speculative. It has been demonstrated that the combustion behavior of unmetalized propellants is not spontaneously oscillatory; also, combustion of AP-Al pellets is typically spontaneously oscillatory. As will be seen in the following, the spontaneously oscillatory behavior of AP-Al pellets does couple with pressure oscillations, permitting preferred-frequency, phase-coupled instability. It is not obvious that aluminized propellants exhibit spontaneously oscillatory behavior in the microscopic sense, but

the microstructure permits intermittent metal combustion at local surface sites, the instability exhibits a preferred frequency character in unstable combustors, and the metal combustion is seen to be oscillatory in unstable combustors.

4.1.5. Amplitude-Coupled Combustion Oscillations

Returning to the more conventional concept of combustion oscillations induced by environmental oscillations, it has become customary to characterize such combustion behavior by a single parameter such as the response function or acoustic admittance of the combustion zone. A number of difficulties have arisen in this connection, some of which are not yet resolved. What is required is a description of the flow of acoustic energy into the combustor as a consequence of combustion oscillations. This has proven to be difficult in two respects. First, the status of both theory and experiment regarding acoustic energy in systems like combustors with gas throughflow is only marginally adequate for qualitative work, and neither the response function or acoustic admittance is an adequate measure of acoustic energy input (Ref. 65, Appendix A), even under conditions where these quantities are well defined. Second, the aspects of the acoustic environment that affect combustion are more complicated than the one-dimensional interaction on which the response function-admittance concepts are based. The combustion zone is exposed to three-dimensional interaction with the acoustic field. At the very least, the interaction must be viewed in terms of components of gas oscillations perpendicular to the burning surface (pressure coupling) and parallel to the burning surface (velocity coupling). In the present program only limited attention has been devoted to velocity coupling (Ref. 67 - 69), primarily because, (a) it is very difficult to study, and (b) its involvement in low frequency instability seems to be less important than pressure coupling.

In later sections of this report, heavy reliance is placed on analytical models of pressure-coupled combustion oscillations - models in which the thermal wave accommodation is the principal transient aspect of the phenomenon. The role of the metal combustion cycle has not been explored analytically and indeed the relative importance of thermal wave and the metal combustion cycle has not yet been determined.

4.2. EXPERIMENTAL OBSERVATION OF COMBUSTION OSCILLATIONS

Ideally, observation of combustion oscillations would consist of space-time resolved measurement of composition and temperature profiles, etc., in the combustion zone. Because of the difficulty in making such measurements, inferences have been made by observation of pressure oscillations, spatially unresolved radiation oscillations, or motion pictures. These procedures have all been used in the present program.

4.2.1. Motion Pictures of Combustion

In Section 3.2, high speed photographic methods were described which permitted observation of the combustion zone in considerable detail during burning. These methods were applied also to transient combustion, and the results will be described in a later section. Here, attention will be directed to the nature of the phenomenon to be photographed, and the difficulties encountered.

Recalling the dimensions of the combustion zone, it should be noted that, even under the best viewing conditions, the smallest structure of the combustion zone is near the limit of resolvability by optical methods (e.g., the one-micron Al_2O_3 droplets). The viewing conditions in a combustion bomb are not the best, and resolution is ordinarily limited to, at best, 10 microns and larger. Further, the depth of field at high magnification is very limited; it is much smaller than the dimensions of the propellant sample - or under some conditions even smaller than the largest particulate structure of the ingredients. There is difficulty in observing self-luminous behavior in the focal plane when similar processes are proceeding also along the line of sight in out-of-focus regions. Further, the most significant processes in the combustion zone are not necessarily self-luminous, and external illumination may be required for photography. This is practical only in regions free from smoke, typically in regions close to the burning surface and in close proximity to the edge of the propellant.

As a result of these limitations to viewing the combustion, prints of individual frames of motion pictures are not very decisive, and the interpretation depends heavily on the motion and color provided by the pictures. Photography of unmetalized propellants usually shows only weak self-luminosity in the form of dull orange streamers or streaks, due in all probability to hot carbon and/or impurities. When external illumination is used, the details of the burning surface are partially resolved, however, the optical contrast between binder and oxidizer is not particularly good, so that no quantitative data has been sought from such pictures.

Motion pictures of metalized propellants ordinarily show a dense cloud of smoke, with brilliantly burning metal droplets seen diffusely through the smoke cloud, for some distance above the burning surface. Available information indicates that the normal extent of this metal combustion-smoke cloud would not be visible in the window bomb, because the flushing flow required to prevent smoke accumulation interacts with the combustion cloud everywhere except near the burning surface. Under conditions of low smoke concentration it is feasible to use external illumination. The accumulation and mobility of metal on the surface, as well as details of the detached metal agglomerates not visible by self-luminosity, can then be seen. In these low density clouds, determination of metal droplet number and size is possible when the droplets are large enough (e.g., 40 microns and up). The small, original metal particles (such as those ordinarily used as the propellant ingredient) which do not

agglomerate into larger spheres, usually move and burn so rapidly that, even at 4000 frames per second, motion pictures show only blurred, elongated images lasting for one or two frames. These fine particles (5-20 microns) are below the optical resolution limit, and are probably surrounded by a glowing smoke cloud, so no detailed data is provided other than a count.

In the present studies, motion pictures were taken of unmetalized propellants, propellants with various powdered metals (primarily aluminum), and pressed pellets of AP, Al, and various ballistic modifiers. Only a limited amount of photography was carried out under oscillating conditions, which will be described in Section 4.4.

4.2.2. Photoelectric Observation

Radiation from the combustion zone can be easily monitored by photoelectric detectors, and extensive observations have been made in both the window bomb and the unstable burners used in this program. Recognizing the results of the motion pictures, it is clear that some care must be exerted in obtaining and interpreting radiation measurements, including consideration of "seeing" conditions, identification and control of the field of view of the detector, identification of the light wavelength response region of the detector, etc. In general, the spatial resolution of observations to date has been poor compared to the dimensions of the oxidizer-binder diffusion flame region, but good compared to the metal combustion field. However, smoke obscuration is a major factor in most of the combustion field with aluminized propellants.

When viewing the combustion of aluminized propellants photoelectrically, the principal source of radiation is the aluminum oxide smoke that is still near enough to aluminum particles to experience sustained heating by heterogeneous reaction. This smoke is at a temperature near the dissociation temperature of Al_2O_3 (Ref. 70), which is around 3800°K. The oxide smoke outside this reaction region is more nearly at the equilibrium temperature of the propellant products, around 3100°K. Considering the fourth power dependence of radiation on temperature, the photoelectric detector will "see" the hotter aluminum oxide smoke closely associated with the aluminum particles. As a result, the radiation records reflect the passage of burning aluminum droplets through the field of view, presumably those droplets nearest the detector-side of the combustion cloud when the smoke is dense. As the field of view is narrowed, radiation records become more ragged, reflecting an integration of radiation over a smaller number of burning droplets in the field; there is also a correspondingly larger fluctuation in radiation about the time average (See Section 6.4). Likewise, the fluctuation becomes greater far from the burning surface because of the lower number of burning droplets present, and the apparent reduction in number of droplets due to smoke obscuration of all droplets except those in the foreground of the combustion volume. These observations are not only important in interpreting results relative to combustion oscillations (which will be

presented in Section 4.4), but are part of the evidence supporting the picture of the aluminum combustion cloud described here.

4.2.3. Observation of Combustion Oscillations by Pressure Oscillations

Ultimately, our concern with combustion oscillations arises from their production of flow oscillations in the combustor. Thus, it is not surprising that a major part of all studies of combustion oscillations has been done by observing pressure oscillations in unstable combustors. Sections 5 and 6 of this report describe extensive studies of such combustor oscillations. While pressure is perhaps the most easily measured perturbation variable, its relation to the combustion oscillations depends upon consideration of the combustor variables and mean flow field, and interpretation of pressure records in terms of details of the combustion process is exceedingly difficult. Consolation for this weakness is found in the fact that pressure measurement focuses attention on those aspects of the combustion that are relevant to instability, but the difficulties of interpretation remain profound.

In early work on this program, efforts were directed at development of combustors that would demonstrate low frequency instability without use of large amounts of propellant; two types of burners were developed. The nonacoustic burner (Section 5; also, Ref. 5 and 15) was developed and exploited as a low cost means of testing, and the previous reports described comparison of behavior of various propellants in such burners. Results were reported primarily in terms of effect of propellant, mean pressure, and combustor variables on frequency of oscillation, with some observations of severity of oscillation. Behavior in this type of combustor has been observed to be highly dependent on combustor geometry, so the trend of instability behavior with propellant variables could not be assessed until some overall model of combustor instability was available to separate the propellant effects from the combustor effects. (This was one of the accomplishments during the present reporting period and is reported in Section 5 and Ref. 15.) Once a stability model is available, the pressure records from tests can be measured to obtain not only frequency, but the rate of growth of oscillations. These quantities can then be used to calculate the acoustic response of the combustion zone, and the role of different combustion steps can be explored by testing the effect of changing propellant variables. Substantial progress has been made along these lines in the present reporting period (See Section 5).

A second burner developed for production and study of combustion oscillations was the double-ended, center-vented (DECEV) burner in lengths up to 60 feet or so (Section 6; Ref. 4 and 5). With propellants located at each end, such burners oscillate at frequencies from 5 cps and up. Early work was concerned with determining the range of frequency, pressure, and propellant variables that would produce instability. Considerable effort was required to obtain controlled behavior

(ignition, steady pressure, etc.) in order to carry out systematic studies and obtain meaningful quantitative measures of pressure oscillations. As in the case of the non-acoustic burner, work during the present reporting period has provided sufficiently good control of tests to permit measurement of the growth rate of pressure oscillations and interpret this growth rate as a quantitative attribute of coupled combustion oscillations. This particular test method is more versatile than the non-acoustic burner in that it will exhibit instability over a wider range of conditions of interest than will the nonacoustic burner; but the test apparatus, propellant and manpower requirements are much greater.

It should be emphasized that study of propellant combustion dynamics by observation of combustor pressure oscillations is strictly a "black-box" approach, i.e., it tells little in detail about the mechanisms involved but does concentrate on the relevant end-product. Mechanistic interpretation of results is dependent on systematic testing involving systematic adjustment of the "unlabeled, uncalibrated" control knobs on the black-box (knobs representing mean pressure, oscillation frequency, propellant variables, etc.). Progress is highly dependent on the development and application of mechanistic models of combustion dynamics and comparison of prediction of stability behavior from the models with experimental results. Work reported earlier on this program was directed towards development of a background of stability behavior sufficient to guide formulation of models. The present work, providing more systematic and reproducible data, is now being compared with relevant combustion models as a basis for selection of models.

4.3. SPONTANEOUS COMBUSTION OSCILLATIONS

In order to study the hypothesis that some propellants might burn at their own "preferred" frequency even in the absence of an oscillatory environment, tests were made on many formulations in a constant-pressure window bomb. Observations were made primarily by photoelectric monitoring of flame radiation, although some motion pictures were taken. Previously reported work (Ref. 5 - 7) had shown that spontaneously oscillating combustion occurred when samples of pressed AP-aluminum powder were burned, and it was suspected that a similar tendency might exist also for aluminized propellants under some conditions. The purpose of the experimental work was to determine whether propellants exhibited spontaneous oscillations, determine why either propellants or pressed AP-Al propellants exhibited oscillations and what materials exhibiting such behavior would be most suitable for further study in oscillating systems.

4.3.1. Experimental Technique

Radiation oscillations in the window bomb were viewed by a photoelectric detector placed in the camera window of the bomb used in high speed photography described in Section 3.2. A typical test record of the radiation from a pressed pellet of AP-aluminum powder is shown in

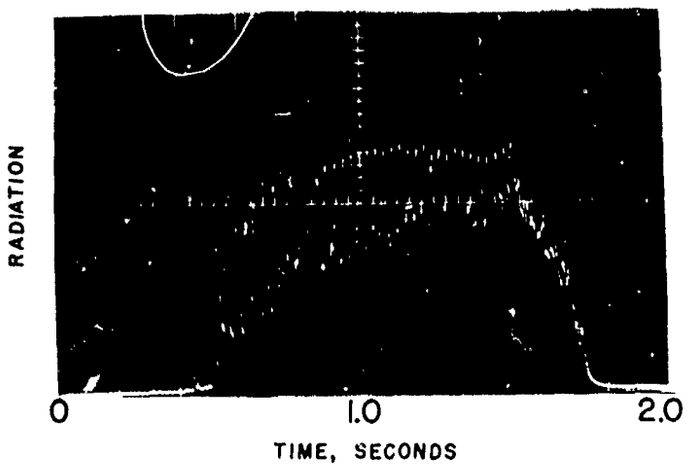

a. Periodic Radiation (J - 12)

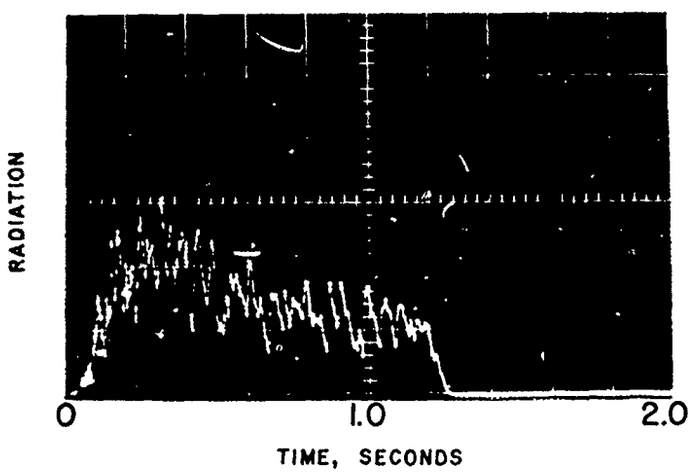

b. Marginally Periodic Radiation (J - 14)

FIG. 4.4. Radiation from AP/Al Pellets Showing Extremes in Observed Periodicity.

Fig. 4.4a. This arrangement resulted in photoelectric "viewing" of the entire combustion cloud without spatial discrimination. A limited number of tests were also made with high speed photography using the arrangement in Fig. 3.4.

The propellants used in this work were a selected few of those listed in Table 3.1 and a few propellants from motor development programs; the materials used in the pressed pellet work were the same as those used in

the propellants (Table 3.2). Pellets were prepared by weighing the ingredients for 10 gram batches, dry-blending them for approximately 16 hours, followed by dry pressing into 0.25 inch long by 0.25 inch diameter cylindrical pellets in a press. Pressing pressures of 10,000, 26,000 and 40,000 psi were evaluated (Fig. 4.5a) and on the basis of the results, a pressure of 40,000 psi was adopted for routine use.

Determination of oscillation frequency was made by measurement of the average oscillation period over an interval during the middle portion of the test when the radiation oscillations were clearly periodic as in Fig. 4.4a. For this type of oscillation, it was observed that the test-to-test reproducibility of the frequency was consistently within 10% and quite often was witnin 3%. These data are indicated by shaded symbols on the graphs (Fig. 4.5). When the radiation oscillations were only "marginally periodic" as in Fig. 4.4b (e.g., at low pressure, low aluminum concentration, etc.), the frequency was determined by averaging the most predominant period in at least three tests. Such data are indicated on the graphs in Fig. 4.5 as open symbols.

4.3.2. Observations of Combustion of AP/Al Pellets

Tests were run to determine the effects of pressure, of AP and Al particle size, of AP/Al mixture ratio, and of various ballistic modifiers on the frequency of spontaneous combustion oscillations. The combinations of ingredients used are shown in Table 4.1 and the frequency trends are shown in Fig. 4.5. The J-numbers noted in the figures correspond to the formulations in Table 4.1.

At lower pressures the samples would not burn reliably. The ballistic modifiers noted in the table were used to promote combustion at low pressures in the range involved in most of the combustor instability testing. Both copper chromite and cupric oxide were observed to extend the low pressure deflagration limit downwards, with cupric oxide being the more effective. In all cases, there tended to be a low pressure region in which the frequency of oscillation was irratic and varied with pressure in a different manner than at higher pressure.

The photographic column in Table 4.1 indicates test conditions under which high speed motion picture observations were made. The results of these observations were decisive. It was seen that under conditions leading to strong spontaneous oscillations, the deflagration of the sample was continuous, yet the combustion of the aluminum was intermittent. The aluminum accumulated on the sample surface without visible combustion for roughly two-thirds of the period of oscillation. Then ignition of the accumulated layer occurred at some local site and the aluminum combustion spread across the surface until the whole layer was enflamed. During this period of propagative combustion, new ignition sites often also developed, and the ignited material moved away from the sample surface, forming a cloud of smoke and burning droplets. For the sample size used, the layer of accumulated aluminum was completely consumed in about one-third of a cycle, and a new "dormant" period of accumulation followed.

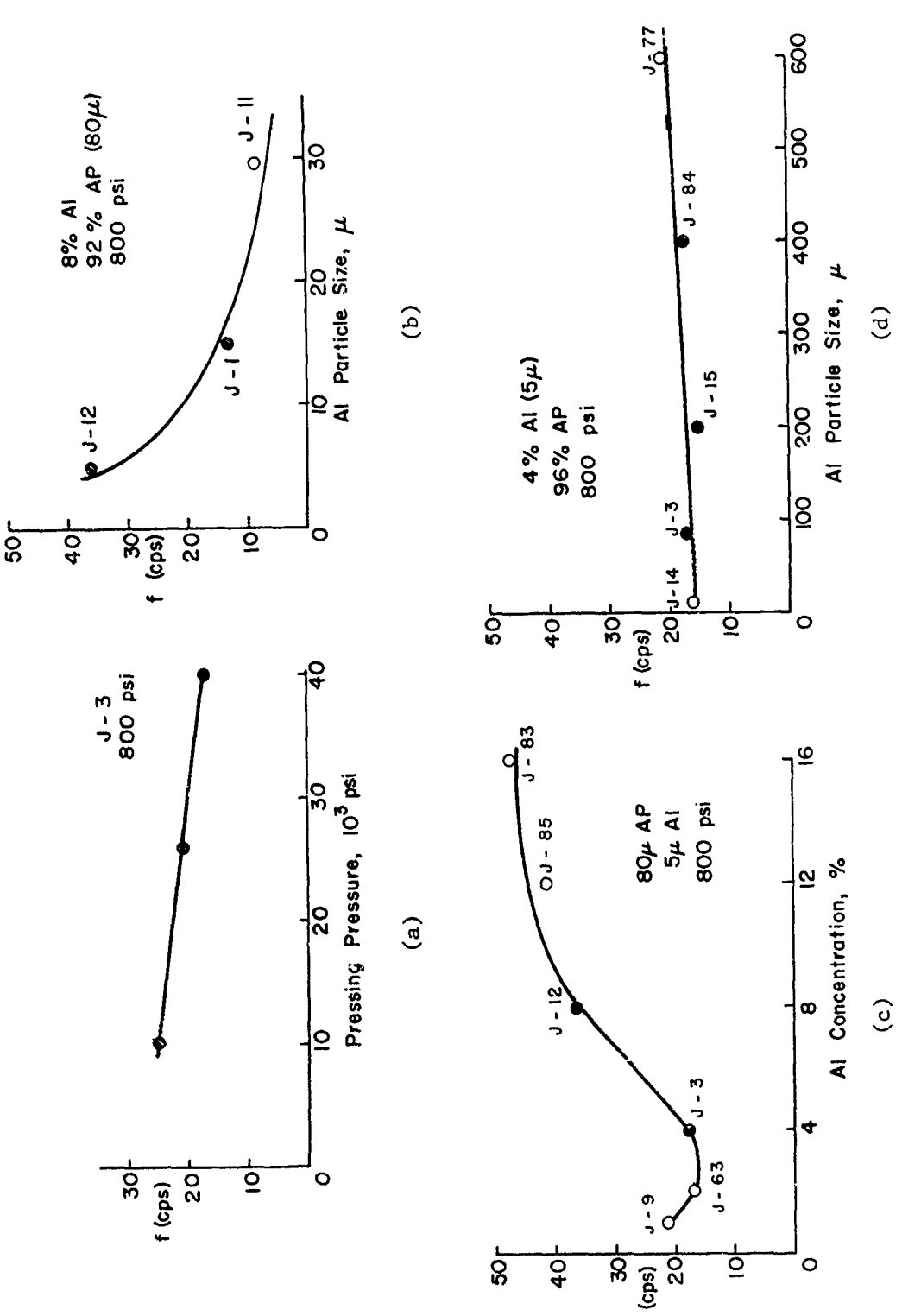

FIG. 4.5. Effect of Various Parameters on the Periodic Nature of AP/Al Combustions.

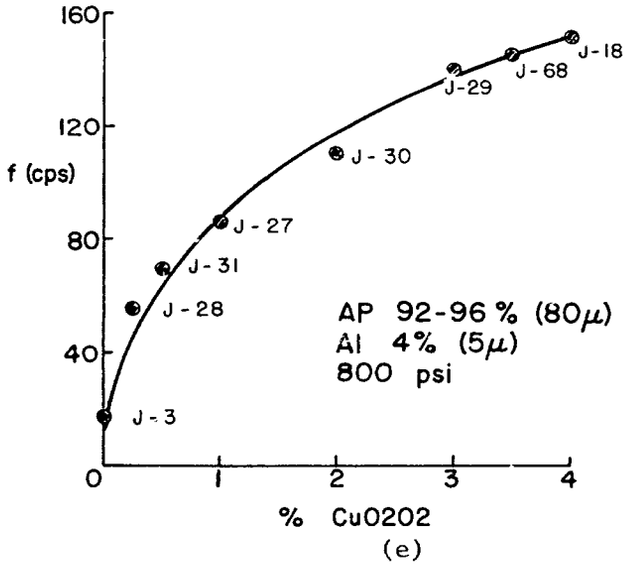

(e)

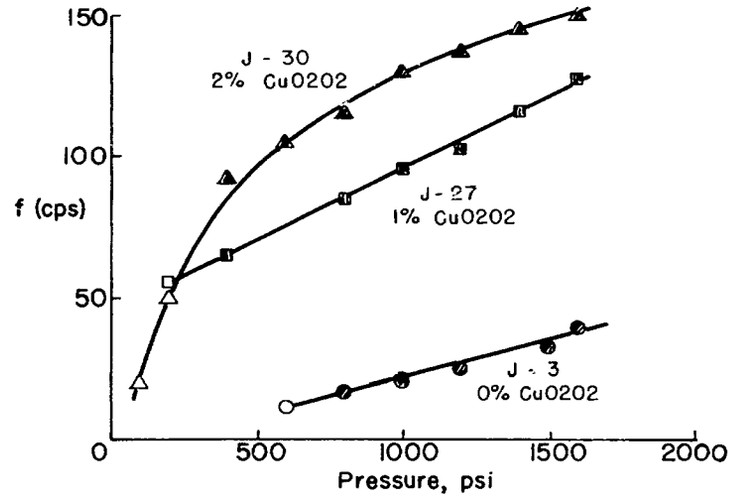

(f)

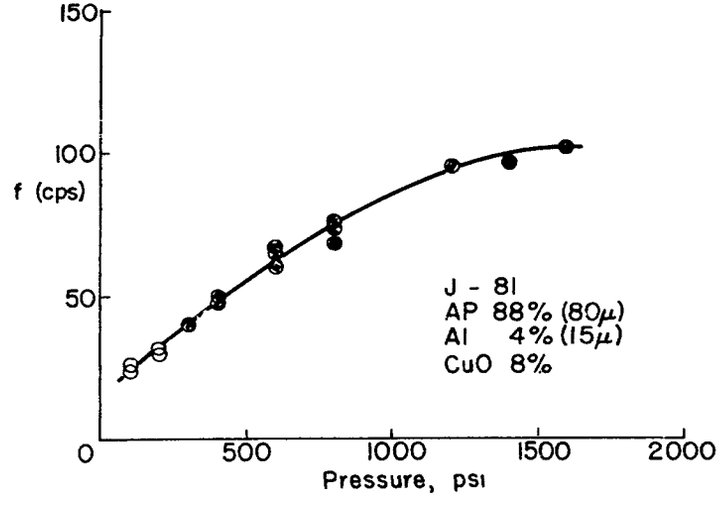

(g)

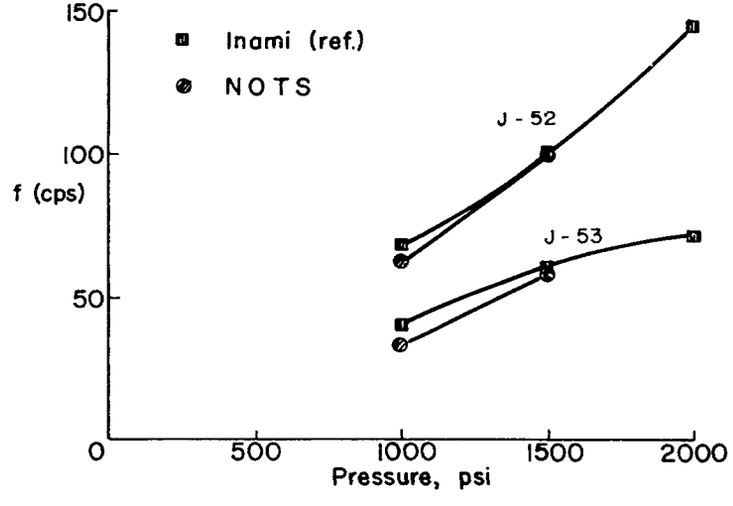

(h)

FIG. 4.5. (Cont'd.)

TABLE 4.1. AP/Al Pellet Formulations

Formulation	%AP	APμ	%Al	Alμ	Other	Photos
J-1	92	80	8	15		800,1600 psi
J-3	96	80	4	5		800 psi
J-9	99	80	1	5		800 psi
J-11	92	80	8	30		800 psi
J-12	92	80	8	5		800 psi
J-14	96	15	4	5		
J-15	96	200	4	5		
J-18	92	80	4	5	4% CuO202	
J-27	95	80	4	5	1% CuO202	400,800 psi
J-28	95 3/4	80	4	5	¼% CuO202	
J-29	93	80	4	5	3% CuO202	
J-30	94	80	4	5	2% CuO202	200,400,800 psi
J-31	95½	80	4	5	½% CuO202	
J-52	90	44	10	6	to duplicate formulations	
J-53	95	44	5	6	in Ref. 75; Alcoa 140 Al	
J-63	98	80	2	5		
J-68	92½	80	4	5	3½% CuO202	
J-77	96	600	4	5		
J-81	88	80	4	15	8% CuO (-325 mesh)	
J-83	84	80	16	5		
J-84	96	400	4	5		
J-85	88	80	12	5		

As noted in Section 4.1.4 (See also Ref. 8), it would be interesting to know to what extent this cycle would be phase-correlated over the entire surface of larger samples (where surface flame propagation would be too slow to produce phase-correlation). Alternately, it would be interesting to know the extent to which this periodic behavior would couple with oscillations in environmental conditions such as pressure, which would be manifested by either phase correlation of behavior over a large surface area or modification of combustion oscillation frequency by mismatch between spontaneous frequency and environmental frequency. These questions are explored further in Section 4.4.

4.3.3. Observation of Combustion of Aluminized Propellants

The study of oscillatory combustion of AP-Al pellets was motivated by the hypothesis that the behavior involved was related to "preferred frequency" character of unstable combustion of aluminized propellants (i.e., their tendency to exhibit instability only over a limited frequency range at a given mean pressure). While it does not necessarily follow that propellants would exhibit uncoupled (spontaneous) combustion oscillations in a constant-pressure atmosphere, tests were made on several propellants to determine whether such behavior was exhibited.

Because the aluminum in propellant flames occurs in a microscopically heterogeneous binder-oxidizer medium with adjoining high temperature diffusion flamelets, it does not ordinarily accumulate in a connected layer over the entire burning surface in the manner of AP-Al pellets. As noted earlier, the aluminum instead accumulates and forms burning droplets in a disorganized manner. This produces a "noisy" signal from a monitoring radiation detector caused by the passage of burning aluminum droplets through the field of view of the detector. Observations were made of several propellants to determine whether there was any underlying periodicity in these noisy radiation signals, suggestive of organized spontaneous oscillations. Table 4.2 summarizes the tests that were made, and Fig. 4.6 illustrates a typical test record. No underlying frequency was observed under the conditions or with the propellants tested.

4.3.4. Interpretation of Results of Spontaneous Oscillation Studies

The results to date are susceptible to fairly reliable mechanistic interpretation. The flame temperature of AP is about 1200°K, and the AP will deflagrate in the absence of aluminum (but with the ballistic modifiers) at the pressures tested. The AP deflagration is apparently not drastically modified by the presence of Al, and proceeds regardless of the momentary state of the Al combustion. The aluminum, on the other hand, does not ignite easily because of the protective oxide coating on each particle. As a result, the Al tends to accumulate on the surface. The oscillatory behavior was not changed when the samples were burned upside down, so the accumulate has some measure of attachment to the surface. It is reasonable to assume that some oxidation of the accumulate occurs during its residence on the surface, since hot oxidizing gases are "percolating" through the accumulate. Some measure of sintering occurs, because residual unburned accumulates recovered after tests possess considerable structural integrity. The sintering is believed to be due to diffusion of Al through its protective oxide coating to the region of particle interfaces followed by oxidation. This hypothesis is supported by the observation that substitution of Al by Al_2O_3 leads to only limited sintering (these latter observations were made of residues from burning in special tests in which pressed AP pellets were provided with small holes filled with Al or Al_2O_3 powders).

TABLE 4.2. Tests to Detect Radiation Periodicity in Propellants

Propellant[a]	%Al	Alμ	Binder	Pressure, psi	Comment
A-50	16.0	15	Polyurethane	800	Non-periodic radiation
E-107(MOD)	17.8	7	"	200,500	" ; Fig. 4
E-107(MOD)	17.8	15	"	400	"
P-1	14.5	9/32	"	400,1000	"
P2	16.0	30	CTBD[b]	"	"
P3	13.0	32	Polyurethane	"	"
P4	13.0	50	"	"	"
P5	20.0	8	N-Polyurethane[c]	"	"
P-6	17.0	32	Polyurethane	"	"
P-7	19.0	32	CMDB[d]	200,800	"
P-8	e	e	DB[f]	50,200	"
P-9	21.6	32	CMDB	200,800	"
P-10	18.0	32	CMDB	"	"

[a] P-numbers refer to classified propellants used in this project

[b] Carboxy-terminated polybutadiene

[c] Nitroplasticized polyurethane

[d] Composite-modified double-base

[e] 3.25% MG/Al alloy (50%-50%)

[f] Double-base

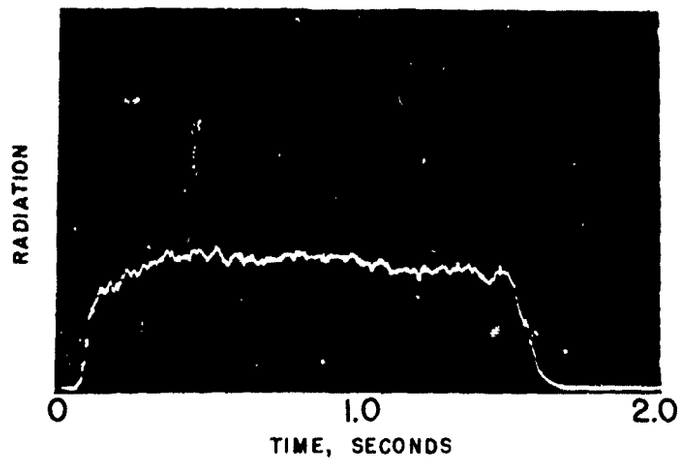

FIG. 4.6. Radiation from an Aluminized Propellant (E-107 MOD.) Showing Absence of Periodic Radiations.

As the sintered layer of Al builds up from the under side during burning of pressed pellets, its resistance to flow of products from the underlying AP decomposition necessarily increases, leading to some stressing of the layer of accumulate. The temperature of the accumulate is probably in excess of the melting point of the Al, in which case the accumulate structure receives its physical integrity primarily from a relatively fragile structure consisting of the Al_2O_3 coatings on the Al. It is reasonable to assume that the stressing will eventually lead to breakage of the accumulate structure, which will expose aluminum in the hot oxidizing flow. Considering the high specific surface of the aluminum accumulate and the low thermal conductivity of "oxide insulated" sintered accumulate, one would expect that the exposure of raw metal might lead to sufficiently rapid local oxidative heating to melt the adjoining oxide structure and thus lead to continued exposure of metal. As observed in the high speed pictures, the local "ignition site" spreads rapidly through the accumulate, which then leaves the surface as a cloud of burning metal spheres. Once the accumulate has been consumed, the "fire" goes out and aluminum starts to accumulate again due to the continued (relatively nonluminous) deflagration of the AP.

In terms of the foregoing interpretation it might be expected that the period of oscillation would be governed by attainment of a critical accumulate layer thickness, which in turn would be governed by the regression rate of the sample and the concentration of Al in the sample. Further, a fine Al particle size would lead to a less permeable and more reactive accumulate layer with correspondingly lower critical thickness. When the experimental results are plotted in terms of accumulate thickness per cycle of oscillation, it is indeed seen (Fig. 4.7) that the accumulate thickness per cycle is relatively independent of pressure and probably independent of all variables except Al particle size, although this generalization breaks down at low pressures where behavior is rather irratic also in other respects.

With respect to propellant combustion, there does not appear to be any spontaneous combustion oscillation on a microscopic scale, nor is the mechanism proposed for AP-Al pellets relevant to propellants except at low pressures (100 psia and below) where surface-wide Al accumulation has often been observed to occur. On the other hand, the behavior of the Al in pellet combustion supports the concept of Al combustion in propellants, supporting in some measure the picture of accumulation-agglomeration-ignition of Al in the "pocket" model advanced in Section 3.4.1. Further, the combustion of the propellant possesses an average periodicity when viewed on a microscopic scale, simply by virtue of the propellant's granular microstructure. The term "average" is used here because the microstructure is not periodic except in a statistical sense. This statistical periodicity cannot provide the basis for surface-wide, phase coordinated combustion oscillations unless there is some phase-correlating influence operative. The experimental results suggest that, if any such influence is operative in the constant-pressure bomb, it is not manifested in the flame radiation.

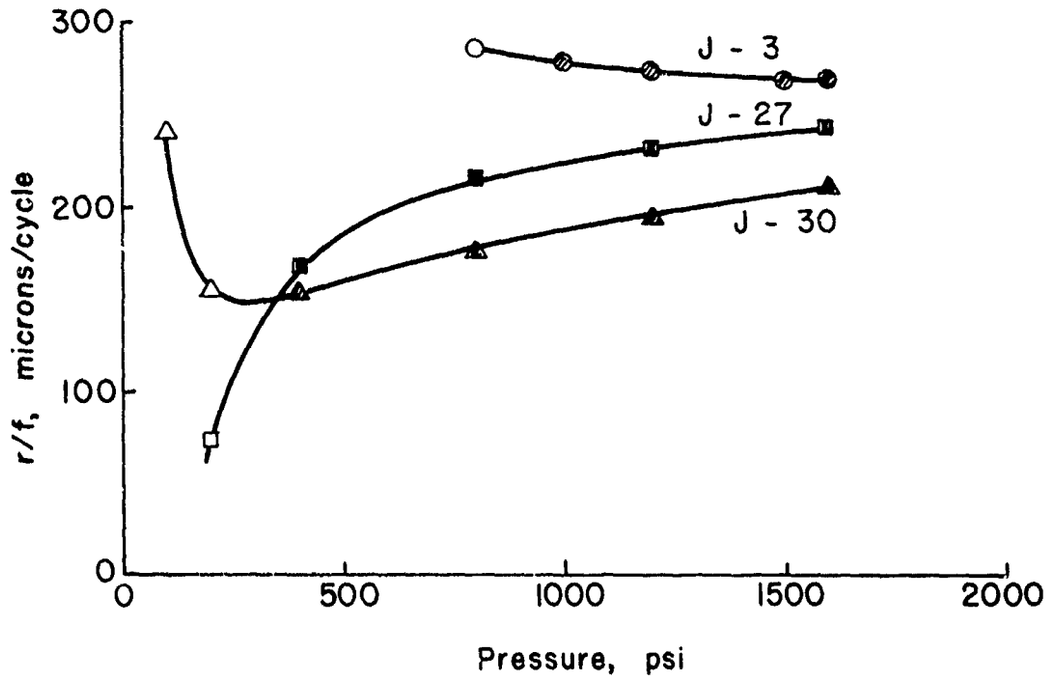

FIG. 4.7. Thickness of Accumulated Aluminum per Cycle for Three AP/Al Pellets.

4.4. COUPLED COMBUSTION OSCILLATIONS

As noted in Section 4.2, an interaction between combustion oscillations and the gas environment oscillations is essential for instability in large combustors even with propellants that burn with spontaneous oscillations. To permit study of this interaction, the flushing system of the window bomb was modified to generate mild pressure oscillations. Observations of the interaction of pressure oscillations and small sample combustion was thus made possible by either high speed photography or photoelectric means. This investigation is described in the following sections.

4.4.1. Experimental Technique

The mechanical arrangement for the pressure driven window bomb is shown in Fig. 4.8. The bomb pressure is oscillated by introducing a sinusoidal gas flow into the downstream end of the bomb flushing system. The oscillatory flow is produced by modulating a secondary gas flow with a sinusoidally-driven needle valve connected to a variable speed motor. The flow system is diagrammed in Fig. 4.9. A radiation transducer and pressure transducers monitor the behavior in the bomb and, after

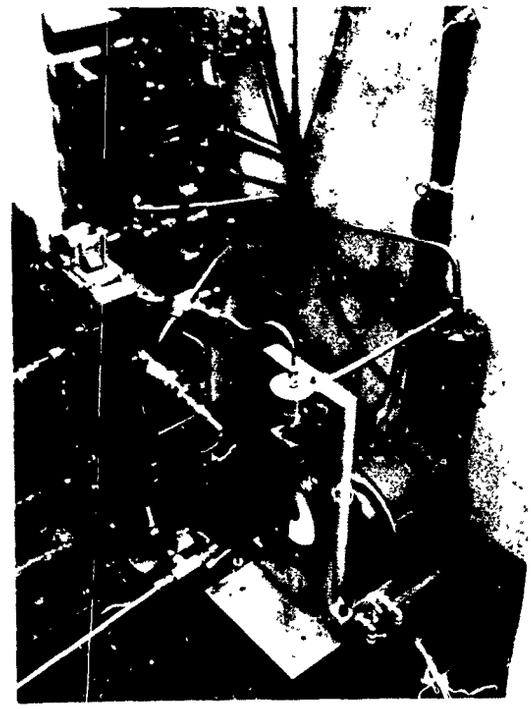

FIG. 4.8. Pressure-Driven Window Bomb.

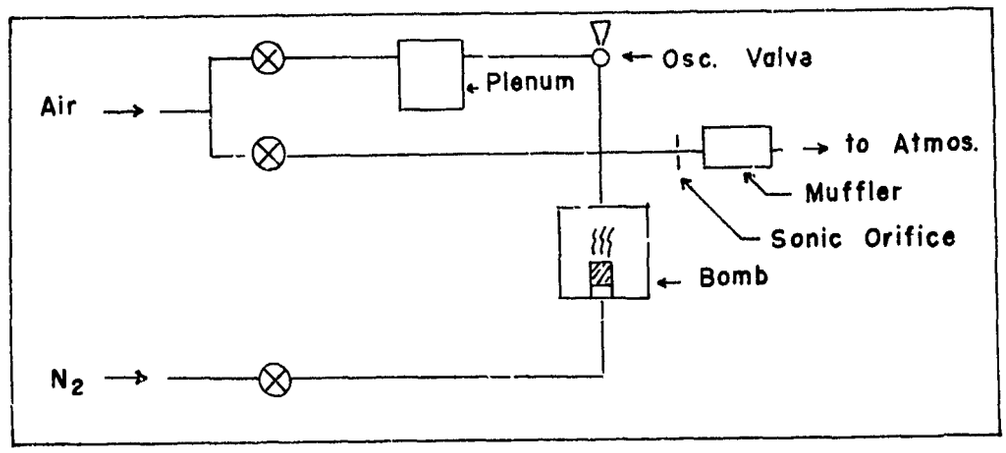

FIG. 4.9. Gas Flow System of Pressure-Driven Bomb.

appropriate electronic filtering, the radiation and pressure signals are recorded on a galvanometer oscillograph. The instrumentation arrangement is shown in Fig. 4.10 and a typical test record of an aluminized propellant (A-91) is shown in Fig. 4.11. A limited number of tests were also made with high speed photography similar to the arrangement in Fig. 3.4.

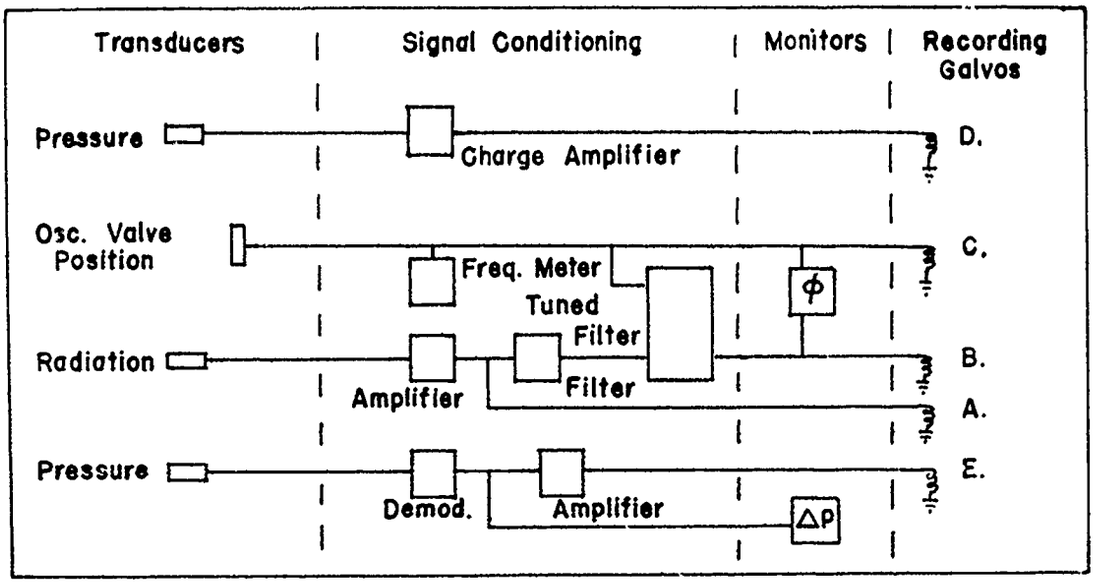

FIG. 4.10. Instrumentation Arrangement Used with Pressure-Driven Bomb. Galvo letters correspond to traces in Fig. 4.11.

Preliminary work with pressed pellets of AP/Al/catalyst has been with J-30 (see Table 4.1); J-81 (Table 4.1) appears to be a better test subject because it is more well-behaved than J-30 at lower pressures, but testing of it in the driven bomb has not yet been initiated. The propellant tested most extensively was A-91 (Table 3.1).

4.4.2. Observations of Coupled Combustion of AP/Al/Catalyst Pellets

An initial attempt was made to determine the degree to which spontaneous combustion oscillations could be altered by imposing pressure oscillation on the combustion. Seven tests were conducted with J-30 pellets (Table 4.1). The test conditions were a mean pressure of 100 psig with pressure oscillations of 5 psi (peak-to-peak) over a frequency range of 18 to 38 cps. From the recorded data, the phase shift between the oscillatory component of the radiation and pressure signals was determined as a function of pressure oscillation frequency and is shown in Fig. 4.12. These initial data seem to indicate (due to the steep slope

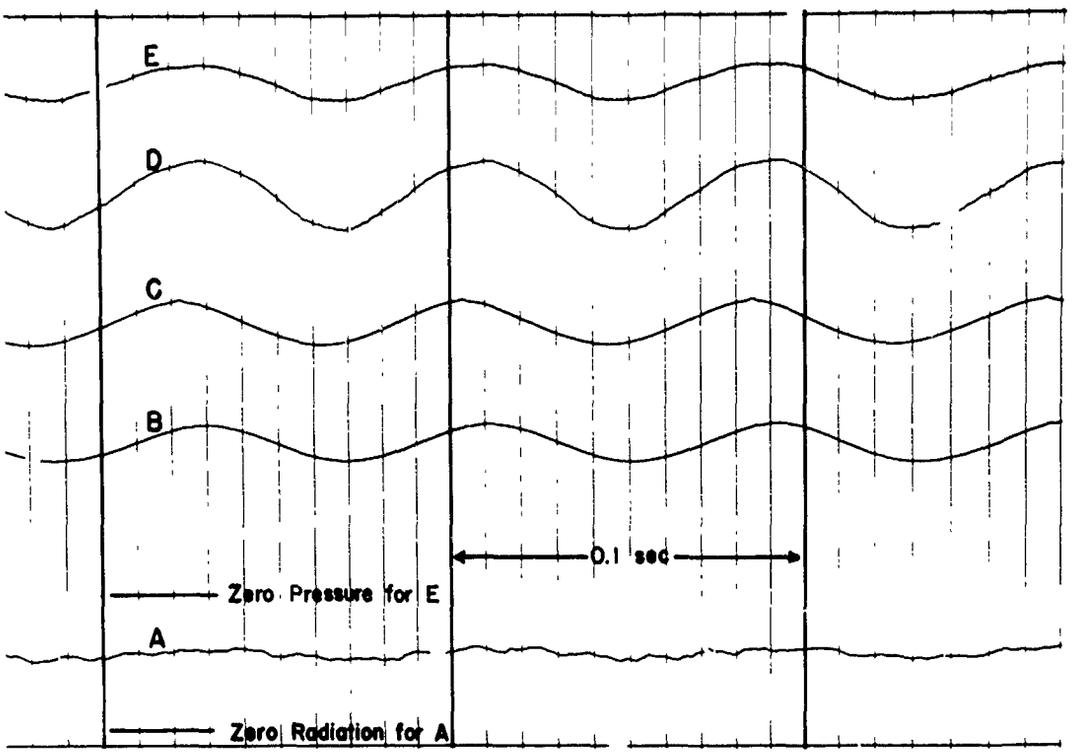

A Total Radiation Signal
B Band-Pass Filtered Radiation Signal
C Reference Signal
D Band-Pass Filtered Pressure Signal
E Total Pressure Signal

FIG. 4.11. Typical Test Record of A-91 Propellant from Pressure-Driven Bomb.

and the rather narrow frequency band over which data could be obtained) that pressure oscillations do interact with the mechanisms responsible for the spontaneous combustion oscillations, but only over a narrow frequency range and hence the combustion oscillations could be described as "sharply tuned". In comparing the spontaneous and pressure-driven combustion oscillations, it seems reasonable to expect that the frequency associated with zero phase shift in the pressure-driven tests should correspond to the spontaneous combustion frequency. The large discrepancy between these frequencies, 31 cps (Fig. 4.12) and 20 cps (Fig. 4.5f), has not been resolved. It could be a real shift due to the influence of the pressure oscillations, or an anomalous shift due to the anomalous spontaneous behavior of the J-30 pellets at low pressure (Fig. 4.5f), or due to the experimental deficiencies (e.g., small angle viewing of combustion region and lack of narrow band-pass electronic filtering) of these initial

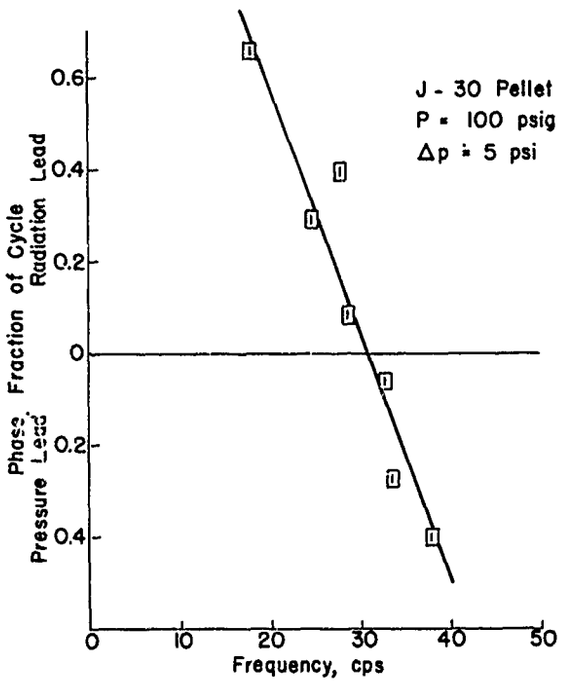

FIG. 4.12. Phase Shift due to Driven Pressure Oscillations for J-30 Pressed Pellets.

pressure-driven tests. If this line of investigation of mechanisms is pursued further, pressure-driven tests will be conducted on the more well-behaved J-81 pellets (Fig. 4.5g).

4.4.3. Observations of Coupled Combustion of Aluminized Propellants

The discussion in Section 4.1.4 pointed out the need for also investigating the possibility of "phase coupling" with aluminized propellants. A series of tests using the pressure-driven bomb technique was initiated with major emphasis on A-91 propellant (Table 3.1), an 8% aluminized propellant tested extensively in the low frequency acoustic burner (Section 6.5). The reduced phase data from these tests is shown in Fig. 4.13. These results are not in good agreement with phase data obtained in the low frequency acoustic burner (Fig. 6.16).

Because of the discrepancy in phase data between the driven and acoustic burners and because of occasional non-periodic radiation oscillations occurring during pressure-driven tests, a few spot checks of the driven tests were made using a framing motion picture camera operating at 400 frames/sec with a magnification of one. The pictures did not

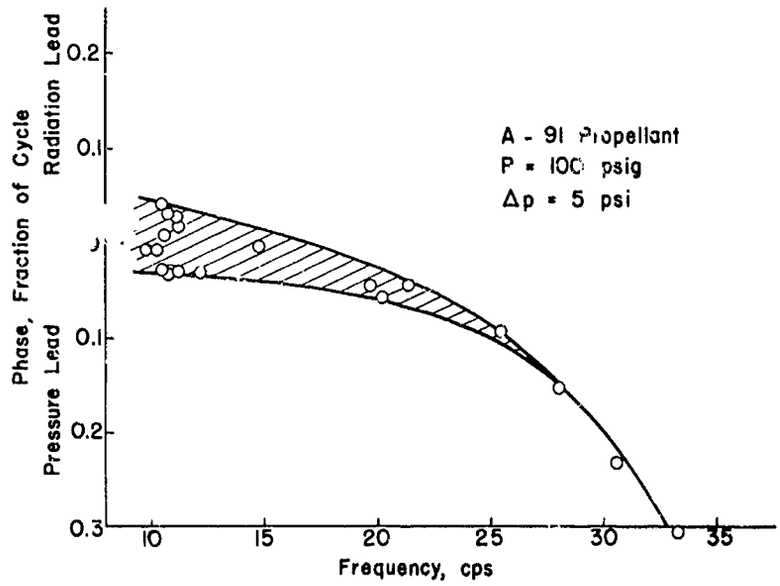

FIG. 4.13. Phase Shift Due to Driven Pressure Oscillations for A-91 Propellant.

reveal fluctuations in the aluminum combustion field visible to the eye and thus did not provide an explanation for the occasional non-periodic behavior from the radiation transducer. Also, the aluminum behavior appeared to be the same as that observed in steady-state combustion, thus implying that the gross behavior of the metal is the same under both steady and pressure-oscillating conditions. The pictures did show periodic variation in the regression rate of the burning surface, but the observation was possibly relative only to the edges of the burning surface, which adjoin the oscillating flow of the flushing gas, and may not reflect behavior of the burning surface as a whole.

4.4.4. Interpretation of Results of Coupled Combustion Oscillations

The data obtained from the pressure-driven combustion bomb on both the pressed pellets of AP/Al/catalyst and the aluminized propellant samples have shown a qualitative demonstration of the "preferred frequency" concept of Section 4.1.4. However, the experiments with pressed pellets have not yet afforded any insight into the mechanisms of interaction of spontaneous combustion oscillations and oscillatory pressure environment due to experimental difficulties. Likewise, the experiments with aluminized propellants have not yielded data that are comparable to those obtained in the low frequency acoustic burner. There are many factors which might account for the discrepancies and they have not been evaluated at the present time. One of the most obvious is the matter of small

propellant sample size and the cold gaseous environment in the pressure-driven burner; the combustion environment is considerably different than that in the acoustic burner. These effects could be minimized by a redesign of the experiment but with an attendant loss in "viewing" and economy. Another factor in the disagreement in phase data could be the manner in which the data is obtained in the acoustic burner. In the pressure-driven burner the radiation transducer is essentially viewing the propellant surface and adjacent combustion volume; in the acoustic burner several radiation transducers are spaced downstream of the burning surface and phase data from these must be extrapolated approximately one inch to the burning surface through a region of large temperature and concentration gradients. There may be unevaluated difficulties in making this extrapolation.

From the foregoing, it is concluded that the driven bomb technique has yielded useful qualitative data but the quantitative relevance to behavior of larger propellant samples or motors is doubtful.

4.5. SUMMARY

Spontaneous combustion oscillations have been observed with pressed pellets of AP and aluminum, and the frequency of the aluminum ignition-shedding has been studied in detail as a function of pressure and pellet composition, providing some insight into the role of aluminum combustion. Similar spontaneous combustion oscillations have not been observed with propellants. However, using a pressure-driven combustion bomb, propellants have been observed to exhibit a "preferred frequency" behavior indicative of a "phase coupling" mechanism. A quantitative correlation with acoustic combustion instability observations has not been achieved, but behavior indicative of phase coupling of the propellant microstructure to produce a statistical "preferred frequency" of propellant has been qualitatively demonstrated. It is anticipated that considerable modification in bomb design would be required to gain quantitative agreement of test results with those obtained in larger burners.

5. NON-ACOUSTIC COMBUSTION INSTABILITY

5.1. INTRODUCTION

Combustion systems often exhibit spontaneous periodic behavior involving spatially uniform, rising and falling internal pressure. This behavior in solid propellant rocket motors was described by Akiba and Tanno (Ref. 12) and by Price (Ref. 4 and 5), and analyzed by Sehgal and Strand (Ref. 13), and Beckstead, Ryan and Baer (Ref. 14). These analyses were committed analytically in varying degrees to rather idealized models of propellant combustion, commitments which limited their applicability and at the same time complicated the analyses and their interpretation. The present paper summarizes an analysis of the non-acoustic instability (NAI) phenomenon based on the same representation of the combustor dynamics as the previous papers However, the representation of the interaction between pressure perturbations and the propellant combustion zone has been employed in a parametric form. The parametric representation of combustion dynamics used here is the "response function" developed originally in connection with analyses of wave mode acoustic instability (Ref. 60), so that the relation between acoustic and non-acoustic instability is established in the analysis. Somewhat similar approaches have been made recently by other investigators (Ref. 72 and 73). The approach of the present paper, however, not only simplifies the analysis and facilitates its interpretation, but also permits the comparison of NAI results with combustion dynamics models, as well as with acoustic-type experimental results such as obtained in T-burners.

Following the analysis of NAI, the present paper describes experimental studies of NAI in which the conditions leading to oscillatory behavior are studied, and the measurements of the frequency and growth rate of oscillations are determined as a function of propellant and combustor variables. These results are then interpreted in terms of the theoretical model and available information regarding combustion response functions.

5.2. THEORETICAL MODEL

The behavior of the combustor in its bulk mode can be represented by the conservation of mass,

$$\frac{M_b}{\overline{M}} - \frac{M_d}{\overline{M}} = \frac{M_a}{\overline{M}} = \frac{m}{\overline{\dot{m}}} - \frac{M_d}{\overline{M}} \qquad (5.1)$$

(see nomenclature). It is assumed that

1. The thickness of the combustion zone above the propellant surface is small, so that the temperature in the combustor volume is spacewise uniform.

2. The flushing time of the combustor is short compared to the period of oscillation, so that the temperature of the gas is constant.

3. The gas conforms to the perfect gas law $p = \rho RT/\mu$.

4. The density of the propellant is much greater than the density of the gas.

5. The nozzle transit time is very short compared to the period of oscillation so that the usual quasi steady isentropic nozzle discharge relation $M_d = C_d A_t p$ may be used to represent either the instantaneous or average discharge rate.

Under the foregoing assumptions, it can be shown that[14] Eq. 5.1 may be written

$$\frac{m}{\bar{m}} - \frac{p}{\bar{p}} = \tau_{ch} \frac{d(p/\bar{p})}{dt} \tag{5.2}$$

In the foregoing, the combustor flushing or residence time which appears in the evaluation of the accumulation term is proportional to the cavity volume-to-vent ratio, L*. It is now assumed that the amplitude of the pressure oscillations grow or decay exponentially with time according to the equation

$$\frac{p}{\bar{p}} = 1 + \frac{P_o}{\bar{p}} e^{\alpha t} \cos \omega t \tag{5.3}$$

and that the mass burning rate per unit burning area responds with a corresponding oscillation about its mean value such that

$$\frac{m}{\bar{m}} = 1 + \frac{M_o}{\bar{m}} e^{\alpha t} \cos \omega(t + \tau)$$

$$= 1 + R \frac{P_o}{\bar{p}} e^{\alpha t} (\cos \omega t \cos \omega\tau - \sin \omega t \sin \omega\tau) \tag{5.4}$$

[14] See, for example, Ref. 14 and 71, also a more complete development of the analytical portions of this report is presented in Ref. 74.

The quantity R is the ratio of the magnitudes of the normalized mass and pressure oscillations

$$R \equiv \frac{M_o/\bar{m}}{P_o/\bar{p}}$$

τ is the time lead of the combustion oscillations relative to the pressure oscillations, and $\omega\tau$ is the phase between mass and pressure oscillations.

Using the above perturbation expressions for $p/\bar{p}$ and $m/\bar{m}$ in Eq. 5.2, the following is obtained

$$[R \cos \omega\tau - 1 - \alpha\tau_{ch}] \cos \omega t - [R \sin \omega\tau - \omega\tau_{ch}] \sin \omega t = 0 \qquad (5.5)$$

This equation can be satisfied in general only if the bracketed expressions each equal zero, yielding the in-phase and out-of-phase components of the response, or the oscillator equations,

$$R \cos \omega\tau = 1 + \alpha\tau_{ch} = 1 + \alpha\, AL^* \qquad (5.6a)$$

$$R \sin \omega\tau = \frac{\tau_{ch}}{\tau} \omega\tau = \frac{AL^*}{\tau} \omega\tau \qquad (5.6b)$$

These equations describe the dynamic behavior of the combustor in terms of the oscillation variables ω and α as functions of the propellant combustion dynamics R and τ and the combustor flushing time τ_{ch}.

The values or trends of R and τ are presently known only in a qualitative way, but for any one propellant they are generally considered to be functions of mean pressure and frequency. Let us first examine the trend of R at low frequency. The steady-state burning rate may be represented by

$$\bar{r} = Cp^{-n} = \bar{m}/\rho_s$$

As the frequency approaches zero, the instantaneous pressure and burning rate approach the steady- state values, thus

$$R_{\omega\to o} = \frac{M_o/\bar{m}}{P_o/\bar{p}} = \frac{\rho_s\, (\partial r/\partial p)\, P_o/\bar{m}}{P_o/\bar{p}} = \frac{\bar{p}}{\bar{r}} \frac{\partial \bar{r}}{\partial \bar{p}} = n \qquad (5.7)$$

Experimental and theoretical studies of the trends of R (Ref. 60 and 75) show an increase to values typically in the range 0.6-2.0 (and possibly more) as frequency increases. Similar studies indicate that τ (Ref. 4, 8 and 60) is positive at low frequencies, and goes to zero and less as frequency increases. Theoretical studies of combustion instability (Ref. 60, 62 and 71) indicate that these trends are more typically a function of ω/r^2, and that the functions $R(\omega)$ and $\omega\tau(\omega)$[15] tend to be shifted to higher frequency at higher pressures due to the higher burning rate. In the following sections, these general properties of the response characteristics R and $\omega\tau$ will be used in combination with Eq. 5.6 to describe the instability behavior in NAI and interpret the experimental results.

5.3. STABILITY TRENDS

Quantitative prediction of stability trends would require detailed knowledge of the functions $R(\omega,\bar{p})$ and $\tau(\omega,\bar{p})$ in the frequency range in question. However, the general behavior of NAI can be anticipated on the basis of qualitative knowledge regarding R and τ in combination with Eq. 5.6a and 5.6b.

5.3.1. Relation of Time Constants in the Unstable Domain

If Eq. 5.6b is solved for $(\tau_{ch}/\tau)/R$, it will be seen that, in the interval $-\pi < \omega\tau < \pi$,[16] solutions exist only if the combustion oscillations lead the pressure oscillations, i.e., $\tau > 0$. In this same region of $\omega\tau$, it can be seen from Eq. 5.6a that growing oscillations ($\alpha > 0$) occur only if $R > 1$ and $0 < \omega\tau < \pi/2$. Thus the unstable domain is restricted to the range of combustion time lead

$$0 < \tau/\tau_{\omega} < 1/4 \tag{5.8}$$

Eliminating R between Eq. 5.6a and 5.6b and solving for τ_{ch}/τ, it can be seen that τ_{ch}/τ is always greater than one in the potentially unstable range $0 < \omega\tau < \pi/2$. However, real oscillatory solutions are limited by Eq. 5.6b to $\tau_{ch}/\tau\, R < 1$, so that the unstable domain is restricted to values of τ_{ch}/τ such that

$$1 < \tau_{ch}/\tau < R \tag{5.9}$$

[15]Note that it is the phase, $\omega\tau$, that tends to be a unique function of ω/r^2 for a given propellant, not the function $\tau(\omega)$.

[16]Consideration is restricted to the range $-\pi < \omega\tau < \pi$ in order to be consistent with experimental observations and results of combustion instability analyses.

If, as experimental results discussed later indicate, R is restricted to values only slightly greater than one, the range of variation of τ_{ch}/τ for unstable behavior is very limited.

The foregoing conditions on τ/τ_ω and τ_{ch}/τ may be combined to yield the range of values of flushing time of the combustor in the unstable domain,

$$0 < \tau_{ch}/\tau_\omega < R/4 \tag{5.10}$$

This result supports the assumption made earlier, that the flushing time is short compared to the period of oscillation, except possibly when R is large.

5.3.2. Stability

A more complete picture of the relation among variables can be obtained by solving Eq. 5.6a for $\alpha\tau$ and using Eq. 5.6b to eliminate either R or τ_{ch}. With these two solutions one may construct Fig. 5.1. In this figure, the unstable domain is bounded by the lines $\alpha\tau = 0$, $\omega\tau = 0$ and $R = \infty$: the region below $\alpha\tau = 0$ and $R = \infty$ corresponds to decaying oscillations, and other regions have no oscillatory solutions. The stability limit, $\alpha = 0$, is satisfied (see Eq. 5.6a) by the condition

$$\cos \omega\tau = 1/R \tag{5.11}$$

For any particular values of R and τ, the oscillatory solutions occur on the corresponding R line in Fig. 5.1, with the particular situation being defined by the value of the burner geometry L*.

In a practical situation, R and τ very likely depend on frequency as discussed above. Starting at the zero frequency limit, $\omega\tau$ may be expected to increase with increasing frequency to a maximum value at which point the decrease in τ begins to dominate. From this point, $\omega\tau$ decreases to zero where τ reaches zero at the frequency, ω_o. Recalling the increase in R with ω discussed earlier, a path may be traced in the $\alpha\tau - \omega\tau - R$ diagram (referred to in the following as a "stability curve") corresponding to conditions with increasing ω. This is illustrated in Fig. 5.2 by using hypothetical R and τ functions, where R has been plotted on the left-hand ordinate and τ on the right-hand ordinate as functions of the frequency. The bottom half of the figure represents the $\alpha\tau - \omega\tau$ curves corresponding to the four cases of hypothetical R and τ curves. The examples in the figure are chosen to illustrate the trends resulting from a particular response function with a sequence of $\tau(\omega)$ functions corresponding to increasing values of ω_o. This set of trends was chosen primarily to illustrate the importance of the location of the

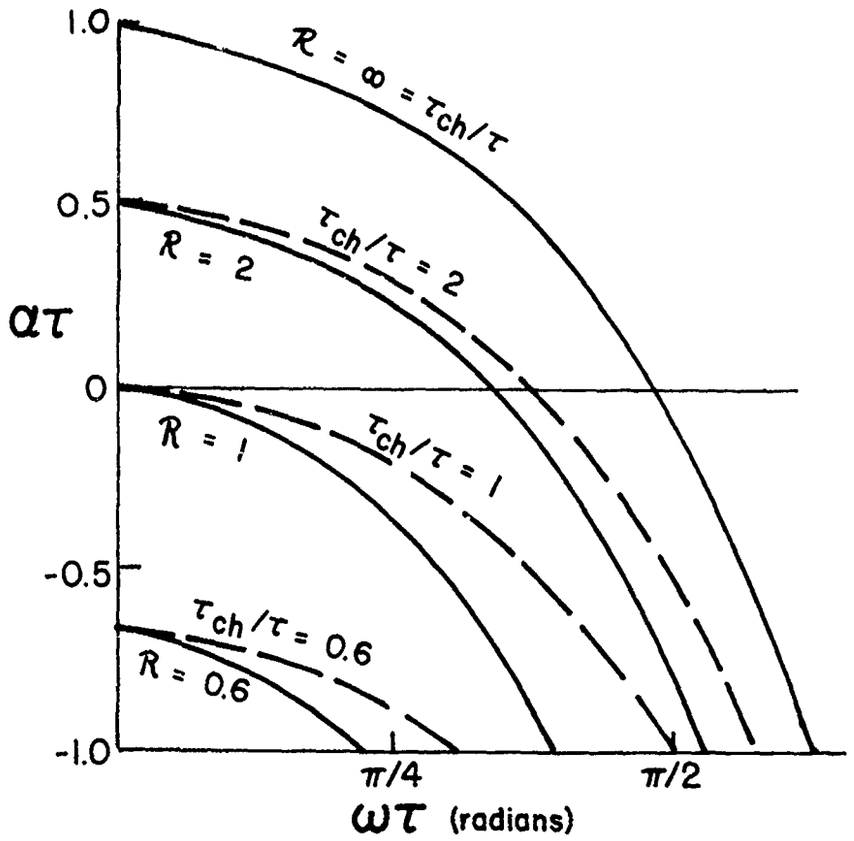

FIG. 5.1. Combustor Stability Diagram Based on Eq. 5.6a and 5.6b Showing Lines of Constant R and Constant τ_{ch}/τ. The unstable region is where $\alpha\tau > 0$.

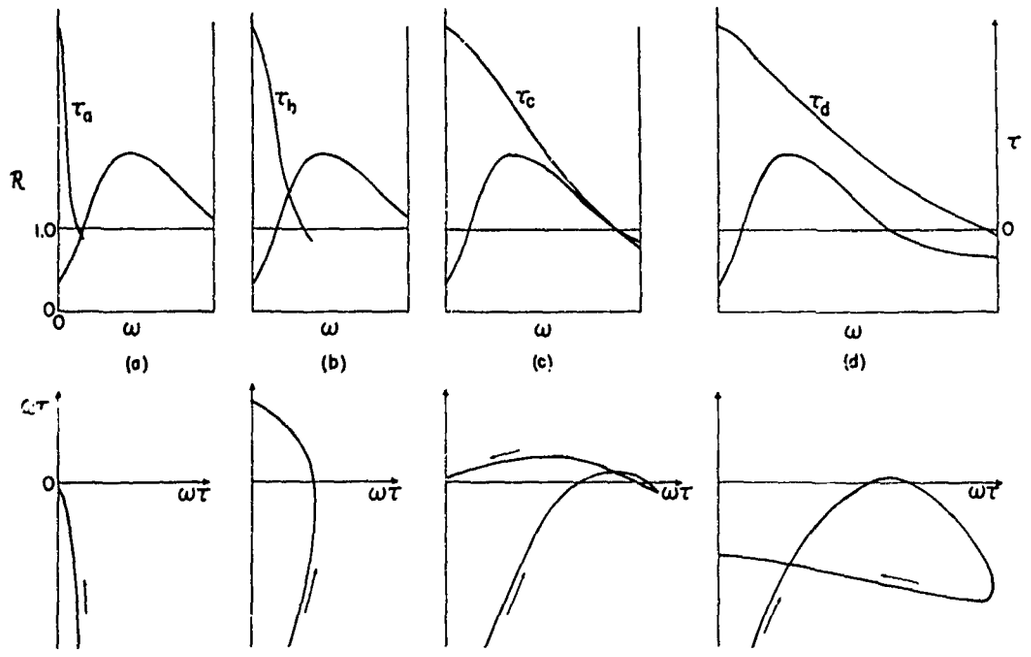

FIG. 5.2. Examples of Various Combination of τ (ω) that Might Occur with a Typical R (ω) and the Corresponding $\alpha\tau$-$\omega\tau$ Stability Curves.

τ = 0 condition, and the resulting stability trends. The examples in Fig. 5.2b and 5.2c are presented in the form of α versus ω and L* versus ω graphs in Fig. 5.3, using the original examples, Eq. 5.6a, and the relation $L^* = \tau_{ch}/A$. The case of Fig. 5.2b is considered to be the most typical of experimental results to date.

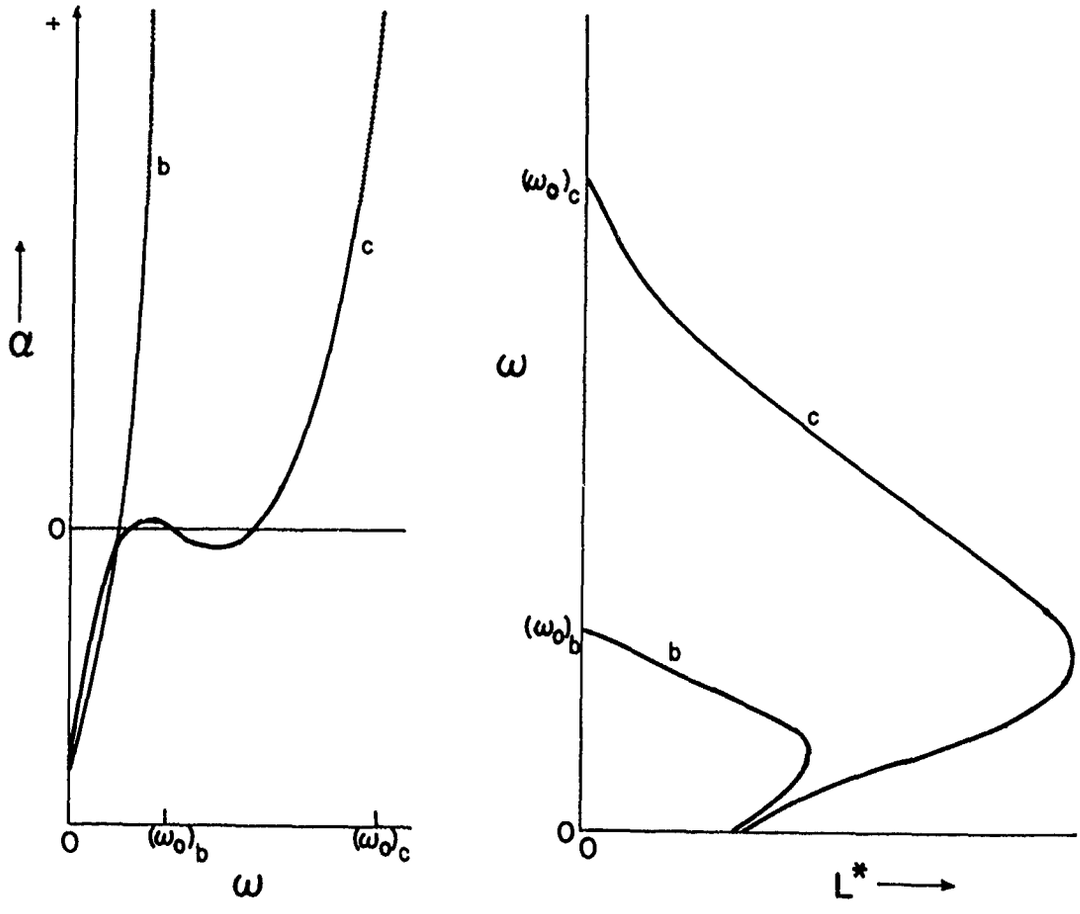

FIG. 5.3. Examples (b) and (c) of Fig. 5.2 Reduced to Values of α, ω and L*.

From the examples given in Fig. 5.2, it is evident that it would be difficult to make a comprehensive summary of stability trends. However, a more precise statement of the problem can be made by a representation of the pertinent variables in differential form. Differentiating Eq. 5.6a and 5.6b, expressions can be obtained relating the differentials of α, L*, ω, and $\bar{p}$, in terms of the partial derivatives of R and τ with respect to pressure and frequency. Equations 5.12 and 5.13 show the results of such an exercise.

$$d\alpha = \frac{1}{R \sin \omega\tau} \left\{ \frac{\omega}{R} \frac{\partial R}{\partial \omega} + R \frac{\omega\tau}{\sin \omega\tau} \left(\frac{1}{R} \cos \omega\tau - 1 \right) \left(\frac{\omega}{\tau} \frac{\partial \tau}{\partial \omega} + 1 \right) + R \cos \omega\tau - 1 \right\} d\omega$$

$$+ \frac{\omega}{R \sin \omega\tau} \left\{ \frac{\overline{p}}{R} \frac{\partial R}{\partial \overline{p}} + R \frac{\omega\tau}{\sin \omega\tau} \left(\frac{1}{R} \cos \omega\tau - 1 \right) \frac{\overline{p}}{\tau} \frac{\partial \tau}{\partial \overline{p}} \right\} \frac{d\overline{p}}{\overline{p}} \qquad (5.12)$$

and

$$\frac{d\omega}{\omega} = \frac{\frac{dL^*}{L^*} - \left(\frac{\omega\tau}{\tan \omega\tau} \frac{\overline{p}}{\tau} \frac{\partial \tau}{\partial \overline{p}} + \frac{\overline{p}}{R} \frac{\partial R}{\partial \overline{p}} \right) \frac{d\overline{p}}{\overline{p}}}{\frac{\omega\tau}{\tan \omega\tau} \left(\frac{\omega}{\tau} \frac{\partial \tau}{\partial \omega} + 1 \right) + \left(\frac{\omega}{R} \frac{\partial R}{\partial \omega} - 1 \right)} \qquad (5.13)$$

Combination of these equations permits prediction of the trends of α and ω as functions of L^*, $\overline{p}$, and the properties of $R(\omega,\overline{p})$ and $\tau(\omega,\overline{p})$. The complexity of these expressions makes it clear that any brief discussion of stability trends is contingent on some advance restriction on the form of $R(\omega,\overline{p})$ and $\tau(\omega,\overline{p})$ such as provided by the samples in Fig. 5.2 and 5.3, or some suitable combustion dynamic theory or experiment providing R and τ.

In the framework of Fig. 5.2 and 5.3, these expressions are considerably simplified by considering trends at constant $\overline{p}$, in which case Eq. 5.12 becomes

negative for $\frac{\omega}{R} \frac{\partial R}{\partial \omega} < 1$ (negative for $R > 1$) negative for $\frac{\omega}{\tau} \frac{\partial \tau}{\partial \omega} > -1$

$$\frac{d\alpha}{d\omega} = \frac{1}{R \sin \omega\tau} \left[\left(\frac{\omega}{R} \frac{\partial R}{\partial \omega} - 1 \right) + \left(\frac{\omega\tau}{\tan \omega\tau} - R \frac{\omega\tau}{\sin \omega\tau} \right) \left(\frac{\omega}{\tau} \frac{\partial \tau}{\partial \omega} + 1 \right) + R \cos \omega\tau \right] \qquad (5.14)$$

From the previous discussion, it is known that $\alpha < 0$ for $R < 1$, so that the above expression is of only limited interest until the frequency is high enough for R to be above one. If, as in Fig. 5.2a, τ has already become negative at that frequency, there is no unstable domain. If τ is approaching zero rapidly at that point as in Fig. 5.2b and 5.3, the term $(\omega/\tau)(\partial\tau/\partial\omega)$ will dominate and give $d\alpha/d\omega$ a positive value (this observation is evident only after a comparison of probable values of the other terms). When $\tau \to 0$ at higher frequency, the term $\partial R/\partial\omega$ may dominate in the frequency range where it is large, giving an interval in which α decreases with increasing frequency (Case c in Fig. 5.2 and 5.3). In all cases, the trend of α with ω is positive as $\tau \to 0$ at $\omega = \omega_o$, although this trend may occur in the stable region if R becomes less than $1/\cos \omega\tau$ before τ reaches zero, as in case d of Fig. 5.2. The factor $1/\sin \omega\tau$ in Eq. 5.14 indicates that $d\alpha/d\omega \to \infty$ as $\tau \to 0$

in all cases. In summary, it may be seen that $d\alpha/d\omega$ can be either positive or negative at the low frequency portion of the unstable domain, but always becomes positive as the condition $\tau = 0$ is approached, becoming infinite at that limit.

The stability trends can be visualized in general terms in a plot such as Fig. 5.4. Here, a grid of R curves is obtained by plotting Eq. 5.11 for different constant values of R. Thus, the grid is a stability limit map, i.e., each R, τ, ω point on the grid corresponds to $\alpha = 0$. The region in the upper right corresponds to unconditional stability (no oscillatory solution to Eq. 5.6), and is bounded by the $R = \infty$ line. Below this line, instability will occur wherever the actual value of R is greater than the value indicated by the grid of constant R curves. Considering a specific R (ω) function, Eq. 5.11 may be used to determine a corresponding τ - ω stability limit curve which bounds the shaded area of Fig. 5.4. Within this area, the actual value of R is greater than indicated by the constant R grid, τ is less than at $\alpha = 0$, and instability will occur. The instability behavior of an actual propellant at a given mean pressure would be indicated by the points on the τ (ω) curve for that propellant, as indicated by the solid section of the two sample τ (ω) curves. The shaded areas represent all possible unstable solutions for the given response function and for a given burning rate (i.e., all possible τ (ω) functions). It can be shown that as $\tau \to 0$, α increases without limit. As a result, experimental measurements of the growth constant will not be obtained as $\tau \to 0$ because oscillations grow too fast to permit measurements in the linear domain. Likewise, experimental measurements near the zero-frequency axis are not obtained because $R < 1$ at low frequency and the system is stable (oscillatory decay rates and frequencies might be obtainable in pulsed systems). Thus, experimental measurements may be expected in a region of Fig. 5.4 parallel to the constant R curves (e.g., in the vicinity of the 1.1 line) with no data near the coordinate axes, and certainly no data above the $R = \infty$ line.

5.3.3. Effect of Combustor Geometry

In the present problem the geometry of the combustor enters in two ways. The steady-state mass balance requires (Ref. 76)

$$\bar{p} = \left(\frac{C \rho_s}{C_d} K \right)^{\frac{1}{1-n}} \tag{5.15}$$

i.e., the mean pressure is dependent on the ratio of propellant burning area to nozzle throat area to the $1/(1-n)$ power. Thus, in arguments regarding trends at constant pressure, it is implicitly presumed that K is constant.

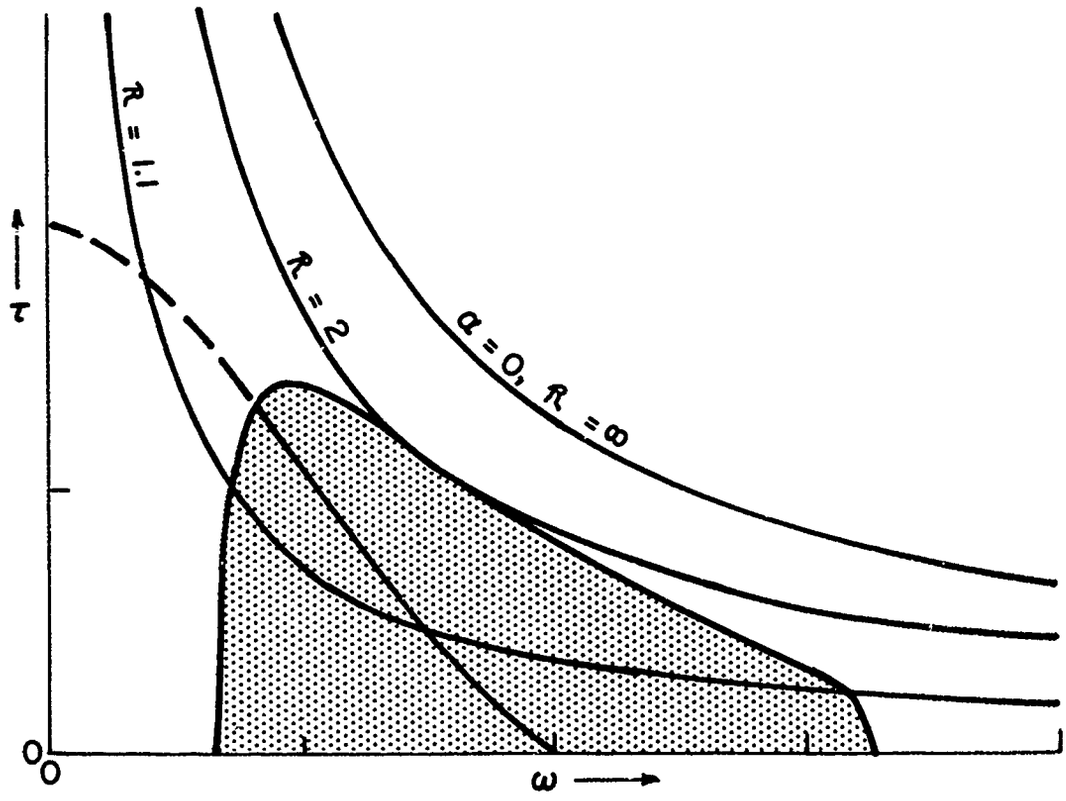

FIG. 5.4. Stability Map in the τ-ω Plane. Shaded area represents the unstable region for a typical R (ω) curve. Solid portion of the τ (ω) curve represents instability for a particular propellant and pressure.

The other geometrical variable, which is related to the instability trends, is L*. The trend of stability with L* can be inferred from Fig. 5.3 and is shown more explicitly in Fig. 5.5 by plotting the growth constant against L* for the samples of Fig. 5.2b and 5.2c and Fig. 5.3. The lowest point on the curves in Fig. 5.5 corresponds to the condition $\omega = 0$, which implies $L^* = (R\tau/A)_{\omega = 0}$ (see Eq. 5.6b). For increasing frequency, L* will increase along the stability curve if the rate of increase of R is greater than the rate of decrease of τ. When such an increasing trend of L* with frequency occurs, it must eventually change to a decreasing trend ending with $L^* \to 0$ as $\omega \to \omega_o$ and $\tau \to 0$ (Eq. 5.6b). In an experiment, L* typically starts at a low value, and increases with time. Thus, if L* is sufficiently small, then α will be greater than zero and oscillations will occur.

It is evident from the figure that more than one frequency is possible at a given L* with the one corresponding to the highest growth constant, presumably being that which would be observed. In the case of a

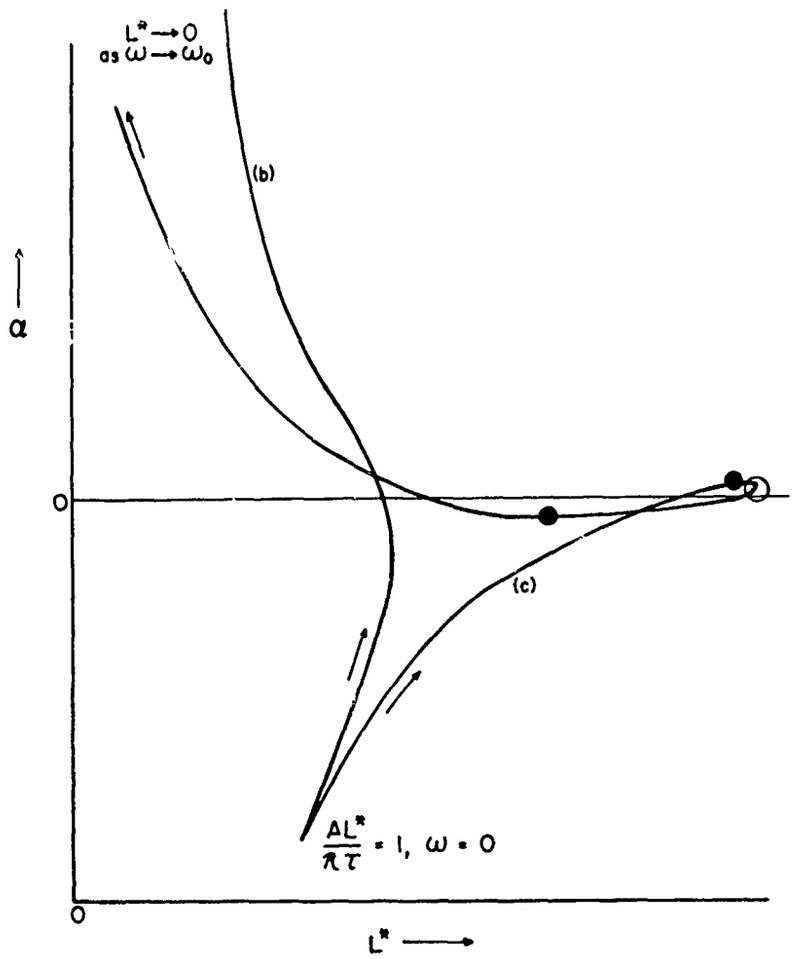

FIG. 5.5. Examples (b) and (c) of Fig. 5.2 Plotted as α Versus L*. The loop in curve (c) provides a possible explanation for two frequencies occurring at one value of L*.

loop in the stability curve as in case (c) (Fig. 5.5), a more abrupt transition in frequency may occur if the loop is in the positive α region and L* ranges through the intersection point of the loop. The oscillations would presumably favor the section of the loop with higher α, with the possibility of oscillations at two frequencies at once if both sections of the stability loop are in the positive α domain. In all cases, a value of L* may be reached beyond which no combination of R, τ and ω given by R (ω) and τ (ω) can satisfy Eq. 5.6b, i.e., there is no oscillatory solution. This maximum value of L* for oscillatory solutions is not necessarily at α = 0, and is a property of R (ω) and τ (ω) rather than the experiment.

The stability trends illustrated above in terms of the R and τ functions in Fig. 5.2 can be stated more generally by suitable manipulation of Eq. 5.13 and 5.14. Thus, the trends of α and ω with L* are given by

$$L^*\left(\frac{\partial \alpha}{\partial L^*}\right)_{\overline{p}} = \frac{\omega}{R \sin \omega\tau} \frac{R \frac{\omega\tau}{\sin \omega\tau}\left(\frac{1}{R}\cos \omega\tau - 1\right)\left(\frac{\omega}{\tau}\frac{\partial \tau}{\partial \omega} + 1\right) + \frac{\omega}{R}\frac{\partial R}{\partial \omega} + R\left(\cos \omega\tau - \frac{1}{R}\right)}{\frac{\omega\tau}{\tan \omega\tau}\left(\frac{\omega}{\tau}\frac{\partial \tau}{\partial \omega} + 1\right) + \left(\frac{\omega}{R}\frac{\partial R}{\partial \omega} - 1\right)} \tag{5.16}$$

near one, $< \pi/2$ — negative, of order 0.1 — positive, of order 0.1

positive, < 1

$$\left(\frac{L^*}{\omega}\frac{\partial \omega}{\partial L^*}\right)_{\overline{p}} = \frac{1}{\frac{\omega\tau}{\tan \omega\tau}\left(\frac{\omega}{\tau}\frac{\partial \tau}{\partial \omega} + 1\right) + \left(\frac{\omega}{R}\frac{\partial R}{\partial \omega} - 1\right)} \tag{5.17}$$

A careful study of these equations in the context of the functional forms of R (ω) and τ (ω) suggested by combustion theory and Fig. 5.2 shows that one reversal in sign of the denominator in Eq. 5.16 and 5.17 will occur (Fig. 5.2b-d) except when $\tau \to 0$ before $\partial R/\partial \omega$ becomes dominant (Fig. 5.2a). The reversal occurs at the L* and frequency for which

$$1 - \frac{\omega}{R}\frac{\partial R}{\partial \omega} = \frac{\omega\tau}{\tan \partial \omega}\left(\frac{\omega}{\tau}\frac{\partial \tau}{\partial \omega} + 1\right) \tag{5.18}$$

and corresponds to the maximum L* point in Fig. 5.3 and 5.5 referred to above, marked by the open circle in the figures. The trend of ω with L* is determined by the dominance of $\partial\tau/\partial\omega$ or $\partial R/\partial\omega$ in this equation, and the resulting sign of $\partial\omega/\partial L^*$.

Comparison of terms in the numerator of Eq. 5.16 indicates that either $\partial\tau/\partial\omega$ or $\partial R/\partial\omega$ may dominate, with $\partial\tau/\partial\omega$ always dominating as $\omega \to \omega_o$ where L* $(\partial\alpha/\partial L^*) \to -\infty$, as suggested by the examples. At the $\omega = 0$ limit, L* $(\partial\alpha/\partial L^*)$ may be either negative or positive. If positive, it will change signs at least once (corresponding to the maximum L* point, the sign change in the denominator, (the open dot in Fig. 5.3 and 5.5). Further sign changes (closed dots, Fig. 5.5) result from sign changes in the numerator of Eq. 5.16, with the closed loop (Case c) resulting from the sign change in the denominator occurring at a value of $\omega\tau$ between the values for which sign changes in the numerator occurred. It should be stressed that the diagnosis of the stability trends is made here by use of Eq. 5.16 and 5.17 and the qualitative form of the R (ω) and τ (ω) functions for the propellant. The question of what will happen in an experiment depends on what values of L* actually occur.

5.3.4. Effect of Burning Rate and Pressure

The value of L* at which NAI occurs has been seen (Ref. 13, 71 and 77) to be highly dependent on the mean pressure in the combustor and burning rate of the propellant. In the framework of the present analysis, an explanation of these observations is contingent on some speculation regarding the trends of the response function and combustion time lead with pressure and burning rate. As noted earlier, current theories of combustion dynamics of solid propellants generally predict that (for the particular model and associated physical and kinetic parameters) the response and the phase are unique function of ω/r^2. Under these conditions it can be shown from Eq. 5.6a and 5.6b that a stability curve such as in the $\alpha\tau$-$\omega\tau$ diagrams in Fig. 5.2 approximates the behavior of a particular propellant over a range of burning rates and pressures. This being the case, the stability limit, $\alpha = 0$, is characterized by a particular value $(\omega/r^2)_{\alpha = 0}$ corresponding to the $\alpha\tau = 0$ intercept of the stability curve. The stability limit is thus determined in terms of frequency for various burning rates as

$$\omega_{\alpha = 0} = r^2 \, (\omega/r^2)_{\alpha = 0} = \text{constant} \times r^2 \qquad (5.19)$$

The value of L* at the stability limit can be determined from Eq. 5.6b, taking advantage of the fact that under the present assumptions, R, $\omega\tau$ and ω/r^2 are independent of r at the stability limit

$$L^*_{\alpha = 0} = \frac{1}{r^2} \left[\frac{R \sin \omega\tau}{A \frac{\omega}{r^2}} \right]_{\alpha = 0} = \text{constant}/r^2 \qquad (5.20)$$

This trend of L* with r for the stability limit is equivalent to that noted by previous authors (Ref. 12, 13 and 71) and can be expressed as the L* - $\overline{p}$ stability limit similar to that reported earlier (Ref. 13 and 71) by replacing r by the equivalent pressure-dependent expression Cp^n. Then,

$$L^*_{\alpha = 0} \propto \overline{p}^{\,-2n} \qquad (5.21)$$

From the foregoing, it is evident that for conditions where R and $\omega\tau$ are unique functions of ω/r^2, the frequency on the stability limit is higher when burning rate (and hence pressure) is high, and the L* producing this frequency is lower. This generalization can be inferred from previous theories (Ref. 12, 13, 14 and 71) and is supported to the extent reported in experimental work (Ref. 13,14, 71,77 & 82). It merits future elaboration in terms of situations where the burning rate law $\overline{r} = Cp^{-n}$ does not apply, or situations such as Fig. 5.2c, where $(\omega\tau)_{\alpha = 0}$ and

$(\omega/r^2)_{\alpha = 0}$ each have three values (see Fig. 5.3), or where the maximum L* for stability is higher than the L* for $\alpha = 0$.

Looking to conditions in the unstable domain, the $\alpha\tau$-$\omega\tau$ stability curve may be used in combination with the $\omega\tau$-ω/r^2 relation to determine a curve in the α-ω plane for each value of r (like the curves in Fig. 5.3). In such a family of α-ω curves, those corresponding to high burning rates (and high pressures) would be on the right, corresponding to higher frequencies. This could be anticipated from the trend along the $\alpha = 0$ line discussed above, and similar reasoning shows that the high burning rate curves correspond also to low values of L*. As in Fig. 5.3, the α curve approaches infinity as $\omega \to \omega_o$ and this limit depends upon r according to

$$\omega_o = r^2 \, (\omega/r^2)_{\omega\tau = 0} \tag{5.22}$$

The implications of the assumption that R and $\omega\tau$ are functions of ω/r^2 are further elucidated to advantage in terms of the resulting burning rate dependent families of $\tau(\omega)$ and $R(\omega)$ curves. These functions are plotted as stability maps (analogous to Fig. 5.4) in Fig. 5.6, in which the unstable domains and the corresponding $\tau(\omega)$ curves are shown for

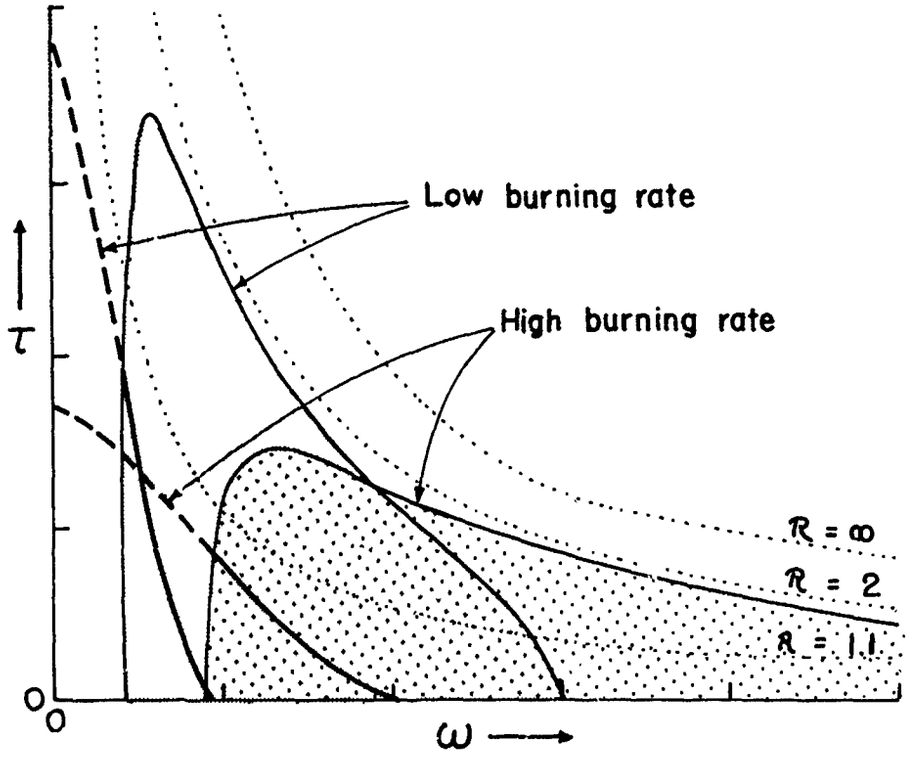

FIG. 5.6. Stability Maps in the τ-ω Plane for Different Pressures or Burning Rates.

different burning rates. The interpretations noted earlier are relevant here, with the added feature that the trend with burning rate becomes evident. Since the value of $\bar{R}$ at the stability limit is presumed constant in the present case, the stability limit is a member of the family of $\alpha = 0$ constant $\bar{R}$ lines in Fig. 5.4 and 5.6.

5.4. EXPERIMENTAL PROCEDURES AND RESULTS

5.4.1. Experimental Apparatus and Data Analysis

The burner used in the present program is a slightly modified version of the previously reported L* burner (Ref. 14). Figure 5.7 is a schematic drawing of the burner as now in use. The propellant surfaces are restricted in such a way as to give a constant burning area and result in constant pressure tests. When aluminized propellants were fired, irregularities were observed in the pressure trace and were attributed to restrictions in the nozzle throat caused by the condensing and shedding of aluminum oxide on the nozzle surfaces. In order to reduce this effect, Teflon inserts have been used in the converging nozzle entrance. Figure 5.8 contains the traces of two firings of the same propellant (A-91) under exactly the same conditions except that the upper trace was obtained with a graphite nozzle while the lower trace was obtained with a copper nozzle containing a Teflon insert. The lower trace is clearly more desirable for the purpose of obtaining data. A third modification consists of exhausting into a pressurized tank. When exhausting to the atmosphere, a sample will often extinguish after a chuff. Exhausting to the pressurized tank causes the propellant to reignite after a chuff and continue burning, enabling the test conductor to obtain additional data from such a test. However, care is exercised in order to maintain sonic conditions at the nozzle throat while the propellant is burning.

One or two propellant discs, 0.25-inch by 1.6-inch diameter are fitted into a glass tube that serves as the burner wall. For the propellants studied during the present reporting period, the configuration described resulted in test conditions that were optimum with respect to obtaining data between pressures of 50 to 200 psia and L* values of 20 to 100 inches.

Three NOTS propellants have been studied systematically over a wide range of conditions, and one Aerojet propellant has been studied somewhat more limitedly. The compositions, physical properties and burning rates of these propellants (and a reference propellant) are reported in Table 1 and Fig. 5.9. Other propellants were fired in the burner to aid in developing experimental techniques and also in a screening process to find propellants suitable for testing in the 5½-inch acoustic burner and the driven burner as well as the L* burner.

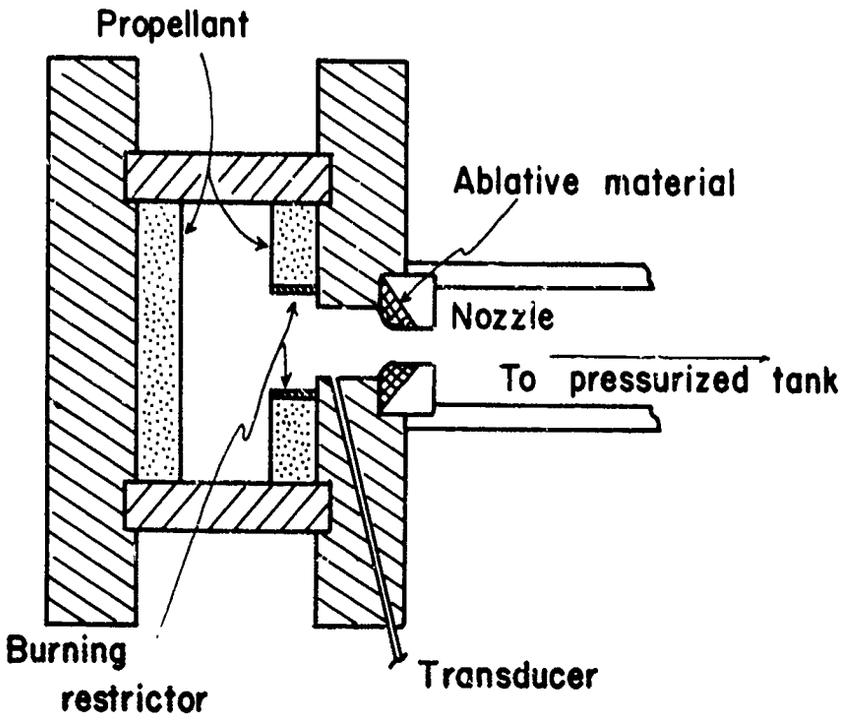

FIG. 5.7. The L*-Burner.

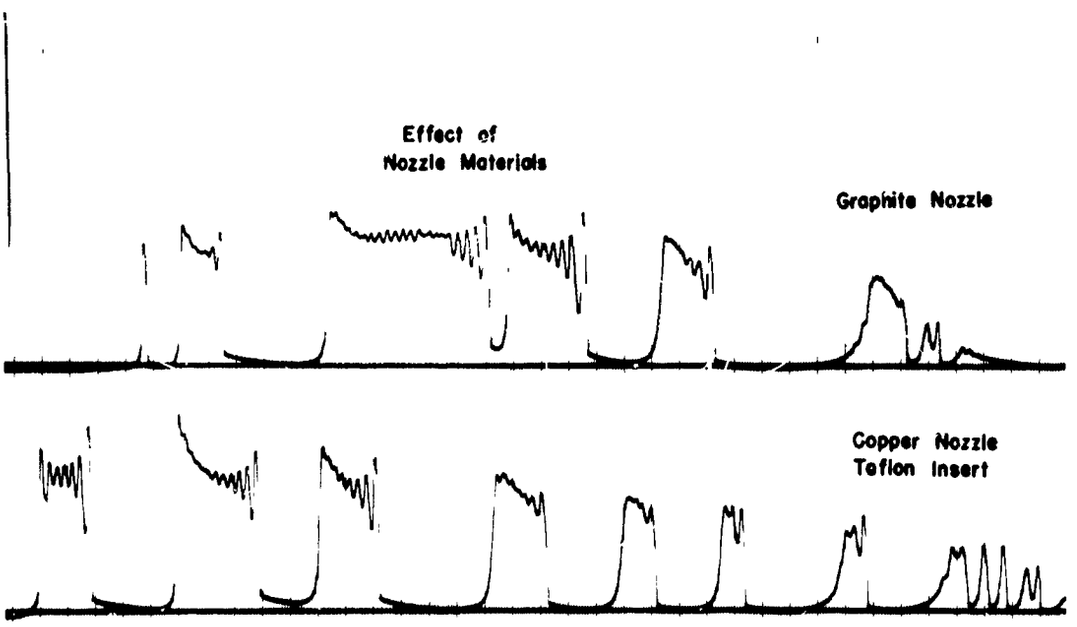

FIG. 5.8. The Effect of Nozzle Material on the Recorded Results. Note the irregularity in the long chuff of the upper trace.

Table 5.1. Propellant Compcsitions and Properties

	A-35	A-91	A-97	U-TF
Binder (percent-type)	25% PU[a]	25% PU	25% PU	18% PBAA[b]
NH_4 ClO_4 (percent-size)	75% 90μ[c]	67% 90μ	66.5% 90μ	37.5% Coarse[d] 37.5% 15μ
Additives	None	8% 5μ Al	8% 5μ Al .5% Cu0202	5% 25μ Al 2% Cu0202
$\bar{r}$ (in/sec) at 100 psia	0.133	0.108	0.15	0.31
n	0.49	0.52	0.53	0.46
ρ (gm/cc)	1.58	1.65	1.69	1.69
α_t(in^2/sec) x 10^4	1.82	2.71	2.88	3.04
c* (ft/sec)	4490	4710	4702	4920
T_f (°K)	2161	2450	2448	2860
γ	1.25	1.24	1.23	1.22
μ	22.0	23.0	23.09	25.1

[a] Polyurethane plus curing agents

[b] Polybutadiene acrylic acid plus curing agents

[c] The fifty weight percent point

[d] Screened -48 + 100 (approximate 225μ mean size)

Figure 5.10 contains the oscillograph trace of an actual firing made in the L* burner with A-35 propellant (the non-aluminized propellant) and shows several aspects of nonacoustic instability quite clearly. Upon ignition, divergent oscillations occur, leading to recurrent quenching known as chuffing. In the figure, the chuffs each have growing, periodic oscillations superimposed on the crest of the chuff. Data that can be obtained from such a record include the frequency, the exponential growth constant, the mean pressure, and the L* at locations where the other measurements are made. The value of L* is calculated from

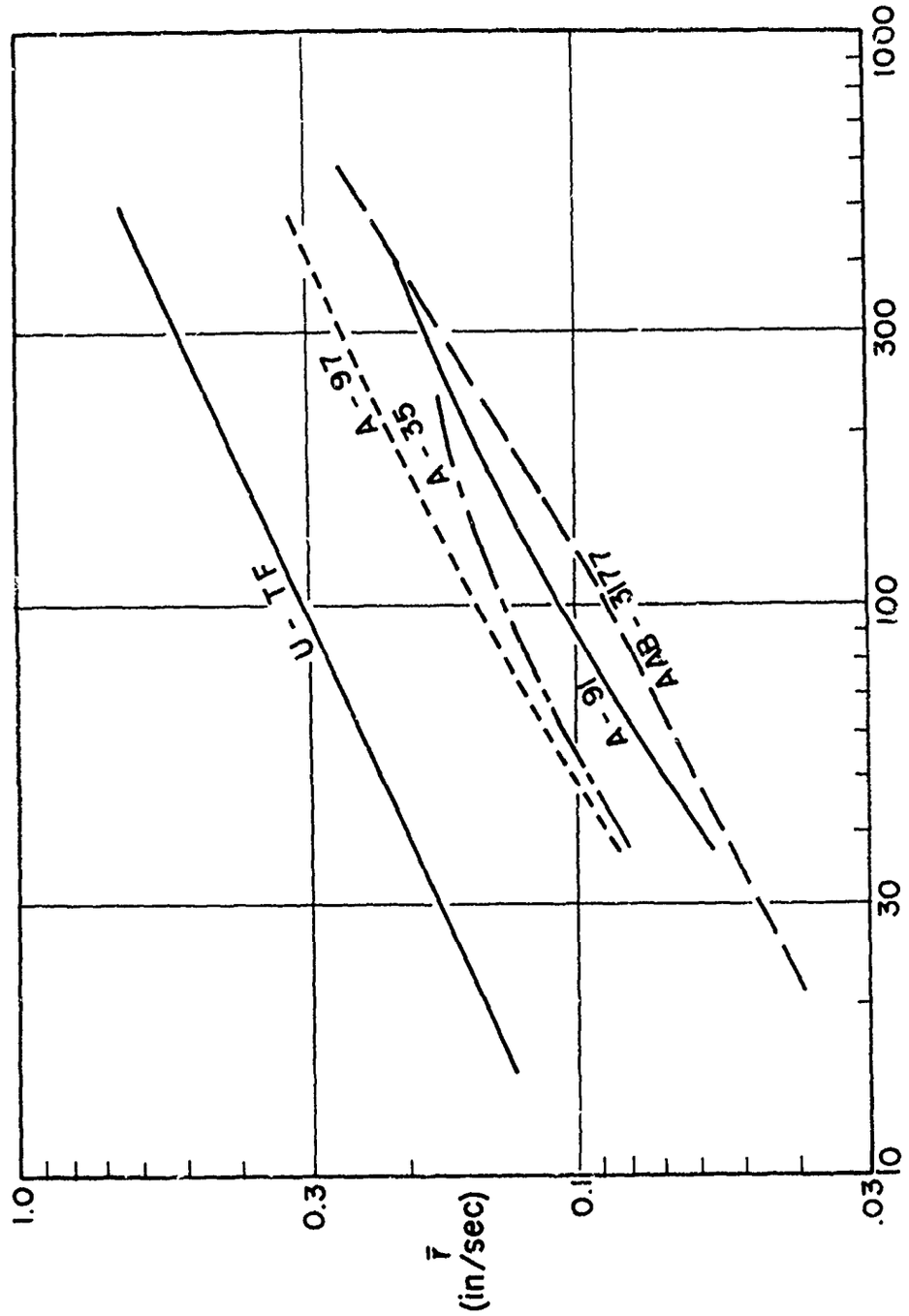

FIG. 5.9. Burning Rate Data for Propellants Reported on in the Present Study.

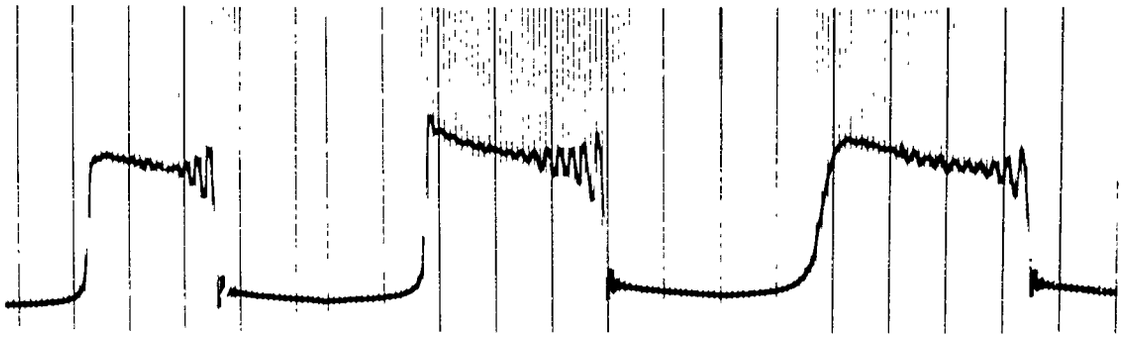

FIG. 5.10. Typical Oscillogram Traces Demonstrating NAI. The propellant is A-35, the mean pressure is approximately 110 psia, and major divisions represent 0.1 sec.

the values of the initial and final L* of the burner, assuming that at any time the fraction of the total area beneath the pressure trace is proportional to the fraction of the total mass of propellant burned and therefore indicative of the change in L*.

The data obtained with the above mentioned propellants have been tabulated in Tables 5.2 to 5.5. In addition to the tabulation of raw data these tables include other quantities such as the chamber and combustion time constants which have been calculated from the raw data and the propellant properties.

5.4.2. Experimental Results

The remainder of this section will be devoted to the discussion of plots of the various quantities. For purposes of reference, data obtained by Beckstead (Ref. 14 and 71) for Utah TF propellant have been included in the majority of the plots. The U-TF propellant is an aluminized, bimodal AP-PBAA propellant containing copper chromite as a burning rate catalyst, and has a much higher burning rate than those propellants being reported here, as can be seen in Fig. 5.9. Because of the inherent differences between this propellant and those being studied (PBAA binder compared to polyurethane binder, bimodal AP compared to monomodal AP, as well as the difference in burning rate), it was expected that comparing the results of the different propellant systems would be illuminating.

5.4.3. Presentation of Basic Data

In previous work (Ref. 4 and 5), data on NAI have been reported in the form of trends of frequency with pressure. The data for the three NOTS propellants, the Aerojet and Utah propellant have therefore been plotted as frequency versus pressure as well as frequency versus burning rate. The results are presented in Fig. 5.11, with the shaded areas representing the regions wherein data were obtained. The data are presented on log-log

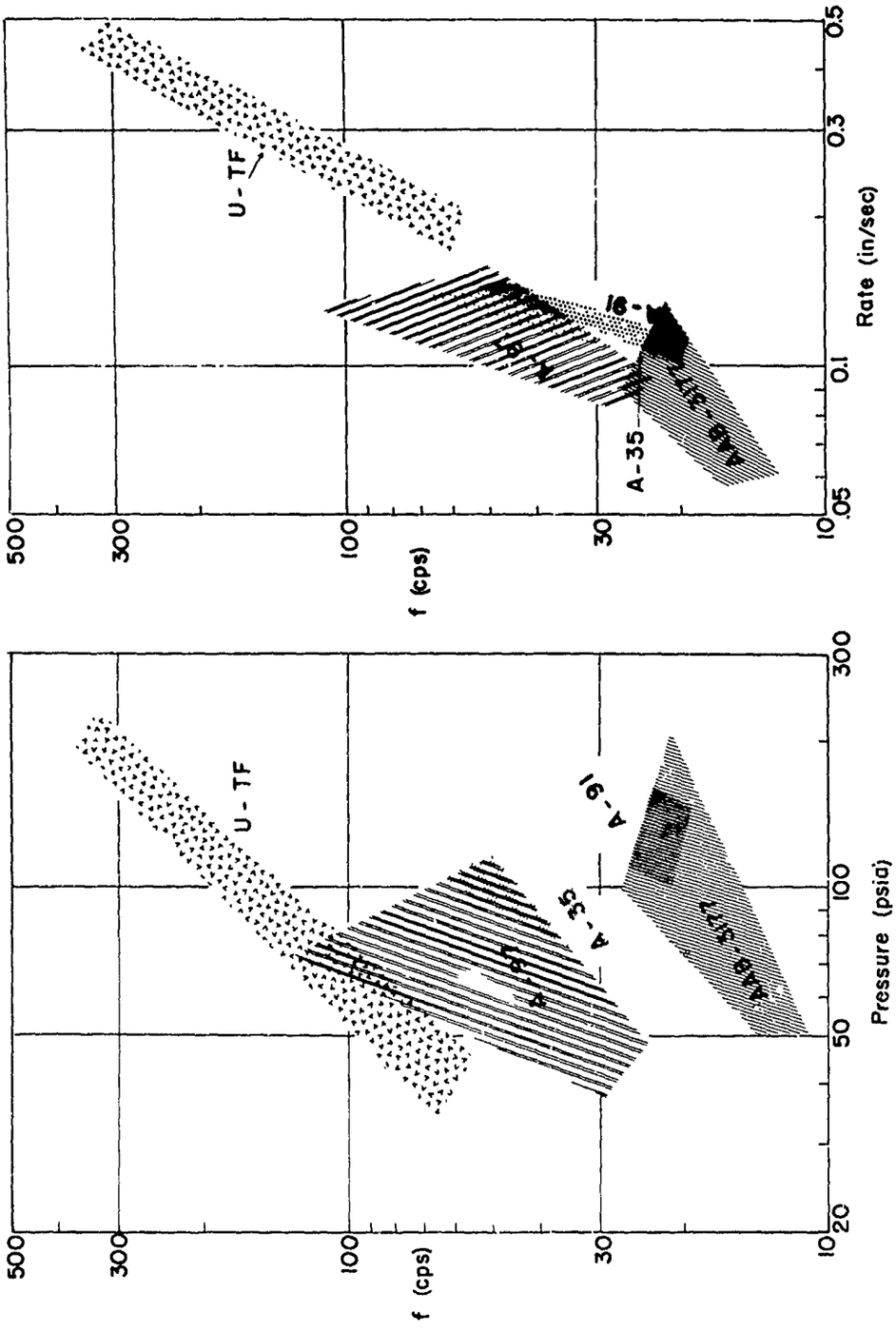

FIG. 5.11. Frequency Versus Pressure and Burning Rate for Several Propellants Demonstrating the Superiority of the Burning Rate in Correlating the Data. (AAB-3177 propellant was supplied by Aerojet General Corporation.)

TABLE 5.2. Data Obtained With A-35 Propellant

Run no.	L*, in.	Frequency, cps	Pressure, psia	Growth constant, sec^{-1}	Chamber time constant msec	Dimensionless frequency, $\frac{4a_t\omega}{\bar{r}^2}$	$\omega\tau_{ch}$	Phase shift, radians	Combustion time constant,	R, Response function
638	53.0	34.0	85	0.0	2.70	10.1	0.578	0.524	2.45	1.156
639	24.0	52.0	100	0.0	1.99	13.5	0.400	0.380	1.165	1.077
do	30.0	40.0	110	0.0	1.53	9.5	0.384	0.375	1.49	1.047
641	25.0	44.0	110	-35.3	1.28	10.4	0.353	0.354	1.28	1.018
do	45.0	38.0	90	10.4	2.30	10.7	0.547	0.490	2.06	1.162
647	48.0	40.0	85	31.8	2.45	11.9	0.615	0.518	2.07	1.241
do	58.0	36.0	85	28.1	2.96	10.7	0.671	0.555	2.46	1.273
do	63.0	33.3	75	29.1	3.21	11.1	0.672	0.552	2.64	1.282
648	16.7	50.0	110	36.2	0.849	11.8	0.267	0.253	0.805	1.067
do	22.5	45.0	110	27.6	1.15	10.7	0.326	0.305	1.08	1.084
do	28.0	42.0	105	24.6	1.43	10.2	0.377	0.349	1.32	1.102
649	24.5	63.0	105	40.4	1.25	15.3	0.493	0.438	1.11	1.162
do	38.0	41.0	100	13.3	1.94	10.6	0.501	0.454	1.76	1.142
do	43.0	40.0	95	20.5	2.19	10.8	0.554	0.487	1.94	1.183
650	52.0	37.5	105	0.0	2.66	9.2	0.627	0.560	2.38	1.181
do	62.0	33.0	100	0.0	3.17	8.6	0.657	0.581	2.80	1.197
651	33.0	47.0	85	37.6	1.68	14.0	0.497	0.436	1.48	1.176
652	30.0	48.0	115	0.0	1.03	10.9	0.460	0.431	1.43	1.102
655	37.0	35.3	105	.....	1.57	8.6	0.349	.....	.....	.....
664	75.0	23.0	80	.....	3.18	7.2	0.459	.....	.....	.....
665	80.0	24.0	80	8.9	4.09	7.6	0.618	0.538	3.56	1.205
666	128.0	19.5	60	9.2	6.52	8.2	0.800	0.648	5.29	1.326
667	65.0	28.0	80	17.7	3.32	8.8	0.581	0.501	2.86	1.210
671	14.0	69.0	140	.....	0.596	13.2	0.258	.....	.....	.....
836	~44.0	38.0	61	.....	2.15	18.2	0.513	.....	.....	.....
837	~60.0	30.0	51	.....	2.55	14.9	0.480	.....	.....	.....
840	~140.0	22.0	50	.....	5.94	11.2	0.822	.....	.....	.....
845	41.0	39.0	66	42.9	2.09	14.7	0.513	0.440	1.80	1.204
846	~40.0	39.0	57	.....	1.70	17.2	0.416	.....	.....	.....
848	~57.0	33.0	66	.....	2.42	12.5	0.503	.....	.....	.....
849	47.0	33.0	70	20.9	2.40	11.9	0.498	0.442	2.13	1.167
850	68.0	28.0	71	17.1	3.47	10.0	0.609	0.522	2.97	1.221
851	~90.0	25.0	56	.....	.....	11.2	0.601	.....	.....	.....

TABLE 5.3. Data Obtained With A-91 Propellant

Run no.	L*, in.	Frequency, cps	Pressure, psia	Growth constant, sec^{-1}	Chamber time constant msec	Dimensionless frequency, $\frac{4a_t\omega}{\gamma^2}$	$\omega\tau_{ch}$	Phase shift, radians	Combustion time constant,	R, Response function
463	35	36.3	180	9.8	1.44	11.5	0.329	0.312	1.34	1.065
do	45	33.3	172	7.8	1.85	11.1	0.389	0.367	1.75	1.097
464	40	33.1	176	.....	1.64	10.9	0.341	.....	.....	.....
470	34	38.8	176	0.0	1.40	1?.8	0.341	0.328	1.35	1.058
472	36	36.4	187	0.0	1.48	11.0	0.339	0.326	1.43	1.057
do	55	28.9	146	16.1	2.26	11.3	0.411	0.379	2.09	1.110
473	32	39.4	178	0.0	1.32	12.5	0.325	0.314	1.27	1.052
475	82	26.2	150	4.1	3.37	9.9	0.556	0.501	3.04	1.158
do	34	36.4	187	.....	1.39	10.3	0.319	.....	.....	.....
476	41	36.4	175	14.4	1.69	11.9	0.385	0.360	1.57	1.094
do	46	33.3	170	21.8	1.89	11.1	0.397	0.365	1.74	1.113
477	36	35.7	195	0.0	1.48	10.4	0.332	0.321	1.43	1.050
do	43	34.5	187	0.0	1.77	14.5	0.385	0.368	1.70	1.070
do	50	31.6	160	17.3	2.06	11.3	0.409	0.377	1.90	1.104
478	39	36.4	175	.....	1.60	11.9	0.366	.....	.....	.....
do	46	31.0	166	7.82	1.89	10.7	0.368	0.347	1.78	1.082
do	50	31.2	163	11.0	2.06	11.0	0.404	0.377	1.92	1.098
482	112	22.5	154	0.0	4.60	8.3	0.652	0.578	4.08	1.193
do	115	22.5	135	20.2	4.73	9.5	0.668	0.548	3.88	1.282
483	77	26.1	154	6.25	3.16	9.7	0.519	0.454	2.77	1.183
488	45	35.0	115	-6.15	1.85	17.4	0.407	0.391	1.78	1.068
489	48	31.0	182	.....	1.97	9.7	0.384	.....	.....	.....
495	29	38.5	145	-12.75	1.19	15.1	0.289	0.284	1.17	1.029
542	67	26.0	163	19.8	2.75	9.1	0.448	0.401	2.46	1.047
do	82	25.0	163	20.2	3.37	8.8	0.530	0.461	2.93	1.190
do	87	23.0	142	10.85	3.58	9.3	0.519	0.464	3.21	1.160
543	102	21.0	142	6.47	4.19	8.5	0.554	0.494	3.74	1.169
544	85	21.5	134	0.0	3.49	9.2	0.472	0.442	3.27	1.106
545	35.0	32.5	170	.....	1.44	11.7	0.293	.....	.....	.....

TABLE 5.3. (Contd.)

Run no.	L*, in.	Frequency, cps	Pressure, psia	Growth constant, sec^{-1}	Chamber time constant msec	Dimensionless frequency, $\frac{4\alpha_t \omega}{r^2}$	$\omega \tau_{ch}$	Phase shift, radians	Combustion time constant,	R, Response function
547	30.0	32.0	131	-17.8	1.23	14.2	0.248	0.250	1.24	1.004
552	100.0	22.0	166	-7.12	4.11	7.55	0.569	0.531	3.84	1.123
553	75.0	23.0	150	21.6	3.08	10.6	0.545	0.473	2.69	1.197
614	53.0	26.7	135	0.0	2.18	11.3	0.366	0.351	2.09	1.065
do	65.0	21.0	125	0.0	2.67	9.6	0.352	0.339	2.57	1.060
615	75.0	26.0	120	0.0	3.08	12.3	0.503	0.466	2.85	1.120
618	30.0	40.0	135	25.1	1.23	16.9	0.310	0.291	1.16	1.080
618a	55.0	25.0	130	16.1	2.26	10.9	0.357	0.332	2.11	1.097
do	65.0	23.0	123	10.8	2.67	10.6	0.388	0.361	2.50	1.098
623	110.0	23.0	130	9.65	4.52	10.0	0.555	0.562	3.19	1.230
624	15.0	57.0	175	39.2	0.658	18.7	0.236	0.225	0.629	1.057
625	50.0	37.0	200	12.6	2.06	10.6	0.480	0.438	1.88	1.132
627	72.0	25.0	120	20.8	2.96	11.8	0.466	0.414	2.63	1.159
do	77.0	23.5	100	.....	3.16	13.7	0.466	.....	.....	.....
628	85.0	27.8	120	18.4	3.49	13.0	0.605	0.518	3.00	1.222
629	57.0	30.0	145	24.4	2.34	11.7	0.443	0.396	2.10	1.150
630	80.0	24.4	120	0.0	3.28	11.7	0.503	0.466	3.13	1.120
631	30.0	37.0	145	32.3	1.23	14.5	0.286	0.269	1.16	1.078
632	15.0	42.0	155	39.1	0.616	15.4	0.163	0.158	0.599	1.037
do	22.0	40.0	150	38.6	0.904	15.2	0.227	0.215	0.854	1.066
633	21.0	44.0	180	0.0	0.863	13.9	0.240	0.236	0.852	1.027
do	23.0	44.0	190	-19.8	0.945	13.3	0.262	0.251	0.909	1.054
711	45.0	36.0	90	0.0	1.85	23.1	0.420	0.398	1.76	1.084
712	101.5	21.0	75	6.25	4.17	16.9	0.552	0.494	3.75	1.164
do	104.0	21.0	75	0.0	4.27	16.9	0.565	0.515	3.90	1.148
do	108.0	21.0	85	-9.8	4.44	14.6	0.588	0.552	4.18	1.122
717	42.0	34.0	170	.....	1.73	11.3	0.369	.....	.....	.....
do	48.0	27.0	150	.....	1.97	10.2	0.334	.....	.....	.....

TABLE 5.4. Data Obtained With A-97 Propellant

Run no.	L*, in.	Frequency, cps	Pressure, psia	Growth constant, sec^{-1}	Chamber time constant msec	Dimensionless frequency, $\frac{4a_t\omega}{\bar{r}^2}$	$\omega\tau_{ch}$	Phase shift, radians	Combustion time constant, msec	R, Response function
685	24.0	46	70	.....	0.990	21.7	0.287	.....	.....	.....
do	26.0	44	70	.....	1.07	20.7	0.296	.....	.....	.....
do	28.0	35	70	.....	1.16	16.5	0.255	.....	.....	.....
686	9.0	55	60	-13.6	0.371	30.9	0.128	0.128	0.37	1.000
687	35.0	36	60	-17.1	1.44	20.2	0.323	0.319	1.41	1.029
688	39.0	36	75	.....	1.61	15.7	0.363	.....	.....	.....
694	16.0	52	90	.....	0.660	18.4	0.215	.....	.....	.....
do	21.0	60	90	.....	0.867	20.2	0.325	.....	.....	.....
695	27.0	44	85	.....	1.11	16.7	0.306	.....	.....	.....
698	11.0	55	50	24.5	0.454	37.9	0.157	0.154	0.44	1.024
do	15.0	54	50	32.7	0.619	37.2	0.210	0.203	0.60	1.045
699	27.0	38	45	14.4	1.11	29.8	0.265	0.255	1.07	1.051
do	31.0	38	43	9.2	1.28	31.5	0.306	0.293	1.23	1.060
700	39.0	33	42	13.8	1.61	27.9	0.335	0.317	1.52	1.073
do	42.0	33	42	11.8	1.73	27.9	0.358	0.338	1.62	1.079
701	58.0	31	40	.....	2.39	27.7	0.465	.....	.....	.....
do	65.0	29	40	.....	2.68	26.0	0.488	.....	.....	.....
743	11.3	68	110	38.8	0.466	19.5	0.199	0.193	0.452	1.039
do	12.2	67	110	45.5	0.503	19.2	0.211	0.204	0.485	1.040
do	13.0	68	110	.....	0.537	19.5	0.229	.....	.....	.....
do	14.0	69	105	41.8	0.577	20.7	0.250	0.239	0.552	1.056
do	14.7	63	95	.....	0.606	21.1	0.239	.....	.....	.....
do	15.4	62	95	.....	0.634	20.8	0.247	.....	.....	.....
do	16.0	62	90	.....	0.659	21.9	0.256	.....	.....	.....
744	20.0	45	110	0.0	0.824	12.9	0.233	0.229	0.810	1.028
754	36.9	38	85	35.2	1.52	14.4	0.363	0.332	1.39	1.114
do	39.6	40	85	24.1	1.63	15.2	0.410	0.375	1.495	1.119
746	57.0	42	100	.....	2.38	13.3	0.628	.....	.....	.....
752	17.8	47	100	34.9	0.733	14.9	0.216	0.208	0.705	1.047
753	19.4	56	100	33.3	0.799	17.8	0.281	0.267	0.758	1.065

TABLE 5.4. (Contd.)

Run no.	L*, in.	Frequency, cps	Pressure, psia	Growth constant, sec^{-1}	Chamber time constant msec	Dimensionless frequency, $\frac{4a_t\omega}{\bar{r}^2}$	$\omega\tau_{ch}$	Phase shift, radians	Combustion time constant, msec	R, Response function
do	21.7	53	100	34.8	0.894	16.8	0.298	0.281	0.873	1.073
do	23.3	55	100	40.3	0.960	17.5	0.332	0.310	0.896	1.089
do	24.6	51	95	.....	1.01	17.1	0.324	.....	.....	.....
776	14.3	95	87	.....	0.590	35.0	0.352	.....	.....	.....
do	15.0	83	87	.....	0.619	30.6	0.322	.....	.....	.....
do	15.9	83	87	.....	0.656	30.6	0.341	.....	.....	.....
778	36.0	44	85	.....	1.49	16.7	0.411	.....	.....	.....
do	37.0	57	85	.....	1.53	21.7	0.549	.....	.....	.....
do	40.0	38	78	.....	1.65	15.7	0.394	.....	.....	.....
779	44.0	36	66	-9.35	1.82	18.0	0.410	0.395	1.74	1.068
do	47.0	45	92	.....	1.94	15.5	0.547	.....	.....	.....
780	15.9	57	69	35.7	0.656	27.2	0.235	0.226	0.63	1.025
781	42.0	36	66	0.0	1.73	18.0	0.391	0.373	1.64	1.073
do	47.0	44	81	.....	1.94	17.5	0.537	.....	.....	.....
785	24.4	42	61	0.0	1.00	23.0	0.265	0.259	0.982	1.034
787	14.9	63	74	0.0	0.615	27.8	0.244	0.239	0.61	1.022
do	17.0	62	71	21.2	0.702	28.7	0.273	0.263	0.68	1.050
788	13.0	110	73	58.7	0.537	49.3	0.371	0.346	0.50	1.098
789	30.0	46	69	0.0	1.24	22.0	0.357	0.343	1.19	1.062
do	31.8	45	74	0.0	1.31	19.6	0.371	0.355	1.26	1.067
790	9.4	102	66	34.3	0.388	51.2	0.249	0.241	0.38	1.012
791	13.0	73	59	.....	0.560	41.4	0.246	.....	.....	.....
792	29.0	48	57	31.1	1.20	28.4	0.361	0.336	1.11	1.095
793	61.0	32	70	.....	2.52	19.8	0.665	.....	.....	.....
794	23.3	57	76	.....	0.962	24.4	0.343	.....	.....	.....
795	9.5	66	64	36.8	0.392	34.2	0.162	0.159	0.38	1.012
796	20.3	60	59	26.3	0.838	34.0	0.316	0.300	0.80	1.067
797	32.3	66	52	25.2	1.33	43.3	0.550	0.488	1.18	1.17
798	54.0	33	51	0.0	2.23	22.1	0.462	0.433	2.08	1.100
do	58.0	30	51	0.0	2.39	20.1	0.449	0.423	2.24	1.095
799	74.0	27	50	.....	3.05	18.6	0.517	.....	.....	.....
do	77.0	28	50	.....	3.17	19.3	0.558	.....	.....	.....
do	80.0	29	50	.....	3.30	20.0	0.601	.....	.....	.....
800	10.1	59	81	.....	0.416	23.4	0.154	.....	.....	.....
do	15.4	54	86	.....	0.634	20.2	0.215	.....	.....	.....
801	22.4	54	84	.....	0.923	20.5	0.313	.....	.....	.....
	30.0	58	91	.....	1.24	20.5	0.450	.....	.....	.....

TABLE 5.5. Data Obtained With AAB-3177 Propellant

Run no.	L*, in.	Frequency, cps	Pressure, psia	Chamber time constant, msec	Dimensionless frequency, $\frac{4a_t\omega}{\bar{r}^2}$	Dimensionless $I^*, \frac{L^*c^* \text{ mw } \bar{r}^2}{4\kappa RT_f}$	$\omega\tau_{ch}$
759	68	22.2	200	2.78	10.1	0.0246	0.388
760	84	22.1	170	3.44	12.3	0.0248	0.478
762	57	27.0	95	2.33	29.3	0.00867	0.395
do	63	19.0	70	2.58	27.8	0.00709	0.308
763	121	6.4	120	4.95	5.35	0.0238	0.199
764_1	103	17.0	105	4.22	16.45	0.0175	0.451
764_2	100	15.0	80	4.09	19.4	0.0127	0.385
765	133	13.6	65	5.44	21.8	0.0137	0.465
do	155	5.7	75	6.34	7.9	0.0184	0.227
766	94	19.0	180	3.85	9.8	0.0300	0.460
802	95	15.0	110	3.89	13.8	0.0170	0.367
do	105	16.0	122	4.30	13.3	0.0208	0.432
803	126	6.0	98	5.16	6.23	0.0199	0.194
do	151	12.0	206	6.18	5.30	0.0562	0.466
804	167	5.3	86	6.84	6.34	0.0230	0.228
805	207	4.5	84	8.47	5.58	0.0274	0.239
do	226	5.8	127	9.25	4.57	0.0473	0.337
807	100	17.0	89	4.09	19.6	0.0143	0.437
808	151	5.4	84	6.18	6.70	0.0200	0.210
do	166	5.2	84	6.79	6.45	0.0220	0.222
809	194	5.4	70	7.94	8.04	0.0214	0.269
do	199	4.5	74	8.15	6.35	0.0231	0.230
810	259	4.7	67	10.60	7.29	0.0274	0.313
811	70	24.0	114	2.87	21.2	0.0130	0.433
do	74	19.0	116	3.03	16.6	0.0139	0.362
do	80	17.0	104	3.27	16.7	0.0134	0.349
812	113	15.0	70	4.63	22.3	0.0125	0.436
813	165	14.0	52	6.75	28.6	0.0133	0.594
do	174	5.4	55	7.12	10.4	0.0149	0.242
814	213	4.6	52	8.72	9.41	0.0171	0.252
816	123	15.0	50	5.03	31.9	0.00953	0.474
do	135	5.1	71	5.53	7.48	0.0151	0.503
817	141	12.0	49	5.77	26.2	0.0106	0.435
818	95	16.0	69	3.89	24.1	0.0104	0.391
do	100	16.0	55	4.09	30.9	0.00851	0.411
819	231	4.9	56	9.46	9.29	0.0202	0.291

coordinates so that the U-TF data at frequencies above 100 cps do not dominate the plot. The pressure range is essentially the same for all of the propellants, but there is no readily apparent correlation between the frequency and the pressure for the different propellants. It is clear that the combined trend of frequency for the whole set of propellants is better corr d by burning rate than by pressure. This would indicate that the burning rate of the propellant is more important in determining the frequency of nonacoustic oscillations than is the pressure level of the combustion chamber. Therefore, the burning rate will be utilized extensively as a correlating parameter throughout the remainder of the discussion.

An interesting phenomenon was observed with the AAB-3177 propellant. Two distinct frequencies were often observed during a single experimental run, one frequency being considerably lower than the expected frequency. Figure 5.12 is an oscilloscope trace of such a firing. The propellant began chuffing with oscillations on the chuffs of about 14 cps and the final[17] oscillations were approximately 6 cps. The possibility of two frequencies occurring for identical test conditions has been discussed in connection with Fig. 5.5. All of the frequency-burning rate data obtained with the AAB-3177 propellant are contained in Fig. 5.13 and the two different trends in the data can readily be seen. The data below 10 cps do not fit the trend observed in Fig. 5.11, but do seem to increase slightly with burning rate. The phenomenon of two different nonacoustic frequencies occurring for a given propellant and at essentially the same test conditions has been reported once before (Ref. 71), and was then reported to be related to radiative heat transfer in depth (the propellant was translucent). In the present case the propellant is not translucent and thus radiative heat transfer would not seem to be so important. However, the propellant does contain mixed oxidizers (ammonium perchlorate and potassium perchlorate) and the anomalous behavior might well be related to this fact. One thing that both propellants do have in common is that each contains a bimodal mixture of AP which could perhaps contribute to the dual frequency phenomenon. These various lines of reasoning have not been pursued and further investigation will be necessary to establish the actual causative factors.

The observation that the frequency of the oscillations is correlated by the burning rate provides some basis for the heavy emphasis of earlier analyses of NAI on transient behavior of the thermal wave in the solid during instability. This point was examined further by calculating the thermal wave accommodation time (τ_{tw}) for each of the experimental data points, and plotting the values against the combustor flushing time τ_{ch}. From this plot, it was possible to determine a stability boundary for each propellant below which α was too small for measurable oscillations. These stability boundaries are shown in Fig. 5.14, and include also boundaries based on data from Ref. 71 and the stability limits for JPL 534 propellant from Ref. 13. Considering the results in Eq. 5.19 and Ref. 13, the trend of the stability limit lines in Fig. 5.14 would be expected to

[17] The firing terminated abruptly when the pyrex wall failed.

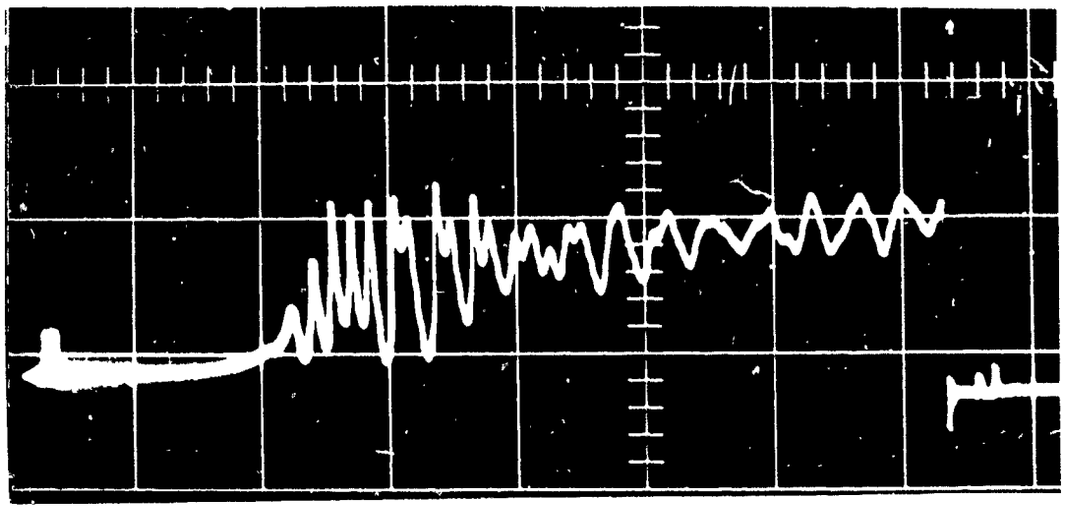

FIG. 5.12. Pressure-Time Trace for AAB-3177. The oscillations pass from a higher frequency to a much lower frequency. The test terminated abruptly when the Pyrex wall failed.

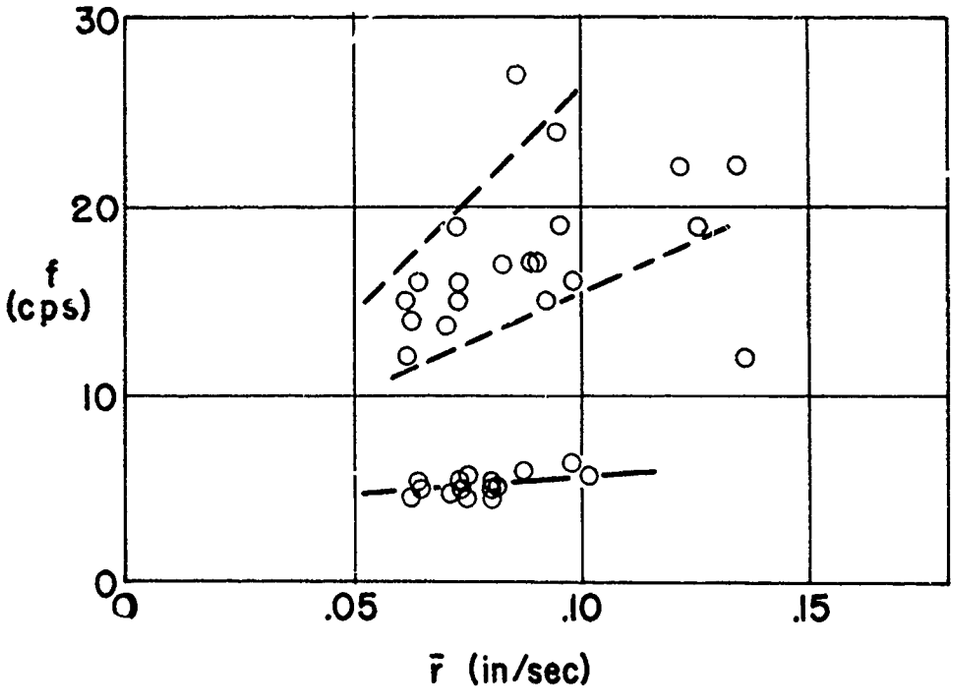

FIG. 5.13. Frequency-Burning Rate Data for AAB-3177 Demonstrating Dual Frequency Nature of Data.

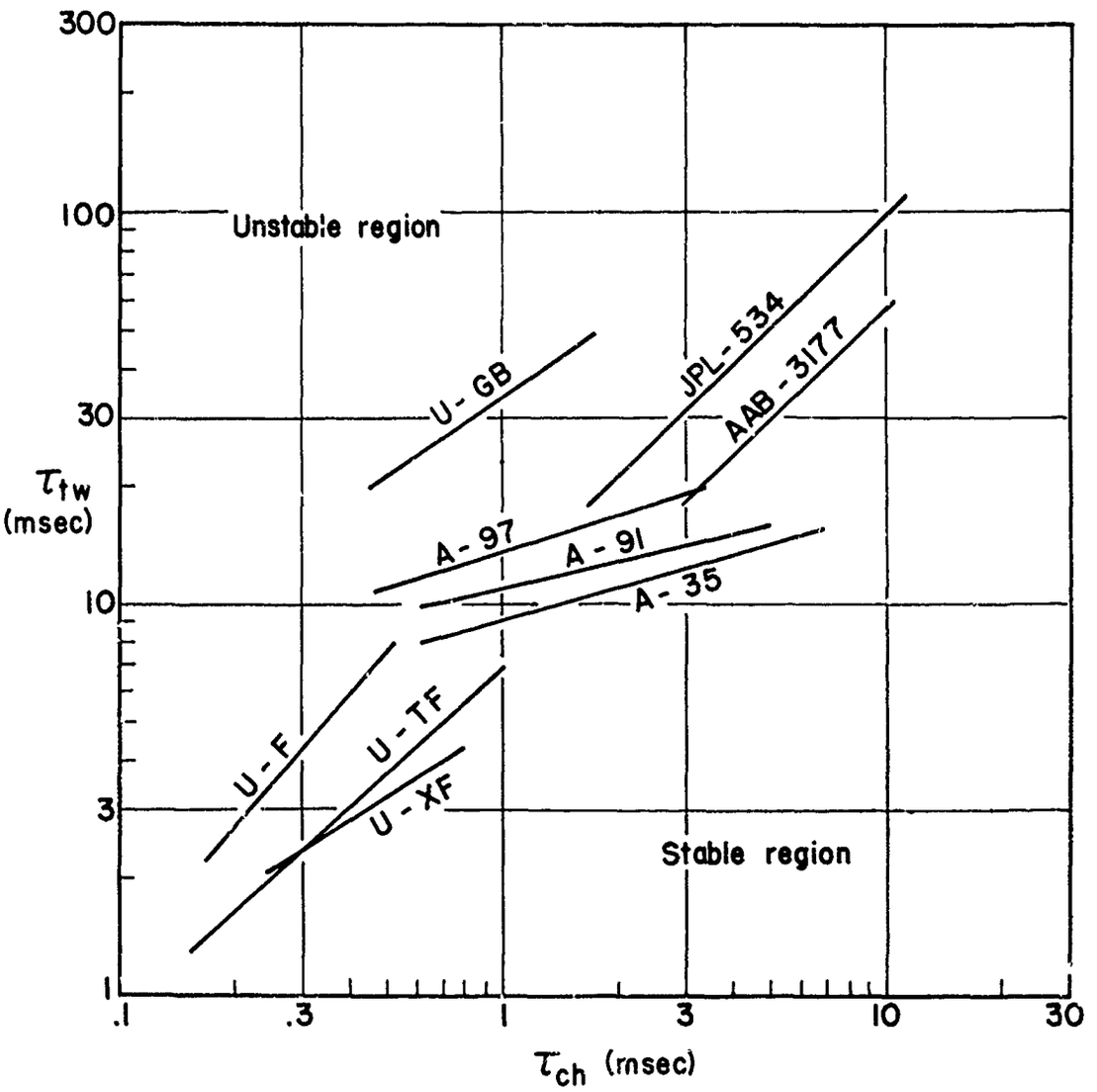

FIG. 5.14. Stability Limits for the Propellants Tested Including Data From Ref. 13 and 71. The coordinates are the thermal wave relaxation time and the chamber residence or flushing time.

have a slope of 1.0 for each propellant (noting that $\tau_{tw} \propto 1/r^2$). Although the conformance of most of the propellants to a general trend seems to indicate the importance of thermal wave accommodation time at these low frequencies, it is clear from the figure that this trend is not supported individually by all propellants. It has been suggested earlier that the dynamics of agglomeration and combustion of the metal fuel ingredient is likely to be a factor also (Ref. 8). This is supported by comparison of the stability limits of the U-F, U-TF, and U-XF propellants, all of which are the same except for content of aluminum of 0, 5 and 10% respectively (with corresponding variations in AP content). These three propellants have practically the same burning rate, but the addition of aluminum caused progressive decrease in the slope of the stability limit line not predicted in the models based on a thermal wave analysis.

The results of the present theoretical analysis (see Fig. 5.5) indicate that the growth constant, α, should correlate with the frequency. The growth constant data from the three NOTS propellants are presented in Fig. 5.15 and there does appear to be some correlation and similarity in the three plots. A dependence of frequency on L* has been reported previously (Ref. 14 and 71) and has been observed in the present work (see Fig. 5.16). It should be noted that in Fig. 5.15 and 5.16 the data are for various burning rates and the effect caused by the burning rate has not been separated.

5.4.4. Calculated Response Functions and Combustion Times

The results of the present theoretical analysis provide a basis for a more discerning interpretation of experimental results than has been possible in the past. Thus, Eq. 5.6a and 5.6b may be combined to permit calculation of the values of τ and R from measured values of α, ω and L*

$$\tau = \frac{1}{\omega} \tan^{-1} \left(\frac{\omega \, AL^*}{1 + \alpha \, AL^*} \right) \tag{5.23}$$

and

$$R = \frac{\omega \, AL^*}{\sin \omega\tau} = \frac{\omega \, AL^*}{\sin \left[\tan^{-1} \left(\frac{\omega \, AL^*}{1 + \alpha \, AL^*} \right) \right]} \tag{5.24}$$

Utilizing these equations, data obtained with several propellants have been employed to calculate values for the response function and the time lead. The remainder of this section will be devoted to the discussion of these results and their relationship to the stability trends discussed in the preceding section.

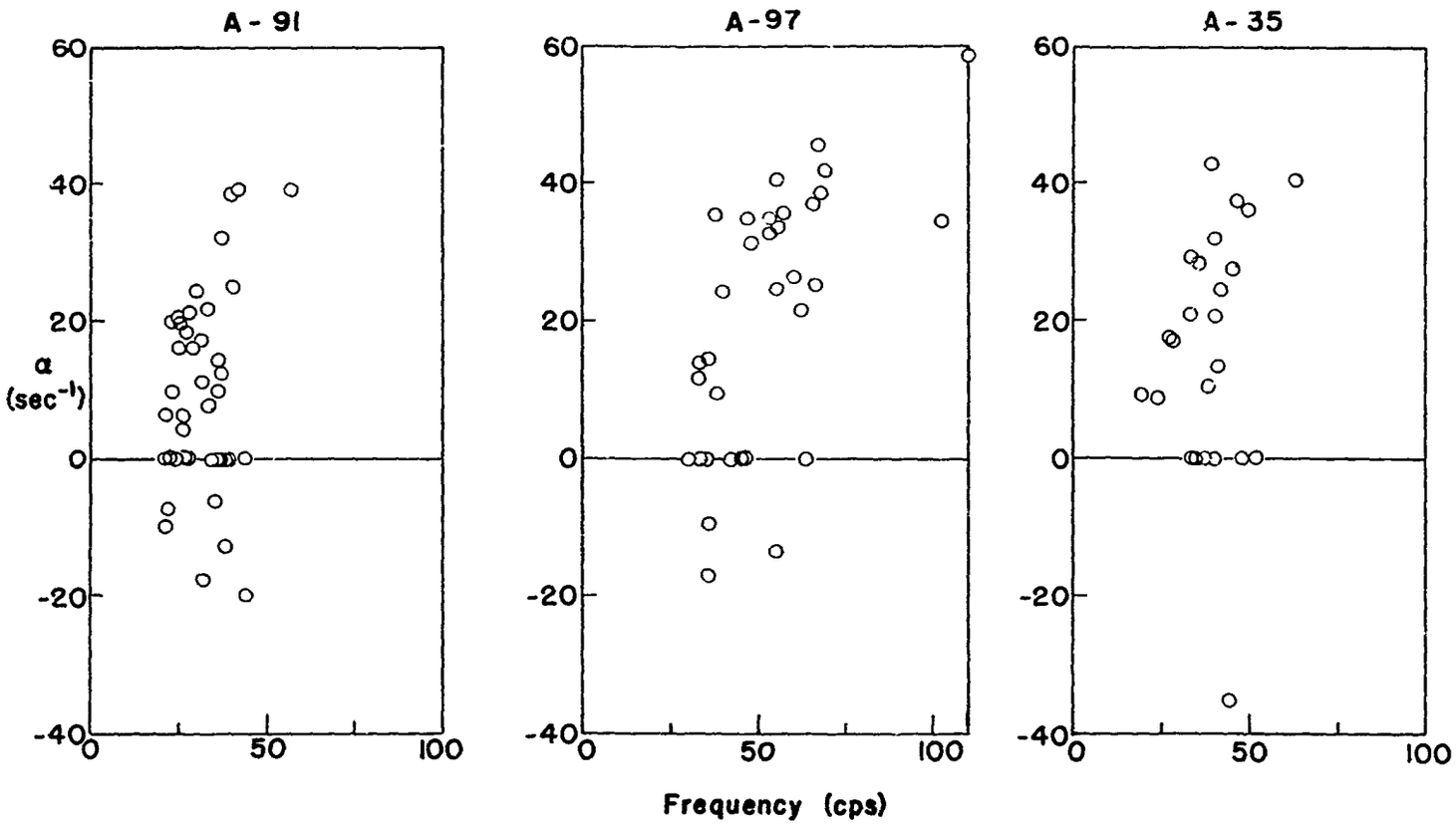

FIG. 5.15. Growth Constant as a Function of Frequency for Three Different Propellants. No burning rate dependence has been accounted for.

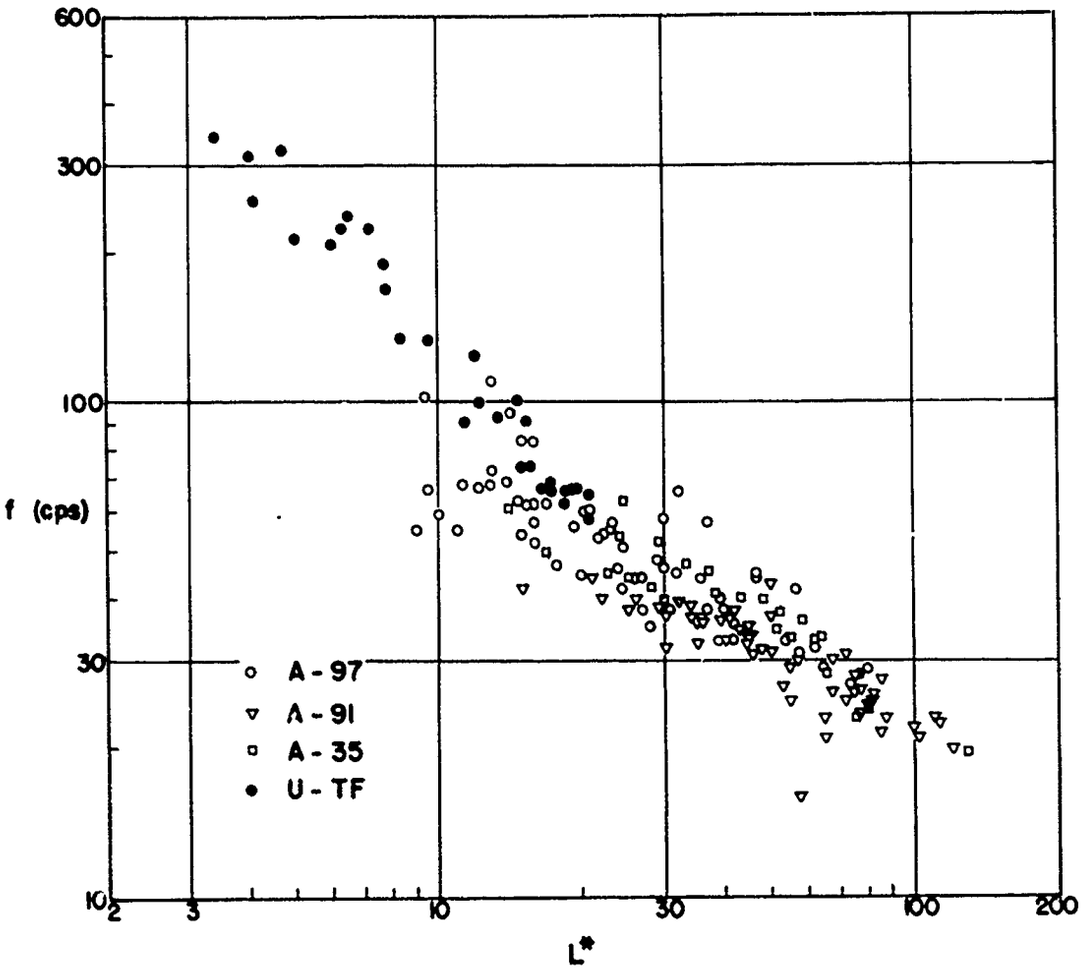

FIG. 5.16. Frequency Versus L* for Different Propellants

Equation 5.9 implies very stringent restrictions on the relation between combustion time lead and combustor flushing time. A comparison of the experimental results (using Eq. 5.23) is shown in Fig. 5.17, where the conformance of the results with the restrictions expressed in Eq. 5.9 offers impressive support for the theoretical model, and re-emphasizes the extremely limited range of conditions under which NAI can occur.

A further comparison of theory and experiment can be made in the context of Fig. 5.4 and 5.6 by plotting the experimentally determined values of the combustion time lead versus frequency. These results are contained in Fig. 5.18 and 5.19. Figure 5.18 contains data for several propellants at many different pressures, while the data of Fig. 5.19 are for one propellant with pressure as a parameter. The latter is analogous to Fig. 5.6 and the trends are seen to be similar in the two figures.

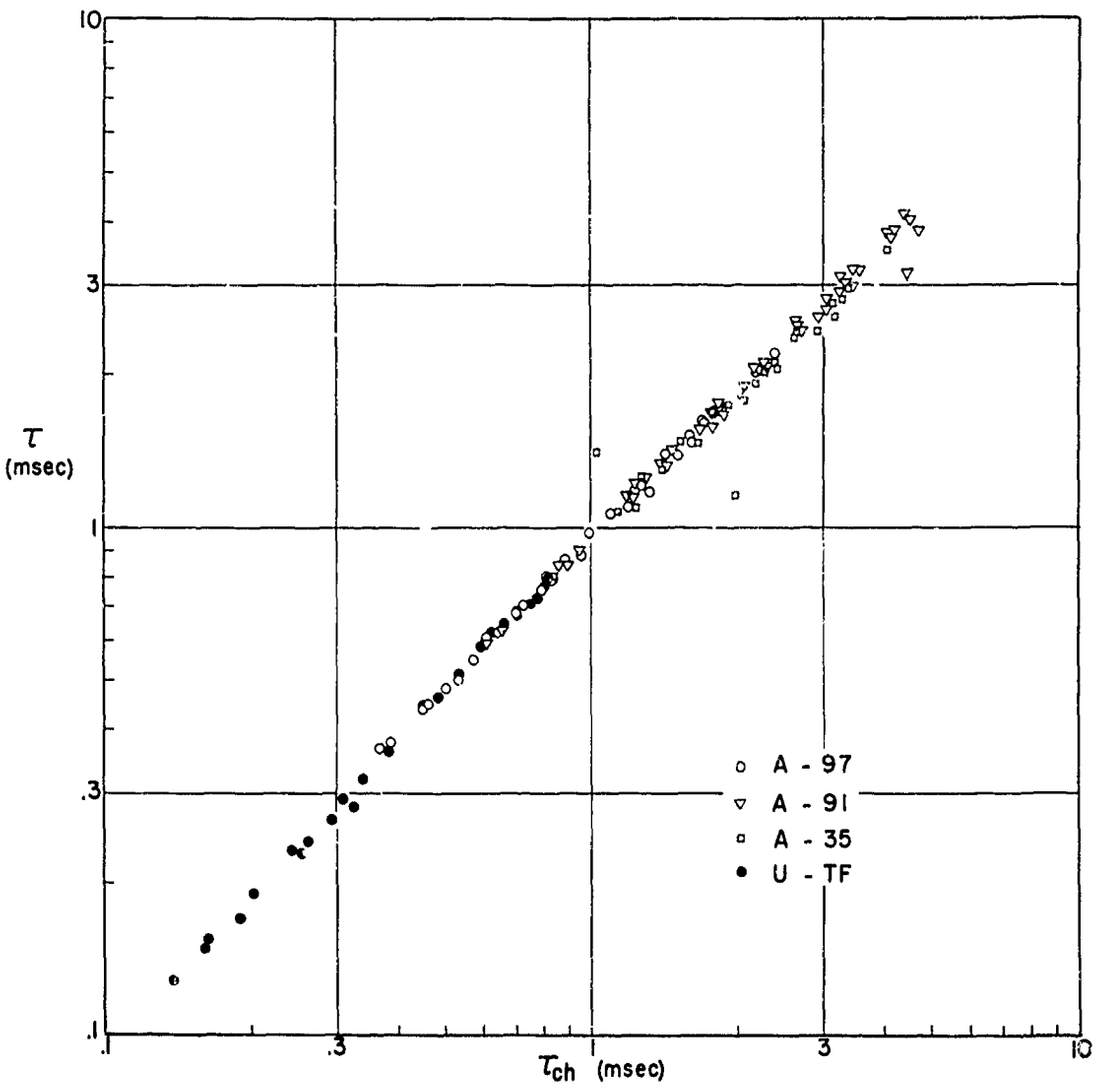

FIG. 5.17. The Combustion Time Versus the Chamber Time Constant Showing the Very Restricted Nature of NAI.

In Fig. 5.18, the data are observed to fall in a band parallel to the constant R stability lines. The upper right portion of the band represents data having very small values of α and hence, are close to the stability limit for the individual propellants. Proceeding through the band of data at approximately constant pressure (such as in Fig. 5.19) it can be observed from the raw data that with increasing frequency and decreasing τ, L* decreases and α increases. The lower edge of the data band thus lies in a region of high α where data are difficult to obtain because of the tendency for nonlinearities and chuffing to occur. These experimental trends are consistent with the illustrative examples, where

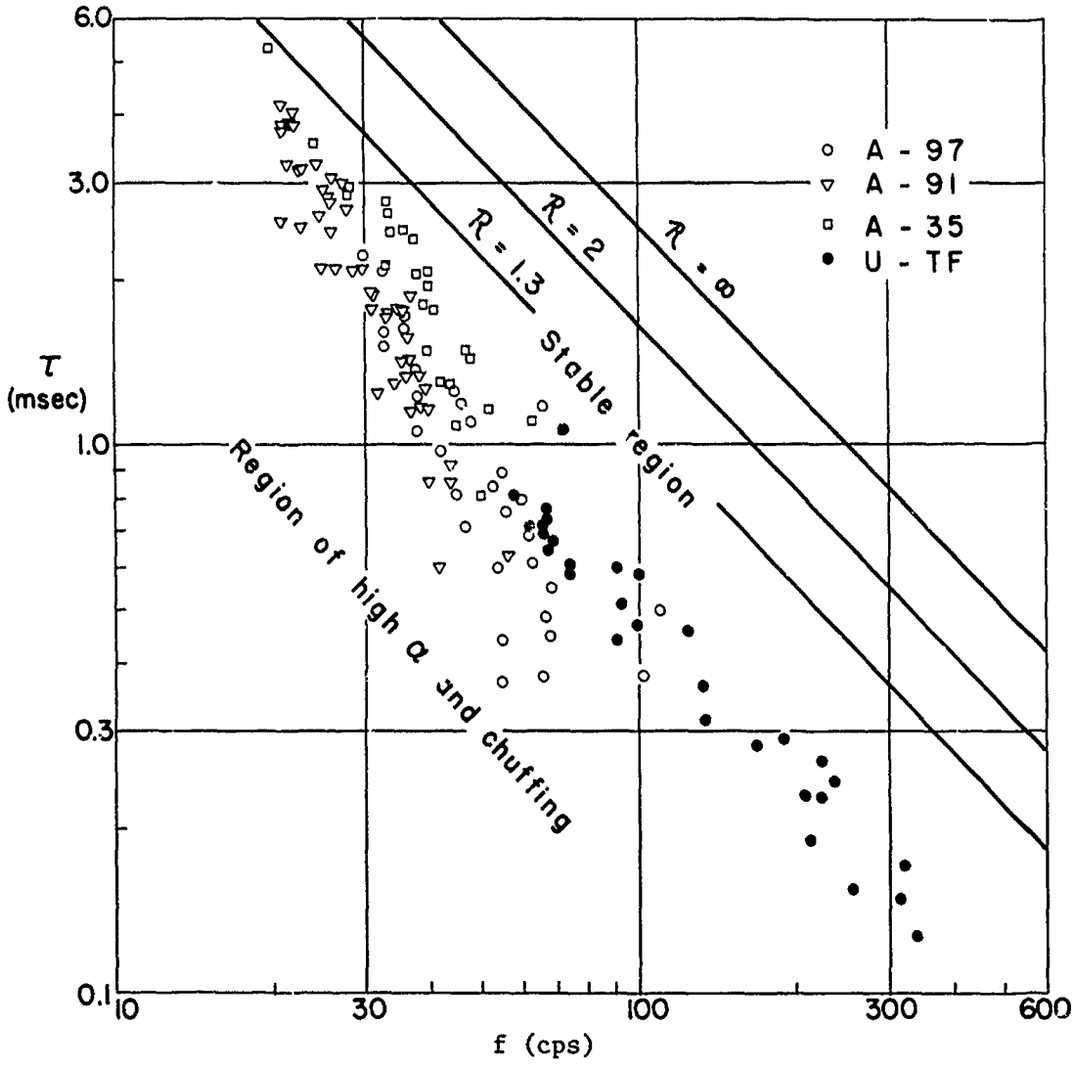

FIG. 5.18. The Combustion Time Versus Frequency Showing the Constant R Lines of Fig. 5.4 and the Region of High α and Chuffing.

the trend to high values of α corresponds to the condition of τ approaching zero. This detailed agreement between trends of experimental results and theoretical predictions lends further credence to the analytical model and to the functional forms of $R(\omega)$ and $\tau(\omega)$ used in the examples.

A figure analogous to Fig. 5.6 can be constructed in the R-ω plane. In this case a stability limit is established with Eq. 5.11 and the τ-ω relation for a given burning rate or pressure. Figure 5.20 represents

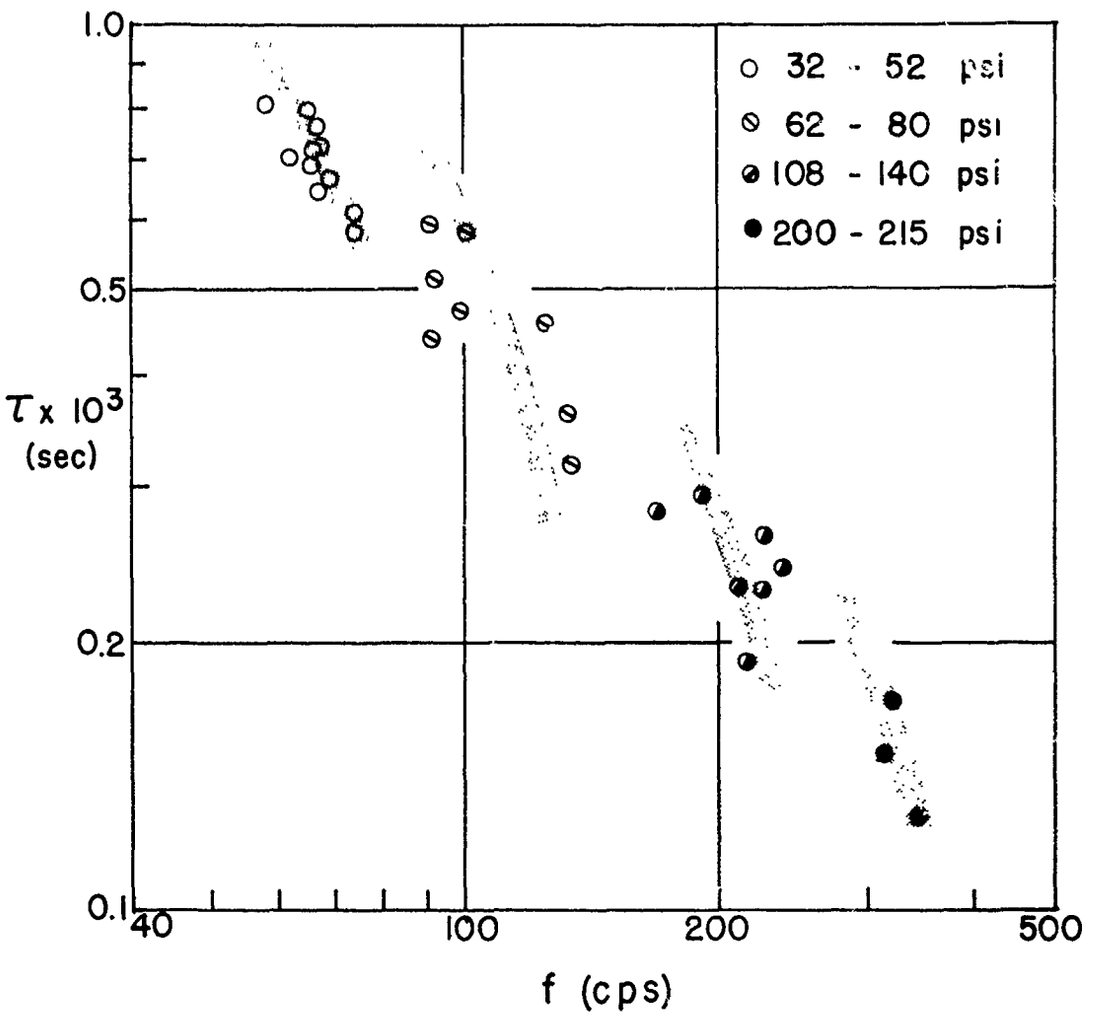

FIG. 5.19. τ Versus Frequency Data for U-TF Propellant (See Ref. 71) With Pressure as a Parameter.

such a plot. In this case the unstable domain (shaded area) is above the neutral stability curve. When the corresponding R-ω relation is plotted in the figure, the points that conform to Eq. 5.6 are along the R-ω curve in the shaded area, with α increasing from zero at the stability limit and approaching infinity as ω_o is approached. Experimental data would presumably be obtainable exhibiting such a trend, with the location of the band of data in the R-ω diagram being dependent on burning rate in a manner discussed before, i.e., high burning rate data to the right.

Utilizing Eq. 5.24, the magnitude of the response can now be calculated directly from L* burner data as a function of both frequency and

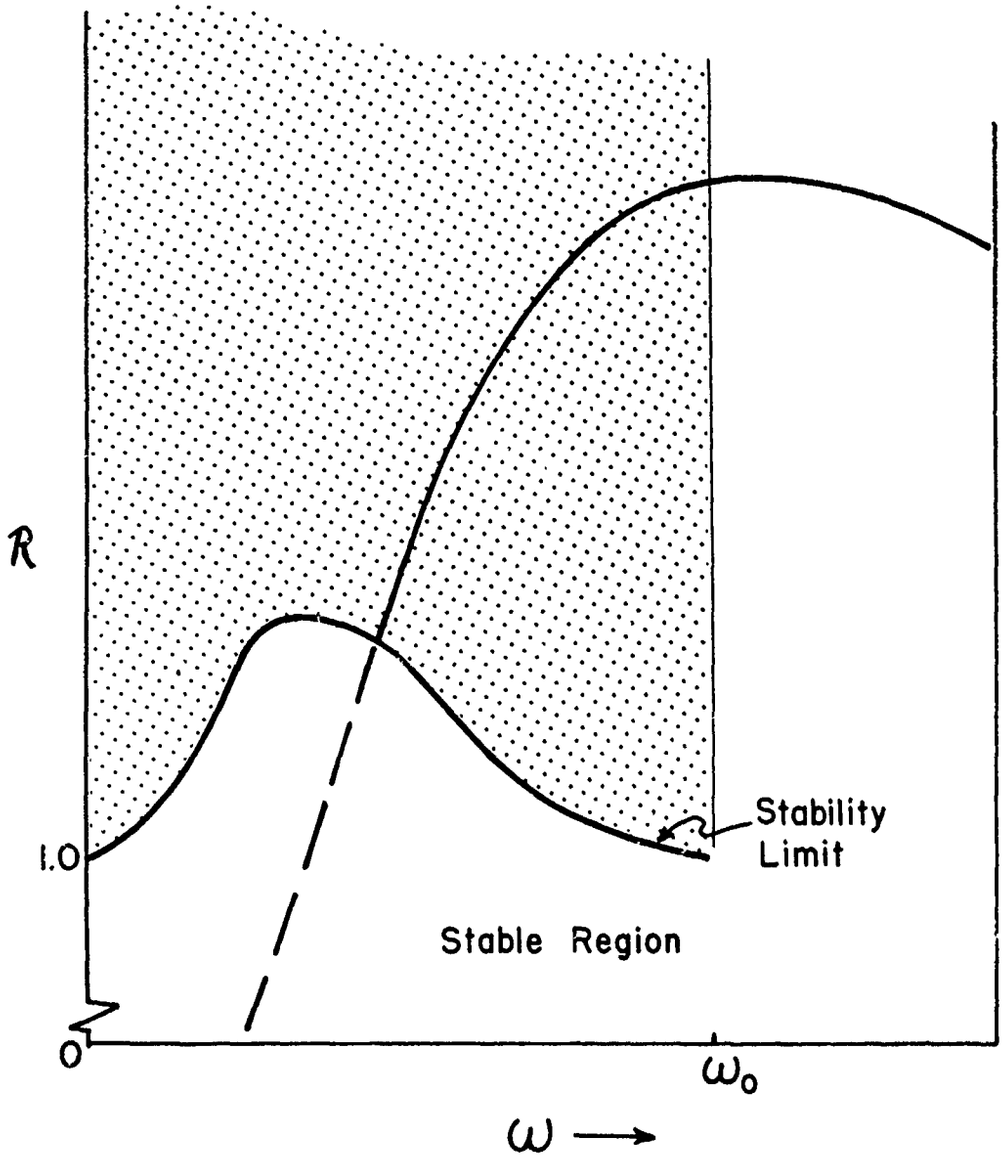

FIG. 5.20. R Versus ω Stability Map Which Shows the Possible Unstable Conditions (Shaded Area). The dotted portion of the R curve would represent stable conditions for that example.

pressure. Figure 5.21 shows the calculated values of R for two propellants at several different pressures. While the reproducibility of the experiment does not provide an accurate representation of the trends, it is clear that the data are qualitatively consistent with the examples of Fig. 5.2, corresponding to the low frequency portion of the curve where R is greater than one and increasing with frequency. The reasons that

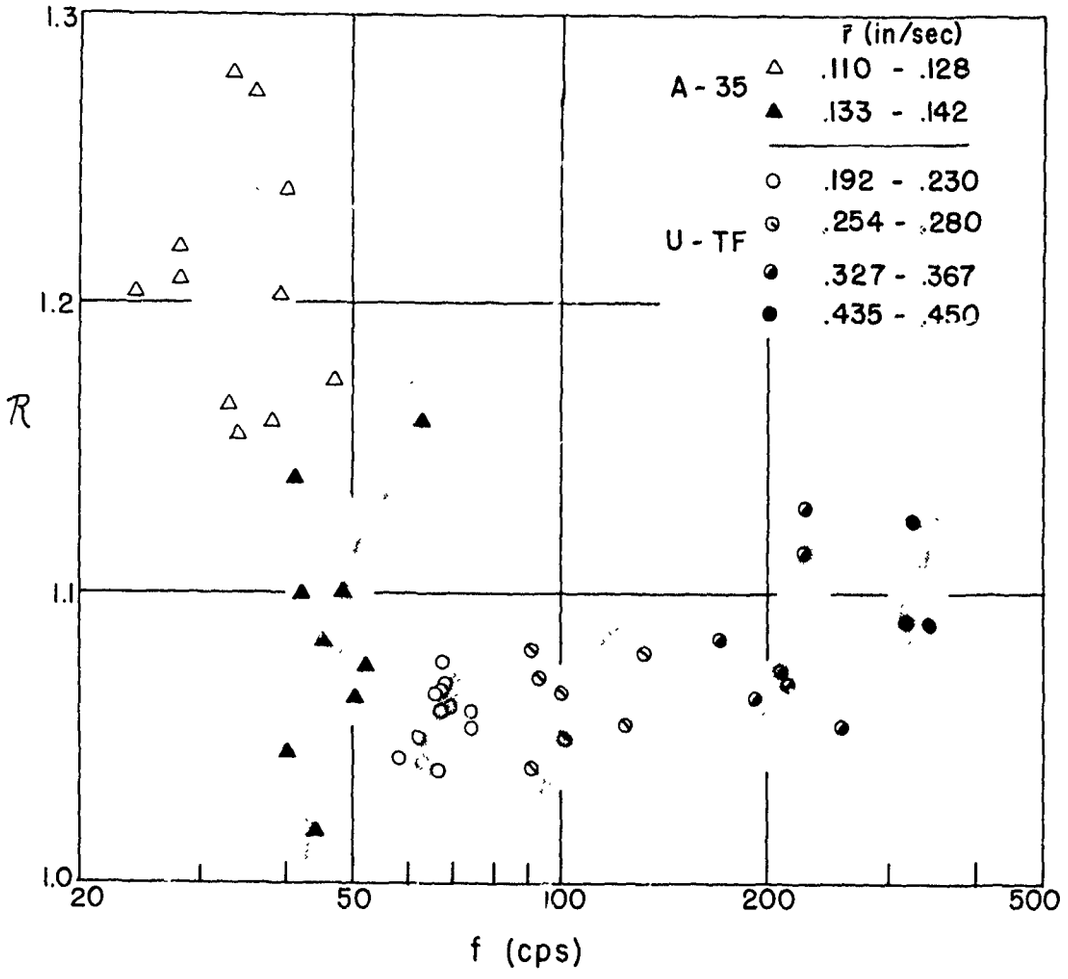

FIG. 5.21. Calculated Values of R as a Function of Frequency From the Data of A-35 and U-TF Propellants With Burning Rate as a Parameter.

the peak in the response function is not observed in Fig. 5.21 is apparently due to the combustion time approaching zero in this neighborhood. As pointed out above, this is related to nonlinearities which prohibit the obtaining of experimental data. It should also be noted that the effect of pressure (through burning rate) is qualitatively as implied in Fig. 5.4, with the unstable domain shifting to lower frequency at lower burning rate.

5.5. DISCUSSION AND SUMMARY

The objective of the present work was to develop an analytical model of NAI that would provide good physical insight into the instability mechanism, and then compare the model with results from concurrent experiments. The analysis is based on the conservation of mass for a rocket chamber with the combustion being represented parametrically by the magnitude of the response function, R, and the time lead, τ. By using these parameters it was possible to separate the effects of the dynamics of the combustor from those of the combustion without assuming a particular combustion model and at the same time provide a simple description of NAI that is easily related to acoustic instability.

In the interpretation of the theory, hypothetical forms of $R(\omega)$ and $\tau(\omega)$ were chosen to conform to the information currently available. The results indicate that instability will occur only for very restricted values of R and τ. The combustion time lead must be positive and is restricted by the values of other time constants in the system, while R must be greater than one and is usually increasing with frequency for instability to occur. Relating these results to the experimentally determinable variables α, ω, and L*, it is found that the predicted trends generally conform with the experimental results. Also, by combining experimental NAI data with the above model, R and τ can be calculated from L* burner data. This has been done and is reported here for the first time with the results supporting the above observation that the relationship between these two parameters is indeed very restricted. The effects of pressure and propellant variables are seen to be roughly correlated by the assumption that the combustion dynamics are dominated by the accommodation of the thermal wave in the solid. However, other factors are also manifested, one being the effect of metal combustion.

From a practical viewpoint, the results of the present work agree with previous observations that for a particular propellant, pressure, and temperature, there is a value of L* above which bulk mode oscillatory behavior will not occur. At lower values of L*, either decaying or growing oscillations may occur depending on the values of the various parameters and variables. The value of L* at which spontaneous instability will occur appears to be inversely proportional to the burning rate. The phenomenon of chuffing which leads to L* "quenching" is a nonlinear aspect of NAI which overrides the linear theory as τ approaches zero, resulting in very large values of α.

An obvious extension of the present work would be to compare the trends of R and τ as predicted by present as well as future combustion instability theories with those that have been predicted and observed for NAI from the present combustor model (such a study has been initiated). These theories would in most cases have to be extended to provide a common basis for application (e.g., express the results in terms of $R(\omega,p)$ and $\tau(\omega,p)$ or equivalent parameters), but such a comparison

could provide further insight concerning the driving forces that are important in NAI. Finally, it would seem desirable to attempt to extend the combustor dynamics model to encompass the thick-combustion-zone case, since the combustion zone volume is often comparable to the total rocket chamber volume at low L*.

6. ACOUSTIC INSTABILITY STUDIES

6.1. INTRODUCTION

Oscillatory combustion is not always in the form of spacewise uniform pressure fluctuations, as in non-acoustic instability, and more often in practice unstable combustion involves the growth and propagation of pressure waves within the combustor. In order to study such "acoustic" instability, burners have been developed with large enough dimensions to permit low frequency acoustic modes. In order to simplify interpretation of test results, the propellant is arranged so that axial mode gas oscillations in the burner impinge perpendicularly on the burning surface. Thus the interaction between the acoustic wave in the gas and the combustion zone is pressure-coupled (Ref. 78-80). While this test method does not simulate all acoustic environment factors encountered in a rocket motor, it does produce a precisely characterized environment which is relevant to both the rocket motor and to non-acoustic instability. The effect of velocity-coupled interaction is not considered in this section although it is an important factor in combustion instability. Experiments have been contrived in order to measure the effect of velocity coupling (Ref. 68 and 81), but the prospects of achieving an accurate method appear to be remote.

Considerable progress has been made during the reporting period in modifying the low frequency acoustic instability apparatus so that quantitative information can be obtained. Primary effort has been toward gaining control of burner pressure and the improvement of instrumentation and measurement techniques. Measurements of acoustic response function, stability limit, and metal combustion-acoustic pressure phase have been obtained using polyurethane-ammonium perchlorate propellants containing aluminum powder.

6.2. DESCRIPTION OF BURNER

The burner currently in use has evolved from smaller burners developed for studies at higher frequency. In order to obtain oscillatory behavior at low frequency it was necessary to go to a burner with larger diameter. Initial development and use of such a burner has been reported previously (Ref. 5, 6, 82 and 83). The design (Fig. 6.1) consists of a 6-inch diameter tube assembled from sections to provide total lengths of 6, 12, 24, 36, 48 and 60 feet. Discs of propellant are mounted in the end closures to provide for perpendicular incidence of axial pressure

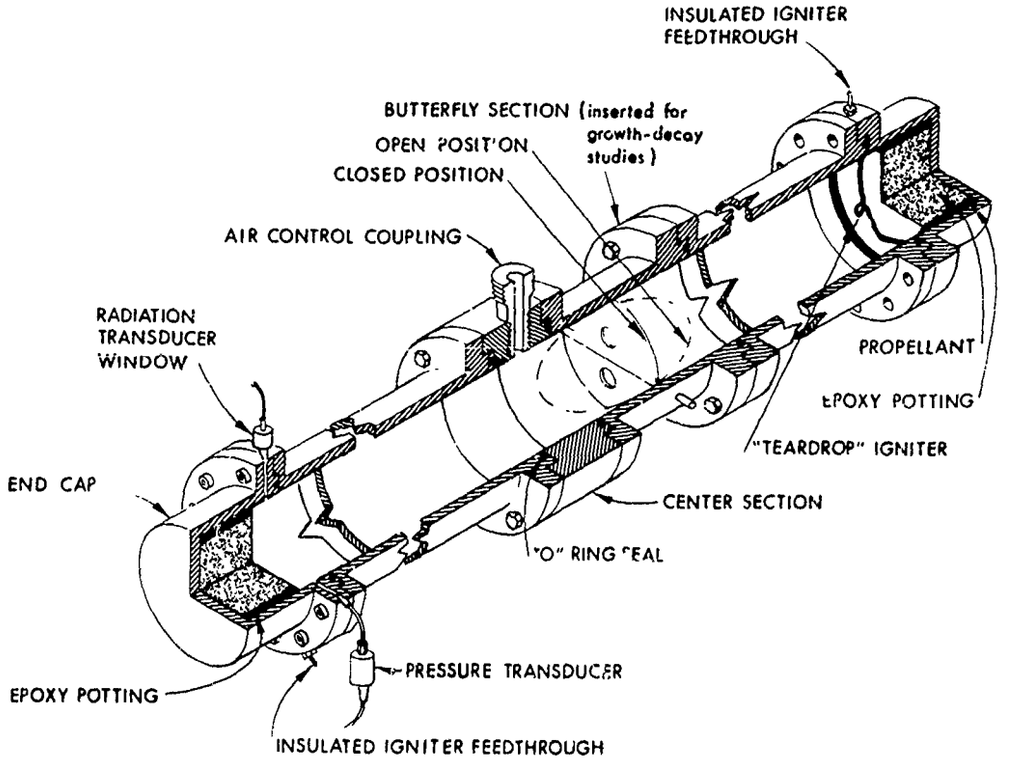

FIG. 6.1. Section of the Burner Used for Low Frequency Pressure-Coupled Acoustic Combustion Instability Research.

waves on the burning surface. The vent is located midway between the ends to minimize acoustic attenuation in the first axial mode.

The relatively large amount of propellant required for this burner precludes its being operated on a surge tank as is done with smaller burners to control mean pressure. Originally, the combustion products were simply discharged to the atmosphere through the vent. Because of the large heat capacity and free volume of the burner, considerable difficulty was encountered in controlling the mean pressure. In addition, the onset of oscillatory combustion could not be limited to the time when burner conditions were at desired values so that measurement of the growth rate of pressure oscillations could not be used effectively as a measure of stability. During the present report period several revisions to the burner have been made to remedy these limitations.

6.3. CONTROL APPARATUS

6.3.1. Control of Burner Pressure

Lack of adequate pressure control has plagued testing in these burners since inception of the low frequency program. Most of the earlier difficulties have been circumvented by inserting an auxiliary air-flow system between the burner and the nozzle. The air-flow system controls burner pressure by providing the majority of gas flow through the nozzle. Proper control of the dome pressure on the main regulator permits the burner to be operated at a preselected steadily increasing pressure. The control system is shown in Fig. 6.2. The progressive pressurization feature is useful as a means of "screening" new propellants for determining the pressures and frequencies at which unstable combustion occurs (Fig. 6.3). Care is needed in selecting pressurization rate in order to assure that the amplitude of oscillations at each moment approximates maximum amplitude for the prevailing pressure. Under ideal conditions a relatively small quantity of propellant (about 30 lbs.) is required to characterize a propellant for unstable combustion behavior from 15 to 250 cps and up to 200 psig, and involves about 15 firings. When conditions for unstable burning have been determined by this type of test sequence, the air-flow system can be programmed for constant pressure behavior and more definitive tests can be made on the propellant (Fig. 6.4).

6.3.2. Control of Acoustic Pressure

A recent advance in control of low frequency burner behavior involves the use of a mechanical damper to hold off oscillations. This device resembles a loose fitting butterfly valve or stove damper (Fig. 6.5). It is built into a short section of burner and can be inserted in place of a blank section of the same length. The damper is electropneumatically controlled and can be opened and closed several times during a test. Use of this device and the ability to provide constant pressure operation permits the determination of growth and decay constants for pressure oscillation. Such data can then be used to compute propellant response functions.

6.4. MEASUREMENTS

Measurement capability, which includes detection, signal conditioning, and recording of data, has been modified and extended during the reporting period.

6.4.1. Detection of Radiation

In order to relate the acoustic behavior to combustion processes, observations have been made of oscillations in radiation from the combustion zone. Techniques for detection of radiation from the propellant gas

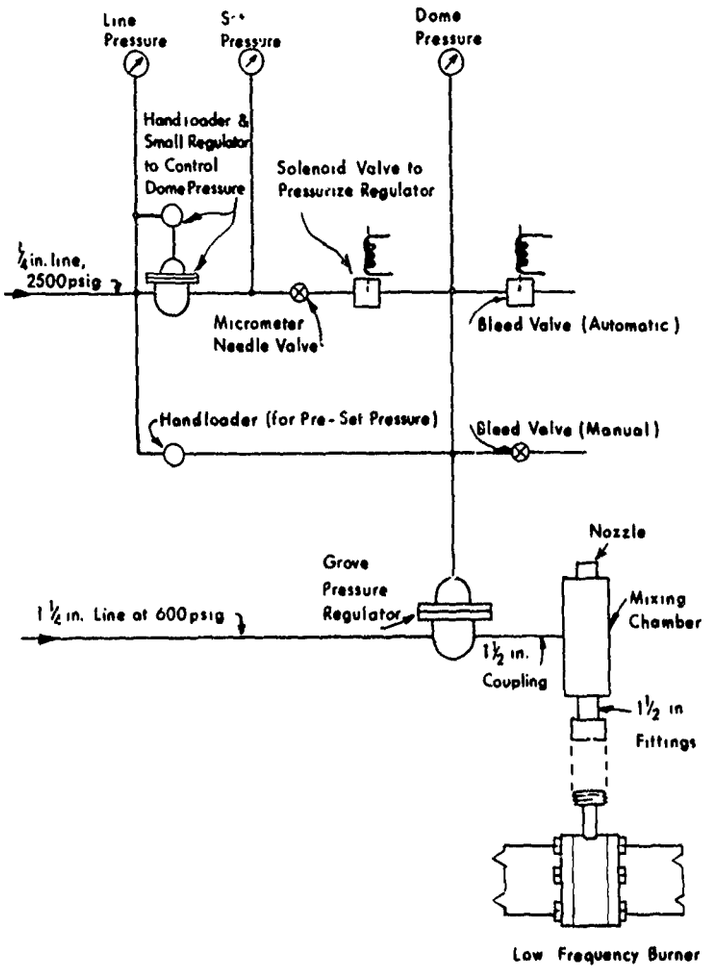

FIG. 6.2. Flow Diagram of the Burner Pressure Control System.

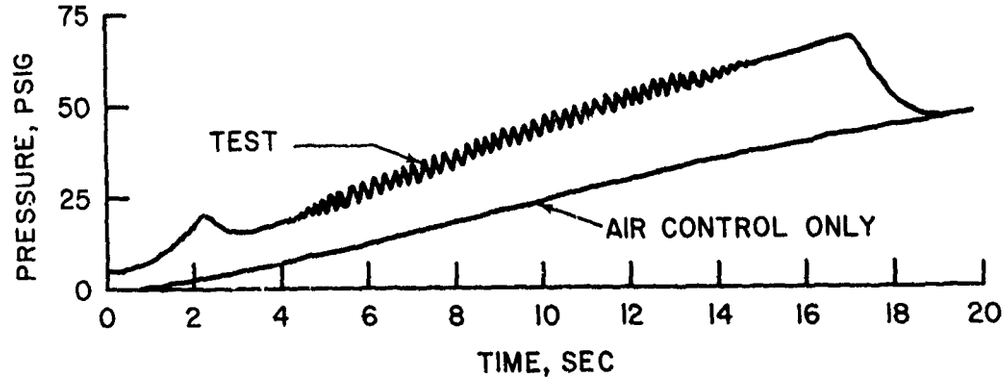

FIG. 6.3. Pressure-Time History Reproduction of a Test in Which Burner Pressure was Programmed to Provide a Progressive Pressure. A-91 propellant was used in this test and was unstable over the entire pressure range.

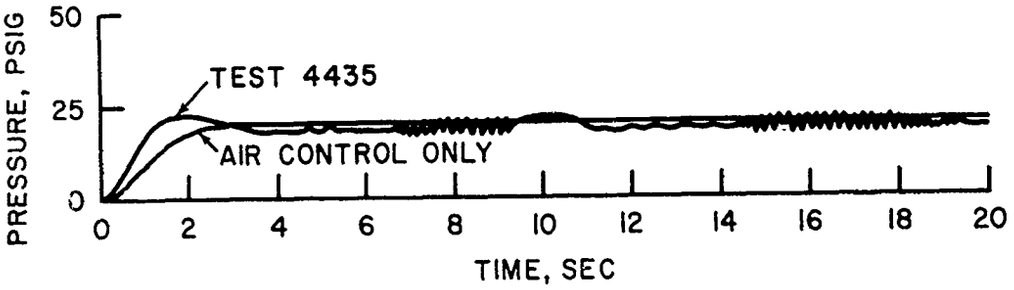

FIG. 6.4. Constant-Pressure Test in Which Burner Pressure Controller was Programmed to Maintain Constant Pressure Following Ignition of Propellant. In this test, oscillatory combustion was controlled by opening and closing the butterfly section.

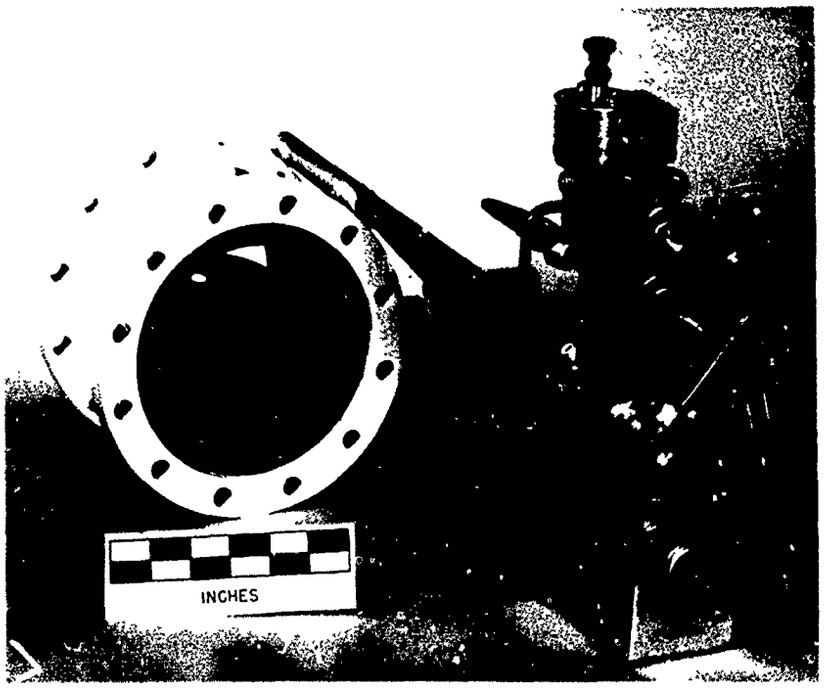

FIG. 6.5. Butterfly Damper Used to Control Initiation and Termination of Acoustic Oscillations.

in the visible and near infrared have been improved with modifications to the window section (Fig. 6.6) which include use of a porous, sintered metal sleeve to distribute the window flushing gas (nitrogen) without vortex formation, and narrowing of the field of view to an included angle of about 9^{o}. The photo-diode detector circuit is of relatively high

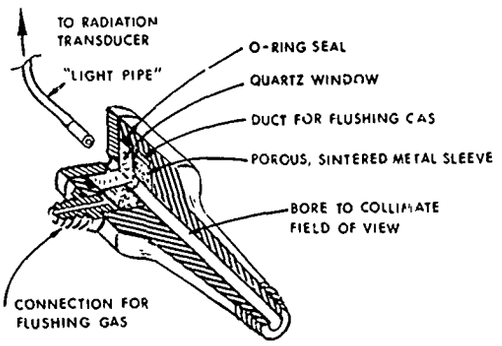

FIG. 6.6. Section of Window Assembly Used to View Conditions Inside Low Frequency Burner.

frequency response, being flat to 500 cps (Fig. 6.7). Three radiation detection stations are currently being utilized at the instrumented end of the burner. These are distributed along the burner at different distances from the propellant surface (Fig. 6.8). The viewing axis of each station is directed along a diameter of the burner and is thus perpendicular to the gas flow. Initial attempts to view combustion at the propellant surface met with difficulty partly due to opacity of the gas and partly due to the difficulty of keeping the window clean as it was facing into the flow of propellant gas.

6.4.2. Pressure Measurement

Two pressure channels are routinely in use on the low frequency acoustic burner. One channel incorporates a low frequency capability (Wiancko) transducer which is used to record mean and acoustic chamber pressure. This channel is to provide an accurate and reliable source of data - linearity is typically within a 2% error band and provides a relatively trouble-free source of information. The second channel uses a high frequency capability system (Photocon Research Products-Dynagage) which incorporates a variable capacitance transducer. This channel has an advertised flat frequency capability from d.c. to about 10 kcps. Both pressure channels are limited in their present application by the frequency response of the recording apparatus. The recording galvanometer response in the case of the low frequency channel is down 5% at 180 cps and the high frequency channel is down 5% at 5 kcps.

6.4.3. Instrumentation System

The low frequency pressure channel is unfiltered and it records both the net pressure and any pressure fluctuations onto a recording oscillograph. The high frequency response pressure channel is filtered and amplified to provide a sensitive acoustic pressure channel on the

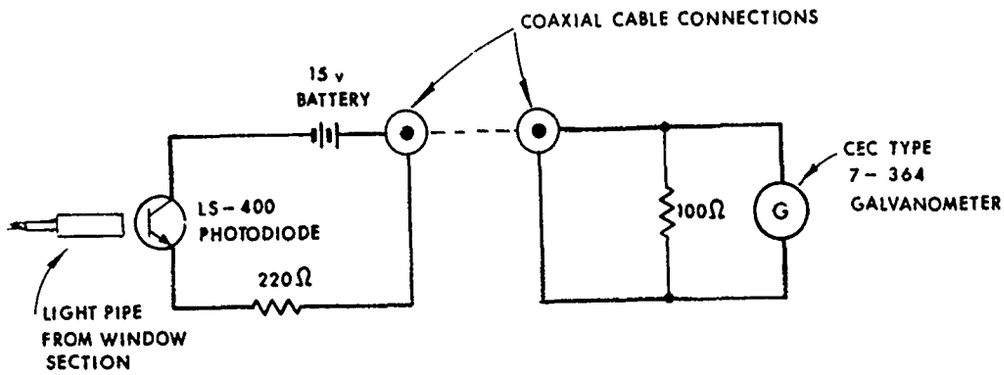

FIG. 6.7. Photo Detector Circuit. Upper frequency limit of about 500 cps is limited by response of the galvanometer used to record data.

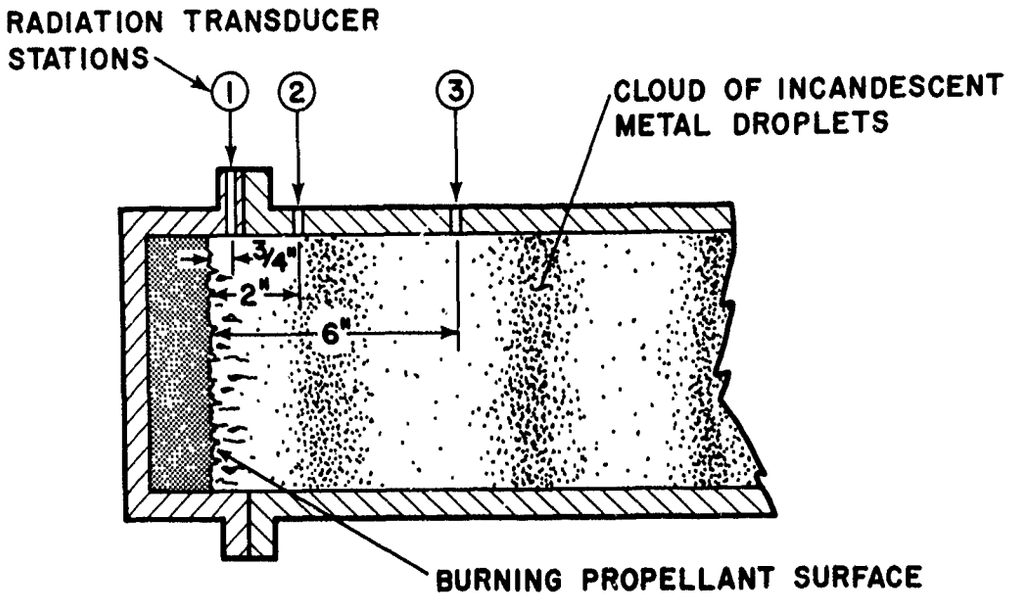

FIG. 6.8. Diagram of Sectioned End of Burner Showing Locations of Radiation Detection Stations Located Along Burner Wall.

recording oscillograph. All three radiation channels are recorded on the oscillograph with the pressure traces. A portion of a typical oscillogram is shown in Fig. 6.9. Chamber pressure is also recorded on an X-Y plotter for the convenience of the person conducting an experiment. This permits him to view the pressure-time history of a test as it progresses during a firing. A diagram of the instrumentation system appears in Fig. 6.10.

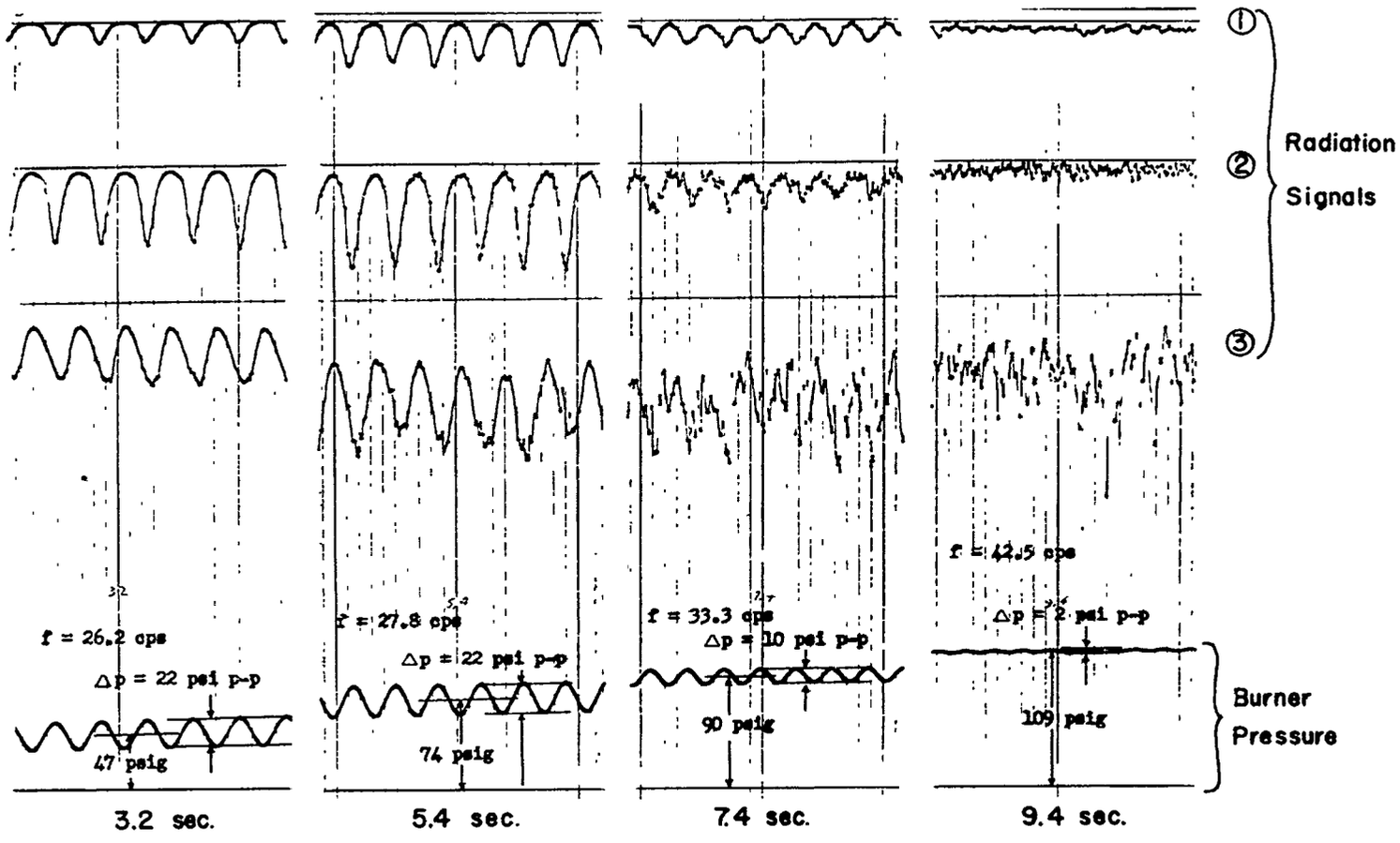

FIG. 6.9. Portions of a Typical Oscillogram Showing Multiple Radiation Channel Recording and Two Pressure Channels Recorded. Chamber pressure was programmed to increase during the test. Degradation of periodic nature of radiation signals as pressure increases suggests that the metal agglomerate shedding process gets out of phase with the acoustic pressure. Radiation channel gains increase with distance from the propellant: Channel 2 has about four times the gain of Channel 1 and Channel 3 has over six times the gain of Channel 1. Timing lines are 10 milliseconds apart.

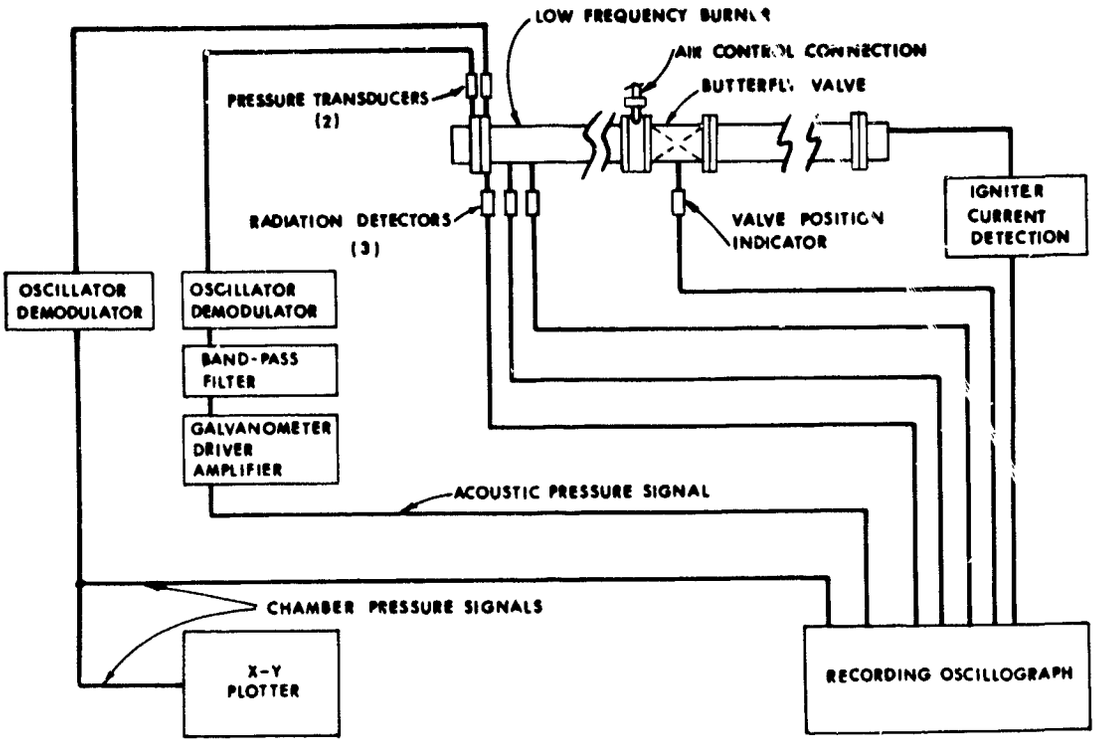

FIG. 6.10. Instrumentation System Used for Low Frequency Combustion Instability Research in the DECEV Burner.

6.5. PROPELLANTS TESTED

An extensive series of tests has been initiated on a family of polyurethane binder propellants in which the constituents are systematically varied. The effects of oxidizer particle size, aluminum particle size, and aluminum concentration are being studied in a window bomb using high speed photography (see Section 3), in the non-acoustic burner (see Section 5), and in a strand burning race bomb, as well as in the low frequency acoustic burner.

Propellant constituents are carefully selected. The oxidizer is either screened or purchased to provide an approximately mono-modal particle size distribution. The aluminum powders are specially purchased narrow cut, spherical materials. Compositions which have been fired in the low frequency burner to date appear in the shaded areas in Table 6.1. Data on some of these propellants is too sparse to permit further comment at present. The table indicates that within the variations listed there is a total of 40 compositions. An attempt to test all of these would lead to an excessive expenditure of time and money. The selection of the types identified by shading is expected to provide an indication of the effect of compositional variation with a minimum of testing. Primary

TABLE 6.1. NOTS Series "A" Propellants Used in Low Frequency Acoustic Instability Research[a]

OXIDIZER SIZE	ALUMINUM CONCENTRATION 0 %	4 %	8 %	16 %	ALUMINUM SIZE
15μ	A—76		A—138		5μ
					15μ
					30μ
80μ	A—35	A—83	A—91	A—32	5μ
			A—140	A—50	15μ
			A—39		30μ
200μ	A—58		A—141		5μ
				A—49	15μ
					30μ
600μ	A—108		A—142		5μ
					15μ
					30μ

[a]All propellants in this series contain 25% polyurethane binder. The remaining 75% is composed of ammonium perchlorate and aluminum powder. Shaded compositions are those on which low frequency acoustic instability research has been concentrated.

emphasis has been on improving methods of determining combustion changes as related to variations in the acoustic pressure. A rather well standardized approach to measurement of radiation and pressure has been developed and has been used during the latter portion of the reporting period.

6.6. SUMMARY OF RESULTS

6.6.1. Stability Diagrams

Results of screening tests on five propellant compositions are presented in Fig. 6.11 and 6.12, which indicate the range of frequency and pressure within which unstable combustion occurred. Conditions for the most severe oscillations are also indicated by a dashed line designated "Max ΔP". Data for A-91 propellant appears in the center of each figure for reference purposes. This data was obtained from tests conducted with

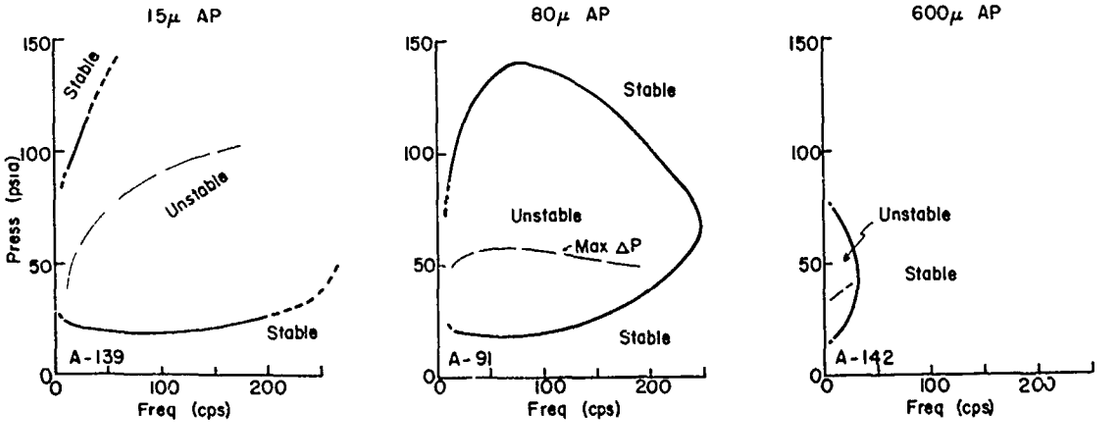

FIG. 6.11. Stability Diagrams for Three Polyurethane-Ammonium Perchlorate Propellants Which Differ Only in Perchlorate Particle Size.

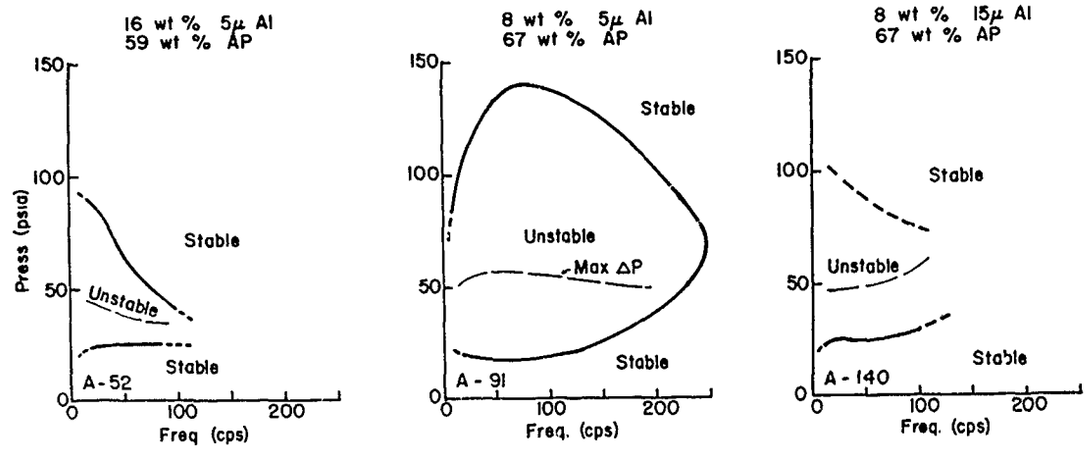

FIG. 6.12. Stability Diagrams for Three Polyurethane-Ammonium Perchlorate Propellants Which Contain Various Amounts and Sizes of Aluminum Powder.

a progressive pressure-time history as indicated in Fig. 6.3. The pressure at which oscillatory combustion was observed to initiate and to die out was noted for each propellant and frequency and the results plotted as shown in the figures. The propellants shown in Fig. 6.11 differ only in oxidizer particle size. The propellants shown in Fig. 6.12 contain different amounts or sizes of aluminum powder.

Each of the propellants tested in the acoustic instability program is also tested in the non-acoustic burner (see Section 5) and are burned in the photographic strand bomb as part of the steady-state investigations being conducted (see Section 3). Results of strand bomb photography and tests in a burning rate bomb are shown in Table 6.2.

TABLE 6.2. Data on "A"-Series Propellants Obtained from Photographic and Strand Bomb Investigations[a]

Composition	Agglomerate Diameter	Burning Rate	Remarks
A-139	25-50 μ	.060 ips	Few agglomerates formed. Most of metal appears to burn at size originally incorporated into propellant.
A-91	50-90 μ	.064 ips	Agglomerates ignite at surface. Presence of smaller particles suggests not all available metal forms into agglomerates.
A-142	100-300 μ	.049 ips	Very large agglomerates which cling to propellant surface even after ignition. Relatively few smaller particles.
A-52	~90-100	.045 ips	Good ignition of agglomerate at propellant surface. Some smaller particles evident.
A-140	90-100	.052 ips	Very poor ignition of agglomerates, most metal leaves propellant surface unignited.

[a]Pressure approximately 50 psia.

Comparison between data in Table 6.2 and Fig. 6.11 and 6.12 indicates that propellants with small agglomerates oscillate at higher frequencies than those with large agglomerates. This observation suggests that the combustion time or the formation time of metal agglomerates is a significant factor in the unstable combustion characteristics of these propellants. However, since the stability limit is also influenced by the losses in the burner, it is possible that particle damping is also a contributing factor.

6.6.2. Response Function Measurements

The determination of the combustion zone response to incident pressure disturbances using a double-ended, center-vented burner has been described previously, Ref. 8 and 80, and is applicable to the burner used for low frequency acoustic instability studies with some modification. The response function is determined by a method which depends on the relation between the exponential growth rate of pressure oscillations in the burner and the rate of increase in acoustic energy in the cavity (Fig. 6.13). Two problems were considered in the present work that have not been considered to be important in earlier work. The first is the deviation in the acoustic field from that usually assumed because of the wide difference in temperature of gases in the combustion zone compared to the temperature in the gas column (as indicated by the low frequency of oscillations). To correct for this effect, the usual analysis was modified by assuming that the temperature in the gas column was that indicated by the frequency of oscillation rather than the temperature of the combustion zone. This leads to a correction to the usual equation for calculation of the pressure-coupled mass response function, consisting of the factor $(c_o/c_{ob})^2$. The derivation of this factor is discussed in Appendix B. The response function, then, is given by

$$\frac{\mu}{\epsilon} = \frac{p}{4\, c_o \rho_s \bar{r}} \left(\frac{\alpha_1 + \alpha_2}{f}\right)\left(\frac{c_o}{c_{ob}}\right)^2 .$$

The second correction considered in the present work involves a still unevaluated aspect of the acoustic theory. In the analysis of acoustic energy input in combustion-flow systems, there are two terms that occur in a sum with the response function:

$$\frac{\mu}{\epsilon} - \frac{\sigma}{\epsilon} + \frac{1}{\gamma} .$$

The physical effects represented by these two terms normally cancel each other at high frequency. At low frequency these terms are not expected to cancel each other. Further, the theoretical basis for the third term in this sum is not entirely satisfactory, and appears to be dependent on the heat-loss situation in the burner (Ref. 84). Because the magnitude

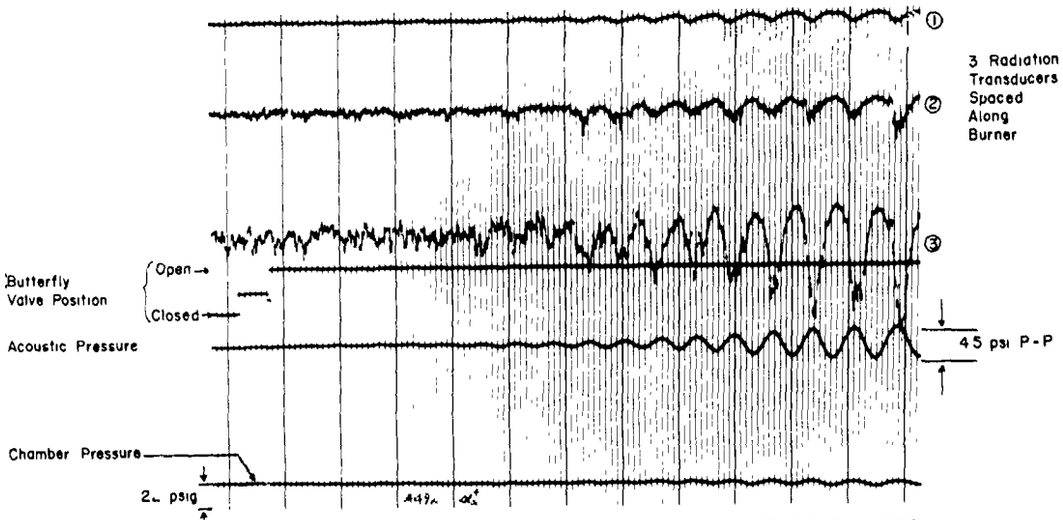

FIG. 6.13. Portion of an Oscillograph Record Showing Growth of Oscillatory Combustion Following Opening of Butterfly Damper.

of μ/ε in the present work was much larger than any plausible value of the rest of the above sum, no correction was introduced (the value of the sum of the other two terms is around 0.1). Data for growth and decay rate constants have been obtained in four different burner lengths using A-91 propellant (Table 6.3). In tests where more than one growth was obtained, the rate constant for the final growth is used because combustor conditions more nearly correspond to those during post-burnout decay of oscillations.

Response function calculations are made from data read off graphs of growth and decay rate constants plotted against pressure. Burning rate, frequency of oscillation, and other information is determined for each chamber pressure (Table 6.4). Since the growth and decay frequency are generally not the same at a given pressure, a slightly modified form of the response function equation was used in the calculations. The effect is due to heat transfer from the gas following extinguisiment of the propellant and is also seen in smaller double end burners. The frequency variation is accounted for by rewriting the term containing the growth and decay constants as follows:

$$\frac{\alpha_1 + \alpha_2}{f} = \frac{\alpha_1}{f_1} + \frac{\alpha_2}{f_2} .$$

TABLE 6.3. Growth and Decay Rate Data for A-91 Propellant

Test No.	Burner Length	Growth Data			Decay Data		
		Pressure	Frequency	α_1	Pressure	Frequency	α_2
4699[a]	12'	23.5	60.0	1.35	24.0	52.0	2.33
4698		42.5	90.0	4.64	36.5	70.0	3.54
4697		63.5	100.0	1.63	53.5	80.0	3.07
4693		63.5	100.0	1.06	....	....	....
4696		83.5	Stable	....	83.5	Stable	....
4665	24'	29.0	26.0	1.10	31.0	26.6	0.80
4661		39.0	40.0	5.04	....	....	....
4666		40.0	40.0	4.79	38.5	25.0	1.07
4662		48.5	42.0	1.89	46.5	26.2	0.98
4602		....	....	....	53.5	28.8	0.91
4663		62.0	42.0	0.834	61.5	25.5	0.844
4692	36'	22.5	18.3	2.16	23.0	17.3	0.692
4691		23.5	18.0	2.33	....	....	....
4694[a]		25.5	18.0	3.00	25.5	16.6	0.643
4690		30.5	22.0	4.86	30.5	17.4	0.748
4735		37.5	22.0	6.08	37.5	16.7	0.642
4736		46.5	22.0	4.27	46.0	16.3	0.658
4688		53.5	25.5	1.35	....	....	....
4689		54.5	26.0	2.51	53.5	17.0	0.556
4695		58.5	23.0	2.51	60.0	16.2	0.568
4660	48'	21.0	13.8	2.31	21.0	13.2	1.96
4435		31.5	15.0	5.24	32.5	13.2	2.49
4436		38.0	16.8	3.77	38.5	12.9	1.41
4436		....	....	....	38.5	12.9	0.62
4421		40.5	17.5	3.0	41.5	13.0	2.34
4437		46.5	16.5	1.25	47.0	13.5	1.08
4437		....	....	....	47.0	13.5	0.54
4420		51.5	17.7	1.08	51.5	13.4	0.56

[a]Data obtained with one end burning.

TABLE 6.4. Response Function Data
for A-91 Propellant

Burner Length	p psia	r m/sec	f_1	$\frac{g\,p}{4\,c_o\,\rho_s\,r}$	$\frac{\alpha_1}{f_1} + \frac{\alpha_2}{f_2}$	$\left[\frac{c_o}{c_{ob}}\right]^2$	$\frac{\mu}{\epsilon}$
12'	23.5	0.030	60.0	73.6	0.136	0.175	1.75
	40.0	0.051	90.0	49.3	.104	0.546	2.81
	63.5	0.080	100.0	44.8	.415	0.608	1.13
	83.5	0.100	....	Stable	Stable	Stable	0.00
24'	30.0	0.038	26.0	84.9	0.0827	0.134	0.941
	39.0	0.050	40.0	54.7	0.171	0.310	2.90
	40.0	0.051	40.0	55.0	0.151	0.310	2.57
	47.0	0.060	42.0	52.4	0.083	0.345	1.50
	62.0	0.078	41.8	53.4	0.051	0.342	0.934
36'	23.5	0.030	18.0	81.8	0.320	0.141	3.70
	25.5	0.035	18.0	76.2	0.353	0.141	3.80
	37.5	0.048	22.0	66.9	0.320	0.211	4.52
	46.5	0.059	22.0	67.4	0.231	0.211	3.29
	54.0	0.068	26.0	57.4	0.126	0.297	2.15
48'	21.0	0.027	13.8	79.8	0.215	0.148	2.54
	31.5	0.040	15.0	74.0	0.538	0.175	6.98
	38.5	0.049	16.8	66.6	0.429	0.226	6.45
	41.5	0.053	17.5	63.4	0.333	0.242	5.12
	47.0	0.060	16.5	65.9	0.179	0.208	2.45
	51.5	0.065	17.7	62.2	0.083	0.244	1.25

The velocity of sound for the gas in the burner was computed from the relation $c_o = 2Lf_1$, where L is the burner length and f_1 is the frequency observed during the growth of oscillations. The sonic velocity in the combustion zone was determined from data obtained from thermochemical calculations which indicated a value of 3,440 ft/sec. Propellant density was determined to be 0.0594 lb/in.^{3}. Figure 6.14 shows how the response function of A-91 propellant varies with pressure. Numbers within the figure indicate frequency.

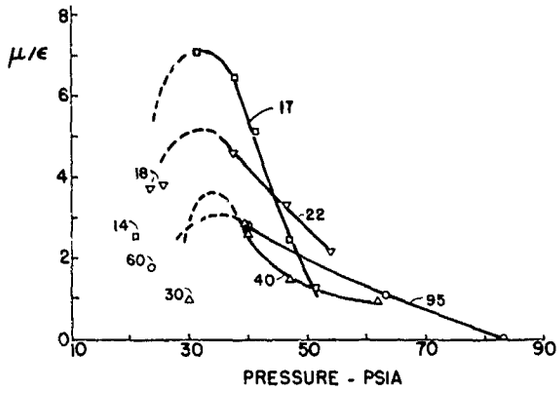

FIG. 6.14. A-91 Propellant Response Function as a Function of Pressure.

6.6.3. Combustion Phase Determination

One of the more notable characteristics of metalized propellant combustion is a tendency for the propellant to exhibit spontaneous combustion oscillations at a particular frequency. Such "preferred frequency" behavior has been discussed previously for propellants (Ref. 4 and 8) and results for pressed AP-Al pellets are covered in Section 4 of this report. Preferred frequency behavior appears to be exhibited by A-91 propellant but the oscillations are not spontaneous as with the pressed pellets. Measurement of the phase between the acoustic pressure and combustion of the metal must be resorted to in the case of A-91 under conditions of oscillatory pressure. Tests in which unstable combustion occurs are suitable for such measurements but the dense smoke in the combustion products interferes with direct observation of metal at the surface of the propellant, thus the multiple station radiation detection described in Section 6.4.1 is resorted to.

Portions of an oscillograph record are shown in Fig. 6.9 which contains three radiation channels. Channels 2 and 3 have gains four and six times the gain of Channel 1 respectively and they are located on the burner as shown in Fig. 6.8. While the relative brightness of radiation

diminishes with distance (Fig. 6.15), it is not clear at present whether the cause is due to increased smoke density or a reduction in combustion activity. The presence of measurable radiation intensity to distances as great as six inches from the burning propellant surface does reveal that combustion reactions are distributed far from the surface. This effect is probably due to a combination of relatively low pressure and long combustion times of metal agglomerates.

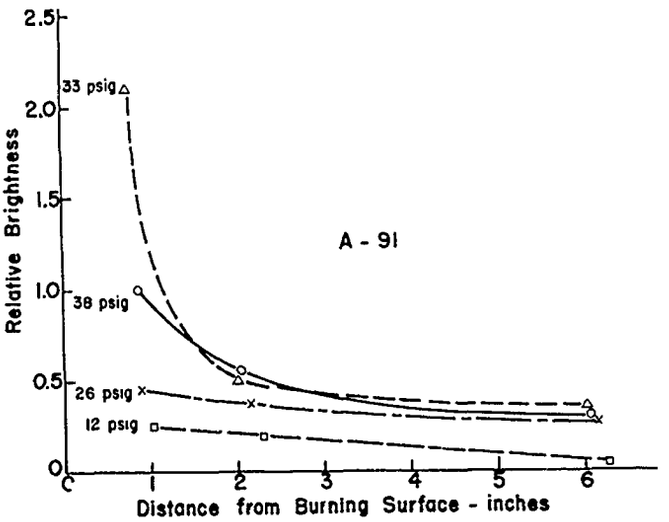

FIG. 6.15. Normalized Radiation Level as a Function of Distance from the Burning Propellant Surface.

The well organized, cyclic character of the radiation at the lowest pressure in Fig. 6.9 suggests that the "preferred frequency" of the propellant is close to the burner frequency. Under these conditions, combustible material is released from the propellant surface very nearly in phase with the acoustic pressure and the acoustic pressure is near maximum amplitude. As the test progresses the burner pressure increases, driving the preferred frequency to values higher than the frequency of the burner. Since the combustible material tends, under these conditions, to be shed at a frequency greater than the acoustic frequency, the combustion oscillations will lead the acoustic oscillations. This is in fact verified by measurement of the combustion phase. However, direct assessment of phase between the radiation traces and the acoustic pressure from the oscillograph record will lead to a systematic error since none of the radiation transducers are viewing the burning surface directly. This difficulty is circumvented by plotting the radiation signal phase as a function of distance along the burner and extrapolating back to the propellant surface. The procedure, illustrated in Fig. 6.16, includes allowance for regression of the burning surface. Plotting the

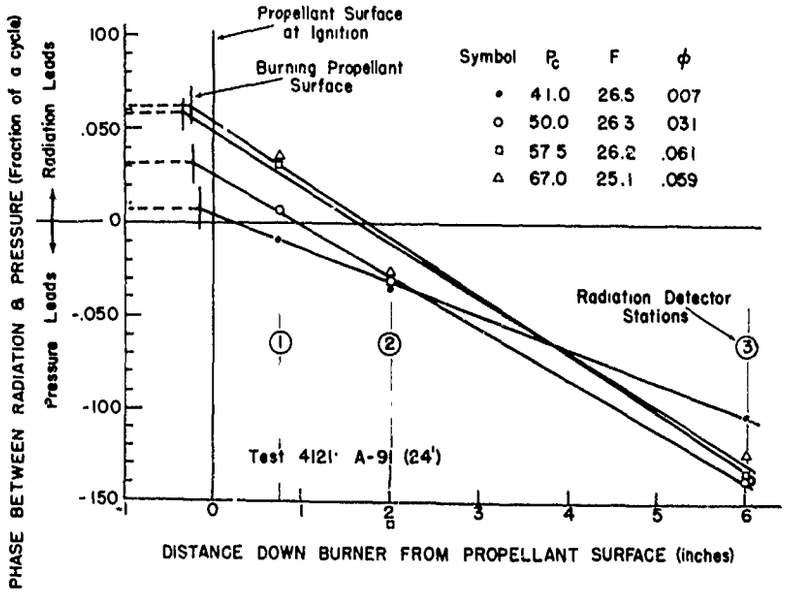

FIG. 6.16. Radiation Signal Phase, Relative to Acoustic Pressure, as a Function of Distance From the Burning Surface of the Propellant. Extrapolation back to burning surface permits assessment of events at surface in relation to acoustic wave.

corrected data as a function of frequency and pressure provides the information on combustion phase depicted in Fig. 6.17. This data will be extended below the zero phase line by additional testing.

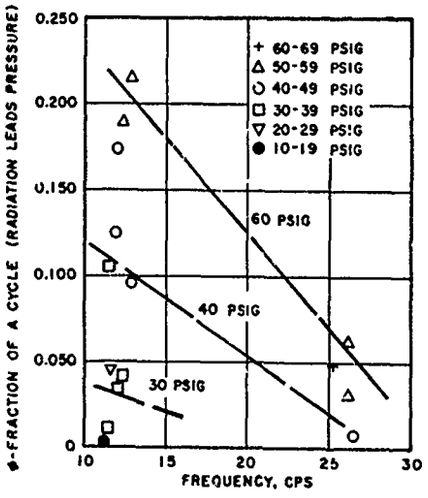

FIG. 6.17. Radiation-Acoustic Pressure Phase as a Function of Pressure and Frequency.

Further investigation into mechanisms of low frequency acoustic instability appears to be warranted now that the experiments yield quantitative information. Refinements in measurement techniques are possible, particularly the combustion phase measurement, and it appears possible to construct a unified theory for low frequency acoustic and non-acoustic instability as the theory can now be tested on the low frequency acoustic burner.

7. ACOUSTIC ATTENUATION

The stability of a combustor is dependent not only on the destabilizing contribution sometimes produced by the combustion dynamics, but also on a number of dissipative processes that suppress oscillatory behavior. Some of these processes, such as wall drag and bulk viscosity, can be evaluated on the basis of theory to a level of accuracy sufficient for stability analysis. As a result, study of attenuation has been rather limited. However, there are several important problem areas that have not been treated adequately; including (a) effect of net through-flow on losses, especially as it pertains to attenuation of axial modes by the nozzle, (b) solution of relevant acoustic equations when the combustor geometry is very complicated, and (c) determination of attenuation due to condensed phase material in the gas flow. In the present program, problems (a) and (b) were judged to merit study, and a laboratory method for experimentation was available in preliminary form. This section of the report describes very briefly the development of this "cold flow" experiment for study of axial mode attenuation. Because the work has been reported extensively in separate reports (Ref. 85, 86 87 and 88), only highlights are presented here.

7.1. EXPERIMENTAL TECHNIQUE

In order to avoid the cost of rocket motor testing, it was decided to simulate rocket motors by geometrically correct scale models having air flow introduced at the head end to maintain sonic flow at the nozzle throat (Fig. 7.1). Air was introduced through a porous wall at the head end, and was supplied from a variable-frequency oscillating source to provide oscillatory behavior. The amplitude of the combustor oscillations was monitored while the frequency of the driving in-flow oscillations was run slowly over the frequency range. Such a test showed amplitude-frequency curves reflecting the axial mode resonances (Fig. 7.2), and the attenuation of these modes was determined by measuring the half-power bandwidth of the resonance peaks. Measurements were also made from oscillation decay rates following pulsing of steady flow and following interruption of steady driven oscillations. Currently a standing wave ratio method of measurement is also being explored. Each of these methods has advantages and disadvantages. Most of the data to date have been obtained with the varying-frequency, half-power bandwidth method.

The original objective of the cold-flow experiment was to provide a low-cost method for determining the effect of geometrical variables on

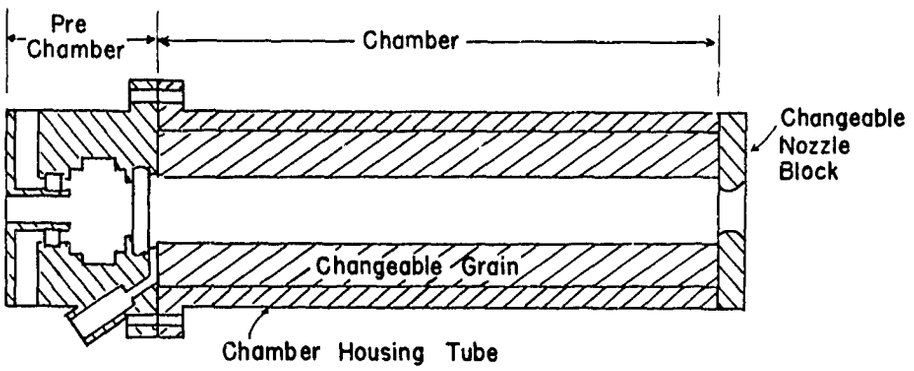

FIG. 7.1. Cutaway of Acoustic Test Model Hardware.

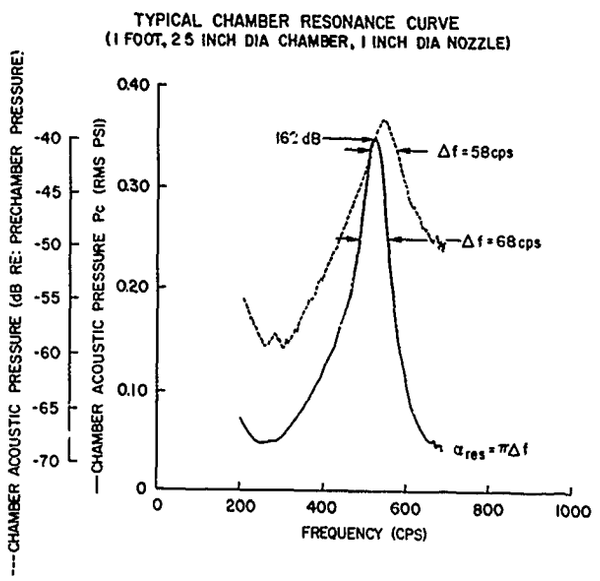

FIG. 7.2. Typical Chamber Resonance Curve for Acoustic Tests.

axial-mode attenuation in geometries that were too complicated for theoretical evaluation of losses. Inherent in the low cost concept was the development of a test apparatus and procedure that could be operated by relatively unskilled personnel with a minimum of guidance. Such a test capability is currently accomplished, with testing now being successfully conducted by two high school students. A block diagram of the test apparatus is shown in Fig. 7.3. An operating manual is in preparation, with the first version being prepared by the high school students (as a science project) as a means of further evaluating the technical level required for operation.

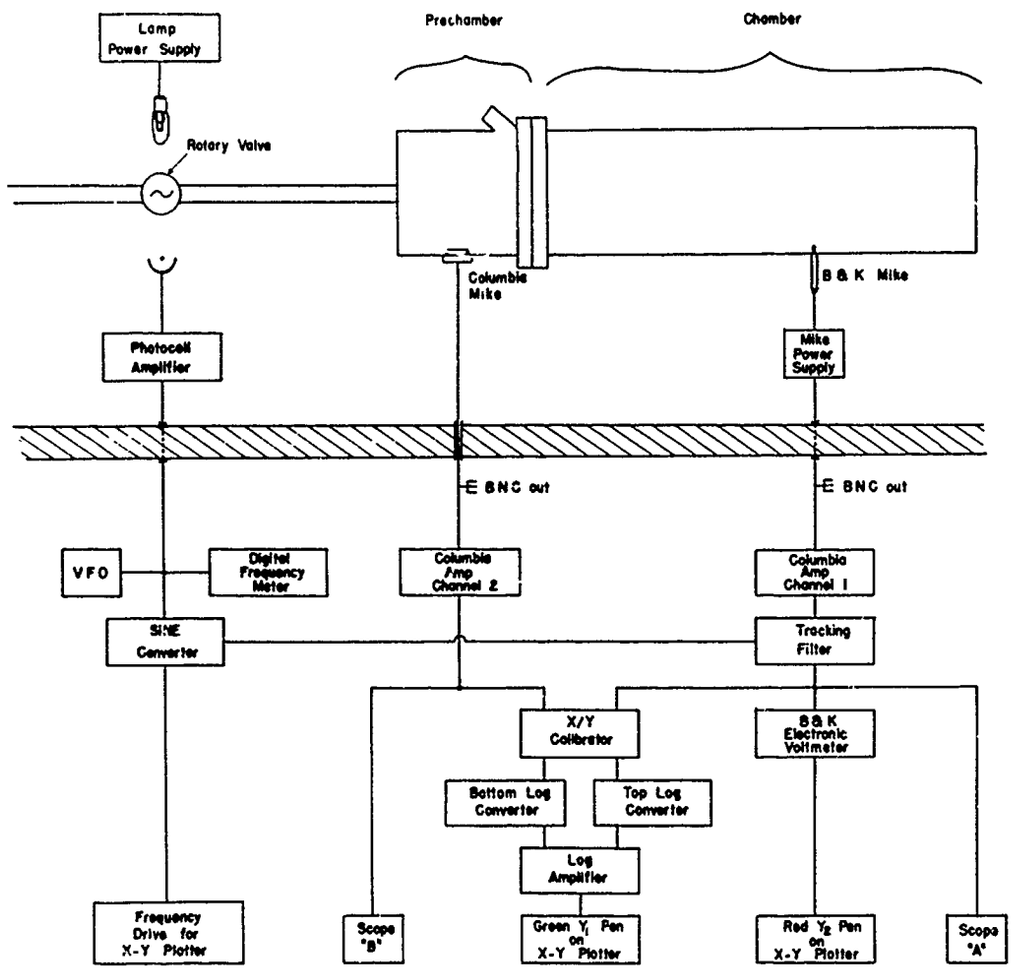

FIG. 7.3. Block Diagram of Acoustic Test Apparatus.

The original aspirations for a comparative test of effects of geometrical variables have been superseded by a goal of quantitative determination of attenuation, which has led to more intensive development of the experimental technique, and subsequent application to more basic problems, including evaluation of current theories. As a result, the test capability has continued to evolve in the direction of more precise measurements and refined interpretation, and a series of tests have been run on simple combustor geometries for which comparison with theory is possible. These activities have been reported extensively (Ref. 85-88), and are summarized briefly below.

7.2. ATTENUATION BY THE NOZZLE FLOW

It can be shown by fairly elementary analysis that the two principal sources of acoustical attenuation of axial modes are energy transmitted out of the combustor through the nozzle and dissipation by velocity lag of condensed phase material in the flow field, with the latter being important primarily at frequencies higher than those of interest in the present program. The accuracy of the theory for energy transmission through the nozzle was suspect, and a series of tests have been run to evaluate the theory and/or supply a source of experimental data (Ref. 88). Simple circularly cylindrical geometrics were used, and the effect of variation of the "J" ratio (nozzle throat area)/(combustor cross sectional area) was tested with different "motor" sizes. The results are summarized in Fig. 7.4, where it is seen that a linear relation exists between attenuation "α" and "J" in the range tested. The value of α was about six times higher than the value predicted by the Crocco theory. No explanation of the descrepancy between experiment and theory has emerged. The current development of a standing wave ratio technique for measuring α is being carried out primarily to obtain an independent method for determination of attenuation, in order to minimize the probability of error in the experimental method.

7.3. EFFECT OF NOZZLE CONTOUR

Because of the increasing use of unconventional nozzle entrance sections, a series of tests were run to determine under what conditions significant effects on attenuation occur. The family of reversible nozzle contours tested is shown in Fig. 7.5, while Fig. 7.6 shows the results obtained. It was found that attenuation was relatively insensitive to nozzle configuration except when a very long re-entrant section was used.

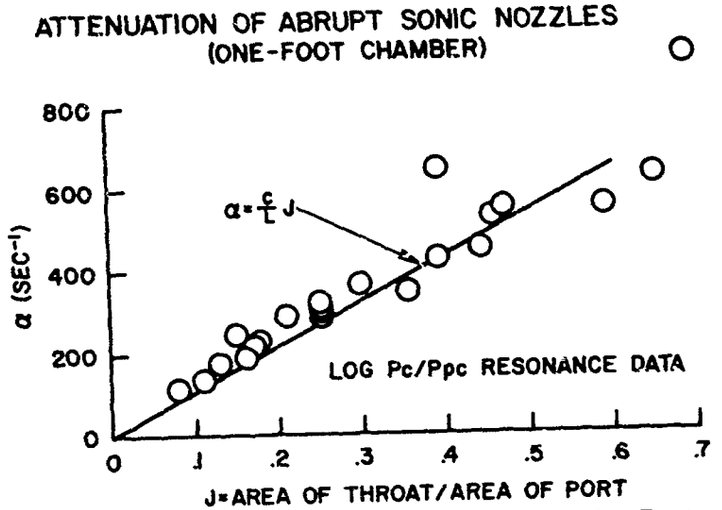

FIG. 7.4. Results of Abrupt Sonic Nozzle Tests. One-foot chamber, different grain and nozzle sizes.

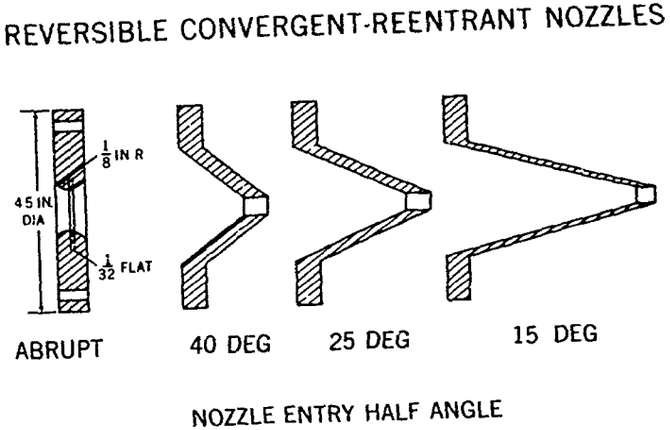

FIG. 7.5. Cutaway of Family of Reversible Convergent Re-entrant Conical Nozzles.

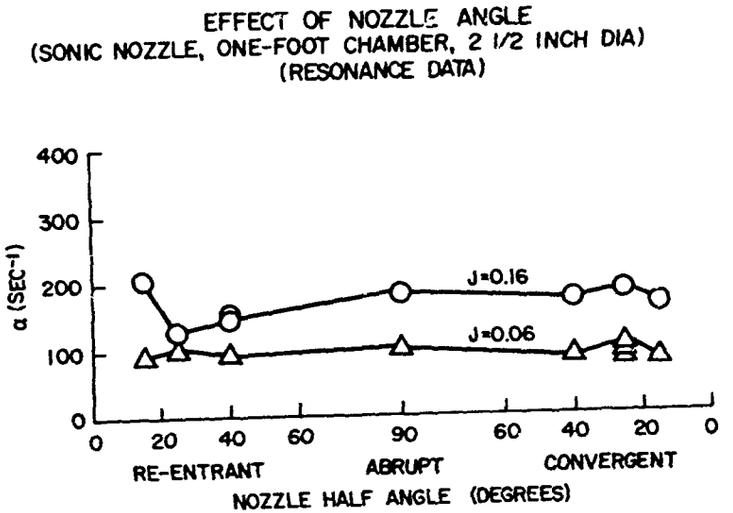

FIG. 7.6. Effect of Nozzle Half Angle for Sonic Nozzle Tests, One-Foot Chamber, 2½-Inch Diameter Port.

8. SUMMARY

In view of the scope of the effort described in this report, each section has contained a discussion of the particular area of activity. In the present summary, the accomplishments are listed without elaboration, to provide a brief summary of the entire program.

8.1. EXPERIMENTAL METHODS

Major developments were made in the following experimental methods:

1. Photography of combustion of propellants, including provision of non-recirculating ventilation, provision for high intensity external illumination, provision for high speed photography (up to 7000 frames per second) and magnified imaging (4 to 1).

2. Quenching of burning samples and studies of quenched surfaces. This includes adaptation of the window bomb for rapid depressurization, concurrent photography, and photomicrography of quenched samples, including application of a scanning electron microscope.

3. Use of large single oxidizer crystals in combustion studies, including deflagration and decomposition of ammonium perchlorate and combustion of AP-binder "sandwiches".

4. Development of the nonacoustic (L*) burner, application to low-cost, "first look" studies of low frequency instability characteristics of propellants, and adaptation to measurement of response functions.

5. Development of a pressure control system for the window bomb that permits oscillatory pressure during burning and photography, at controlled frequency, amplitude and mean pressure. Study of phase of combustion radiation relative to pressure.

6. Development and application of the double-ended, center vented burner for stability testing. This includes the 6-inch diameter burner in lengths from 6 to 72 feet, a technique for programming the mean pressure during a firing, and a technique for holding off and stopping oscillations on demand, which permits several determinations of response function in each test.

7. Development of a photoelectric technique for monitoring oscillatory combustion and interpretation in terms of phase and droplet population for metal combustion.

8. Development of a laboratory scale, cold flow apparatus for measuring the acoustic attenuation of axial mode oscillations in scale models of rocket motors. The facility is designed for operation by relatively untrained technicians, and can be used to evaluate attenuation coefficients in motor configurations that are too complicated for theoretical evaluation of coefficients.

8.2. DECOMPOSITION AND DEFLAGRATION OF AMMONIUM PERCHLORATE

Primarily as a result of studies with large single crystals, a number of important observations were made about AP:

1. At temperatures around 230°C, AP crystals decompose by nucleation of decomposition sites on the surface. These sites increase in number and spread until the entire crystal surface is covered and the decomposition front proceeds inwards at constant rate. A porous layer constituting about 65% of the original AP remains behind the decomposition front. The activation energy of the decomposition (based on propagation rate of the front into the crystal) was observed to be 21.9 kcal/mole.

2. The residual AP from low temperature decomposition was observed to be an interconnected structure somewhat like a sponge, suggesting that the previous concept of preferential decomposition of intermosaic material is incorrect.

3. The decomposition (∿230°C) of AP crystals was found to be non-isotropic, particularly with respect to surface nucleation and spreading of decomposition sites and structure of the residual AP.

4. Doping of AP crystals with MnO_4^- increased the surface nucleation rate for low temperature decomposition about 100 fold, but had only mild effect on the propagation of the decomposition front into the crystal. The residual AP was similar to that of pure AP crystals.

5. Granular AP was observed to give off an explosive gas when mildly heated in a test tube at one atmosphere. As temperature was increased, an orange flame was established above the granular material, which extinguished when the external heat was removed. These observations suggest that oxidation of ammonia does not occur too readily in AP decomposition and very likely occurs primarily in gas phase reactions.

6. The "burning rate" of single AP crystals was easily measured, was found to be slightly higher than previously reported values for pressed granular AP and was not dependent on direction relative to crystal axis. The low pressure deflagration limit was somewhat lower than previously reported values for pressed pellets; it was approximately 275 psia. Crystals doped with 0.04% MnO_4^- would not burn in the range of pressures tested (up to 1500 psia).

7. The surface of ammonium perchlorate was observed during deflagration by motion pictures, which revealed a very complex structure with evidence of bubbling. Observations of quenched surfaces revealed a bubbly residue (about 2 microns thick at 400 psia) indicative of a decomposing liquid. X-ray diffraction patterns of the residue indicated it to be AP. The collected evidence leaves little doubt that a decomposing liquid layer exists in the deflagration wave. Present interpretations indicate that the reacting liquid layer plays a decisive role in providing heat transfer from the exothermic reactions to the solid.

8. The surface of deflagrating AP is not flat on a microscopic scale, but is characterized by intricate patterns of depressions and ridges on a lateral scale of 50 to 150 microns and height scale of 20 microns. The patterns are fairly stable during regression of the surface, are of smaller lateral dimensions at high pressure, and do not seem to be geometrically related to the crystal structure. The results suggest that a flat deflagration wave may not be dynamically stable, but it seems unlikely that the "non-flatness" of the wave is important to the combustion characteristics of usual interest; i.e., the deflagration of individual AP particles in a propellant.

9. Studies of quenched crystals reveal very little evidence of subsurface decomposition, but clearly show a subsurface layer that has been physically (optically) modified by crystal phase change in the combustion wave prior to quenching. Measurements of this layer were used to calculate the temperature of the solid surface during burning, the results indicating that the surface temperature is pressure-independent and is about 560°C. Independence of pressure is consistent with the concept of a surface melt.

8.3. STEADY STATE BURNING OF PROPELLANTS

As a result of combustion studies of AP-binder sandwiches and photographic studies of combustion of propellants of systematically varied formulation, a number of trends and mechanistic arguments were evaluated:

1. Cross-sections of quenched "sandwiches" showed that the leading edge of the deflagration wave was always in the AP - not in the binder or at the binder-AP interface. This held true for several binders (non-explosive type), with and without ballistic modifiers. The leading edge of the wave was, however, located fairly close to the interface during low pressure burning, indicating the contribution of the diffusion flame under these conditions where the AP will not burn by itself. The surface characteristics of deflagrating AP described above were also evident in sandwich-burning.

2. Photography of combustion of metalized propellants revealed that aluminum accumulates on the burning surface with relatively little

oxidation, and eventually leaves the surface as relatively large agglomerates (100 to 100,000 particles of the original aluminum. In the case of composite propellants with modest solids loading and correspondingly large volume elements of binder in the microstructure, the aluminum accumulation was governed by the size of these binder elements, with aluminum apparently accumulating until the volume element of aluminum-loaded binder was "consumed" and the aluminum accumulate became exposed to an oxidizing atmosphere. At this point the aluminum accumulate is often seen to ignite, melt into a sphere, and leave the surface concurrently.

3. Aluminum agglomeration occurs even in the case of propellants with very fine microstructure (e.g., propellants with high solids loading and multimodal particle size blends) but underlying trends are difficult to determine in this case. Accumulation is particularly extensive at low pressures, where agglomerates sometimes do not all ignite in the window bomb environment. Accumulation and agglomeration were seen to occur in all of the metalized propellants tested, including ones with magnesium, boron, and magnesium-aluminum alloys.

4. Interpretation of results to date indicates that aluminum particles, with protective oxide coating and transpiring fuel vapors from the binder, reside on the propellant surface at temperatures up to about 1400°C without igniting. The accumulation is favored so long as the concentration of oxidizing species and/or the temperature remains low. Particles are apparently sintered together, probably by accumulation of oxide between particles resulting from "slow" diffusion of aluminum vapor. A number of factors contribute in varying degree to separation of the accumulate from the surface, including: rising temperature due to oxidative self-heating and increasing extension into the diffusion flame; increasing exposure to oxidizer decomposition products; increasing obstruction to flow of decomposition products from underlying material. The key event is often local breakdown of the oxide structure somewhere in the accumulate, leading to oxidative self-heating, propagative breakdown of the oxide structure, complete melting of the accumulate to a burning droplet with the oxide drawn by surface tension into a "cap" on the droplet. The sequence of inflammation, separation from the surface, and transformation to a droplet varies according to propellant and environmental variables, and even statistically according to local conditions at the surface of a given propellant sample. Indeed, these processes are probably mutually interdependent and not necessarily sequential in nature.

8.4. LOW FREQUENCY INSTABILITY (LFI)

At the outset of this program, very little was known about oscillatory behavior in rocket motors in the 0 - 100 cps range, primarily because testing of motors capable of such behavior had been very limited. As a result, the early phase of the program was concerned first with

development of laboratory scale experiments exhibiting LFI. This was followed by a period devoted to exploration of the qualitative aspects of LFI and their dependence on propellant variables. With increasing insight and improving experimental technique, it has become possible to make quantitative measurements of combustion dynamics. This has made possible meaningful comparison between theory and experiment, and a new period of up-grading analytical models is now beginning. In the course of these developments, the following major advances in knowledge were achieved on this program:

1. The qualitative nature of low frequency instability characteristics has been determined for many different propellants, including practically every type of commercial propellant and many experimental formulations prepared for systematic studies of the effect of propellant variables (see also previous reports on this program (Ref. 5, 6 and 82).

2. It was found that most propellants will exhibit oscillatory combustion in low-loss burners somewhere in the frequency range 5 - 200 cps and pressure range 10 - 500 psig. Propellants containing appreciable amounts of aluminum were found to be at least as unstable as unaluminized propellants, but tended to be unstable over a narrower range of test conditions, typically at pressures below 300 psia.

3. The "preferred frequency" characteristics of aluminized propellants were linked with the periodic accumulation and ignition of metal on the burning surface. This process was clearly visible with burning of pressed samples of AP and aluminum, even in constant-pressure environments. With propellants, this behavior occurs locally on the surface on a microscopic scale, but becomes visible only when environmental oscillations exist and organize the microscopic fluctuations into a "phase-correlated" oscillation capable of amplifying the acoustic oscillations. Such behavior is visible by radiation detectors that measure the phase and amplitude of the combustion oscillations, and such behavior is sometimes discernible also in motion pictures of oscillatory combustion of propellants.

4. An overall combustor stability analysis was made for the case of bulk-mode (chugging) oscillatory behavior (NAI). This analysis of NAI differed from previous ones in that the dynamic behavior of the combustion wave was represented by a response function, instead of an idealized one-dimensional model. The advantages of this are that the analysis is not restricted to a particular combustion wave model, and may even use experimentally measured response function data; the analysis establishes the much-needed link between nonacoustic and acoustic instability; the analysis is mathematically simple and direct, preserving always the connection between the mathematical and physical problem. Through use of this analysis it has been possible to calculate response function data from test data, and to understand the general behavior of nonacoustic instability.

5. Both the NAI and acoustic burner techniques have progressed to the point of making quantitative measurements of dynamic combustion behavior in the frequency range 10 - 200 cps, and an assessment of the accuracy and range of applicability is in progress. Methods include measurements of growth constants, phase and frequency of oscillations, in both non-acoustic and acoustic burners. While these methods promise to provide quantitative results that are consistent internally and with combustion theory, this goal has not yet been achieved. The results do provide an excellent means for comparative testing of the effect of propellant variables.

6. A comparison of existing one-dimensional analytical models for combustion perturbation behavior has been made, which shows these models to be closely alike insofar as low frequency instability is concerned. They show the transient mass burning rate response to pressure perturbations below about 500 cps to be dependent primarily on the accommodation time of the thermal wave in the solid. The behavior of unmetalized propellants tends to confirm this. However, the presence of metal, or of heterogeneity in the propellant is inconsistent with the analytical models, and apparently causes significant (sometimes conspicuous) differences between experiment and theory. The most significant result of theory is the prediction (for homogeneous propellants) of a maximum in the response function at a frequency of about $f \approx 5{,}300\ r^2 = 212$ cps, where r is the linear burning rate of the propellant, in inches per second, and has been taken as 0.2 in/sec for the right-hand equality. For a propellant with a typical burning rate function $r = Cp^n$, this gives a frequency of $f \approx C^2p^{2n} = 69p$ (where p is in psia, and r is 0.2 in/sec, n = 0.5 in the equality on the right). In terms of practical applications, one should obviously be concerned about instability when the motor has conservative acoustic modes around the frequency given by this equation. In addition, propellant heterogeneity and metal combustion may modify the range of frequency over which oscillatory behavior may be sustained.

7. Determinations were made of the attenuation constant of first axial mode oscillations in model rocket motors, to test the effect of motor geometry. For simple geometrics the attenuation was given by $\alpha = (c/L)\ J$ which is larger than predicted by present theories. The method has not yet been adapted for measurement of convective transport of acoustic energy, although the result above does show the radiative transport in the presence of sonic flow in the nozzle. Measurements were made of the effect of entrance angle of nozzles, and of the effect of varying the degree of submergence of the nozzle. These effects were not dramatic, but could be important in marginally stable motors.

8.5. STATUS

Results of the present investigations establish that some occurrences of combustion instability in future development programs are almost inevitable unless consideration to circumvention is given before selection

of design and propellant is made. Low frequency instability seems unlikely in motors operating above 500 psi, except possibly during the starting and ending transients. Use of aluminum and other powdered metal fuels definitely does not reduce the risk of instability.

Laboratory scale methods exist for evaluating the low frequency combustion dynamic behavior of propellants, and cost of testing is quite moderate. These methods allow comparative testing of propellants and determination of trends with frequency and pressure. Quantitatively reproducible measurements of combustion response to pressure oscillations are now possible, but additional work is needed to determine the absolute accuracy of these measurements. Initial testing shows the same trends as predicted by theory, but the validity of the theory is not sufficient to evaluate the absolute accuracy of measurements.

The general nature and mechanisms of instability are now understood. Quantitative evaluation of the absolute importance of different contributing factors to losses and gains is not yet possible. Further, it is not clear that quantitative evaluation is economically practical on a short term basis, as it involves solution of a host of fundamental problems that have resisted previous attacks. In any case, it seems clear that a more valid detailed understanding of the steady state combustion process is needed before quantitative understanding or prediction of instability will be feasible, and that a theory providing accurate prediction of combustion instability will have to be much more complicated than present ones. Further, there is a large gap between present understanding and its use in development programs, indicating the need for education is as great as the need for research.

The present qualitative understanding of combustion instability has been dependent in part on the advances in understanding the steady state combustion process (has motivated many of the advances), and future advances appear to be extensively dependent on resolution of further questions regarding the steady state process. Most important are the questions of the relative importance of surface and gas phase reactions, controlling mechanisms of metal accumulation and ignition on the burning surface, and importance of the heterogeneous character of the propellant.

From the practical standpoint, it seems prudent to continue to explore the instability trends resulting from systematic propellant variations, with primary attention to variations that (a) provide a test of existing theories or otherwise show large or unexpected effects, (b) are expected to be of interest in development programs, or (c) have exhibited instability in motor firings. Anomalies between results obtained by different experiments should be explored, and discrepancies between experiment and theory should be explained. All such activities should be conducted in concert with development needs and with the need to bridge the "educational gap".

Appendix A

A REVIEW OF CALCULATIONS OF THE ADMITTANCE FUNCTION FOR A BURNING SURFACE*

F. E. C. Culick
Associate Professor of Engineering
Daniel and Florence Guggenheim Jet Propulsion Center
California Institute of Technology, Pasadena, Calif.

Abstract

All oscillatory or transient motions in solid propellant rocket chambers are excited and sustained by a coupling between the motion and the burning near the solid propellant surface. This interaction is often conveniently expressed in terms of an admittance function which, therefore, becomes a necessary quantity for stability analyses. The function may also be useful, eventually, as a relative measure of the tendency for propellants to drive waves. There exist at the present time a number of calculations of the admittance function; an increasing amount of laboratory data is being obtained from T-burners, L*-burners, and similar devices. However, there is a substantial gap between theory and experiment, such that it is not clear which, if any, of the available calculations are valid. The main purpose of this review is to discuss the various analyses within a common framework, perhaps simplifying the tasks of choosing among them, and of interpreting data. No attempt is made to compare theory and experiment, although a short relevant discussion is given.

I. Introduction

The numerous oscillatory and transient motions which have been found in solid propellant rocket motors share an obvious common feature: their existence depends ultimately on some kind of coupling between the motion and combustion. Although it is possible that residual chemical reactions within the gas phase may, under some circumstances, be important, it appears at the present time that they may be ignored. A truly significant interaction occurs principally in a relatively thin region near the burning solid surface. The coupling may be associated, in general, with either changes of pressure or of velocity parallel to the surface. By far, most of the attention given to this problem has been concerned with pressure coupling, and the emphasis of this paper is set accordingly. However, there is evidence that "velocity-coupling" may be important in some cases.

Perhaps the simplest problem which requires knowledge of the response of a burning surface is that involving small amplitude acoustic waves. This was the earliest case treated, and hence the term ' admittance function, ' borrowed from acoustics, is commonly used. In the analysis of acoustic waves in a chamber, [1-3] it is necessary to specify the component of velocity normal to the boundary. Following traditional acoustics practice, it has usually been assumed that the fluctuation of velocity, u', is proportional to the fluctuation of pressure, p, at the surface; the coefficient of proportionality, in suitably normalized form, is the admittance function A_b for the burning surface. The definition used here is

$$A_b = \frac{u'/\bar{a}}{p'/\gamma\bar{p}} = \bar{M}_b \frac{u'/\bar{u}}{p'/\gamma\bar{p}} \qquad (1)$$

where $\bar{a}$ is the average speed of sound, $\bar{p}$ is the mean pressure, and γ is the ratio of specific heats. The Mach number and speed of the mean flow leaving the surface are $\bar{M}_b$ and $\bar{u}$. This is in fact a natural definition so far as the burning process is concerned, since in response to a pressure change, there is a change in the rate at which solid is converted to gas, and this must appear partly as a velocity fluctuation.

It is generally easier to compute the small change m' of mass flux ($m = \rho u$ where ρ is the gas density) in response to a small change of pressure. Obviously, since $m' = \bar{\rho}u' + \rho'\bar{u}$, (1) gives

$$A_b = \bar{M}_b \left[\frac{(m'/\bar{m})}{(p'/\gamma\bar{p})} - \frac{(\rho'/\bar{\rho})}{(p'/\gamma\bar{p})} \right] . \qquad (2)$$

Superscript bar ($\bar{}$) denotes time averaged quantities and prime, ( )', denotes fluctuations. The bracket is evaluated just downstream of the burning region so that if one assumes that the oscillations are isentropic, $p \sim \rho^\gamma$, the second term is unity. Further remarks on this point will be offered later. The real part of the first term is often given the symbol $\gamma(\mu/\epsilon)$,

$$\frac{\mu}{\epsilon} = \gamma e \frac{m'/\bar{m}}{p'/\bar{p}} \qquad (3)$$

and much of the later discussion will be concerned with μ/ϵ, or the entire complex ratio, rather than A_b.

The function A_b is, in general, a complex quantity, depending on the properties of the materials involved as well as frequency. It is helpful to think in terms of harmonic motions, and to measure phases with respect to the pressure oscillation. The real part of A_b gives that fraction, u'_r, which is in phase with the pressure. Consequently, the rate at which work is done by the surface region on the waves in the chamber is $u'_r p' = (\gamma\bar{p}/\bar{a}) A_b^{(r)} p'^2$, $A_b^{(r)}$ being the real part of A_b. Hence, the attenuation, or growth constant for steady waves has a part proportional to $A_b^{(r)}$ such that the waves are driven if $A_b^{(r)}$ is positive. A larger value of $A_b^{(r)}$ implies a greater tendency for combustion to drive the waves. Although it is a useful relative measure, the admittance function alone is not sufficient to describe the stability of waves in a given chamber; there is a further contribution, of comparable magnitude, due to interaction between the fluctuating and mean flows at the

* This work was performed under a personal services contract with the Naval Ordnance Test Station, China Lake, California.

surface[3, 4]. A valid statement of the stability of waves must be based on a proper accounting of all energy losses and gains.

A similar interpretation of the admittance function arises in connection with the reflection of a traveling wave from a surface. Consider, for example, a plane wave travelling to the left and reflected from a flat surface oriented normal to the direction of propagation. If the interaction between the mean flow and the fluctuations is ignored, then it is quite easy to show that the complex amplitude (i.e., both magnitude and phase are included) of the reflected wave is $(1+A_b)/(1-A_b)$ times the amplitude of the incident wave. Appendix A contains further and more detailed remarks on the meaning and use of the admittance function.

For the classical acoustic modes, therefore, the velocity fluctuation v' parallel to the surface does not enter in a natural, direct way. However, it may clearly be important because of its possible erosive influence on the burning rate, thereby causing a fluctuation of velocity normal to the surface. The function analogous to A_b might be defined as $\mathcal{A}_b = u'/v'$ and the rate at which work is done on the waves would be $p'(\mathcal{A}_b v')^{(r)}$ if phases are again measured with respect to p'. However, a serious difficulty arises because the surface responds to the magnitude of the total velocity parallel to the surface, which includes the mean flow. Moreover, there may be a threshold to the magnitude of the net velocity, below which the erosive response is essentially zero. The analysis in any case becomes non-linear. Since these questions have not been thoroughly treated analytically, and there seems to be no useable relevant data in the literature, they will not be discussed here.

On the other hand, an increasing amount of experimental information is being obtained for the case of pressure coupling. Unfortunately, systematic interpretation of the data is lagging considerably. One would like to be able, eventually, to classify propellants at least roughly according to correlations between composition and the admittance function. This will probably be accomplished, if at all, only if one understands something of the effects that changes of composition have on the various steps in the unsteady combustion process. Hence, it is clear that analytical work is a necessary guide to interpretation of the experimental work, even though precise quantitative results cannot be expected.

Soon after it had been recognized that the admittance or response function must be known for the study of oscillations in rocket chambers, a laboratory apparatus, the T-burner, was devised[5-8] for measuring this quantity without firing a complete rocket. Full usefulness of this technique has not yet been realized, partly because there is not available a good analysis of the T-burner itself, which is required for indirect determination of the admittance function from the direct measurement of pressure only. More recently[9-13] it has become apparent that a different device, the L*-burner, can also be used to measure the admittance function. Although this provides again an indirect measurement, the analysis used is considerably simpler and probably more accurate. To cover the entire frequency range of interest, both kinds of measurement seem to be necessary. One therefore has a means of experimentally determining a boundary condition required for analytical treatment of waves in a chamber.

The subject of this review is consequently of considerable importance, not only in application to problems encountered in rocket motors, but also for the treatment of laboratory data which should eventually be useful in the design of solid propellant rockets. Calculation of the admittance function is by no means a closed subject at the present time, and indeed, it is only now becoming possible (maybe) to extract sufficient information from observations that one may select the "correct" or "valid" analyses. Thus, only brief and qualitative mention of comparison of theory and experiment is included in the present work.

In a very rough way, the various analyses fall into three categories: time lag theories, purely heat transfer theories, and (more or less) "complete" calculations. Truly useful calculations fall mainly in the third class, which includes those attempts to describe the entire burning process from the solid phase to the burnt combustion products. Much of this work has appeared since Cheng[14] published his useful survey of the subject. Geckler[15] and Schultz, et al.[16] have also prepared brief summaries.

II. Time Lag Theories

It appears that the earliest published treatment of acoustic oscillations in a solid propellant rocket chamber is due to Grad[17]. Although his analysis of the stability problem is unnecessarily complicated and yields some incorrect quantitative results (particularly the prediction that the most unstable modes are of much higher order than those actually observed), the formulation of the overall problem is interesting and partially similar to those now used. Moreover, he is led naturally to introduce an admittance function in the following way. Consider a burning surface placed normal to the x-axis and at the origin so that the solid phase is along the negative axis (as in Figure 1). Suppose that the mass flux leaving the solid is a given function f(p, T) of the pressure and temperature downstream of the burnt gases; f(p, T) = ρu is the result one would obtain by steady state measurements.* Let m be the actual mass flux under unsteady conditions and assume that the rate of change of m with time is proportional to the difference between the actual mass flux and that which would exist in steady state for the same pressure and temperature:

$$\frac{dm}{dt} = \frac{1}{\tau}(f - m) . \qquad (4)$$

The relaxation time, or time constant, or time lag is τ, and (4) is merely a statement that the burning process tends to return the mass flux to its instantaneous equilibrium value (f). Thus, for a step change of f (due to a change of pressure, say), the mass flux changes as $e^{-t/\tau}$. Both f and m may be represented as sums of mean values (independent of time) and fluctuations: $f = \bar{f} + f'$ and $m = \bar{m} + m'$. In steady burning, $\bar{f} = \bar{m}$ so that (4) gives

* Since here u is a positive outward from the solid, u = -v in Grad's formula (8), f = -ρv.

$$\frac{dm'}{dt} = \frac{1}{\tau}(f'-m') \quad . \qquad (5)$$

The small change f' in f is due to small changes p' and T' in the pressure and temperature:

$$f' = \left(\frac{\partial f}{\partial p}\right)_T p' + \left(\frac{\partial f}{\partial T}\right)_p T' \quad .$$

Now for an isentropic acoustic wave, $T/\bar{T}_c = (p/\bar{p})^{(\gamma-1)/\gamma}$ and expansion in the small quantities T', p' gives

$$T' = \bar{T}_c(\gamma-1)\frac{p'}{\gamma\bar{p}} \qquad (6)$$

where $\bar{T}_c$ is the mean chamber temperature. With (6), f' is

$$f' = bp' \qquad (7)$$

and

$$b = \left(\frac{\partial f}{\partial p}\right)_T + (\gamma-1)\bar{T}_c\left(\frac{\partial f}{\partial T}\right)_p$$

as defined by Grad, is a quantity which may be presumed known from the ballistic properties of the propellant. After (7) is substituted, and p' is assumed to vary harmonically in time, $p' \sim e^{i\omega t}$, Eq. (5) is easily solved for m':

$$\frac{m'/\bar{m}}{p'/\bar{p}} = \frac{b\tau(\bar{p}/\bar{m})}{1+i\omega\tau} \quad . \qquad (8)$$

Grad treats τ and b as independent quantities, neither a function of frequency. But in fact, they must be related if (8) is to correspond to the correct low frequency behavior of real propellants. For usually, the linear burning rate r varies as a power of pressure, $r \sim p^n$. Hence, for a very slow, small change of pressure, $r'/\bar{r} = n(p'/\bar{p})$, and since $m = \rho_p r$ where ρ_p is the density of the solid,

$$\frac{m'}{\bar{m}} = n\frac{p'}{\bar{p}} \qquad (\omega \to 0) \qquad (9)$$

in the limit of zero frequency. This limit will be used many times; it amounts to satisfaction of the surface energy balance (Eq. (38)) in steady burning[27]. Application of (9) to (8) gives

$$\tau = \frac{nm}{b\bar{p}} \qquad (10)$$

and (6) becomes

$$\frac{m'/\bar{m}}{p'/\bar{p}} = \frac{n}{1+i\omega\tau} \quad . \qquad (11)$$

Grad takes $b \approx .02$ and $\tau \sim O(10^{-5} - 10^{-9})$ sec, the latter being, roughly, the characteristic times of response for many chemical reactions. With this value of b, $\rho_p = 1.6$ gm/cm^3, $\bar{r} = 1$ cm/sec and $\bar{p} = 50$ atm $= 50.5 \times 10^6$ dynes/cm^2, Eq. (10) gives $\tau = 1.5 \times 10^{-5}$ sec, which is consistent with the range of values assumed by Grad. It is perhaps useful to exhibit τ explicitly as a time lag by rewriting (11) as

$$\frac{m'}{\bar{m}} = \frac{r(1-i\omega\tau)}{1+\omega^2\tau^2}\frac{p'}{\bar{p}} = \frac{n}{\sqrt{1+\omega^2\tau^2}}\epsilon e^{i\omega(t-\tau)} \qquad (12)$$

where ϵ is the dimensionless amplitude of the pressure oscillation.

More to the point, however, is the behavior of (11) as a function of frequency. The real part is

$$\frac{\mu}{\epsilon} = \frac{n}{1+\omega^2\tau^2} \qquad (13)$$

which starts at n for $\omega = 0$ and vanishes as $\omega \to \infty$. All measurements which have been reported show a definite peak in μ/ϵ at some moderate frequency, generally less than a few thousand cycles per second. Hence, this very simple picture, perhaps the most elementary one can devise, is wholly inadequate to describe the interaction between pressure waves and the burning. The essential reason for the failure is that the "time lag" τ is in fact a very strong function of frequency which, in the more detailed computations discussed later, can apparently be determined to a rather good approximation.

Much more extensive work was done by Cheng[14, 17-21] using the idea of a time lag, although defined quite differently from Grad's response time. The formulation was in this case strongly influenced by, and is quite similar to, the extensive development of the time lag for analysis of instabilities in liquid propellant rocket motors[22-24]. Consider an element of propellant which, having been heated in the solid phase as the burning surface recedes, departs the surface at some time $t-\tau$. There is, in general, a relatively small energy change associated with the surface reaction (either exothermic or endothermic). But the main exothermic release of energy, from the element considered, occurs at some later time t after the element has progressed some distance downstream in the gas phase. Thus, τ is the time lag, for a given amount of propellant, between the moment of pyrolysis at the surface and combustion in the homogeneous flame region. Let $m_s(t-\tau)$ denote the instantaneous mass flux at the surface, so that $m_s(t-\tau)d(t-\tau)$ grams of solid are converted to gas in the interval $d(t-\tau)$ at time $t-\tau$; this later burns in the interval dt at the time t, and at the rate $m(t)$, the same mass flux appearing in the definition of the admittance function. Thus, conservation of mass implies

$$m(t)dt = m_s(t-\tau)d(t-\tau)$$

or

$$m(t) = \left(1 - \frac{d\tau}{dt}\right)m_s(t-\tau) \quad . \qquad (14)$$

Now the essential assumption is made that before burning (i.e., in the interval τ), the propellant absorbs a fixed amount of energy ("activation energy"?) and that this is related to the pressure according to

$$\int_{t-\tau}^{t} p^{\nu}(t')dt' = \text{const.}$$

It may be noted, as later remarks will amplify, that in all computations of the admittance function, the pressure may be assumed uniform, though varying in time, in both the solid and gas phases. Differentiation of the last equation gives

$$1 - \frac{d\tau}{dt} = \left[\frac{p(t)}{p(t-\tau)}\right]^{\nu}$$

so that (14) relates the total mass flux at the surface, that at the gas phase, and the pressure

$$m(t) = \left[\frac{p(t)}{p(t-\tau)}\right]^{\nu} m_s(t-\tau) \quad .$$

The further assumption is made that the instantaneous surface mass flux is related to the instantaneous pressure, with no phase or time lag, according to

$$m_s(t-\tau) = \text{const.}\,[p(t-\tau)]^n = \frac{\bar{m}}{\bar{p}^n}\,[p(t-\tau)]^n ,$$

the second inequality following in order to satisfy the condition that in steady burning $m_s = \bar{m}$, and of course, $p = \bar{p}$ at all times. (Cheng[14] also includes dependence on erosion but that will be ignored here.) Combination of the last two equations gives

$$\frac{m(t)}{\bar{m}} = \frac{1}{\bar{p}^n}\,\frac{p^\nu(t)}{[p(t-\tau)]^{\nu-n}} \qquad (15)$$

which is Eq. (5) of Reference 18. Roughly, then, n is interpreted as the index in the linear burning rate law $r \sim p^n$ and ν is an index associated with the gas phase reactions.

As before, a relation between m' and p' is found by writing $m = \bar{m} + m'$, $p = \bar{p} + p'$, and after expansion of (15), one finds, to first order of small changes:

$$\frac{m'}{\bar{m}} = \nu\,\frac{p'(t)}{\bar{p}} - (\nu-n)\,\frac{p'(t-\tau)}{\bar{p}} .$$

For harmonic oscillations, $p'(t) \sim e^{i\omega t}$, $p'(t-\tau) \sim e^{i\omega(t-\tau)}$ and

$$\frac{m'(t)/\bar{m}}{p'(t)/\bar{p}} = \nu - (\nu-n)\,e^{-i\omega\tau} . \qquad (16)$$

Note that for $\omega \to 0$, (16) tends to the correct limit, if n is interpreted as remarked above. For comparison with Grad's result (Eq. (11)), (16) can be written in the form:

$$\frac{m'/\bar{m}}{p'/\bar{p}} = \frac{n}{1 + \left\{\frac{(\nu-n)[e^{-i\omega\tau}-1]}{\nu-(\nu-n)\exp(-i\omega\tau)}\right\}} . \qquad (17)$$

Obviously, the time lags defined by Grad and Cheng are not related in a particularly simple way.

The real part of (16) is

$$\mu/\epsilon = \nu - (\nu-n)\cos(\omega\tau) . \qquad (18)$$

As a function of frequency, for fixed τ (again assumed to be independent of frequency), (18) exhibits infinitely many peaks. Figures 2-4 of Reference 14 show some numerical results computed by Cheng. By proper choice of ν, and by letting τ vary with frequency (Cheng[14] chooses $\tau \sim \omega^{-2/3}$), it is possible to force only a single peak. This is clearly an unsatisfactory situation; one is merely fitting a curve, and is not in a position to predict results or to interpret given results in any detail, a shortcoming thoroughly recognized by Cheng.

The result (16) was used in studies of the stability of waves in chambers[18-21] for various configurations and types of propellants. However, statements about stability depend rather strongly on the shape of the admittance function (or μ/ϵ) as a function of frequency. Hence, conclusions based on formulas such as (11) or (17) are suspect.

As in the case of Grad's computation, the representation in terms of a time lag is evidently oversimplified. One gain,[19] however, is that (16) does not vanish as $n \to 0$, whereas (11) does. Even if $n = 0$, so that the burning rate is insensitive to pressure changes in the low frequency limit, there is no reason to expect a similar result at high frequencies. More detailed analyses support this contention.

Moore and Maslen[25] also introduced a time lag in their discussion of the stability of waves. Their final result, expressed in their equation (16) for the growth constant, shows that their assumptions are equivalent to the statement that the admittance function is a complex number. As already noted, the attenuation constant λ for acoustic waves (i.e., $p' \sim e^{-\lambda t} e^{i\omega t}$) has a contribution proportional to the real part of A_b. For a cylindrical grain, and assuming irrotational mean flow (see, for example, Eq. (23) of Reference 3),

$$-\lambda = \frac{\bar{M}_b(\bar{a}/R)}{1 - m_1^2}\,A_b^{(r)} \qquad (19)$$

where R is the radius of the chamber and m_1 is a constant whose value depends on the mode considered: $m_1 = 1/1.84$ for the lowest mode commonly observed. In terms of the magnitude and phase ϕ of A_b, $A_b^{(r)} = |A_b|\cos\phi$ and $\phi = \tan^{-1}(A_b^{(i)}/A_b^{(r)})$. Obviously, a time lag can be defined by $\omega\tau = -\phi$ so that

$$A_b^{(r)} = |A_b|\cos(\omega\tau) \qquad (20)$$

$$\tau = \frac{-1}{\omega}\tan^{-1}(A_b^{(i)}/A_b^{(r)}) . \qquad (21)$$

Thus, according to the definition (1), τ evidently represents the lag between the pressure and velocity fluctuations (if u_r' lags p', then $A_b^{(i)}$ and ϕ are negative and τ is positive). In complex notation, $A_b = |A_b|e^{-i\phi}$ and (1) becomes

$$\frac{u'}{\bar{u}} = |A_b|e^{-i\omega\tau}\,\frac{p'}{\gamma\bar{p}} = \frac{1}{\gamma}|A_b|\,\epsilon\,e^{i\omega(t-\tau)} \qquad (22)$$

A more direct comparison may be made with Eqs. (11) and (17) by solving (2) for $(m'/\bar{m})/(p'/\bar{p})$ and inserting (22) for A_b:

$$\frac{m'/\bar{m}}{p'/\bar{p}} = \frac{n}{1 + \dfrac{[(\gamma n-1) - \bar{M}_b^{-1}|A_b|e^{-i\omega\tau}]}{[1 + \bar{M}_b^{-1}|A_b|e^{-i\omega\tau}]}} . \qquad (23)$$

The low frequency limiting condition has been applied; at $\omega = 0$, when $A_b = A_b^o$, the condition implies

$$A_b^o = \bar{M}_b(\gamma n - 1) . \qquad (24)$$

In fact, (23) is not especially useful or enlightening; the only point is that so far as the relation between velocity and pressure fluctuations at the surface is concerned, the natural "time lag" is defined in terms of the real and imaginary parts of the admittance function.

It appears that Moore and Maslen used a definition of τ like that of Eq. (20). However, it was introduced arbitrarily, following quite a different approach, and they had no way of computing or estimating it. Once again, τ is a strong function of frequency as well as the properties of the propellant.

Three distinct definitions of a time lag have been discussed in this section; more will arise shortly. They all suffer from the inevitable weaknesses of any ad hoc hypothesis, that they are known only by a more detailed analysis (in which case they become trivial definitions) or they must

be measured. If a time lag is used in a complete analysis of waves in a chamber, then an inverse problem must be solved: if all other quantities are known, what values of τ (and perhaps additional parameters) lead to unstable waves? This has been a reasonably successful approach for liquid rockets (Reference 23, for example), principally, it seems, because the time lag is at most a very slow function of frequency; the dependence on combustion parameters (fuel/oxidizer ratio particularly) may be inferred from observation of the stability boundary. This happens to be a fortunate situation, since there exists no way of computing τ for a liquid rocket. On the other hand, the situation in a solid propellant rocket is just reversed: although τ is a function of frequency (and therefore geometry and mode), it may, possibly, be not only measured but calculated.

III. Formulation of the More Complete Problem

While it is quite easy to classify those analyses which rely heavily on some sort of arbitrary time lag, there is a great deal of overlap among the remaining treatments -- in fact much more than one would gather from a brief perusal. It therefore seems advisable to construct at this stage a rather broad description of the problem, providing a reference framework. There is fairly obvious and general agreement concerning the gross aspects of the combustion process: cold solid is heated, perhaps decomposes in a region near the solid-gas interface, vaporizes (the "pyrolysis" reaction) and burns in the gas phase. These features are sketched in Figure 1. Naturally, there are many more details which must be accounted for: differences between composite and double-base propellants, burning of metallic particles, influence of ballistic additives, inhomogeneities of the various regions, and the complicated character of the gas phase. Some of these will be treated subsequently; some have yet to be studied adequately.

It happens, however, that all calculations with which the author is acquainted may be treated as "three-region" models: the solid phase, the gas phase, and the interface region. The last is generally collapsed to a plane and provides a very important matching condition between the solid and gas phases. Except for one recent calculation, the solid has been treated as a single homogeneous layer up to the interface, and there is virtual unanimity on the solution for the condensed phase. Hence the analyses differ importantly only in regard to handling the gas phase.

The problem will, of course, be analyzed in one-dimensional form, and unless otherwise specified, all material properties are averaged over the chemical composition. Three-dimensional properties, such as those necessarily present in composite propellants, are therefore hidden; at present, there is no way of treating such complications, and the problem may perhaps best be regarded as one of determining the appropriate averaging procedure. There are several attempts to approximate the difference between composite and double-base (i.e., homogeneous) propellants, but inhomogeneities in the interface and the influence of metal particles have not been studied.

During unsteady burning the interface moves relative to its mean position: when the pressure oscillates harmonically, the surface does so as well. In all but two works[26, 27], a coordinate system attached always to the burning surface is used; this is not an inertial system. The author prefers an inertial system, with origin fixed to the average position of the burning surface, which moves at rate r in the laboratory. This system, which is similar to the choice made in thin airfoil theory, was first used in this problem by Williams[26]; the equivalence of results obtained in the two systems is demonstrated in Appendix B. Thus, in Figure 1, the solid appears to be moving from the left at the steady linear burning rate r. Since the actual burning surface oscillates about the origin, some care must be taken with the boundary conditions.

a. Solid Phase

Because the conservation of mass and momentum are trivially satisfied, the energy equation alone, written for the temperature, needs to be considered in the solid phase:

$$\lambda_p \frac{\partial^2 T}{\partial x^2} - \bar{m} c \frac{\partial T}{\partial x} - \rho_p c \frac{\partial T}{\partial t} = - \dot{Q}_d \qquad (25)$$

where $\dot{Q}_d$ is the rate of generation of heat, per unit volume, accompanying decomposition. Only in Reference 27 is $\dot{Q}_d$ taken to be non-zero in a finite region, so for simplicity here, only the case $\dot{Q}_d = 0$ will be treated in a detailed manner. With dimensionless variables,* $\tau = T/\bar{T}_s$, $\xi_p = \bar{m} c x/\lambda_p$, (25) is

$$\frac{\partial^2 \tau}{\partial \xi_p^2} - \frac{\partial \tau}{\partial \xi_p} - \left(\frac{\lambda_p \rho_p}{\bar{m}^2 c}\right) \frac{\partial \tau}{\partial t} = 0 . \qquad (26)$$

The normalized mean temperature satisfies

$$\frac{d^2 \bar{\tau}}{d \xi_p^2} - \frac{d \bar{\tau}}{d \xi_p} = 0 \qquad (27)$$

with solution

$$\bar{\tau} = \bar{\tau}_i + (1 - \bar{\tau}_i) e^{\xi_p} \qquad (28)$$

meeting the conditions $\bar{T} = \bar{T}_s$ at the surface and $\bar{T} = \bar{T}_i$ far downstream in the cold propellant.

For harmonic motions, $\tau' \sim e^{i\omega t}$, Eq. (26) is

$$\frac{d^2 \tau'}{d \xi_p^2} - \frac{d \tau'}{d \xi_p} - i \frac{\omega_p}{4} \tau' = 0 \qquad (29)$$

where the important dimensionless frequency parameter is

$$\omega_p = \frac{4 \lambda_p \rho_p \omega}{\bar{m}^2 c} . \qquad (30)$$

The spatial dependence of τ' is clearly also exponential, $\tau' \sim \exp(\lambda \xi_p)$, and λ satisfies the equation

$$\lambda(\lambda - 1) = i \frac{\omega_p}{4} \qquad (31)$$

which has two solutions; only the one with positive real part is used, since then $\tau' \to 0$ for $x \to -\infty$:

$$\lambda = \lambda_r + i \lambda_i \qquad (32)$$

* Subscript s refers to the burning surface and subscript o will refer to the origin of the coordinate system.

$$\lambda_r = \frac{1}{2}\left\{1 + \frac{1}{\sqrt{2}}\left[(1+\omega_p^2)^{\frac{1}{2}}+1\right]^{\frac{1}{2}}\right\} \quad (33)$$

$$\lambda_i = \frac{1}{2\sqrt{2}}\left[(1+\omega_p^2)^{\frac{1}{2}}-1\right]^{\frac{1}{2}} \quad (34)$$

It will be apparent shortly that what one really requires is the expression for the fluctuation of heat transferred from the solid-gas interface to the solid; in dimensionless form, this is

$$q'_{s-} = (\lambda_p/\bar{m}c\bar{T}_s)(\partial T/\partial x)'_{s-}$$

and in Appendix B, the result is shown to be

$$q'_{s-} = \left(\lambda + \frac{A}{\lambda}e^{-i\omega\tau_1}\right)\tau'_s + \frac{n_s}{\lambda}e^{-i\omega\tau_2}\frac{p'}{\bar{p}} \quad (35)$$

where $A = E_s(1-\bar{\tau}_1)/R_o\bar{T}_s$ contains the activation energy E_s associated with surface pyrolysis. The time lags τ_1, τ_2 are defined in Eq. (41). If a decomposition region of finite thickness within the solid phase is included, then q'_{s-} has the same form,

$$q'_{s-} = X_{\tau-}\tau'_s + X_{p-}\frac{p'}{\bar{p}} , \quad (36)$$

but the expressions for the coefficients $X_{\tau-}$ and X_{p-} are considerably more complicated (Ref. 27).

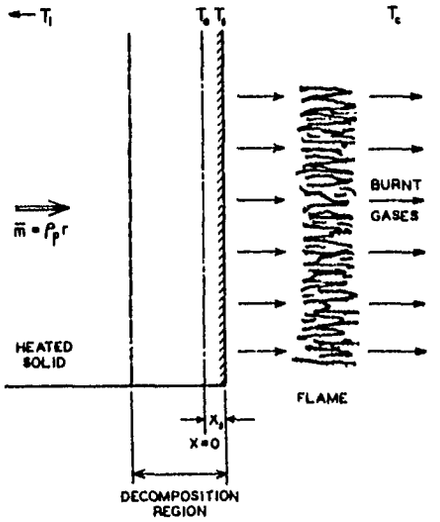

Figure 1. Sketch of Model Used.

b. Solid-Gas Interfacial Region

Conservation of mass and energy, and the law for conversion of solid to gas, give three important relations. The first two are easily found by considering a small control volume placed about the true burning surface which is located at $x = x_s$ and moves with speed $\dot{x}_s$ (Figure 2). Thus, if the region can be collapsed so that negligible amounts of mass and energy are contained within it, one finds "jump" conditions associated with total unsteady mass and energy transfer on the upstream (s+) and dowrstream (s-) sides:

$$\frac{\rho_p \dot{x}_s}{\bar{m}} = -\left(1 - \frac{\bar{\rho}}{\rho_p}\right)\frac{m'_s}{\bar{m}} \approx -\frac{m'_s}{\bar{m}} , \quad (37)$$

* The mean gas density $\bar{\rho}$ near the surface is always much smaller than the solid density in the cases of current interest, so that the term $\bar{\rho}/\rho_p$ will hereafter be dropped.

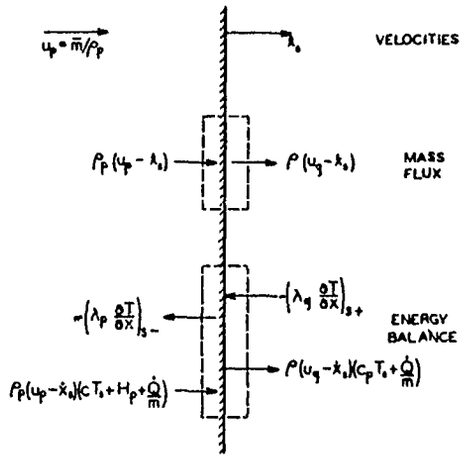

Figure 2. Control Volumes for Interface Conditions.

$$\lambda_g\left(\frac{\partial T}{\partial x}\right)_{s+} = \lambda_p\left(\frac{\partial T}{\partial x}\right)_{s-} + \bar{m}\left(1 - \frac{\rho_p \dot{x}_s}{\bar{m}}\right)[-H_p + (c_p - c)T_s] . \quad (38)$$

The energy change, H_p, accompanying the surface reaction is positive for an exothermic reaction; note that $\lambda_p(\partial T/\partial x)_{s-}$ is the heat flux from the interface to the solid, and $\lambda_g(\partial T/\partial x)_{s+}$ is the heat flux to the interface from the gas phase.

Usually, an Arrhenius law has been assumed for the conversion of solid to gas, giving the total surface mass flux

$$m_s = B p^{n_s} e^{-E_s/RT_s} . \quad (40)$$

In most cases, the dependence on pressure has been ignored ($n_s = 0$). A general perturbed form of (40), to first order of small quantities, is

$$\frac{m'_s}{\bar{m}} = E\frac{T'_s}{\bar{T}_s}e^{-i\omega\tau_1} + n_s\frac{p'}{\bar{p}}e^{-i\omega\tau_2} \quad (41)$$

with $E = E_s/R_o\bar{T}_s$ the dimensionless activation energy for the surface reaction. The time lags τ_1, τ_2 are arbitrarily introduced to represent the lag (or lead) between the fluctuations of surface temperature and pressure, and the corresponding contributions to the fluctuation of surface mass flux. At the present time, there is no way of computing them on the basis of known chemical kinetics. Hence, they will be ignored for the most part, but they have been included as unknown parameters in several of the works discussed later.

So far as a linearized problem is concerned, the assumption of an Arrhenius law, (40), has little significance. What matters is the statement that the surface mass flux responds to both surface

temperature and pressure changes; the linear relation (41) must then hold. If one chooses to deduce (14) from (40), then this merely provides a familiar interpretation of the parameters E and n_s. Incidentally, the use of (41) is not universal; in some of the work of McClure and co-workers, it was assumed that the mass flux was sensitive to heat transfer fluctuations. (See Eq. 73.)

The dimensionless perturbed form of (38) is readily found to be

$$\frac{c_p}{c} q'_{s+} = q'_{s-} + \left(\frac{c_p}{c} - 1\right)\tau'_s + \left(\frac{c_p}{c} - 1 - H\right)\frac{m'_s}{\bar{m}} \qquad (42)$$

where the normalized heat transfer from the gas to the interface is $q'_{s+} = (\lambda_g/\bar{m}c_p)(\partial T/\partial x)'_{s+}$. In some way or other, all calculations must involve the above conditions, although perhaps in slightly modified forms which will be noted as required. Since the various studies differ mainly in respect to the treatment of the gas phase, it seems best to use (42) as the pivotal matching condition; and if, in addition, (41) is assumed, one has

$$\frac{c_p}{c} q'_{s+} = q'_{s-} + X_\tau \tau'_s + X_p \frac{p'}{\bar{p}} \qquad (43)$$

with

$$X_\tau = \left(\frac{c_p}{c} - 1\right)\left(Ee^{-i\omega\tau_1} + 1\right) - EHe^{-i\omega\tau_1} \qquad (44)$$

$$X_p = n_s\left(\frac{c_p}{c} - 1 - H\right)e^{-i\omega\tau_2} \qquad (45)$$

Moreover, with (36), Eq. (43) is

$$\frac{c_p}{c} q'_{s+} = (X_{\tau-} + X_\tau)\tau'_s + (X_{p-} + X_p)\frac{p'}{\bar{p}} \qquad (46)$$

and once q'_{s+} has been determined as a function of τ'_s, $p'/\bar{p}$ and perhaps q'_{s-}, the problem is solved. For then (46) can be solved for $\tau'_s/(p'/\bar{p})$, and substitution into (41) gives $(m'_s/\bar{m})/(p'/\bar{p})$. The solution for the gas phase will provide both q'_{s+} and a relation between m'_s and the fluctuation of mass flux, m', at the outer gas boundary, which is required in the admittance function, Eq. (2). For subsequent use, it should be remarked that the normalized form of the mean energy balance at the surface is, from (38):

$$\frac{c_p}{c}\bar{q}_{s+} = \bar{q}_{s-} + \left(\frac{c_p}{c} - 1 - H\right) = \frac{c_p}{c} - \bar{\tau}_1 - H \ . \qquad (47)$$

c. Gas Phase

This is by far the most involved part of the problem: not only are the equations more difficult to handle, but it is not clear what approximations are appropriate for which propellants. Thus, practically, the limited success achieved to the present time has been gained with the simplest analyses. An essential reason for this is that much of the behavior in the frequency range of interest is evidently dominated by the response of the solid phase; and it appears that the straightforward solution reproduced in Appendix B is adequate. Hence, the gas phase can be simplified considerably without destroying certain major features of the problem. It remains to be seen just how simple yet representative it can be.

If diffusion of the separate species is accounted for, a familiar form for the conservation equations of mass, concentration, and energy, is

$$\frac{\partial\rho}{\partial t} + \frac{\partial m}{\partial x} = 0 \qquad (48)$$

$$\rho\frac{\partial k_i}{\partial t} + \rho u\frac{\partial k_i}{\partial x} - \frac{\partial}{\partial x}\left(\rho D\frac{\partial k_i}{\partial x}\right) = w_i \qquad (49)$$

$$\rho\frac{\partial h}{\partial t} + \rho u\frac{\partial h}{\partial x} - \frac{\partial}{\partial x}\left(\frac{\lambda_g}{c_p}\frac{\partial h}{\partial x}\right) = \frac{\partial p}{\partial t} + \frac{\partial}{\partial x}\left[\frac{\lambda_g}{c_p}(Le-1)\Sigma h_i^o\frac{\partial k_i}{\partial x}\right] \qquad (50)$$

where the enthalpy for each species is

$$h_i = h_i^o + \int_0^T c_{p_i}\,dT$$

and $h = \Sigma k_i h_i$. The only calculations[26, 28, 29] including diffusion explicitly do so for Lewis number, Le, equal to unity, in which case the energy equation (50) can be written

$$\frac{\partial}{\partial x}\left(\lambda_g\frac{\partial T}{\partial x}\right) - mc_p\frac{\partial T}{\partial x} - \rho c_p\frac{\partial T}{\partial t} = -\dot{Q} - \frac{\partial p}{\partial t} \ . \qquad (51)$$

The local rate at which heat is released per unit volume is

$$\dot{Q} = -\Sigma w_i h_i^o \ . \qquad (52)$$

The equation for conservation of momentum reduces to the statement that the pressure is approximately uniform throughout the region treated but of course varies with time. This is a consequence of the low speeds and long wavelengths involved; a closer estimate may be found in Reference 26, p. 3160.

Apart from the obvious complications if diffusion is accounted for, the truly serious obstacle to solving the equations for the gas phase is that in general (48) and (50) or (51) are coupled through the density in $\partial\rho/\partial t$. The simplest and usual means of avoiding the difficulty is to assume that the frequency is sufficiently "small" that all time derivatives in the gas phase can be ignored; this is the "quasi-static" or "low-frequency" approximation, and (48) and (51) become:

quasi-static approximation

$$m = m_s \qquad (53)$$

$$\frac{\partial}{\partial x}\left(\lambda_g\frac{\partial T}{\partial x}\right) - mc_p\frac{\partial T}{\partial x} = -\dot{Q} \qquad (54)$$

In the first instance, this approximation may be motivated by estimating magnitudes of the terms dropped. For example, if (51) is written in terms of dimensionless variables, with $\xi_g = \bar{m}c_p x/\lambda_g$, corresponding to ξ_p in the solid phase, then the frequency parameter for harmonic oscillations is ω_g:

$$\omega_g = \frac{4\lambda_g\bar{\rho}_c\omega}{\bar{m}^2 c_p} = \left(\frac{\lambda_g}{\lambda_p}\frac{c}{c_p}\frac{\bar{\rho}_c}{\bar{\rho}_p}\right)\omega_p \ . \qquad (55)$$

That is, the left hand side of (49) becomes, when written for the first order perturbations,

$$\frac{d^2T'}{d\xi_g^2} - \frac{dT'}{d\xi_g} - \frac{m'}{\bar{m}}\frac{d\bar{T}}{d\xi_g} - i\frac{\omega_g}{4}T' \ ,$$

and the last term one assumes to be negligible if $\omega_g \ll 1$. A similar argument applies to $\partial\rho/\partial t$ in (48) and the term $\partial p/\partial t$ on the right hand side of (51). Some representative properties are given in

Table I; with those values and $\bar{p} < 100$ atmospheres, (55) shows that $\omega_g < \omega_p/100$. It is easy to show that $\omega_p \approx f/40r^2$ where f is the frequency (cps) and r is the linear burning rate (cm/sec). In the range $f < 1000$ cps, $r \approx 1$ cm/sec, $\omega_p < 25$, and ω_g is "small," but certainly not negligible.

$\lambda_p = \lambda_g$	$= 5 \times 10^{-4}$ cal/gm-cm-$^\circ$K
ρ_p	$= 1.5$ gm/cm^3
$\bar{T}_c$	$= 2000^\circ$K
$R = R_o/24$	$= 34.2 \frac{\text{cm}^3\text{-atm}}{\text{gm-}^\circ\text{K}}$
$\bar{\rho}_c$	$= 1.7 \times 10^{-4} \bar{p}$ (atm) gm/cm^3
$c_p = c$	$= 1/3$ cal/gm-$^\circ$K
$\bar{T}_s$	$= 900^\circ$K
T_i	$= 300^\circ$K

TABLE I
Representative Numerical Values

The ratio ω_g/ω_p is effectively a measure of the ratio of the thermal response time in the gas to that in the solid; the gas responds more quickly because, owing to a lower density, the volumetric heat capacity is much smaller. Since for many (but certainly not all) chemical reactions, the response time is also much less than the thermal response time for the solid phase, one might expect the quasi-static approximation to be fairly good under some conditions. Brief discussions of this simplification will also be found in some of the references (e.g. 1, 26, 27, 28, 30). Bird, et al.[30] found that for their treatment of the gas phase, the approximation seems to be quite good up to 10^4 cps. The accuracy of the approximation cannot be verified without having more elaborate solutions, but the only work in which the assumption of quasi-static behavior is not eventually made is Reference 1.

Practically all of the following discussion will therefore not involve explicit time derivatives in the gas phase. This means that expressions found for q'_{g+} required in Eq. (46) will be independent of frequency. Hence, variations of m'_g and the admittance function with frequency will be solely consequences of the relatively slow response of the solid, i.e., due to the propagation of thermal waves inward from the solid-gas interface.

IV. Intermediate Theories

As it has been formulated here, and indeed, as it has been treated in the literature, the problem reduces principally to computation of q'_{g+}, the fluctuation of heat transfer from the gas phase to the interface. Except for those labelled earlier as "time lag theories," all of the computations focus essentially on heat transfer and are perhaps justly called "thermal theories" in the sense that whatever might be claimed at the beginning of an analysis, diffusion of mass eventually winds up in very much a minor position. However, the calculations covered in this section fall, in a more or less loose sense, somewhere between the time lag theories and those treated later as the most complete calculations available.

Some of these involve fluctuations of velocity parallel to the surface, so that they are, in effect, concerned with velocity-coupling rather than pressure-coupling. However, they are not concerned with the non-linear aspects of velocity-coupling, which, as noted earlier, seem to be the distinctive features of that problem. Moreover, certain questions, such as "self-excited" oscillations were first raised by them.

In particular, two papers by Green[31] and Nachbar and Green[32] generated a certain amount of interest[14, 16, 33, 34]. The relevant part of Green's[31] work consists first in the assumption of an Arrhenius law, Eq. (41) here, with $n_s = 0$ but non-zero time lag (τ_1) between mass flux and surface temperature fluctuations, thus giving as a special case of (41):

$$\frac{m'_s}{\bar{m}} = Ee^{-i\omega\tau_1}\tau'_s \,. \tag{56}$$

The total heat transfer to the surface (Green's eq. (1)) is assumed to be expressed in terms of a film thickness δ, or heat transfer coefficient h:

$$q_{s+} = \frac{\lambda_g}{\delta}(T_f - T_s) = h(T_f - T_s) \tag{57}$$

in dimensional form, with T_f the flame temperature. The argument is then offered that the film thickness must increase if the mass flux from the surface increases; thus, h is assumed to have the form

$$h = F/r = \rho_p(F/m_s) \tag{58}$$

where F is an unknown factor, roughly expressed as $F = \lambda_g \bar{\rho} v/\rho_p \ell$, ℓ being the distance from the downstream stagnation point in a rocket chamber--i.e., the distance for development of a boundary layer -- and v being the velocity parallel to the burning surface. Since Green assumes that F may fluctuate ($F = \bar{F} + F'$) as a consequence of fluctuations of the parallel velocity, (56) and (57) give for the normalized heat transfer fluctuation, q'_{s+} (normalization factor is $\bar{m}c_p\bar{T}_s$):

$$q'_{s+} = \frac{(\bar{\tau}_f - 1)}{\bar{m}c_p\bar{r}} F' - \frac{\bar{F}}{\bar{m}c_p\bar{r}}\left[(\bar{\tau}_f - 1)\frac{m'_s}{\bar{m}} + \tau'_s\right] *$$

where $\bar{\tau}_f = \bar{T}_f/\bar{T}_s = T_f/\bar{T}_s$.

Combination of the last equation and (56) gives

$$q'_{s+} = \frac{(\bar{\tau}_f - 1)}{\bar{m}c_p\bar{r}} F' - \frac{\bar{F}}{\bar{m}c_p\bar{r}}\left[(\bar{\tau}_f - 1)Ee^{-i\omega\tau_1} + 1\right]\tau'_s \,. \tag{59}$$

The normalized mean heat transfer to the surface from the gas phase, based on (57) and (58), is

$$\bar{q}_{s+} = \frac{\bar{F}}{\bar{m}c_p\bar{r}}(\bar{\tau}_f - 1)$$

which, according to (47), is equal to

$$(c/c_p)(c_p/c - T_i/\bar{T}_s - H_p/c\bar{T}_s) \,.$$

Consequently, the mean value of the coefficient F is not an independent quantity but is given by

* The flame temperature is assumed constant here.

$$\bar{F} = \frac{\bar{m}\bar{c}\bar{r}}{(\bar{\tau}_f - 1)}\left(\frac{c_p}{c} - T_i/\bar{T}_s - H_p/c\bar{T}_s\right) \quad . \quad (60)$$

However, the point is that (59) is the principal result of Green's analysis, and is to be used in the general matching condition (46), with $X_{p-} = X_{p+} = 0$ and $X_{T-} = \lambda + A\lambda^{-1}\exp(-i\omega\tau_1)$. The equation can then be solved for τ_s':

$$\tau_s' = \frac{\frac{1}{\bar{m}\bar{c}\bar{r}}(\bar{\tau}_f - 1)F'}{\lambda + \frac{A}{\lambda}e^{-i\omega\tau_1} + \frac{\bar{F}}{\bar{m}\bar{c}\bar{r}} + E\left(\frac{c_p}{c} - \bar{\tau}_i - 2H\right)e^{-i\omega\tau_1} + 1) + \left(\frac{c_p}{c} - 1\right)\left(Ee^{-i\omega\tau_1} + 1\right)} \quad .$$

In his Eq. (4), the surface energy balance, Green fails to include the contribution of convection $[(c_p - c)T_s$ in Eq. (38) here]. This amounts to setting $c_p = c$ and the last equation simplifies to

$$\tau_s' = \frac{\left(\frac{T_f}{\bar{T}_s} - 1\right)\frac{F'}{\bar{m}\bar{c}\bar{r}}}{\lambda + \frac{A}{\lambda}e^{-i\omega\tau_1} + \frac{\bar{F}}{\bar{m}\bar{c}\bar{r}} + E\left(1 - \frac{T_i}{\bar{T}_s} - 2H\right)e^{-i\omega\tau_1}} \quad . \quad (61)$$

This is exactly the result obtained by Green (his $L = -H_p$ here) although it was not expressed in the same notation; for large ω_p, τ_s' ($= \Delta T_s/\bar{T}_s$ in his notation) is given as Eq. (29) of reference 31 and for ω_p unrestricted it appears as Eq. (13) of reference 32. There seems to be little point in showing the complete correspondence of symbols, but a few of the more pertinent identifications are shown in Table II.

This Work	Refs. 31, 32
τ_1	τ
λ	λ_2
$Ae^{-i\omega\tau_1}$	A
$-H_p$	L
ω_p	Ψ
$\lambda_p = \lambda_g$	k
$\rho_p\lambda_p/c$	α
$\bar{r}$	r_o
$\frac{\bar{F}}{\bar{m}\bar{c}\bar{r}} + E\left(1 - \frac{T_i}{\bar{T}_s} - 2H\right)e^{-i\omega\tau_1}$	$\frac{k}{\bar{m}c}C$

TABLE II
Correspondence of Symbols with Refs. 31, 32.

Green and Nachbar sought conditions under which the denominator of (61) vanishes, and identified this with the occurrence of "resonance," presumably by analogy with, say, the behavior of a simple second-order system. If all other quantities are fixed, the condition, if it can be satisfied, gives particular values ("eigenvalues") of the frequency ω_p; actually, they chose to permit both the frequency and the time lag τ_1 to vary and sought the critical values for zeros of the denominator.

Since then τ_s' and hence the mass flux change become infinitely large even for vanishingly small values of the "driving force" (F'), it was supposed that this condition corresponds to the existence of pressure oscillations ("resonant" burning) leading to observable increases in the burning rate and mean chamber pressure. It is now recognized that this is a very narrow view of the problem, to be discussed further in the section on "self-excited" or "intrinsic" instabilities: oscillations may very well occur even if the denominator is not zero, or even near zero.

For the sake of comparison with later work, however, several points should be made. First, multiply numerator and denominator of (61) by λ and eliminate λ^2 by use of the equation (31) satisfied by λ. Then write (61) with the real and imaginary parts shown explicitly:

$$\frac{\bar{m}\bar{c}\bar{r}}{(\bar{\tau}_f - 1)}\frac{\tau_s'}{F'} = \lambda\left[A\cos\omega\tau_1 + \lambda_r\left\{1 + \frac{\bar{F}}{\bar{m}\bar{c}\bar{r}} + E(1 - \bar{\tau}_i - 2H)\cos\omega\tau_1\right\} - \lambda_i E(1 - \bar{\tau}_i - 2H)\sin\omega\tau_1\right] +$$

$$+ i\lambda\left[\frac{\omega_p}{4} + \lambda_i\left\{\frac{\bar{F}}{\bar{m}\bar{c}\bar{r}} + E(1 - \bar{\tau}_i - 2H)\cos\omega\tau_1\right\} + A\sin\omega\tau_1 + \lambda_r E(1 - \bar{\tau}_i - 2H)\sin\omega\tau_1\right] . \quad (62)$$

An interesting special case is $\tau_1 = 0$:

$$\frac{m_s'}{\bar{m}} = E\tau_s' = \frac{(\lambda_r + i\lambda_i)\frac{(\bar{\tau}_f - 1)E}{\bar{m}\bar{c}\bar{r}}F'}{\{\lambda_r(P - A) + A\} + i\left\{\frac{\omega_p}{4} + \lambda_i(P - A)\right\}}$$

$$= \frac{E\frac{(\bar{\tau}_f - 1)}{\bar{m}\bar{c}\bar{r}}F'}{\lambda + \frac{A}{\lambda} - (1 + A) + P} \quad (63)$$

where P is defined by

$$P = A + \frac{\bar{F}}{\bar{m}\bar{c}\bar{r}} + E(1 - \bar{\tau}_i - 2H) \quad . \quad (64)$$

Note that if F', which is proportional to velocity fluctuations parallel to the surface, is related to pressure fluctuations as for some acoustic modes, these results would produce $(m_s'/\bar{m})/(p'/\bar{p})$, as required for the problem of pressure coupling. And it will be shown later that for $\tau_1 = 0$, this analysis by Green and Nachbar of the zeros of the denominator in (63) is exactly the same as the computation by Denison and Baum[28] for the conditions under which self-excited motions arise. A non-zero value of τ_1 modifies quantitative results, but is not an essential feature of the model.

The preceding calculation has yielded no quantitative results either for the response function or for the stability of waves in a chamber. Mainly this is a consequence of preoccupation with the very special aspect of intrinsic instabilities which were first noted by Green. Barrère and Bernard[35] tried to generalize the computation by introducing additional time lags and also permitting a continuous distribution of time lags. Their hope was to find a means of representing the behavior of composite propellants, a problem which remains unsolved. A slightly later consideration of the same problem appears in Ref. 36, also making use of a time lag, but defined differently.

Akiba and Tanno[9] proposed an interesting modification to Green's analysis, for use in their experimental study of low frequency (also called L* or "non-acoustic") instability. Two important changes were made: (1) the phase lag $\omega\tau_1$ is set equal to zero, because of the low frequencies involved; and (2) the heat transfer from the gas phase to the solid-gas interface is given by the expression (their Eq. (8) written in the notation used here)

$$\lambda_g \left(\frac{\partial T}{\partial x}\right)_{s+} = k p^n (T_f - T_s) \tag{65}$$

where k is a constant and n is again the index in the linear burning rate law. (In their notation, the index is n/2 and $k = k_g \lambda / L$ for $r = bp^n$.) Thus, (65) involves a heat transfer coefficient changing with pressure only, $h = kp^n$. The flame temperature is again taken to be fixed, and the normalized fluctuation of heat transfer is

$$\frac{c_p}{c} q'_{s+} = - \frac{k\bar{p}^n}{\bar{m}c} \tau'_s + \frac{nk\bar{p}^{n+1}}{\bar{m}c} (\bar{\tau}_f - 1) \frac{p'}{\bar{p}} \tag{66}$$

which corresponds to (59) used by Green.

When (66) is used in the energy matching condition (46), with $X_{\tau_p} = X_p = 0$, and $m'_s/\bar{m}$ is related to τ'_s by (41) with $^p\tau_1 = n_s = 0$, one finds easily

$$\frac{m'_s/\bar{m}}{p'/\bar{p}} = \frac{\dfrac{nk\bar{p}^{n+1}E}{\bar{m}c}}{\lambda + \dfrac{A}{\lambda} + X_\tau + \dfrac{k\bar{p}^n}{\bar{m}c}} .$$

Application of the limiting condition for $\omega \to 0$ shows that, since $\lambda \to 1$ for $\omega \to 0$,

$$X_\tau + \frac{k^{-n}_p}{\bar{m}c} = P - (A+1)$$

where P is here defined as

$$P = \frac{Ek\bar{p}^{n+1}}{\bar{m}c} (\bar{\tau}_f - 1) . \tag{67}$$

The response function based on the above assumptions is therefore finally

$$\frac{m'_s/\bar{m}}{p'/\bar{p}} = \frac{n P}{\lambda + \dfrac{A}{\lambda} - (1+A) + P} . \tag{68}$$

Sehgal and Strand[11] based their discussion on the ideas introduced by Akiba and Tanno; neither paper contains explicitly a formula like (68), although it is of course implied.

This response function involves the unsatisfactory assumption (65) for the heat transfer coefficient, thereby introducing pressure coupling rather than the velocity coupling proposed by Green. The form of (68) is exactly that found by later works (P and A being adjustable parameters independent of frequency) but the basis of the calculations, and hence the interpretations of P, will be more convincing than in the case just discussed.

Another calculation concerned with intrinsic instabilities rather than the complete response function is the work of Shinnar and Dishon[37] who did not produce any numerical results. However, it is useful to discuss their treatment of the gas phase; once again, the only difference in the formal structure is, ultimately, the expression for q'_{s+}. The perturbed Arrhenius law, (41), is used with n_s and the time lags equal to zero; their energy matching condition (their Eq. (3)) also does not include the convection terms, so that $c_p = c$ effectively. The energy equation for the gas phase is taken to have the form of (51) here, except that the term $\partial p/\partial t$ is, incorrectly, not included. It is solved for the case of no heat generation ($\dot{Q} = 0$) in the region between the solid surface and the "flame" assumed to be a plane at $x = \delta$; all heat release occurs at $x = \delta$ and affects only the boundary condition at that position*. This picture of the gas phase is similar to the model of References 1, 30, 39, 40 and 41.

With $\dot{Q} = 0$, Eq. (51), in dimensionless variables for the mean temperature ($\bar{\tau} = \bar{T}/\bar{T}_s$) is

$$\frac{d^2\bar{\tau}}{d\xi_g^2} - \frac{d\bar{\tau}}{d\xi_g} = 0 \tag{69}$$

which is to be solved subject to the conditions $\bar{\tau} = 1$ at $x = 0$ and $\bar{\tau} = \bar{T}_\delta/\bar{T}_s = \bar{\tau}_\delta$ at $x = \delta$.* The solution is

$$\bar{T} = \bar{T}_s + (\bar{T}_\delta - \bar{T}_s) \frac{\exp\left(\dfrac{\bar{m}cx}{\lambda_g}\right) - 1}{\exp\left(\dfrac{\bar{m}c\delta}{\lambda_g}\right) - 1} . \tag{70}$$

The treatment of the unsteady energy equation is not internally consistent. Thus, they don't include the $\partial p/\partial t$ term, and also set m' equal to m'_s when it arises; the second step decouples the energy equation from the continuity equation. But to be consistent, one must also ignore $\partial T/\partial t$, which Skinnar and Dishon did not do. With their basic assumptions, the only correct treatment is a purely quasi-static one, which means computing both T' and the fluctuation of heat transfer by examining small perturbations of the steady state profile (70). The result for q'_{s+}, assuming that T_δ is constant, is

$$q'_{s+} = - (e^{\bar{\delta}} - 1)^{-1} \tau'_s - [(\bar{\tau}_\delta - 1)(e^{\bar{\delta}} - 1)^{-2} e^{\bar{\delta}}] \delta' . \tag{71}$$

Here, $\bar{\delta}$, δ' are the mean and fluctuation values of the flame "stand-off distance", normalized as usual, with respect to $\bar{m}c/\lambda_g$.

If the flame temperature T_δ is known, then the mean profile (70) gives

$$\bar{q}_{s+} = \frac{(\bar{\tau}_\delta - 1)}{(e^{\bar{\delta}} - 1)} \tag{72}$$

and this can be used in the mean energy balance, (47), to find a formula for $\bar{\delta}$. The only remaining part of the problem is to relate δ' to, say, $p'/\bar{p}$. Leaving this unspecified, (71) substituted into (46) leads to

* The x-axis is defined to run in the opposite direction in Ref. 37 so that the outer boundary condition is applied at $x = -\delta$.

$$\frac{m_s'}{\bar{m}} = \frac{E\frac{c_p}{c}\left(\frac{\bar{q}_{s+}e^{\bar{\delta}}}{\bar{\delta}}\right)(-\delta')}{e^{\bar{\delta}}-1} \Big/ \lambda + \frac{A}{\lambda} + X_\tau + \frac{c_p/c}{e^{\bar{\delta}}-1} \qquad (72)$$

if $X_p = X_{p_-} = \tau_1 = n_g = 0$. Note, for example, that one expects the flame distance to decrease if the pressure increases, so $-\delta' \sim p'$ and one arrives once again at a form of the admittance function like (63) and (68) after the limiting $\omega \to 0$ condition is applied.

Shinnar and Dishon did not carry out the above computation. They eventually found a characteristic value problem (their Eq. (28)) in ω and δ which corresponds to finding the zeros of the denominator of a ratio like (72). This may be compared with Green's characteristic value problem in ω and τ. Since the formulation is incorrect, there is no need to discuss the details, but the formula (72) for the response related to the flame "stand-off" distance is interesting.

Finally, there are two other works[37, 38] which are sometimes referred to, but are now rendered wholly obsolete by more recent work. Smith and Sprenger[37], in a paper which contained one of the first experimental verifications that increases in the mean chamber pressure often accompany oscillations, suggested that the coupling was due to the influence of pressure changes on heat release in the gas phase. However, they ignored the important role of heat transfer in the solid phase and assumed that the surface recedes at uniform speed. No calculations were carried out. Smith[38] assumes that the surface temperature is constant and that the heat transfer from the gas phase (q_{g+}') is in phase with the pressure oscillations. Both of these approximations are unacceptable, and the subsequent computations are bound to be seriously in error.

V. More Complete Calculations

Since publication of the work by Hart and McClure[1], more emphasis has, correctly, been placed on computing the admittance function and its variation with frequency, rather than simply being concerned with its poles. Cheng had, of course, worked with this function, but the results obtained are severely limited and not reliable so long as time lags are used. On the other hand, Reference 1 is the first attempt to treat the entire process in the manner already described here. Moreover, it contains also the only calculation (albeit for a simplified model) of the gas phase for frequencies outside the "quasi-static" range.

There is an important difference in the pyrolysis law used in Reference 1, leading to a dependence of mass flux on heat transfer rather than temperature and pressure only. In the notation used here, Eq. (36) of Reference 1 is

$$\frac{m_s'}{\bar{m}} = E\tau_s' + \alpha\frac{q_{s+}'}{\bar{q}_{s+}} \qquad (73)$$

with α found to be -1. This result is based initially on the assumption that solid material decomposes internally at a rate given by the Arrhenius law, and that the conversion of solid to gas is the integrated result of the decomposition:

$$m_g = B_1 \int_{-\infty}^{x=x_s} e^{-E_s/R_oT}\,dx \qquad (74)$$

where B_1 is a constant. If the variable is changed from x to T, and one assumes that the major contribution to decomposition occurs in a region so thin that dT/dx has approximately the value on the gas side of the interface*, (74) becomes

$$m_s \approx \frac{B_1}{(dT/dx)_{s+}} \int_{T_i}^{T_s} e^{-E_s/R_oT}\,dT = \frac{B_1}{(dT/dx)_{s-}} \int_{T_i}^{T_s} \frac{R_oT^2}{E_s}\frac{d}{dT}\left(e^{-\frac{E_s}{R_oT}}\right)dT .$$

Evidently if the decomposition does occur in a thin region, then the behavior of the integrand is dominated by the exponential, and one can set $R_oT^2/E_s \approx R_oT_s^2/E_s$. Hence, approximately

$$m_s \approx \frac{B_1R_oT_s^2}{E_s(dT/dx)_{s+}}\left(e^{-E_s/R_oT_s} - e^{-E_s/R_oT_i}\right) .$$

For $T_s \sim 3T_i$, the first exponential dominates and

$$m_s \approx \frac{B_1R_o}{E_s}\frac{T_s^2}{(dT/dx)_{s+}}e^{-E_s/R_oT_s} . \qquad (75)$$

Linearization of (75) in small quantities gives (73) with $\alpha = -1$. The coefficient of τ_s' in (73) should be (E+2) but the value of E used in Ref. 1 are so large (E = 41.6 and 34.7) that this is an insignificant detail; in any case, one can simply absorb the 2 in E, whose value is not well known.

One might expect that the sensitivity of the surface mass flux to heat transfer could be related to the heating effect of energy gained from the gas. But (73) shows the unexpected (and not explained in the references cited) result that if the heat transferred from the gas is increased ($q_{s+}'>0$) then the mass flux is decreased since $\alpha =$ If $(dT/dx)_{s-}$ had been used in approximating the integrand above, the interpretation of the sign would make more sense, since one would have increased mass flux for a decreased heat loss to the solid phase (q_{s+}' would be replaced by q_{s-}' in (73).) However, other features of the calculation mask this difficulty and will be more important.

References 1, 30, 39, and 40 will be considered together, although Ref. 40 represents somewhat of a break from the earlier three: it does not involve the direct dependence of m_s' on q_{s+}' (i.e., α=0). Most of the details will not be included - some of the calculations are very lengthy - but some relevant steps will be noted. Table III shows the correspondence for the more important symbols used. For simplification, the four papers will be cited as I, II, III, and IV, respectively.

The solution for the solid phase is the same in all these papers and is given by Eq. B-8 of Appendix B

* The "heated solid" side of the interface therefore begins upstream of the decomposition region discussed here.

This Work	Ref. 1 (I)	Ref. 30 (II)	Ref. 39 (III)	Ref. 40 (IV)
T_i	T_c	T_c	T_c	T_c
T_s	T_o	T_o	T_o	T_o
T_f	T_l	T_l	T_l	T_l
$-H_p$	h_v	h_v	h_v	h_v
$-H_p - cT_i$	h	h	h	h
$(\partial T/\partial x)_{s+}$	G_o	G_o	G_o	G_o
$(\partial T/\partial x)_{s-}$	G_{os}	G_{os}	G_{os}	G_{os}
$m'_s/\bar{m}$	$\tilde{\mu}_o$	$\tilde{\mu}_o$	$\tilde{\mu}_o$	$\tilde{\mu}_o$
$(m'/\bar{m})_{x\to\infty}$	$\tilde{\mu}_l$	$\tilde{\mu}_l$	-	-
τ'_s	$dT_o/\bar{T}_o$	$\delta T_o/\bar{T}_o$	$d\bar{T}/\bar{T}_o$	$\tilde{\psi}_o$
λ_p	λ_s	λ_s	λ_s	λ_s
λ_g	λ	λ	λ	λ
λ	$\lambda\gamma'/\bar{m}C_s$	α	Λ	Λ
$\omega_p/4$	ωT_s	ωT_s	ωT_s	ωT_s
E_s	A_s	A_s	A_s	A_s
E	β	β	β	$A_s/R\bar{T}_s - \frac{1}{2}$
ξ_p	$\bar{m}C_s x/\lambda_s$	y	-	$\bar{m}C_s x/\lambda_s$

TABLE III - Correspondence of Symbols with References 1, 30, 39, and 40.

$$q'_s = \lambda\tau'_s + \frac{(1-\bar{\tau}_i)}{\lambda}\frac{m'_s}{\bar{m}} \quad . \tag{76}$$

This may be extracted from the last equation of the Appendix to paper I, but it should be noted that the equation there is for the total heat transfer $\bar{q}_{s-} + q'_{s-}$ and that $\gamma'\lambda_s/\bar{m}C_s = \lambda$ used here.

The gas phase in I - IV is treated according to the model sketched in Figure 3, or slightly modified forms. A boundary condition is set at the downstream edge of the flame region (which is effectively collapsed to a plane) so that the conservation equations are solved without heat release included except as it affects the boundary condition at $T = T_f$; diffusion is also ignored. In I, the coupled continuity and energy equations (Eqs. (48) and (50) with $\dot{Q} = 0$) are solved by transforming the independent variables from (x, t) to (T, t) and without the strict quasi-static assumption. The dependent variable $\psi(T, t)$ is essentially the perturbation of $p^{1/\gamma}x$ where x is the position at which the temperature is T at time t. Thus, the boundary condition at the burning surface is $\psi(T_s, t) = 0$ since the origin of the original coordinate system is always at the burning surface where $T = T_s$. Motion of the flame relative to the burning surface is accounted for and leads to a relatively involved boundary condition there.

Eventually the continuity and energy equations can be combined to give a single second order equation for ψ (Eq. (20) of I), but at the expense of losing interpretation of the formal analysis. From the solution $\psi(T, t)$, the fluctuation of mass transfer can be found by use of the continuity equation and boundary conditions.

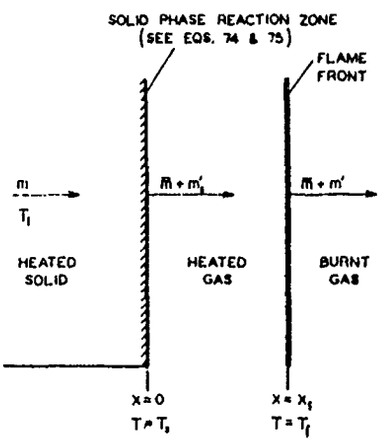

Figure 3. Model Used in Refs. 1, 30, 39, 40.

Unfortunately, the analysis of the gas phase is not done independently of the remainder of the problem. When the single equation for ϕ is formed, the solution for the solid phase, the pyrolysis law and the energy matching condition are used explicitly. However, it follows from the definition of ϕ (Eq. (17c) of I) that

$$\frac{q'_{s+}}{\bar{q}_{s+}} = \frac{p'}{\bar{p}} - \frac{\bar{m}c_p\bar{T}_s}{\lambda_g}(1-H_p-\bar{\tau}_i)\left(\frac{\partial\phi}{\partial T}\right)_{T=T_s}$$

which could be used in the scheme suggested here.

It is perhaps useful to note that a quantity J appears in all four papers; it arises first in Eq. (6a) of I, which is a formula for the total heat transfer from the gas phase to the solid. That equation combines the solution to the solid phase, the pyrolysis law (75), and the energy matching condition; in the present notation, one finds

$$\frac{c_p}{c}(\bar{q}_{s+}+q'_{s+}) = \frac{m_s}{\bar{m}}\left(\frac{c_p}{c}\frac{T_s}{\bar{T}_s}-\bar{\tau}_i-H\right)+\frac{m'_s}{\bar{m}}\frac{J}{c\bar{T}_s}.$$

It can then be shown that the formula for J is

$$\frac{J}{c\bar{T}_s} = \frac{q'_{s-}-\tau'_s}{(m'_s/\bar{m})} - (1-\bar{\tau}_i) \qquad (77)$$

in which τ'_s is found by combining the pyrolysis law (75) and the perturbed part of the energy matching condition, (42),

$$\frac{\tau'_s}{m'_s/\bar{m}} = \frac{1-\alpha\frac{c}{c_p}\left(\frac{1-\bar{\tau}_i}{\lambda}+\frac{c_p}{c}-1-H\right)/\bar{q}_{s+}}{E+\alpha\frac{c}{c_p}\left(\lambda-1+\frac{c_p}{c}\right)/\bar{q}_{s+}}. \qquad (78)$$

In the special case $\alpha = 0$,

$$\frac{J}{c\bar{T}_s} = \frac{1}{E}\left[\left(\lambda+\frac{A}{\lambda}\right)-(1+A)\right]. \qquad (79)$$

Although the quasi-static assumption is not made in the differential equations, an "adiabatic" approximation is used to determine formulas for fluctuations in the burning rate both for the pyrolysis law and for the burning rate in the gas phase. (Cf. Eq. (7) and following remarks of I.) In this way, a comprehensive treatment of the flame region is avoided. It appears, however, that this approximation, reducing the flame to a plane surface, may be very restrictive and probably not at all applicable to composite propellants.

The formula for μ/ε is lengthy and will not be reproduced here. Evidently, numerical calculations were carried out for much wider ranges of parameters than reported in I, for the existence of large peaks (i.e., zeros of the denominator as discussed above in connection with Green's work) was noted. However, the values of the parameters (such as E) associated with the peaks evidently were unrealistic (they were not published), and the numerical results actually given exhibit only broad, rather low peaks. Even so, the values of E (34 - 42) are rather high -- more reasonable values are 10 - 15, that is, E_s = 20 - 30 kcal/mole. The failure to obtain higher peaks, closer to observed results, with acceptable values of the parameters led subsequently to inclusion of thermal radiation (Ref. 39, paper II) and dependence of the surface reaction on pressure (Ref. 40, paper IV).

In Reference 30, the second paper of this series, two main points are important. First, it was found that the effect of propellant compressibility appears to be negligible. This is the only discussion of compressibility, and since it appears to be unimportant, it will not be discussed further here. The more interesting result is that a true quasi-static calculation of the gas phase was given; in all other respects the calculation was the same as in paper I. Numerical results showed that the quasi-static analysis agreed with the more involved treatment of paper I to within 10 per cent for frequencies up to 10,000 cycles per second, somewhat higher than one could reasonably have expected. This of course is the only available check of the quasi-static approximation.

The formula found in paper II (Eq. 23) for q'_{s+} in the quasi-static limit is

$$\frac{q'_{s+}}{\bar{q}_{s+}} = a_o\frac{m'_s}{\bar{m}} + b_o\frac{p'}{\bar{p}} \qquad (80)$$

where, if propellant compressibility is ignored,

$$a_o = \frac{(c_p/c)(1+1/E)-(H+\bar{\tau}_i+\bar{\tau}_i/j)}{c_p/c(1-1/E)-(H+\bar{\tau}_i)} \qquad (81a)$$

$$b_o = \frac{n\,\bar{\tau}_i/j}{c_p/c(1-1/E)-(H+\bar{\tau}_i)} \qquad (81b)$$

Equation (80) is the quantity required from solution to the gas phase, and combination of (80), the pyrolysis law (73), the solution for the solid phase, and the energy matching condition (42), gives

$$\frac{m'_s/\bar{m}}{p'/\bar{p}} = \frac{n}{1+j\frac{J}{c\bar{T}_i}} \qquad (82)$$

where j is the index in the burning law $\bar{m}\sim\bar{p}^n T_i^j$. It is particularly interesting to examine the case when the direct dependence of mass flux on heat transfer is absent ($\alpha = 0$), for which the function J is given by (79). Then Eq. (82) is easily put in the form

$$\frac{m'_s/\bar{m}}{p'/\bar{p}} = \frac{n(\bar{\tau}_i E/j)}{\lambda+\frac{A}{\lambda}-(1+A)+(E/j)\bar{\tau}_i}. \qquad (83)$$

If one writes P for $\bar{\tau}_i E/j$, the formula has exactly the same form found previously, Eq. (68), also to be discussed again shortly. However, in other analyses, the parameter P characterizes the gas phase, whereas here, $P=(E/j)\bar{\tau}_i$, it is the normalized surface activation energy reduced by $\bar{\tau}_i/j$, which is also a property of the solid material. It may be noted that the limiting behavior, $\mu/n\varepsilon \to 1$ for $\omega \to 0$, is correct.

It is quite easy to show from Eq. (83) that large peaks in this function will occur only for quite unrealistic values of surface activation energy. The pole occurs at the frequency $\omega_p = 4\sqrt{AP}$ (see Eq. (118)), and the large peaks occur near this pole, i.e., for values of A and P giving small values of the denominator in (83). Now, experimentally, it is found that maxima in the response function occur in the neighborhood of $\omega_p/4 \approx 8$. Hence, this implies that $AP \approx 64$, or for $P=(E/j)\bar{\tau}_i$

$$E^2 \approx \frac{64j/\bar{\tau}_i}{1-\bar{\tau}_i} . \qquad (84)$$

With $\bar{\tau}_i \approx 1/3$ (Table I) and $j \approx \frac{1}{2} - 1$ (Ref. 1), E must be around 15-25. But for real propellants, E is 10 - 15. One must conclude then, as the original authors found in their numerical work, that with the treatment of the gas phase used in Refs. 1, 30, and 39, it may be difficult to find large values of the admittance function for realistic values of frequency and surface activation energy. The trouble seems to lie not so much with the treatment of the flame as a thin region as with the handling of the boundary conditions on the gas phase region and subsequent manipulations. It is clear from (83) that these have been set in such a way that the final result contains no parameter characterizing the gas phase. On the other hand, later remarks will show that a fairly straightforward analysis leads to the same form as (83) but the parameter P is identified with the behavior of the gas phase.

The preceding discussion applies to the case $\alpha = 0$; for $\alpha \neq 0$ the formula for μ/ϵ is much more complicated. But it appears, judging by the results given in Refs. I and II, that the difficulty is not avoided either by taking $\alpha \neq 0$ or by relaxing the assumption that the gas phase behaves in a quasi-static manner. The calculations of Ref. 39 (paper III) are also based on the model and analysis used in papers I and II, but with some account taken of thermal radiation by the burnt combustion gases. Radiation was included as a perturbation about a quasi-static analysis of the gas phase. This complication was added in an attempt to obtain larger values of μ/ϵ with reasonable values of E and the other parameters. It was found that the response was indeed enhanced at the lower frequencies; a discussion of the results was also given in Ref. 42.

The last paper of this series, Ref. 40 (paper IV), constitutes another attempt to predict larger responses in the lower frequency range. The principal change is that the pyrolysis law contains no dependence on heat transfer from the gas phase ($\alpha = 0$) but it does have a dependence on pressure:

$$m = B_o \frac{p}{\sqrt{T_s}} e^{-E_s/R_o T_s} . \qquad (85)$$

This formula is based partly on the idea that "active constituents" in the gas near the solid surface may return to the surface and thereby alter the reaction rate. From kinetic theory, the flux of particles in one direction through a plane is proportional to $p/\sqrt{T}$ which accounts for the factor in (85). Not all such collisions lead to reaction, and the weighting factor $\exp(-E_s/R_o T_s)$ enters. Thus, the added sensitivity to pressure is associated with an "autocatalytic effect." The perturbed form of (85) is

$$\frac{m'_s}{\bar{m}} = E\tau'_s + \frac{p'}{\bar{p}} \qquad (86)$$

where E stands for $E_s/R_o\bar{T}_s - \frac{1}{2}$.

Once again, the gas phase is treated quasi-statically, but other assumptions and details differ in certain respects from those used in papers I - III. It is supposed that the fluctuation of burning rate in the gas phase is dependent on pressure and on heat transfer from the interface to the unreacted solid:

$$\frac{m'}{\bar{m}} = a_1 q'_{s-} + b_1 \frac{p'}{\bar{p}} \qquad (87)$$

where the coefficients a_1 and b_1 are

$$a_1 = \frac{-j}{\bar{\tau}_i - j[\frac{1}{E} + (1-\bar{\tau}_i)]} \qquad (88a)$$

$$b_1 = \frac{n\bar{\tau}_i - j/E}{\bar{\tau}_i - j[\frac{1}{E} + (1-\bar{\tau}_i)]} \qquad (88b)$$

These results are deduced from an "adiabatic" or quasi-static perturbation analysis of the overall burning process and energy balance for the solid phase; j has the same meaning as in (81a, b) and (82).

The solution for the solid phase is the same as used many times, Eq. (76). By combining (76), (86), and (87), one finds for the response (Eq. (20) of IV, but J_a there is -J here)

$$\frac{m'_s/\bar{m}}{p'/\bar{p}} = \frac{n+N}{1+jJ/c\bar{T}_i} \qquad (89)$$

where J is the same J defined in (79) and

$$N = \frac{j}{E\bar{\tau}_i}(\lambda - 1) . \qquad (90)$$

For comparison with other formulas, (89) may be written

$$\frac{m'_s/\bar{m}}{p'/\bar{p}} = \frac{n(\bar{\tau}_i E/j) + (\lambda - 1)}{\lambda + \frac{A}{\lambda} - (1+A) + (\bar{\tau}_i E/j)} \qquad (91)$$

which differs from the earlier result, (83), of paper II only in the factor $(\lambda - 1)$ in the numerator; if the pyrolysis law had p^{n_s} instead of p, the factor would be $n_s(\lambda - 1)$.

Although the response calculated from (91) does show higher peaks, and relatively good agreement with some data (for one propellant) is obtained[40], the values of E used are still low. A good discussion of this point, as well as certain relevant aspects of steady-state burning, is included in paper IV.

It is fairly clear, even from such a brief coverage, that the last paper, like the other three, contains little information about the gas phase: this part of the problem seems to be too much simplified. Thus, the results, Eqs. (83) and (91), for the quasi-static treatment (which were found to be in good agreement with the non-quasi-static form of the analysis[1] for frequencies up to 10,000 c. p. s.) contain no parameter characterizing the gas phase. It will be evident shortly that this is contrary to results found elsewhere. The interpretation of $P(\neq \bar{\tau}_i E/j)$ is then different and one does not encounter the difficulty (see Eq. (84) and following remarks) with low values of the surface activation energy.

The only elaborate attempt to treat diffusion is that by Williams[26]. However, not only is the quasi-static approximation made, but the final result for the response function $m'_s/\bar{m}$ goes to zero for $\omega \to 0$; that is, it is valid only for $n = 0$, a restrictive case at best. This unfortunate result originates mostly in approximations used to treat the steady-state behavior of the gas phase.

phase; it is not clear just where. In view of this serious failing, although the results might be valid if $n=0$ (i.e., mesa propellants), and because the analysis is lengthy and differs from others only in the treatment of the gas phase, it will not be discussed here. Reference 26 does contain a more complete discussion of diffusion than appears elsewhere.

Denison and Baum[28] first showed a response function explicitly in terms of two parameters, called A and P here, and found an expression for P in terms of the properties of the gas phase. They treated the gas phase quasi-statically; although diffusion is ostensibly included, it is for Lewis number unity, and in the final results the influence of diffusion appears nowhere. The integral of the energy equation was performed in an approximate way, following known laminar flame theory, which leads to an expression for the mass flux in terms of quantities associated with the gas phase:

$$m_g = c\, p^{\nu}\, T_f^{\nu+1}\, e^{-E_f/2R_o T_f} \qquad (92)$$

where c is constant and E_f is the activation energy for the gas phase reaction. Linearization of (92) gives

$$\frac{m_g'}{\bar{m}} = \left(\frac{E_f}{2R_o T_f} + \nu + 1\right)\frac{T_f'}{\bar{T}_f} + \nu\,\frac{p'}{\bar{p}} \qquad (93)$$

Their Eq. (21) is the first integral to the energy equation; linearization gives the quasi-static formula for q_{s+}',

$$q_{s+}' = \frac{m_g'}{\bar{m}}\left[1 + \frac{Q_r \epsilon_r}{c_p \bar{T}_s} - \frac{\bar{T}_f}{\bar{T}_s}\right] - \frac{\bar{T}_f'}{\bar{T}_s} + \frac{T_s'}{\bar{T}_s}$$

and after substitution from (93) for $T_f'/\bar{T}_s$,

$$q_{s+}' = \frac{c}{c_p} X_{\tau+}\, \tau_s' + \nu \mathcal{E}\,\frac{p'}{\bar{p}} \qquad (94)$$

with

$$\frac{c}{c_p} X_{\tau+} = 1 - \frac{E}{\mathcal{E}} - E\left\{\frac{\bar{T}_f}{\bar{T}_s} - 1 - \frac{Q_r \epsilon_r}{c_p \bar{T}_s}\right\} . \qquad (95)$$

The total mean rate of heat release is Q_r and ϵ_r is a reference concentration of one constituent; $\mathcal{E} = \bar{T}_s/\bar{T}_f(\nu+1+E_f/2R_o\bar{T}_f)$ and the pyrolysis law used to eliminate $m_g'/\bar{m}$ is (41) with $\tau_1 = n_s = 0$. Correspondence of some of the symbols is given in Table IV.

This Work	Reference 28
T_s	T_w
T_f	T_f
E_s	E_w
λ_p	K_s
λ_g	K
ξ_p	$-y^*$
λ	$-\lambda$
$\omega_p/4$	ω/Ω
A	A
P	$A\alpha$
α	α
$nP/E\alpha$	B

This Work	Reference 28
$\mathcal{E}(\bar{T}_s/\bar{T}_f)$	$\mathcal{E}$
$\nu = n$	$n/2$
H_p	$-L$
D	$-4b/\omega_p$
F	$4a/\omega_p$

TABLE IV

Correspondence of Symbols with Ref. 28.

Thus, (94) is exactly what is required in the matching condition (42); the solution for the solid phase is simply (35) with $\tau_1 = n_s = 0$. One finds after these substitutions,

$$\frac{m_s'/\bar{m}}{p'/\bar{p}} = \frac{\nu P}{(\lambda + \frac{A}{\lambda}) - X_{\tau+} + X_\tau} \qquad (96)$$

where

$$X_\tau = \left(\frac{c_p}{c} - 1\right)(E+1) - EH , \qquad (97)$$

$$P = \frac{c_p}{c}\,\frac{E}{\mathcal{E}} . \qquad (98)$$

To obtain correspondence with Ref. 28, $\nu = n^*$ and for $\omega \to 0$ $(\lambda \to 1)$,

$$1 + A - X_\tau + X_{\tau+} = P$$

and (96) becomes

$$\frac{m_s'/\bar{m}}{p'/\bar{p}} = \frac{nP}{(\lambda + \frac{A}{\lambda}) - (1+A) + P} \qquad (99)$$

The real part of this formula is

$$\frac{\mu}{\epsilon} = \frac{nPD}{D^2 + F^2} \qquad (100)$$

where

$$D = (\lambda_r - 1) + A\left(\frac{4\lambda_i}{\omega_p} - 1\right) + P \qquad (101a)$$

$$F = \lambda_i - \frac{4A}{\omega_p}(\lambda_r - 1) . \qquad (101b)$$

The equality of (100) and E times the Eq. (71) of Ref. 28 is easily shown.

Equation (99) has the form seen already several times, but it is especially important that the parameter P depends very much on properties of the gas phase and not merely on E. Thus, the difficulty of finding large values of μ/ϵ for reasonable values of the surface activation energy does not arise. Denison and Baum emphasize this with use of a quantity α,

$$\alpha = \frac{P}{A} = \frac{c_p}{c\mathcal{E}(1-\bar{\tau}_1)} . \qquad (102)$$

Referring again to the zeros of the denominator (Eq. (118)), the condition is $\omega_p = 4\sqrt{AP} = 4A\sqrt{\alpha}$, and, as quoted earlier, $\omega_p/4 \approx 8$ according to observations of peaks in μ/ϵ. For A = 10, this means $\sqrt{\alpha} = .8$ and $\alpha \approx 0.6$. Values of α around 0.6 seem to fit some experimental results[13], and can be estimated for reasonable values of the quantities required: suppose $T_f = 3000^\circ$K, $n = \frac{1}{2}$, $E_f = 30,000$ cal/mole ($R_o = 2$ cal/mole), and other values given in Table I; then $\alpha = 0.5$. Moreover, as shown in

*$\nu = n$ implies $T_1' \to 0$ for $\omega \to 0$ (Eq. (93)).

Figure 4,† the shape of the response function seems to be in reasonably good agreement with observations (see also Refs. 13, 27, and 43).

However, it would be surprising if the result (99) containing only two parameters should work for all real propellants. For example, no account has been taken of inhomogeneities, decomposition of the solid phase in a finite region, of pressure dependence of pyrolysis, or of the obvious differences between composite and double-base propellants.

Some interesting results relevant to the last question have recently been obtained by Marxman[43]. The computation is basically that of Denison and Baum, but with the addition of "surface-coupled" reactions. Arrhenius' law for pyrolysis, with pressure dependence, is still used. However, it is assumed that in the gas phase very near the burning surface (effectively in the region denoted by s+ here), two distinct contributions to energy release can be identified: an amount Q_H dependent upon the local gas phase conditions and an amount Q_D independent of the gas phase. The second is associated with solid-phase reactions, but it is supposed to have no effect in the s- region of the solid: unlike the analysis of Ref. 27, then, the familiar solution (35) ($\tau_1 = n_s = 0$) for the solid phase can be used. The result (94) for the gas phase is used* and the only change in the analysis is in the energy matching condition. When this is formed, the two terms $-(Q_H+Q_D)$ appear on the right hand side of (38) and the linearized form is

$$\frac{c_p}{c}\, q'_{s+} = q'_{s-} + \left(\frac{c_p}{c} - 1\right)\tau'_s + \left(\frac{c_r}{\quad} - 1 - H\right)\frac{m'_s}{\bar{m}} - (Q'_H + Q'_D) \qquad (103)$$

In accord with their meanings, Q_H and Q_D are represented as

$$Q_H = H_H m_s \left(\frac{p}{T_s}\right)^m e^{-E_H/R_o T_s} \qquad (104a)$$

$$Q_D = H_D m_s e^{-E_D/R_o T_s} . \qquad (104b)$$

Using the linearized forms of (104a, b) for Q'_H and Q'_D, and substituting (94) for q'_{s+}, (35) for q'_{s-}, one eventually obtains from (103)

$$\frac{m'_s/\bar{m}}{p'/\bar{p}} = \frac{\nu(P + \frac{m}{\nu} E\theta_H)}{\lambda + \frac{A}{\lambda} - X_{\tau+} + X_\tau - I(\theta_H+\theta_D) - \theta_s} \qquad (105)$$

where

$$\theta_s = \theta_H\left(\frac{E_H}{R_o\bar{T}_s} - m\right) + \theta_D \frac{E_D}{R_o\bar{T}_s} , \qquad (106)$$

$$\theta_H = \frac{\bar{Q}_H}{\bar{m}c\bar{T}_s} , \quad \theta_D = \frac{\bar{Q}_D}{\bar{m}c\bar{T}_s} . \qquad (107)$$

By combining previous definitions, and with $\bar{q}_{s+} = 1 + Q_r\epsilon_r/c_p\bar{T}_s - \bar{T}_f/\bar{T}_s$ from Denison and Baum's calculation, one can show that

$$X_\tau - X_{\tau+} = P - (A+1) + E(\theta_H + \theta_D)$$

so that (105) is

$$\frac{m'_s/\bar{m}}{p'/\bar{p}} = \frac{\nu(P + \frac{m}{\nu} E\theta_H)}{\lambda + \frac{A}{\lambda} - (1+A) + (P - \theta_s)} . \qquad (108)$$

To obtain the proper limit for $\omega \to 0$, one must require

$$n = \frac{\nu P + mE\theta_H}{P - \theta_s} = \frac{\nu\alpha + mE\theta_H/A}{\alpha - \theta_s/A} \qquad (109)$$

Hence, as one might have anticipated, the addition of chemical reactions near the burning surface but in the gas phase leads to a new formula for the parameter P characterizing the gas phase, but the form of the response function is unchanged. Note that $m\theta_H$ is the coefficient of $p'/\bar{p}$ in $Q'_H/\bar{m}c\bar{T}_s$, found from Eq. (104a),

$$\frac{Q'_H}{\bar{m}c\bar{T}_s} = \theta_H \frac{m'_s}{\bar{m}} + \theta_H\left(\frac{E_H}{R_o\bar{T}_s} - m\right)\frac{T'_s}{\bar{T}_s} + m\theta_H \frac{p'}{\bar{p}} \qquad (110)$$

Put another way, the same result would be obtained if $(Q'_H+Q'_D)$ were not included in the energy balance (103) but rather arise as part of q'_{s+} in the solution (94) to the gas phase.

Only a re-definition of one parameter is required to reduce Marxman's result to Denison and Baum's. Marxman works with α, and uses (instead of $P_M = P - \theta_s$)

$$\alpha_M = \alpha - \theta_s/A \qquad (111)$$

where α is Denison and Baum's α. This is useful only if one assumes that α is known. Certain features of the behavior of the response may then be examined as θ_s (or θ_H) is varied, i.e., for different surface-coupled reactions. This is, of course, an interesting and useful result, for the structure of the gas phase region undoubtedly changes among the various propellants. In particular, it is likely that composite and double-base propellants as classes will have very different surface-coupled reactions and hence θ_s. This subject is pursued further in the discussion of self-excited instabilities.

Friedly and Petersen[29] have carried out a calculation which differs from that of Denison and Baum only by the use of a different flame theory (Zel'dovitch's formulation). As a result, the coefficients in the formula for q'_{s+} differ in detail; the response function again has the form (99). It appears, however, judging by their Figures 3 and 7, for example, that they did not force the limiting behavior for $\omega \to 0$. As a result, they have too many parameters free to be specified, when in fact only (n, A, P) can be arbitrarily set; P, of course, will depend on other variables in the problem as Eq. (98) shows here.

All of the work discussed so far involves the assumption that purely solid phase reactions occur in a plane of infinitesimal thickness - maybe a good approximation, but maybe not, because not only is the surface rough, but there are reactions in the solid phase (decomposition) which do take place at temperatures lower than the surface temperature. The analysis of a decomposition region greatly complicates the calculations for the solid phase; the only treatment at the present time is given in Ref. 27. Decomposition, and the associated heat release, or absorption, affects mainly the temperature gradients, and the response

* Owing to the additional heat release near the surface, the mean temperature profile is changed and this affects the coefficient $X_{\tau+}$; however, it vanishes from the problem when the limiting condition ($\omega \to 0$) is applied.

† See page 24, before references.

* $\nu \neq n$ generally, so $T'_1 \neq 0$ for $\omega \to 0$.

function is subsequently rather strongly affected.

The gas phase is treated with the quasi-static assumption but with no further approximations* concerning the structure of the region between the solid surface and downstream of the flame. It is shown that the solution for the gas phase will lead generally to the form for q'_{g+} found by Denison and Baum, with P simply a parameter representing the sensitivity of the gas phase to pressure fluctuations. Hence the results obtained can be reduced to (99) which appears to be the simplest form of the response function, at the same time containing the fewest dominant features of the solid and gas phases.

As additional refinements are included, the number of parameters increases; so far, apart from ω_p, only P and A appear in (99). These three, of course, depend further on particular properties of the propellants (such as $\bar{T}_s$, E_s, T_i, etc.), but the point is to group these into the simplest combinations. In Ref. 27, there are, in addition, four associated with the decomposition region, two (besides A) for the burning surface with only P for the gas phase. The interpretation, but not the precise values, of these are known. One interesting result is that while the latent heat (H_p here) doesn't appear in (99), it does remain explicitly whe.. the surface reaction depends on pressure ($n_s \neq 0$).

Fortunately, it appears[27] that the qualitative behavior of the calculated response function is sufficiently sensitive to the various effects that the differences might be distinguished in experimental results. Available measurements and their interpretation have not yet progressed far enough to merit discussion at this time. Several points are worth noting, however. According to the calculations[27], if A and P are fixed, sensitivity of the pyrolysis to pressure ($n_s \neq 0$) depresses the response, to an extent which depends quite strongly on both the sign and magnitude of the surface latent heat (H_r); moreover, the response function is broadened in frequency. Inclusion of decomposition also tends to depress the response function; in particular, it acts rather like a damping effect with respect to the zeros of the denominator of the ratio $(m'/\bar{m})/(p'/\bar{p})$. That is, if decomposition is included, it may not be possible to find infinite values of (99) within reasonable ranges of A and P.

VI. Self-Excited or Intrinsic Instabilities

It has already been noted that both Green and Denison and Baum, among others, have attempted to identify the occurrence of infinite values of $(m'/\bar{m}_s)/(p'/\bar{p})$ with the conditions for oscillations in a rocket motor. If the response is indefinitely large, then an infinitesimally small pressure change (unavoidably present in a real chamber) causes a large fluctuation in the mass flux, which in turn reinforces the original pressure disturbance**. Such an event of course has nothing to do with oscillations in the chamber and in fact would occur (see below) at frequencies determined by the propellant. An inherent, or intrinsic, or self-excited instability of this sort may be possible - it has not been proven experimentally - but is almost certainly not the kind of instability present in rocket chambers. But it seems quite clear that the overall problem involves both strong coupling (expressed as a response function) of the burning solid to the gas phase, and the geometry of the chamber. This combination mainly determines the frequency of the motions, whether they be standing or traveling waves.

However, it is true that the propellant most strongly drives oscillations in the frequency range where the real part of the response function is largest, and this occurs rather close (in a sense shown below) to the infinite values[27]. As an aid to qualitative argument, then, it is indeed useful to locate the poles of the response function. It happens that this is very simply done for the form (99). The denominator vanishes if

$$\lambda(\lambda-1) - \lambda(A-P) - A = 0 \qquad (112)$$

which can be solved for λ to give

$$\lambda = \tfrac{1}{2}(A-P+1) \pm \tfrac{1}{2}[A-P+1)^2-4A]^{\frac{1}{2}} .$$

After using this for λ in (112), and with $\lambda(\lambda-1) = i\omega_p/4$, one finds

$$i\frac{\omega_p}{4} = -[A-\tfrac{1}{2}(A-P)(A+1-P)] \pm \tfrac{1}{2}(A-P)[(A+1-P)^2-4A]^{\frac{1}{2}} \qquad (113)$$

Now ω (i.e., ω_p) appeared originally as the frequency of harmonic time variations, $T' \sim e^{i\omega t}$, etc., so that if one treats ω_p as a complex quantity, $\omega_p = \omega_p^{(r)} + i\omega_p^{(i)}$, the real and imaginary parts of (113) are equal:

$$\frac{\omega_p^{(r)}}{4} = +\tfrac{1}{2}(A-P)[4A-(A+1-P)^2]^{\frac{1}{2}} \qquad (114)$$

$$\frac{\omega_p^{(i)}}{4} = A - \tfrac{1}{2}(A-P)(A+1-P) . \qquad (115)$$

For stable oscillations†, $\omega_p^{(i)} \geq 0$ and the last equation can be put in the form

$$(A+P) \geq (A-P)^2 \qquad (116)$$

or, since $P = A\alpha$,

$$(1+\alpha) \geq A(1-\alpha)^2 . \qquad (117)$$

Equality holds on the boundary between stable and unstable oscillations; (114) then gives

$$\omega_p^{(r)} = 4\sqrt{AP} = 4A\sqrt{\alpha} . \qquad (118)$$

This appears to be a very useful formula for estimating the location of the maximum in the response function. Note that the frequency at which the peak occurs increases with both the surface activation energy and the sensitivity of the gas phase. With (118), the real and imaginary parts of λ are $\lambda_r = A/(A-P)$; $\lambda_i = \omega_p/4(A-P)$.

Equation (117) with the equality sign is plotted as the limiting line in Figure 1 of Ref. 28. Marxman[43] has used the shift of this limit, for changes

* Except that the question of isentropic or non-isentropic behavior downstream of the flame was avoided, a restriction which can be relaxed (Ref. 49).

** In some earlier works, this process, presumably leading also to increases in the mean burning rate, was called "resonance" as opposed to "sonance," the occurrence of relatively small amplitude oscillations. This usage of the terms has fortunately disappeared.

† In fact, for stable transient motions generally, as one can see if $i\omega_p$ is treated as a Laplace transform variable[28,49p].

of α, in connection with observations of traveling waves to estimate qualitative differences between composite and double-base propellants. For his result (108), α is replaced by $\alpha_M = \alpha - \theta_s/A$. (117) is

$$(1+\alpha - \theta_s/A) = A(1-\alpha+\theta_b/A)^2 \quad . \qquad (119)$$

The limit line shown as A vs. $1/\alpha$ shifts drastically as θ_s is changed,* and in different directions for different signs of θ_s. The argument is then based on the observation that composite propellants probably involve "surface-coupled" reactions (i.e., θ_H and hence θ_s non-zero), whereas double-base propellants may not, or at least are likely to have small values of θ_H. Experimental evidence** supporting the theoretical predictions is given. This is indeed a striking use of the admittance functions to interpret measurements. Use of (119) related to the poles of the admittance function should be regarded as a qualitative indication of trends and not as support of the view that the oscillations are "self-excited."

Figure 4 shows the response function (99) for a fixed value of A and three values of P (or α), one of which meets the condition (117) for a pole. In all cases, there seems to be the abrupt change of phase at the pole (velocity changes from a "lead" to a "lag" with respect to pressure). If decomposition is included[27], the infinite value does not occur, and if the decomposition region releases heat, the real part of the response is always positive.

VII. Isentropic or Non-Isentropic?

Several years ago, an interesting question was raised by Summerfield[44, 45] regarding the behavior of the coupled burning and pressure oscillations, particularly at low frequencies. Although the oscillations in the burnt gases may apparently, to a good approximation, be regarded as isentropic, if they are small amplitude waves, the assumption is less credible in the region near the flame. The boundary condition required for analysis of the chamber problem is the normal velocity component produced by a small pressure change. But this depends also on the density (or temperature) changes associated with the pressure flucuation, as shown by Eqs. (1) and (2). The second term in the bracket of (2) is unity only if the process is isentropic at the edge of the burning region, which must be considered thin so far as the entire chamber is concerned. Moreover, of course, the "edge" must constitute a proper outer boundary to solution of the unsteady combustion problem: for example, it is convenient to retain the assumption that the pressure is uniform but varying in time.

The point raised by Summerfield concerns the validity of the common assumption that at the edge of the boundary the fluctuations are isentropic so that $\gamma(\rho'/\bar{\rho})/(p'/\bar{p}) = 1$. Certainly this is not the case within the flame, so that successive elements of the flow passing through have different values of entropy. The possibility exists that these entropy variations persist to the downstream edge of the flame region and are therefore carried with the flow. In the absence of dissipative processes, the entropy satisfies

$$\rho \frac{\partial s}{\partial t} + \rho u \frac{\partial s}{\partial x} = 0 \qquad (120)$$

so that entropy fluctuations behave according to

$$\frac{\partial s'}{\partial t} + \bar{u} \frac{\partial s'}{\partial x} = 0 \quad .$$

If s'_o is the fluctuation at $x = \delta$ and variations are harmonic, then downstream of the plane $x = \delta$,

$$s'(x,t) = s'_o e^{i\left(\omega t + \frac{(x-\delta)}{\omega \bar{u}}\right)} \quad . \qquad (121)$$

The real part, say, is

$$s' = s'_o \cos\left(\omega t - \frac{\omega(x-\delta)}{\bar{u}}\right) \quad ,$$

and as a function of x there is an entropy wave, of wavelength $2\pi\bar{u}/\omega$, which is much smaller than the acoustic wavelength $2\pi\bar{a}/\omega$.

In fact, of course, there are dissipative actions tending to smooth out entropy variations so that the fluctuations s' decay as they propagate away from the flame. If s' is negligible at some plane $x = x_f$, and the region $0 < x < x_f$ is "thin," then the admittance function may be computed with the isentropic condition and the result used as a boundary condition on the waves in the chamber. All applications of the admittance function so far have been based on this assumption. The damping length is in fact quite large[47] if only ordinary thermal conduction is accounted for; the influence of viscous stress is even less important.

Thus, it appears that, apart from the certain influence of turbulence, entropy waves, if they are present, are not significantly attenuated near the surface. The problem comes down to determining the conditions under which such waves might be observed; one is then forced to treat the interaction of the pressure changes and the flame more precisely than in the works discussed so far. In particular, the transition region between the flame and the outer pressure field is especially important. Arguments have been advanced[44-46] that the existence of such waves is more likely in the low frequency range although observation of them has thus far been unsuccessful.

If the pressure doesn't change much during the time required for an element of gas to pass through the combustion region, then the temperature tends to a constant value. But since the entropy for a perfect gas is

$$s = s_r + c_p \ln \frac{T}{\bar{T}_f} - R \ln \frac{p}{\bar{p}}$$

where s_r is the value at $T = \bar{T}_f$, $p = \bar{p}$, then the fluctuation is

$$s' = c_p \frac{T'}{\bar{T}_f} - R \frac{p'}{\bar{p}} \quad . \qquad (122)$$

Hence, if the flame is truly isothermal even in the presence of small pressure changes, s' is nonzero and so far as the motions downstream of the flame are concerned, (122) gives s'_o in (121):

* An essential assumption in the argument is that α, expressing the sensitivity of the outer flame region, is the same for the propellants compared.

** A similar shift can be found from the analysis of Ref. 27, except that A rather than P is altered. One can show that in the limit of small Q and ℓ, one again has (108), except $\theta_s = \theta_H = 0$ and A is replaced by $A - Q\ell^2/2$; ℓ is the dimensionless thickness of the decomposition region and Q is the normalized heat release.

$$s'_o = -R_o \frac{p'}{\bar{p}} \quad \text{(isothermal)} \tag{123}$$

The other extreme is normally assumed, namely that the downstream edge of the flame matches the isentropic acoustic fluctuations: $T'/\bar{T} = (R/c_p)p'/\bar{p}$ and $s'_o = 0$. A calculation exhibiting intermediate values, using the work of Ref. 1 as a basis, has been given in Ref. 47. Very little change in the response function was found except at low frequencies, and at higher frequencies where the analysis is not valid.

A very much simpler calculation appears in Ref. 46. The solution for the solid phase and the energy matching condition are the same as usual; the pyrolysis law is simply $m'_s/\bar{m} = E\tau'_s$. A quasi-static formula for q'_{s+} is found not by considering the gas phase but by perturbing the steady state form of the energy matching condition (38). One finds

$$\frac{c_p}{c} q'_{s+} = \frac{n}{E}(A+1+X_\tau)\frac{p'}{\bar{p}} \tag{124}$$

where X_τ is given by (44) ($\tau_1 = 0$). Substitution of (124) and (B-8) for q'_{s-} into (43) gives

$$\frac{m'_s/\bar{m}}{n(p'/\bar{p})} = \frac{A+1+X_\tau}{\lambda + \frac{A}{\lambda} + X_\tau} , \tag{125}$$

which again has the form (99). However, since the gas phase has effectively not been considered, no parameter associated with it appears in (125).

Now if one simply integrates the steady-state energy equation (54) from the solid surface to some position downstream of the flame where $\partial T/\partial x = 0$, the result is

$$-mc_p T_f = \lambda_g \left(\frac{\partial T}{\partial x}\right)_{s+} - mc_p T_s + mH_f \tag{126}$$

with H_f the total heat release in the gas phase. The steady-state and perturbed (i.e., quasi-static linearization) forms of (126) are

$$\frac{\bar{T}_f}{\bar{T}_s} = 1 - \bar{q}_{s+} - \frac{H_f}{c_p \bar{T}_s} \tag{127}$$

$$\frac{T'_f}{\bar{T}_s} = \tau'_f = -q'_{s+} + \tau'_s\left[1+E\left(1 - \frac{\bar{T}_f}{\bar{T}_s} - \frac{H_f}{c_p \bar{T}_s}\right)\right] \tag{128}$$

The flame temperature T_f and $H_f/c_p\bar{T}_s$ can be eliminated from (128) by use of (127), with $\bar{q}_{s+}$ given by (47); and with q'_{s+} from (124), the fluctuation of temperature at the outer edge of the flame is

$$\frac{\tau'_f}{p'/\bar{p}} = \frac{cn}{c_p E}(A+1+X_\tau)\left[\frac{A+1+X_\tau}{\lambda + \frac{A}{\lambda} + X_\tau} - 1\right] . \tag{129}$$

For low frequencies, $\lambda \to 1 + \omega_p^2/16 + i\omega_p/8$ and to first order in ω_p, (129) gives

$$\frac{\tau'_f}{p'/\bar{p}} = i\frac{\omega_p}{8}\frac{cn}{c_p E}(A-1) . \tag{130}$$

The temperature T'_f is treated as the boundary value to be used in the admittance function (2). Thus, in general,

$$\gamma\left(\frac{\rho'/\bar{\rho}}{p'/\bar{p}}\right)_f = \gamma - \gamma\frac{T'_f/\bar{T}_f}{p'/\bar{p}} = \gamma - \gamma\frac{\tau'_f}{p'/\bar{p}}\left(\frac{\bar{T}_s}{\bar{T}_f}\right)$$

which is unity if $T'_f/\bar{T}_f$ corresponds to isentropic changes, and γ if the isothermal limit is used. But if (130) is used, an intermediate, non-zero result is obtained. The corresponding entropy fluctuations are

$$\frac{s'_o}{p'/\bar{p}} = \begin{cases} 0 & \text{isentropic limit} \\ -R_o & \text{isothermal} \\ -R_o + i\frac{\omega_p}{8}\frac{cn\bar{T}_s(A-1)}{c_p E \bar{T}_f} & \text{low frequency (Eq. 130)} \end{cases} \tag{131}$$

According to this argument, then, one might expect to find entropy waves, observable as temperature waves, having a phase less than 180° (the isothermal limit) with respect to pressure fluctuations. The low frequency limit can be written as

$$s'_o = \sqrt{R_o^2 + \left(\frac{\omega_p}{8}\right)^2\left(\frac{cn\bar{T}_s}{c_p E \bar{T}_f}\right)^2 (A-1)^2}\; e^{i\phi}\frac{p'}{\bar{p}}$$

where

$$\tan\phi = \frac{\omega_p\, cn(A-1)}{-R_o\, c_p E}$$

and the decrease from 180° is proportional to the frequency.

The preceding calculation is interesting partly because of its simplicity, leading nevertheless to the form (125) which is now so familiar. It is of course restricted at best to the very low frequency range, and has the unfavorable feature that it does not depend on properties of the gas phase; the reason for this is clear from the argument leading to (125). A recent paper[48] contains a calculation which, with different assumptions, yields a result only slightly different. One finds that Eqs. (6) and (7) of Ref. 48 give, in the notation used here:

$$q'_{s+} = \frac{c}{c_p} X_{\tau+}\tau'_s + \frac{c}{c_p} X_{p+}\frac{p'}{\bar{p}} \tag{132}$$

with

$$X_{\tau+} = (1-\bar{\tau}_i)\left[2n\left(1 - \frac{H}{1-\bar{\tau}_i} + \frac{c_p/c - 1}{1-\bar{\tau}_i}\right) + \frac{n}{m}\right]$$

$$X_{p+} = m\left(\frac{H}{1-\bar{\tau}_i} - 1 - \frac{c_p/c - 1}{1-\bar{\tau}_i}\right) + \frac{c_p}{c} - 1 .$$

It may be noted that m, H of Ref. 48 are A, $H/(1-\bar{\tau}_i)$ here. The corresponding formula for the response is (125), but with

$$X_\tau = 2E\left(\frac{c_p}{c} - 1 - H\right) . \tag{133}$$

The fluctuation of "flame temperature" is the same as (129), with (133) used for X_τ. A non-linear calculation and a few experimental measurements are also reported in Ref. 48; the entropy waves have yet to be observed.

This interesting aspect of the response function remains unsettled; it appears that it may not be relevant to the frequency ranges characteristic of rocket motors. However, in order to treat the question properly, one must be concerned, much more than in the past, with certain details of combustion in the gas phase. The behavior at higher frequencies may subsequently be better understood. The crux of the matter is the way in which the flame temperature

responds to pressure in the low frequency limit, and what temperature fluctuation exists at the chamber side of the flame. In this connection, it should be remarked, as implied, for example in Eq. (109), that many of the computations discussed here will accommodate a non-zero value of T_f' for $\omega \to 0$. For example, Marxman's calculation includes this, and those of Refs. 27 and 28 are easily modified to do so.

VIII. Concluding Remarks

The eventual purpose of calculating the admittance or response function must be to motivate interpretation of experimental results and thereby to classify propellants according to a small number of parameters. Quite obviously the problem is too complicated to be analyzed quantitatively in all respects. To the present time, very little effort has been expended on the comparison of computations and measurements; this is due partly to the relatively unsystematic nature of existing measurements, and partly to difficulties of using available calculations.

It seems, however, that the situation is changing quite rapidly in a favorable way. The response function can be inferred from both T-burner and L*-burner measurements, so that a rather broad

Reference		$\frac{m'/\bar{m}}{n(p'/\bar{p})}$	Equation Number	Meaning of
Green	31	$E\frac{(\bar{\tau}_f-1)}{n\bar{m}c\bar{r}}\frac{F'}{(p'/\bar{p})}$ $\lambda+\frac{A}{\lambda}-(1+A)+P$	63	F' : Eq. (58) P : Eq. (64)$_{T_i}$ $A = E\left(1-\frac{\bar{T}_i}{\bar{T}_s}\right)$
Akiba and Tanno	9	$\frac{P}{\lambda+\frac{A}{\lambda}-(1+A)+P}$	68	$P = \frac{Ek\bar{p}^{n+1}}{\bar{m}c}(\bar{\tau}_f-1)$
Hart, McClure, et al.	1 30	$\frac{P}{\lambda+\frac{A}{\lambda}-(1+A)+P}$	83	$P = \bar{\tau}_i E/j$
Hart, Farrell, and Cantrell	40	$\frac{P+\frac{n_s}{n}(\lambda-1)}{\lambda+\frac{A}{\lambda}-(1+A)+P}$	91	$P = \bar{\tau}_i E/j$ $\bar{\tau}_i = T_i/\bar{T}_s$
Denison and Baum	28	$\frac{P}{\lambda+\frac{A}{\lambda}-(1+A)+P}$	99	$P = A\alpha$ $\alpha = \frac{c_p/c}{(1-\bar{\tau}_i)e}$ $e = \frac{\bar{T}_s}{\bar{T}_f}\left(n+1+\frac{E_f}{2R_o\bar{T}_f}\right)$
Marxman	43	$\frac{(P-\theta_s)}{\lambda+\frac{A}{\lambda}-(1+A)+(P-\theta_s)}$	108	$P = A\alpha$ θ_s : Eq. (106)
Waesche and Summerfield Kier, et al.	46 48	$\frac{1+A+X_\tau}{\lambda+\frac{A}{\lambda}+X_\tau}$	125	X_τ : Eq. 44 (Ref. 46)($\tau_1=0$) or Eq. 133 (Ref. 48)
Culick	27	$\frac{P_1}{X_{\tau-}-X_{\tau-0}+\frac{P_1}{1-n_s/n}}+\frac{n_s}{n}$ (This reduces to Eq. (99) for no decomposition and $n_s = 0$.)	-	$P_1 = P-\frac{E}{n}(X_p+X_{p-})$ X_p : Eq. (43) n_s : Eq. (40) $X_{\tau-}, X_{p-}$: Eq. (36)

TABLE V

Summary of Response Functions with Quasi-Static Approximation for the Gas Phase.

frequency range can be covered. Indeed (at least for some propellants), overlapping data[13] in the region of the peak in the response have been obtained from both kinds of experiment: the L*-burner can be used for lower frequencies (ω_p) through the peak, and the T-burner provides results for higher frequencies down through the peak. The response cannot be measured directly, and in each case a rather careful analysis of the apparatus itself is required; the T-burner presents greater and presently unresolved difficulties in this respect. Other attempts to measure the admittance function, such as an impedance tube, have been considerably less successful.

Given an increasing amount of data, one must now choose among the various calculations. It seems quite clear that the starting point is the two-parameter form; actually, there are three parameters (A, P, ω_p), but ω_p will always appear as the basic frequency variable. There are, of course, a large number of other properties which must be known - surface temperature, specific heats, flame temperature, for example - but these are either of less importance because they don't vary much or they appear in A, P, and ω_p. It should be noted that ω_p contains a very strong dependence on mean burning rate ($\omega_p \sim \omega/r^2$) and hence on mean pressure. Thus, one might expect that the real frequency ω for maximum of the response, which, according to Eq. (118) occurs roughly at $\omega_p = 4\sqrt{AP}$, will vary as $\bar{p}^{2n}$ if AP is constant. This offers perhaps the simplest test of this form of the response function. Existing data do not seem to define the peak well enough to check the shift with mean pressure.

One interesting conclusion of this discussion is that a surprising number of existing calculations do in fact reduce to the two-parameter form, although P in particular may have different meanings; these are summarized in Table V.

The two basic parameters are therefore $A = E(1-T_i/\bar{T}_s)$, essentially the surface activation energy, and P, which is related (usually) to sensitivity of the gas phase to pressure changes. Evidently, the logical first step is to determine how well measurements can be correlated with these parameters only. It appears[13] that for reasonable values of A and P, fairly good agreement with some data can be obtained. If, as more data are examined, A and P are found to be inadequate, then further complications must be considered. Thus, for example, Marxman finds a split interpretation of P, part for the flame far from the surface and part for surface-coupled reactions. In Ref. 27, additional groups associated with decomposition and pressure sensitivity of solid phase reactions and pyrolysis are introduced. Certainly more detailed considerations of the gas phase will lead to a more precise definition of P and perhaps further dimensionless groups.

So far as the linear problem is concerned, the general scheme suggested here seems to offer a convenient means for comparing calculations of the response function. The procedure is simple: treat the solid and gas phases separately, and match the results for heat transfer fluctuations by using the energy matching condition, Eq. (42). This will lead to an equation involving T_s', p', and m_s'. One then uses a pyrolysis law to eliminate m_s', and the equation can be solved for the surface temperature fluctuation, or the ratio T_s'/p'. The pyrolysis law is then used again to give m_s'. If the analysis does not involve the approximation of quasi-static behavior in the gas phase, then further work is required to find m', the fluctuation of mass flux at the downstream edge of the flame region.

All of the computations and results discussed here are for the response of the burning process to a steady sinusoidal pressure fluctuation. Other pressure disturbances can be handled simply by treating $i\omega_p/4 = s$, a Laplace transform variable, as, for example, in Ref. 28. It is perhaps worthwhile to point out, however, that the calculation presented there can be greatly shortened[49]. If $F(s)$ is the Laplace transform of the pressure, then the response is given by the inverse transform of $m'/\bar{m}(s)$; for the simplest form (99), one has

$$\frac{1}{n}\frac{m_s'}{\bar{m}}(t) = \frac{P}{2\pi i}\int_{\sigma-i\infty}^{\sigma+i\infty} \frac{\lambda F(s) e^{s\tau} ds}{\lambda^2 + \lambda(P-A-1) + A}$$

where $\tau = (4c\rho_p F^2/\lambda_p)t$ is the normalized time. The roots s_1, s_2 of the denominator treated as a function of s are given by (113), and since $\lambda = (1+\sqrt{1+s})/2$, the above formula can be written

$$\frac{1}{n}\frac{m_s'}{\bar{m}}(t) = \frac{P}{\pi i}\int_{\sigma-i\infty}^{\sigma+i\infty} \frac{(1+\sqrt{1+s})F(s)e^{s\tau} ds}{(\sqrt{1+s}-\sqrt{1+s_1})(\sqrt{1+s}-\sqrt{1+s_2})}.$$

For the functions $F(s)$ normally of interest (step functions, damped sinusoids, etc.), the integrand can easily be written as a partial fraction expansion and the inverse transforms found in standard tables. Reference 49, for example, gives the important result for a damped sinusoidal pressure disturbance.

It is clear that much remains to be done before measurements will be satisfactorily correlated, and before the various parameters are related even in a gross way to the composition of propellants. At the same time, there are several important pieces of the problem which have not been satisfactorily analyzed: the differences between double-base and composite propellants; the response of a propellant with metallic particles; the question of entropy wave generation, which is closely related to a more thorough study of the outer flame region; velocity coupling and other non-linear problems; and extension of the results to frequencies outside the "quasi-static" range for the gas phase.

Appendix A

Consider a burning surface placed at $x = 0$ with the burnt gases moving at speed $\bar{u}$ to the right as in the sketch. To examine the connection between the admittance function and the attenuation of small amplitude waves in the burnt gases, the combustion region is collapsed to a plane and the oscillatory motion of the surface is ignored. It there are no chemical reactions in the gases, and the mean flow properties are uniform, the acoustics equations for one-dimensional velocity and pressure fluctuations are:*

$$\frac{\partial u'}{\partial t} + \bar{u}\frac{\partial u'}{\partial x} + \frac{1}{\bar{\rho}}\frac{\partial p'}{\partial x} = 0 \qquad (A1)$$

$$\frac{\partial p'}{\partial t} + \bar{u}\frac{\partial p'}{\partial x} + \bar{\rho}\bar{a}^2\frac{\partial u'}{\partial x} = 0 \qquad (A2)$$

* These may be found, for example, as special cases of Eqs. (1) and (2) of Ref. 3 and in many other places.

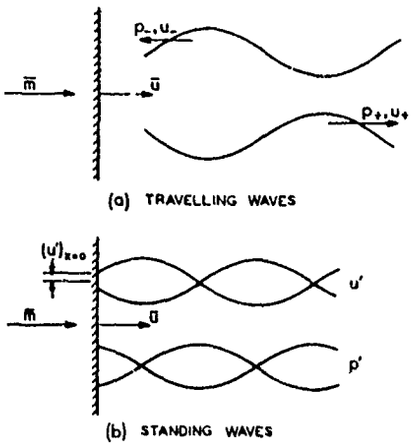

Figure 5. Burning Surface in Presence of Waves.

For traveling waves, part (a) of the sketch, both u' and p' have the form $\exp(i\omega t \mp k_{\pm}x)$ where + stands for a wave traveling to the right and - for a wave traveling to the left; superposition of both waves gives

$$u' = u_+ e^{i(\omega t - k_+ x)} + u_- e^{i(\omega t + k_- x)} \qquad (A3)$$

$$p' = p_+ e^{i(\omega t - k_+ x)} + p_- e^{i(\omega t + k_- x)} \qquad (A4)$$

Substitution of the + and - waves separately into (A1) and (A2) leads to the relations

$$k_+ = \frac{\omega/\bar{a}}{1+\bar{M}} \quad , \quad k_- = \frac{\omega/\bar{a}}{1-\bar{M}} \qquad (A5)$$

$$u_+ = \frac{p_+}{\bar{\rho}\,\bar{a}} \quad , \quad u_- = \frac{-p_-}{\bar{\rho}\,\bar{a}} \qquad (A6)$$

Hence, at $x = 0$, the propellant surface, after use of (A3), (A4), and (A6), one finds

$$A_b = \left(\frac{u'\sqrt{\bar{a}}}{p'/\sqrt{\bar{\rho}}}\right)_{x=0} = \frac{p_+ - p_-}{p_+ + p_-}$$

which can be solved for p_+:

$$p_+ = \frac{1+A_b}{1-A_b}\, p_- \; . \qquad (A7)$$

This gives the amplitude and phase of the reflected pressure wave with respect to the incident pressure wave; in particular, the amplitude is increased to $|1+A_b|/|1-A_b|$ of the original value.

Now for standing waves, part (b) of the sketch, in which the envelope of the oscillation is shown by by so. d line, the boundary condition on the gradient of the pressure field is set in accordance with (A1),

$$\left(\frac{\partial p}{\partial x}\right)_{x=0} = -\bar{\rho}\left(i\omega u' + \bar{u}\,\frac{\partial u'}{\partial x}\right)_{x=0} \qquad (A8)$$

for harmonic oscillations. In the absence of mean flow and for a rigid wall, the right hand side vanishes at the boundary. With burning, the response of the surface produces a non-zero velocity fluctuation, of the order of the mean flow Mach number. The second term in (A8) already has a factor $\bar{u} = \bar{M}\bar{a}$, so that to first order, $\partial u'/\partial x$ must be evaluated from Eq. (A2) with $\bar{u} = 0$: $\partial u'/\partial x \approx -i\omega p'/\bar{\rho}\,\bar{a}^2$. With this approximation, and after using the definition of the admittance function to replace u', (A8) is

$$\left(\frac{1}{p'}\,\frac{\partial p'}{\partial x}\right)_{x=0} = -i\,\frac{\omega}{\bar{a}}\,(A_b - \bar{M}). \qquad (A9)$$

Equation (A9) contains an indication that the admittance function is not the only consideration for the stability of standing waves. It is not obvious from these remarks (a more complete discussion appears in Ref. 3), but the $\bar{M}$ in (A9) can eventually be identified with convection of wave energy into the gas phase. There is an equal contribution arising from interaction between waves and the mean flow within the chamber. So far as the stability of waves in a chamber is concerned, the burning surface is characterized by the admittance function reduced by a factor depending on the mean flow Mach number normal to the surface[3].

The equivalence of (A9) with the representation of a standing wave in terms of traveling waves is readily established. From (A4) one has at $x = 0$

$$\left(\frac{1}{p'}\,\frac{\partial p'}{\partial x}\right)_{x=0} = i\,\frac{-k_+ p_+ + k_- p_-}{p_+ + p_-}$$

and p_- may be eliminated by use of (A7) to give

$$\left(\frac{1}{p'}\,\frac{\partial p'}{\partial x}\right)_{x=0} = \frac{i}{2}\left[-k_+(1+A_b) + k_-(1-A_b)\right]$$

$$= \frac{i}{2}\,\frac{\omega}{\bar{a}}\left[-\frac{1+A_b}{1+\bar{M}} + \frac{1-A_b}{1-\bar{M}}\right] .$$

To first order in $\bar{M}$, $(1\pm\bar{M})^{-1} = 1 \mp \bar{M}$ and the last equation is exactly (A9).

Appendix B

In the inertial coordinate system, the equation for temperature fluctuations in the solid phase is Eq. (29), with solution $\tau' = C\exp(\lambda\xi_p)$; or, since C is the fluctuation at the origin (i. e., the mean position of the surface)

$$\tau' = \tau'_o\, e^{\lambda \xi_p} \; . \qquad (B1)$$

Thus, the oscillatory heat transfer at the mean position is

$$q'_{o-} = \lambda \tau'_o \; . \qquad (B2)$$

It is q'_{s-}, the heat transfer at the burning surface itself ($x = x_s$), that is required. In the usual manner of treating linearized boundary conditions, both the temperature and temperature gradient can be expanded about the origin to give

$$T'_s \approx T'_o + x_s \left(\frac{d\bar{T}}{dx}\right)_{o-} \qquad (B3)$$

$$\left(\frac{\partial T'}{\partial x}\right)_{s-} \approx \left(\frac{\partial T'}{\partial x}\right)_o + x_s \left(\frac{d^2\bar{T}}{dx^2}\right)_{o-} \qquad (B4)$$

where the derivatives of $\bar{T}$ are found from the average temperature field in the solid.

With dimensionless variables, (B3) and (B4) are

$$\tau'_s = \tau'_o + \xi_{ps}\left(\frac{d\bar{\tau}}{d\xi_p}\right)_{o-} \qquad (B5)$$

$$q'_{s-} = q'_{o-} + \xi_{ps}\left(\frac{d^2\bar{\tau}}{d\xi_p^2}\right)_{o-} . \qquad (B6)$$

According to (37), since $\dot{x}_s = i\omega x_s$, it follows that

$$\xi_{ps} = -\frac{1}{i\omega_p/4}\frac{m'_s}{\bar{m}} = -\frac{1}{\lambda(\lambda-1)}\frac{m'_s}{\bar{m}} \qquad (B7)$$

where (31) has been used. The last three equations can be combined with (B2) and $(d\bar{\tau}/d\xi_p)_{o-} = (d^2\bar{\tau}/d\xi_p^2)_{o-} = 1-\bar{\tau}_i$ to give

$$q'_{s-} = \lambda\tau'_s + \frac{(1-\bar{\tau}_i)}{\lambda}\frac{m'_s}{\bar{m}} . \qquad (B8)$$

Note that the second term is associated with the motion of the surface. In particular, for the Arrhenius law giving (41), (B8) yields

$$q'_{s-} = \left(\lambda + \frac{A}{\lambda}e^{-i\omega\tau_1}\right)\tau'_s + \frac{n_s}{\lambda}e^{-i\omega\tau_2}\frac{p'}{\bar{p}} \qquad (B9)$$

which is used as Eq. (35) in the main text.

Now in the case that the coordinate system attached to the burning surface is used, the coefficient $\bar{m}c$ in (25) must be written as $mc = (\bar{m}+m'_s)c$, since the entire solid is fluctuating. The perturbed form, with $\dot{Q}_d = 0$, becomes

$$\frac{d^2\tau'}{d\xi_p^2} - \frac{d\tau'}{d\xi_p} - i\frac{\omega_p}{4}\tau' = \frac{m'_s}{\bar{m}}\frac{d\bar{\tau}}{d\xi_p} = (1-\bar{\tau}_i)e^{\xi_p}\frac{m'_s}{\bar{m}} \qquad (B10)$$

The solution to (B10) is the sum of the homogeneous solution $C\exp(\lambda\xi_p)$ and a particular solution:

$$\tau' = Ce^{\lambda\xi_p} - \frac{4}{i\omega_p}(1-\bar{\tau}_i)e^{\xi_p}\frac{m'_s}{\bar{m}} . \qquad (B11)$$

Since the origin of the coordinate system is now at the burning surface, $\tau' = \tau'_s$ at $\xi_p = 0$ and

$$C = \tau'_s + \frac{(1-\bar{\tau}_i)}{\lambda(\lambda-1)}\frac{m'_s}{\bar{m}} .$$

The first derivative of (B11), evaluated at $\xi_p = 0$, gives q'_{s-},

$$q'_{s-} = \lambda\tau'_s + \frac{(1-\bar{\tau}_i)}{\lambda}\frac{m'_s}{\bar{m}}$$

in agreement with (B8).

Partial List of Symbols

Some symbols having commonly accepted meanings or used but briefly are not included.

A	$A = E(1-\bar{\tau}_i)$
A_b	admittance function, Eq. (1)
c, c_p	specific heats of solid and gas
E_s	activation energy for surface reaction
E	$E = E_s/R\bar{T}_s$
H_p	latent heat for surface reaction; $H_p > 0$ for exothermic surface reaction
H	$H = H_p/c\bar{T}_s$
$\bar{m}$	average mass flux
m'_s	fluctuation of mass flux at the surface
n	index in the linear burning rate law, $r = ap^n$
n_s	index in the surface pyrolysis law, Eq. (40)
P	sensitivity of gas phase to pressure changes
$\dot{Q}_d$	average heat release (per unit volume) in solid
$\dot{Q}$	heat release in gas phase
$q'_{o\pm}$	fluctuations of heat transfer at the average position of the surface (x=0)
$q'_{s\pm}$	fluctuations of heat release at the burning surface
r	linear burning rate
R_o	universal gas constant
T_i	initial temperature of propellant ($x \to -\infty$)
T_s	temperature of burning surface
T_f	flame temperature
$\bar{T}_c$	average chamber temperature ($x \to +\infty$)
$x_s, \dot{x}_s$	surface displacement, velocity
$X_{\tau-}, X_\tau$	functions defined in Eqs. (36) and (43)
X_{p-}, X_p	functions defined in Eqs. (36) and (43)
α	Equation (102)
ϵ	stands for $p'/\bar{p}$
λ	Equations (31)-(34)
λ_p, λ_g	thermal conductivities of solid and gas
μ	stands for $(m'_s/\bar{m})_r$
ρ_p, ρ	density of solid propellant and gas phase
ρ_c	average density in chamber
τ	normalized temperature or a time lag in §II.
ω_p, ω_g	dimensionless frequency parameters for the solid and gas phases; Eqs. (30) and (55)
ω	real angular frequency
$\bar{(\ )}$	mean value
$(\ )'$	fluctuating value
$(\ )_s$	evaluated at the solid-gas interface
$(\ )_{s\pm}$	evaluated on the gas (+) or solid (-) side
$(\ )_{o\pm}$	evaluated on the gas or solid side of the mean position of the burning surface
$(\ )_r$	real part
$(\ )_i$	imaginary part

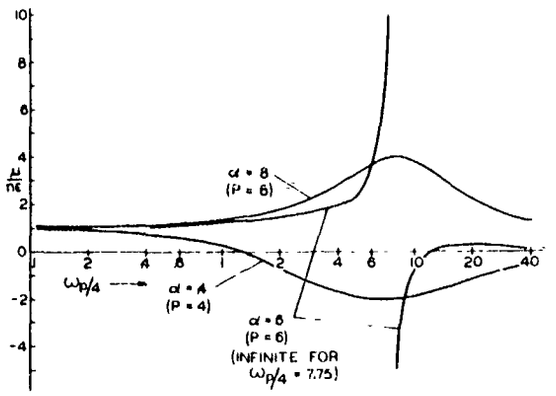

Figure 4. Real Part of $\frac{(m_s'/\bar{m})}{n(p'/\bar{p})}$ According to Equation (99) with A = 10. Case for α = .4 Is Intrinsically Unstable According to Equation (117).

References

1. Hart, W. R. and McClure, F. T., "Combustion Instability: Acoustic Interaction with a Burning Propellant Surface," J. Chem. Phys. 30 (Sept. 1959), pp. 1501-1514.

2. McClure, F. T., Hart, R. W., and Bird, J. F., "Acoustic Resonance in Solid Propellant Rockets," J. Appl. Phys. 31 (Apr. 1960), pp. 884-896.

3. Culick, F. E. C., "Acoustic Oscillations in Solid Propellant Rocket Chambers," Astronautica Acta 12 (Mar.-Apr. 1966), pp. 113-126.

4. Cantrell, R. H. and Hart, R. W., "Interaction Between Sound and Flow in Acoustic Cavities: Mass, Momentum, and Energy Transfer," J. Acoust. Soc. Amer. 36 (April 1966), pp. 697-706.

5. Horton, M. D., "One-Dimensional Solid Propellant Oscillatory Burner," ARS J. 31 (Nov. 1961), pp. 1596-1597 (also, unpublished Ph. D. Thesis, University of Utah, May 1961).

6. Horton, M. D., "Acoustic Admittance of a Burning Solid Propellant Surface," ARS J. 32 (April 1962), pp. 644-645.

7. Horton, M. D. and Price, E. W., "Dynamic Characteristics of Solid Propellant Combustion," in Ninth Symposium (International) on Combustion, Academic Press (1963), pp. pp. 303-310.

8. Horton, M. D. and Rice, D. W., "The Effect of Compositional Variables upon Oscillatory Combustion of Solid Rocket Propellants," Combustion and Flame 8 (March 1964), pp. 21-28.

9. Akiba, R. and Tanno, M., "Low Frequency Instability in Solid Propellant Rocket Motors," in Proceedings of the First Symposium (International) on Rockets and Astronautics (Tokyo, 1959), pp. 74-82.

10. Coates, R. L., Cohen, N. S., and Harvill, L. P., "An Interpretation of L* Combustion Instability in Terms of Acoustic Instability Theory," to be published in AIAA Journal, May 1967.

11. Sehgal, R. and Strand, L., "A Theory of Low Frequency Combustion Instability in Solid Rocket Motors," AIAA J. 2 (April 1964), pp. 696-702.

12. Beckstead, M. W., Ryan, N. W., and Baer, A. D., "Non-Acoustic Instability of Composite Propellant Combustion," AIAA J. 4 (Sept. 1966), pp. 1622-1628.

13. Beckstead, M. W., "Low Frequency Instability: A Comparison of Theory and Experiment," presented at Western States Section of the Combustion Institute (Paper 67-13), Univ. of Calif. at San Diego, April 24, 25 (1967).

14. Cheng, Sin-I, "Unstable Combustion in Solid-Propellant Rocket Motors," in Eighth Symposium (International) on Combustion, Williams and Wilkins (1962), pp. 81-96.

15. Geckler, R. D., "Unsolved Problems in Solid Propellant Combustion," in Fifth Symposium (International) on Combustion, Reinhold, New York (1955), pp. 29-40.

16. Schultz, R., Green, L., Jr., and Penner, S., "Studies of the Decomposition Mechanism, Erosive Burning, Sonance and Resonance for Solid Composite Propellants," Third AGARD Colloquium on Combustion and Propulsion, Pergamon Press (1958), pp. 367-420.

17. Grad, H., "Resonance Burning in Rocket Motors," Commun. in Pure Appl. Math. 2 (March 1949), pp. 79-102.

18. Cheng, Sin-I, "High Frequency Combustion Instability in Solid Propellant Rockets," Jet Propulsion (1954), Part I, pp. 27-32, Part II, pp. 102-109.

19. Cheng, Sin-I, "On 'Unstable Burning of Solid Propellants'," Jet Propulsion 25 (Jan. 1955), pp. 79-80.

20. Cheng, Sin-I, "Combustion Instability in Solid Rockets Using Propellants with Suspended Metallic Powders," First Symposium (International) on Rockets and Astronautics (Tokyo, 1959), pp. 62-70.

21. Cheng, Sin-I, "Combustion Instability in Solid Rockets Using Propellants with Reactive Additives," in Progress in Astronautics and Rocketry, Vol. 1, Academic Press (1960), pp. 393-422.

22. Crocco, L. and Chang, Sin-I, "Theory of Combustion Instability in Liquid Propellant Rocket Motors," AGARDOGRAPH No. 8, Butterworths Scientific Publications, London (1956).

23. Crocco, L., Grey, J., and Harrje, D. T., "Theory of Liquid Propellant Rocket Combustion Instability and Its Experimental Verification," ARS J. 30 (Feb. 1960), pp. 159-168.

24. Crocco, L., "Theoretical Studies on Liquid Propellant Rocket Instability," in Tenth Symposium (International) on Combustion, The Combustion Institute, Pittsburgh, Pa. (1964), pp. 1101-1128.

25. Moore, F. K. and Maslen, S. H., "Transverse Oscillations in a Cylindrical Combustion Chamber," NACA TN 3152 (Oct., 1954).

26. Williams, F. A., "Response of a Burning Solid to Small Amplitude Pressure Oscillations," J. App. Phys. 33 (Nov. 1962), pp. 3153-

27. Culick, F. E. C., "Calculation of the Admittance Function for a Burning Surface," Astronautica Acta 13, no. 3 (1967).

28. Denison, M. R. and Baum, E., "A Simplified Model of Unstable Burning in Solid Propellants," ARS J. 31 (Aug. 1961), pp. 1112-1122.

29. Friedly, J. C. and Petersen, E. E., "Influence of Combustion Parameters on Instability in Solid Propellant Motors," AIAA J. 4 (1966), Part I: Development of Model and Linear Analysis (pp. 1604-1609); Part II: Nonlinear Analysis (pp. 1932-1937).

30. Bird, J. F., Haar, L., Hart, R. W., and McClure, F. T., "Effect of Solid Propellant Compressibility on Combustion Instability," J. Chem. Phys. 32 (May 1960), pp. 1423-1429.

31. Green, L., Jr., "Some Properties of Solid Propellant Burning, Jet Propulsion 28 (June 1958), pp. 386-392.

32. Nachbar, W. and Green, L., Jr., "Analysis of a Simplified Model of Solid Propellant Resonant Burning," J. Aero/Space Sc., 26 (Aug. 1959), pp. 518-526.

33. Price, E. W., "Combustion Instability in Solid Propellant Rockets," ARS J. 30 (June 1960), pp. 574-576.

34. Nachbar, W. and Green, L., Jr., "Closure," ARS J. 30 (June 1960), pp. 576-577.

35. Barrere, M. and Bernard, J. J., "Combustion Instability of Solid Propellant with Time Delay Distribution," in Eighth Symposium (International) on Combustion, Williams and Wilkins (1962), pp. 886-894.

36. Wood, W. A., "Oscillatory Burning of Solid Composite Propellants," Ninth Symposium (International) on Combustion, Academic Press, New York (1963), pp. 335-344.

37. Smith, R. P. and Sprenger, D. F., "Combustion Instability in Solid Propellant Rockets," in Fourth (International) Symposium on Combustion, Williams and Wilkins (1954), pp. 893-906.

38. Smith, A. F., "A Theory of Oscillatory Burning of Solid Propellants Assuming a Constant Surface Temperature," in Progress in Astronautics and Rocketry, Vol. 1, Academic Press (1960), pp. 375-391.

39. Cantrell, R. H., McClure, F. T., and Hart, R. W., "Effects of Thermal Radiation on the Acoustic Response Function of Solid Propellants," AIAA J. 3 (March 1965), pp. 418-426.

40. Hart, R. W., Farrell, R. A., and Cantrell, R. H., "Theoretical Study of a Solid Propellant Having a Heterogeneous Surface Reaction. I - Acoustic Response, Low and Intermediate Frequencies," Combustion and Flame 10 (Dec. 1966), pp. 367-380.

41. Hart, R. W. and Cantrell, R. H., "Amplification and Attenuation of Sound by Burning Propellants," AIAA J. 1 (Feb. 1963), pp. 398-464.

42. Cantrell, R. H., Hart, R. W., and McClure, F. T., "Linear Acoustic Gains and Losses in Solid Propellant Rocket Motors," AIAA J. 2 (June 1964), pp. 1100-1105.

43. Capener, E. L., Dickinson, L. A., Kier, R. J., Marxman, G. A., and Wooldridge, C. E., "Response of a Burning Propellant Surface to Erosive Transients," Stanford Research Institute, SRI Project FRU-5818, Annual Report (Dec. 31, 1966). Also, Marxman, G. A. and Wooldridge, C. E., "Non-Linear Theory of Transient Combustion Processes in Solid Propellants," Second ICRPG/AIAA Solid Propulsion Conference (June 6-8, 1967), Proceedings, p. 66.

44. Waesche, R. H. W., Wenograd, J., and Summerfield, M., "Research on Solid Propellant Combustion Instability," Aeronautical Engineering Report No. 564b, Princeton University (Dec. 1961).

45. Waesche, R. H. W., Wenograd, J., and Summerfield, M., "Entropy Wave Observations in Oscillatory Combustion of Solid Propellants: A Progress Report," AIAA Solid Propellant Rocket Conference (1964), Preprint No. 64-154.

46. Waesche, R. H. W. and Summerfield, M., "Solid Propellant Combustion Instability: Oscillatory Burning of Solid Rocket Propellants," Aerospace and Mechanical Sciences Report No. 751, Princeton University (Aug. 1965).

47. Hart, R. W. and Cantrell, R. H., "Amplification and Attenuation of Sound by Burning Propellants," AIAA J. 1 (Feb. 1963), pp. 398-404.

48. Krier, H., Tien, J., Sirignano, W., and Summerfield, M., "Non-steady Burning Phenomenon of Solid Propellants: Theory and Experiment," Proceedings, Second ICRPG/AIAA Solid Propulsion Conference (June 6-8, 1967), p. 75.

49. Culick, F. E. C., "Remarks on the Simplest Form for the Response Function of a Burning Surface," submitted to AIAA Journal, 1967.

Appendix B

DERIVATION OF THE ACOUSTIC RESPONSE FUNCTION EQUATION, ACCOUNTING FOR LOSS OF HEAT FROM THE GAS

The effect of heat loss from the gas in a double-ended, center-vented burner can be accounted for in the derivation of the acoustic response equation by retaining the identity of terms which refer to properties at the burning surface and to gas properties. The exponential growth constant, due to propellant driving in a side vented burner, is given below and is the basic expression to be evaluated (Ref. B1):

$$2\alpha_b = \frac{\dfrac{-\gamma M_b}{\rho_{ob}\, c_{ob}} \displaystyle\int_{S_b} < p_{1b}^2 > \left(Re\ y_b - \frac{1}{\gamma} \right) dS}{< \displaystyle\int_V dV \left(1/2\rho_o V_1^2 + p_1^2/2\rho_o c_o^2 \right) >} \qquad \text{(B1)}$$

In this expression the subscripts 0 and 1 refer to zero order and first order quantities respectively and the subscript b refers to the burning surface. Since an approximate correction is sought, it is assumed that the first mode pressure perturbation can be approximated by the first normal axial standing mode with a pressure antinode at each end of the burner tube. It is further assumed that the pressure amplitude change during a cycle of oscillation is small and therefore the time average value of the denominator can be approximated by the instantaneous value and the time average value in the numerator will be obtained by integrating over a period.

After employing the above simplifications, Eq. B1 reduces to

$$\alpha_b = \frac{-2\gamma M_b}{L} \frac{\rho_o c_o^{\,2}}{\rho_{ob} c_{ob}} \left(Re\ y_b - \frac{1}{\gamma} \right) \qquad \text{(B2)}$$

In Eq. B2, the subscript b was retained where present in Eq. B1 and in evaluating the volume integral effective average value ρ_o and c_o were assumed for gas density and sonic velocity respectively.

In order to reduce Eq. B2 to a form more easily evaluated, c_o will be assumed to be given by $c_o = 2\,L\,f$, the velocity of sound at the burning surface will be assumed equal to $\sqrt{\gamma p_{ob}/\rho_{ob}}$, and the sonic velocity is taken as $\sqrt{\gamma p_o/\rho_o}$ for the bulk gas. From continuity at the propellant

surface the Mach number M_b is replaced in Eq. B2 by the expression $\rho_b r_b / \rho_{ob} c_{ob}$.

After the appropriate substitutions, α_b is given by the relation

$$\alpha_b = \frac{-4\rho_s r_s c_o f_o}{p_o} \left(Re\ y_b - \frac{1}{\gamma} \right) \left[\frac{c_{ob}^2}{c_o^2} \left(\frac{p_o}{p_{ob}} \right)^2 \right] \tag{B3}$$

For the Mach numbers involved, less than 0.01 for the data of Ref. B1, the pressure drop is small and the pressure ratio (p_o/p_{ob}) is assumed to be equal to unity.

As in Ref. B2, α_b is set equal to $(\alpha_g - \alpha_d)$ and $Re\ y_b$ equal to $-Re\ (\frac{\mu}{\varepsilon} - \frac{1}{\gamma})$ resulting in the expression

$$Re(\mu/\varepsilon) = \left[\frac{(\alpha_g - \alpha_d)\ p_o}{4\rho_s r_s c_o f_o} \right] \left(\frac{c_o}{c_{ob}} \right)^2 \tag{B4}$$

for the propellant response. Equation B4 differs from the relation for $Re\ (\mu/\varepsilon)$, Eq. 7, given in Ref. B2, by the factor $(c_o/c_{ob})^2$.

A discussion of the errors inherent in the calculation of propellant response from "T-burner" data is presented in Ref. B2 and the limitations of Eq. B1, above, are pointed out in Ref. B1. Equation B4 is subject to the same limitations.

However, the effect under consideration can be of major importance as was borne out by experimental data obtained at this laboratory, the correction factor $(c_o/c_{ob})^2$ ranging from 0.15 to 0.24 for different chamber pressures employing a 48-foot long burner. For tests in a 12-foot long burner, the corrective factor ranged between 0.18 and 0.49. The need for a modification to the response function equation of Ref. B2 appears to be confirmed. It should be pointed out that changing the channel diameter, thus altering the relative heat loss by changing the ratio of channel area to perimeter, should provide an experimental means of investigating the effect under consideration and could thus provide a method of evaluating the adequacy of the present analysis or any other more fundamental analysis that may become available.

NOMENCLATURE

c	Sonic velocity
f	Frequency of oscillation
L	Length of gas column
M_b	Mean Mach number of gas at burning surface
p	Pressure
r_o	Mean burning rate of propellant
Re	Real part of a complex quantity
S_b	Burning surface area
v	Gas velocity
V	Volumn of gas column
y_b	Reduced specific acoustic admittance at burning surface $\left(\frac{\mu}{\varepsilon} - \frac{1}{\gamma} \right)$
α_b	Exponential oscillation growth constant attributable to the burning surface
α_d	Exponential oscillation decay constant
α_g	Exponential oscillation growth constant
γ	Ratio of heat capacities of combustion gas
ε	Amplitude of the fractional pressure perturbation which causes μ
μ	Amplitude of the fractional mass flow rate perturbation at the combustion zone
ρ	Density

SUBSCRIPTS

b Cas property at burning

s Solid propellant property

o Mean value

i First order perturbation quantity

< > Time average value

REFERENCES

B1. Cantrell, R. H. and R. W. Hart. "Interaction Between Sound and Flow in Acoustic Cavities: Mass, Momentum and Energy Considerations," ACOUS SOC AM J, Vol. 36, No. 4 (April 1964), Pp. 697-706.

B2. Horton, M. D. and D. W. Rice. "The Effecc of Compositional Variables Upon Oscillatory Combustion of Solid Rocket Propellants," COMBUST AND FLAME, Vol. 8, No. 1 (March 1964), Pp. 21-8.

Appendix C

PRESENTATIONS UNDER NASA WORK ORDERS WO 11, 294, WO 3034, WO 3035 AND WO 6030

1. "Preferred Frequency Oscillatory Combustion of Solid Propellants," by J. L. Eisel, M. D. Horton, E. W. Price, and D. W. Rice. Presented at the AIAA Solid Propellant Rocket Conference, Palo Alto, Calif., 29-31 January 1964.

2. "Experimental Solid Rocket Combustion Instability," by E. W. Price. Presented at the Tenth Symposium (International) on Combustion, Cambridge Univ., England, 17-21 August 1964.

3. "L* Combustion Instability," by E. W. Price. Presented at the 1st ICRPG Combustion Instability Conference, Orlando Air Force Base, Fla., 16-20 November 1964.

4. "Effect of Geometrical Variables on Losses in Motors as Determined by Cold Flow Model Testing," by H. B. Mathes. Presented at the 1st ICRPG Combustion Instability Conference, Orlando Air Force Base, Fla., 16-20 November 1964.

5. "Review of the Combustion Instability Characteristics of Solid Propellants," by E. W. Price. Presented at the 25th meeting of the AGARD Combustion and Propulsion Panel, San Diego, Calif., 22-24 April 1965.

6. "A Technique for Investigating Low Frequency Velocity-Coupled Combustion Instability," by J. L. Eisel and G. L. Dehority. Presented at the 2nd ICRPG Combustion Conference, Los Angeles, Calif., 1-5 November 1965.

7. "Aluminum Combustion in Composite Propellant," by J. E. Crump. Presented at the 2nd ICRPG Combustion Conference, Los Angeles, Calif., 1-5 November 1965.

8. "Two-Dimensional Experimental Studies of the Combustion Zone of Composite Propellants," by J. D. Hightower and E. W. Price. Presented at the 2nd ICRPG Combustion Conference, Los Angeles, Calif., 1-5 November 1965.

9. "Non-Acoustic Instability of Composite Propellant Combustion," by M. W. Beckstead, N. W. Ryan, and A. D. Baer. Presented at the AIAA 3rd Aerospace Sciences Meeting, New York, 24-26 January 1966.

10. "Acoustic Attenuation Experiments of Subscale, Cold-Flow Rocket Motors," by F. G. Buffum, G. L. Dehority, R. O. [illegible], and E. W. Price. Presented at the 2nd ICRPG Combustion Conference, Los Angeles, Calif., 1-5 November 1965. Also presented at the AIAA 3rd Aerospace Sciences Meeting, New York, 24-26 January 1966.

11. "Experimental Studies of the Combustion Zone of Composite Propellants," by J. D. Hightower and E. W. Price. Presented at the ICRPG/AIAA Solid Propulsion Conference in Washington, D. C., 19-21 July 1966.

12. "Combustion of Solid Rocket Propellants," by E. W. Price. Presented at the 2nd AFOSR Combined Contractors' Meeting on Combustion Dynamics Research, Stanford Research Institute, Menlo Park, Calif., August 1966.

13. "Combustion of Ammonium Perchlorate," by J. D. Hightower and E. W. Price. Presented at the 11th Symposium (International) on Combustion, Berkeley, Calif., August 1966.

14. "Oscillatory Combustion in Rocket Motors," by E. W. Price. Presented at a Seminar given at the Jet, Rocket, Nuclear, Ion and Electric Propulsion - Theory and Design Course, UCLA, Los Angeles Calif., 1 March 1967.

15. "Nonacoustic Combustor Instability," by M. W. Beckstead and E. W. Price. Presented at the 3rd ICRPG Combustion Conference, Kennedy Space Center, Fla., October 1966.

16. "Oscillatory Combustion of Solid Rocket Propellants," by E. W. Price. Presented at a seminar, City College of New York, Dept. of Chemical Engineering, 10 October 1966.

17. "Status of Solid Rocket Combustion Instability Research," by E. W. Price. Presented at the 6th Annual Meeting of the Canadian Armament Research Development Establishment (CARDE), Tripartite Technical Cooperation Program, Panel D-5, October 13, 1966.

18. "Experimental Techniques in Low Frequency Solid Propellant Acoustic Instability," by H. B. Mathes. Presented at the 3rd ICRPG Combustion Conference, Kennedy Space Center, Fla., October 1966.

19. "Nozzle Attenuation of Resonant Model-Rocket Motors," by R. O. Slates and F. G. Buffum. Presented at the 3rd ICRPG Combustion Conference, Kennedy Space Center, Fla., October 1966.

20. "On the Surface Temperature of Deflagrating Ammonium Perchlorate Crystals," by M. W. Beckstead and J. D. Hightower. Presented at the 3rd ICRPG Combustion Conference, Kennedy Space Center, October 1966. Also presented at the AIAA Fifth Aerospace Sciences Meeting, New York City, January 23-25 1967.

21. "Measurement of Combustion Dynamics of Solid Propellants in the Low Frequency Range," by H. B. Mathes and E. W. Price. Presented at the 5th Aerospace Sciences Meeting, New York, New York, January 23-26 1967.

22. "Low Frequency Instability: A Comparison of Theory and Experiment," by M. W. Beckstead. Presented at the Western States Combustion Institute Meeting, San Diego, Calif., 24-25 April 1967.

23. "Solid Propellant Combustion: State of Knowledge 1967," by E. W. Price. Presented at the American Institute of Chemical Engineers Sixty-Second National Meeting, Salt Lake City, Utah, May 21-24 1967. (Paper No. 3b)

24. "Combustion of Solid Rocket Propellants," by E. W. Price. Presented at an invited seminar given at the Georgia Institute of Technology, Atlanta, Georgia, 25 May 1967.

25. "Acoustic Attenuation in Resonant Model-Rocket Motors," by R. O. Slates, F. G. Buffum, and G. L. Dehority. Presented at the 3rd ICRPG Combustion Conference, Kennedy Space Center, October 1966. Also presented at the AIAA/ICRPG 2nd Solid Propulsion Conference, Anaheim, Calif., June 1967.

26. "Basic Problems Associated with Solid Propellant Rocket Combustion," by E. W. Price. Presented at the 3rd AFOSR Contractors Meeting on Combustion Dynamics Research, Cocoa Beach, Fla., 27-30 June 1967.

27. "Classes of Solid Rocket Combustion-Measurement Problems Related to Solid Rocket Combustion Instability," by H. B. Mathes. Presented at the 5th ICRPG Annual Meeting of the Solid Propellant Rocket Static Test Working Group, Aerojet-General Corp., Sacramento, Calif., 18-20 October 1967.

28. "The Effect of Oxidizer Particle Size on Non-Acoustic Instability," by M. W. Beckstead and T. L. Boggs. Presented at the 4th ICRPG Combustion Conference, Menlo Park, Calif., 9-13 October 1967.

29. "Continuing Studies of the Combustion of Ammonium Perchlorate," by J. D. Hightower and E. W. Price. Presented at the 4th ICRPG Combustion Conference, Menlo Park, Calif., 9-13 October 1967.

30. "A Comparison of Theoretical and Experimental Response Functions," by M. W. Beckstead and F. E. C. Culick. Presented at the 4th ICRPG Combustion Conference, Menlo Park, Calif., 9-13 October 1967.

Appendix D

PUBLICATIONS UNDER NASA WORK ORDERS WO 11, 294, WO 3034, WO 3035 AND WO 6030

1. U. S. Naval Ordnance Test Station. Low Frequency Combustion Instability of Solid Rocket Propellants, 1 July - 1 September 1962, by E. W. Price. China Lake, Calif., NOTS, December 1962. (TPR 301, NOTS TP 3107).

2. ------. Low-Frequency Combustion Instability of Solid Rocket Propellants, 1 September 1962 - 1 May 1963, by M. D. Horton, J. L. Eisel, and E. W. Price. China Lake, Calif., NOTS, May 1963. (TPR 318, NOTS TP 3248).

3. Horton, M. D., J. L. Eisel, and E. W. Price. "Low-Frequency Acoustic Oscillatory Combustion," AIAA J, Vol. 1, No. 11 (November 1963), Pp. 2652-4.

4. U. S. Naval Ordnance Test Station. Low-Frequency Combustion Instability of Solid Rocket Propellants, by E. W. Price, D. W. Rice and J. E. Crump. China Lake, Calif., NOTS, July 1964. (TPR 360, NOTS TP 3524).

5. Eisel, J. L., M. D. Horton, E. W. Price, and D. W. Rice. "Preferred Frequency Oscillatory Combustion of Solid Propellants," AIAA J, Vol. 2, No. 7 (July 1964), Pp. 1319-23.

6. Mathes, H. B. "Effect of Geometrical Variables on Losses in Motors as Determined by Cold-Flow Testing," in "1st Combustion Instability Conference, Interagency Chemical Rocket Propulsion Group," comp. and ed. by Chemical Propulsion Information Agency. Silver Spring, Md., CPIA, January 1965. CPIA Publ. No. 68, Vol. 1, Pp. 443-51.

7. Crump, J. E. "Photographic Survey of Aluminum Combustion in Solid Propellants," in "1st Combustion Instability Conference, Interagency Chemical Rocket Propulsion Group," comp. and ed. by Chemical Propulsion Information Agency. Silver Spring, Md., CPIA, January 1965. CPIA Publ. No. 68, Vol. 1, Pp. 367-70.

8. Crump, J. E. "Surface Characteristics of Quenched Samples of Composite Aluminum Propellants," in "1st Combustion Instability Conference, Interagency Chemical Rocket Propulsion Group," comp. and ed. by Chemical Propulsion Information Agency. Silver Spring, Md., CPIA, January 1965. CPIA Publ. No. 68, Vol. 1, Pp. 361-5.

9. Horton, M. D. "Low Frequency Pressure Coupling," in "1st Combustion Instability Conference, Interagency Chemical Rocket Propulsion Group," comp. and ed. by Chemical Propulsion Information Agency. Silver Spring, Md., CPIA, January 1965. CPIA Publ. No. 68, Vol. 1, p. 397.

10. Price, E. W. "L* Combustion Instability," in "1st Combustion Instability Conference, Interagency Chemical Rocket Propulsion Group," comp. and ed. by Chemical Propulsion Information Agency. Silver Spring, Md., CPIA, January 1965. CPIA Publ. No. 68, Vol. 1, Pp. 507-12.

11. Price, E. W. "Review of the Combustion Instability Characteristics of Solid Propellants," presented at the 25th Meeting of the AGARD Combustion and Propulsion Panel, San Diego, Calif., 22-24 April 1965. (To be published).

12. Price, E. W. "Experimental Solid Rocket Combustion Instability," Tenth Symposium (International) on Combustion. Pittsburgh, Pa., Combustion Institute, 1965. Pp. 1067-82.

13. U. S. Naval Ordnance Test Station. Aluminum Combustion in Composite Propellants, a 12½ minute color/sound movie (16mm) produced by the Technical Information Department. China Lake, Calif. (1966)

14. ------. Acoustic Losses of a Subscale, Cold-Flow Rocket Motor for Various "J" Values, by F. G. Buffum, G. L. Dehority, R. O. Slates, and E. W. Price. China Lake, Calif., NOTS, February 1966. (NAVWEPS Report 8971, NOTS TP 3932).

15. Eisel, J. L., and G. L. Dehority. "A Technique for Investigating Low Frequency Velocity-Coupled Combustion Instability," in "2nd Combustion Conference, Interagency Chemical Rocket Propulsion Group," comp. and ed. by Chemical Propulsion Information Agency. Silver Spring, Md., CPIA, May 1966. CPIA, May 1966. CPIA Publ. No. 105, Vol. 1, Pp. 703-12.

16. Buffum, F. G., G. L. Dehority, R. O. Slates, and E. W. Price. "Acoustic Attenuation Experiments on Subscale, Cold-Flow Rocket Motors," in "2nd Combustion Conference, Interagency Chemical Rocket Propulsion Group," comp. and ed. by Chemical Propulsion Information Agency. Silver Spring, Md., CPIA, May 1966. CPIA Publ. No. 105, Vol. 1, Pp. 835-59.

17. Beckstead, M. W. "Non-Acoustic Combustion Instability," in "2nd Combustion Conference, Interagency Chemical Rocket Propulsion Group," comp. and ed. by Chemical Propulsion Information Agency. Silver Spring, Md., CPIA, May 1966. CPIA Publ. No. 105, Vol. 1, Pp. 659-75.

18. Hightower, J. D., and E. W. Price. "Two-Dimensional Experimental Studies of the Combustion Zone of Composite Propellants," in "2nd Combustion Conference, Interagency Chemical Rocket Propulsion Group," comp. and ed. by Chemical Propulsion Information Agency. Silver Spring, Md., CPIA, May 1966. CPIA Publ. No. 105, Vol. 1, Pp. 421-36.

19. Crump, J. E. "Aluminum Combustion in Composite Propellants," in "2nd Combustion Instability Conference, Interagency Chemical Rocket Propulsion Group," comp. and ed. by Chemical Propulsion Information Agency. Silver Spring, Md., CPIA, May 1966. CPIA Publ. No. 105, Vol. 1, Pp. 321-9.

20. Beckstead, M. W., N. W. Ryan and A. D. Baer. "Non-Acoustic Instability of Composite Propellant Combustion," AIAA J, Vol. 4, No. 9 (September 1966), Pp. 1622-8.

21. Beckstead, M. W., and E. W. Price. "Nonacoustic Combustor Instability," Third ICRPG Combustion Conference, Kennedy Space Center, Fla., 17-21 October 1966. To be published in AIAA J.

22. Slates, R. O., and F. G. Buffum. "Nozzle Attenuation of Resonant Model-Rocket Motors," in "3rd Combustion Conference, Interagency Chemical Rocket Propulsion Group," comp. and ed. by Chemical Propulsion Information Agency. Silver Spring, Md., CPIA, February 1967.

23. Beckstead, M. W., and J. D. Hightower. "On the Surface Temperature of Deflagrating Ammonium Perchlorate Crystals," in "3rd Combustion Conference, Interagency Chemical Rocket Propulsion Group," comp. and ed. by Chemical Propulsion Information Agency. Silver Spring, Md., CPIA, February 1967. CPIA Publ. No. 138, Vol. 1, Pp. 107-12. (To be published in AIAA J).

24. Culick, F. E. C. "Calculation of the Admittance Function for a Burning Surface," in "3rd Combustion Conference, Interagency Chemical Rocket Propulsion Group," comp. and ed. by Chemical Propulsion Information Agency. Silver Spring, Md., CPIA, February 1967. CPIA Publ. No. 138, Vol. 1, Pp. 429-40.

25. Mathes, H. B. "Experimental Techniques in Low Frequency Solid Propellant Acoustic Instability," in "3rd Combustion Conference, Interagency Chemical Rocket Propulsion Group," comp. and ed. by Chemical Propulsion Information Agency. Silver Spring, Md., CPIA, February 1967. CPIA Publ. No. 138, Vol. 1, Pp. 237-52.

26. Buffum, F. G., G. L. Dehority, R. O. Slates, and E. W. Price. "Acoustic Attenuation Experiments on Subscale, Cold-Flow Rocket Motors," AIAA J, Vol. 5, No. 2 (February 1967), Pp. 272-80.

27. Culick, F. E. C. "A Review of Calculations of the Admittance Function for a Burning Surface," in ICRPG/AIAA 2nd Solid Propulsion Conference, Anaheim, Calif., American Institute of Aeronautics and Astronautics, June 1967. 26 pp. (Also Appendix A)

28. Hightower, J. D. and E. W. Price. "Combustion of Ammonium Perchlorate," in "Eleventh Symposium (International) on Combustion," Pittsburgh, Pa., Combustion Institute, 1967. Pp. 463-72.

29. Culick, F. E. C. "Calculation of the Admittance Function for a Burning Surface," ASTRONAUTICA ACTA, Vol. 13, No. 3 (1967).

30. Naval Weapons Center. Theory of Nonacoustic Combustor Instability by E. W. Price. China Lake, Calif., NWC. (To be published)

31. Price, E. W. Solid Propellant Combustion: State of Knowledge 1967. New York, N. Y., American Institute of Chemical Engineers, 1967. Paper No. 3b. Also published under U. S. Naval Ordnance Test Station, China Lake, Calif., Technical Note 508-45.

32. U. S. Naval Ordnance Test Station. Status of Solid Rocket Combustion Instability Research, by E. W. Price. China Lake, Calif., NOTS, February 1967. (NOTS TP 4275).

REFERENCES

1. Angelus, T. A. "Solid-Propellant Combustion Instability," Panel Discussion in Proceedings of the Eighth Symposium (International) on Combustion. Baltimore, Md., Williams and Wilkins Company, 1962. Pp. 921-4.

2. Jet Propulsion Laboratory. Solid Propellant Propulsion, Chapter IV, Starfinder Motor Development, by Floyd Anderson. Pasadena, Calif., JPL Research Summary No. 36-3. (No date).

3. Piasecki, L. and W. Gin. "Solid Rockets for Lunar and Planetary Spacecraft," ARS Preprint 1462-60 (December 1960).

4. Eisel, J. L., M. D. Horton, E. W. Price and D. W. Rice. "Preferred Frequency Oscillatory Combustion of Solid Propellants," AIAA J, Vol. 2, No. 7 (July 1964), pp. 1319-23.

5. U. S. Naval Ordnance Test Station. Low Frequency Combustion Instability of Solid Rocket Propellants, 1 July - 1 September 1962, by E. W. Price. China Lake, Calif., NOTS, December 1962. (TPR 301, NOTS TP 3107).

6. U. S. Naval Ordnance Test Station. Low-Frequency Combustion Instability of Solid Rocket Propellants, by E. W. Price, D. W. Rice and J. E. Crump. China Lake, Calif., NOTS, July 1964. (TPR 360, NOTS TP 3524).

7. Inami, Y. H. and H. Shanfield. "Nonacoustic Combustion Pulsations of Ammonium Perchlorate Containing Aluminum," AIAA J, Vol. 2, No. 7 (July 1964), Pp. 1314-18.

8. Price, E. W. "Review of the Combustion Instability Characteristics of Solid Propellants," presented at the 25th Meeting of the AGARD Combustion and Propulsion Panel, San Diego, Calif., 22-24 April 1965. (To be published).

9. Price, E. W. "Experimental Solid Rocket Combustion Instability," Tenth Symposium (International) on Combustion. Pittsburgh, Pa., Combustion Institute, 1965. Pp. 1067-82.

10. Price, E. W. "Axial Mode, Intermediate Frequency Combustion Instability in Solid-Propellant Rocket Motors," AIAA Preprint 64-146, January 1964.

11. U. S. Naval Ordnance Test Station. Axial Mode Combustion Instability in Solid Propellant Rocket Motors (U), by E. W. Price, H. B. Mathes, B. A. Sword and H. J. Sprouse. China Lake, Calif., NOTS, December 1964. (NAVWEPS Report 8658, NOTS TP 3700), CONFIDENTIAL.

12. Akiba, R. and M. Tanno. "Low Frequency Instability in Solid Propellant Rocket Motors," Proceedings of the First Symposium (International) on Rockets and Astronautics (Tokyo, 1959), Pp. 74-82.

13. Sehgal, R., and L. Strand. "A Theory of Low-Frequency Combustion Instability in Solid Rocket Motors," AIAA J, Vol. 2, No. 4 (April 1964), Pp. 696-702.

14. Beckstead, M. W., N. W. Ryan and A. D. Baer. "Non-Acoustic Instability of Composite Propellant Combustion," AIAA J. Vol. 4, No. 9 (September 1966), Pp. 1622-8.

15. Beckstead, M. W. and E. W. Price. "Nonacoustic Combustor Instability," Third ICRPG Combustion Conference, Kennedy Space Center, Fla., 17-21 October 1966. To be published in AIAA J.

16. Hightower, J. D. and E. W. Price. "Combustion of Ammonium Perchlorate," in "Eleventh Symposium (International) on Combustion," Pittsburgh, Pa., Combustion Institute, 1967. Pp. 463-72.

17. Friedman, R., R. G. Nugent, K. E. Rumbel, and A. C. Scurlock. "Deflagration of Ammonium Perchlorate," in Sixth Symposium (International) on Combustion, New York, N. Y., Reinhold Publishing Corp., 1957. Pp. 612-18.

18. Levy, J. B. and R. Friedman. "Further Studies of Pure Ammonium Perchlorate Deflagration," in Eighth Symposium (International) on Combustion, Baltimore, Md., The Williams and Wilkins Co., 1962. Pp. 663-72.

19. Shannon. L. J. and E. E. Petersen. "Deflagration Characteristics of Ammonium Perchlorate Strands," AIAA J, Vol 2, No. 1, (January 1964), Pp. 168-9.

20. Coates, R. L. "Linear Pyrolysis Rate Measurements of Propellant Constituents," AIAA Preprint No. 65-55 (January 1965).

21. Guinet, A. "Vitesse Lineaire de Pyrolyse du Perchlorate d' Ammonium en Ecoulement Unidimensional," in La Researche Aerospatiale No. 109 (1965), Pp 41-49.

22. Bircumshaw, L. L. and B. H. Newman. "The Thermal Decomposition of Ammonium Perchlorate. I. Introduction, Experimental, Analysis of Gaseous Products, and Thermal Decomposition Experiments," in ROY SOC LONDON, PROC, Vol. A 227 (1954), Pp. 115-132.

23. Bircumshaw, L. L. and B. H. Newman. "The Thermal Decomposition of Ammonium Perchlorate. IV The Kinetics of the Decomposition, the Effect of Particle Size, and Discussion of Results," in ROY SOC LONDON, PROC, Vol. A227 (1955), Pp. 228-41.

24. Strunin, V. A. and G. B. Mandelis. "The Effect of Pressure on the Kinetics of Thermal Decomposition of Ammonium Perchlorate," in Bulletin of the Academy of Science, USSR, Division of Chemical Science, Vol. No. 12, December, 1964.

25. United Technology Center. Composite Solid Propellant Ignition Mechanisms, by L. J. Shannon, Annual Scientific Report (May 1966), UTC 2138-ASR1.

26. Jacobs, P. W. M. and A. Russell-Jones. "On the Mechanism of the Decomposition of Ammonium Perchlorate," AIAA J, Vol. 5, No. 4 (April 1967), Pp. 829-30.

27. Galwey, A. K. and P. W. M. Jacobs. "High-Temperature Thermal Decomposition of Ammonium Perchlorate," J CHEM SOC (1953), Pp. 837-44.

28. Levy, J. B. "The Thermal Decomposition of Perchloric Acid Vapor," J PHYS CHEM, Vol. 66 (1962), Pp. 1092-7.

29. Waesche, R. H. W. and J. Wenograd. "The Effects of Pressure and Additives on the Kinetics of Decomposition of Ammonium Perchlorate," Western States Section/The Combustion Institute, San Diego, Calif., (April 1967). (Paper No. WSC1-67-8)

30. U. S. Army Missile Command. The Mechanism of Decomposition of Ammonium Perchlorate: A Review, by 1st Lt. Charles U. Pittman, Jr. Redstone Arsenal, Ala., AMC, August 1966. (Report No. RK-TR-66-13.)

31. Torgesen, J. L., A. T. Horton, and C. P. Saylor. "Equipment for Single Crystal Growth from Aqueous Solution," NATL BUR STANDARDS, J RES, Vol. 67C, No. 1, (1963), Pp. 25-32.

32. Tutton, A. E. H. "The Alkali Perchlorates and a New Principle Concerning the Measurement of Space-Lattice Cells," in ROY SOC LONDON, PROC, A111, 462 (1926).

33. Galwey, A. K. and P. W. M. Jacobs. "The Thermal Decomposition of Ammonium Perchlorate at Low Temperatures," in ROY SOC LONDON, PROC, Vol. A-254, (1960), Pp. 455-69.

34. Manelis, G. B. and Yu. I. Rubtsov. "Kinetics of the Thermal Decomposition of Ammonium Perchlorate," RUSSIAN J PHYS CHEM, Vol. 40 (1966), Pp. 416-18.

35. Land, J. E. "A Study of the Decomposition Mechanism of Ammonium Perchlorate," administered by The Auburn Research Fdn., Auburn Univ., Dept. of Chem. and Chem. Engr., Birmingham Procurement District, U. S. Army (May 1965). Contract No. DA-01-009-ORD-1023 (Z), AD No. 466956.

36. Sammons, G. D. "Application of Differential Scanning Calorimetry to the Study of Solid Propellant Decomposition," in "3rd Combustion Conference, Interagency Chemical Rocket Propulsion Group," comp. and ed. by Chemical Propulsion Information Agency. Silver Spring, Md., CPIA, February 1967. CPIA Publ. No. 138, Vol. 1, Pp. 75-83.

37. Rogers, R. N., and E. P. Morris, Jr. "On Estimating Activation Energies with a Differential Scanning Calorimeter," ANAL CHEM, Vol. 38, (1966), p. 412.

38. Watson, E. S., M. J. O'Neill, J. Justin, and N. Brenner. "A Differential Scanning Calorimater for Quantitative Differential Thermal Analysis," ANAL CHEM, Vol. 36, (1964), p. 1233.

39. Borchardt, H. J. and F. Daniels. "The Application of Differential Thermal Analysis to the Study of Reaction Kinetics," AM CHEM SOC, J, Vol. 79 (1957), pp. 41-6.

40. Kissinger, H. E. "Variation of Peak Temperature with Heating Rate in Differential Thermal Analysis," NATL BUR STANDARDS, J RES, Vol. 57 (1956), Pp. 217-21.

41. Kissinger, H. E. "Reaction Kinetics in Differential Thermal Analysis," ANAL CHEM, Vol. 29 (1957), Pp. 1702-06.

42. Rohm and Haas. Determination of Reaction Kinetics by Differential Thermal Analysis, by D. E. Mastin (1966), Rohm & Haas Report No. S-60.

43. Crump. J. E. "Private Communication," U. S. Naval Ordnance Test Station, China Lake, Calif. (August 1966).

44. McGurk, J. L. "Microscopic Determination of Propellant Combustion Surface Temperatures," in "1st Combustion Instability Conference, Interagency Chemical Rocket Propulsion Group," comp. and ed. by Chemical Propulsion Information Agency. Silver Spring, Md., CPIA, January 1965. CPIA Publ. No. 68, Vol. 1, Pp. 361-65.

45. Whittaker, A. G., and D. C. Barham. "Burning Rate of Ammonium Perchlorate Single Crystals," ARS J, Vol. 32, No. 8 (August 1962), p. 1273.

46. Adams, G. K., B. H. Newman, and A. B. Robins. "The Combustion of Propellants Based Upon Ammonium Perchlorate," in "Eighth Symposium (International) on Combustion," Baltimore, Md., The Williams & Wilkins Company, 1962. Pp. 693-705.

47. The Dow Chemical Company. JANAF Thermochemical Data. Compiled and calculated by The Dow Chemical Company, Thermal Laboratory, Midland, Michigan.

48. Handbook of Chemistry and Physics, 44th Edition, Cleveland, Ohio, Chemical Rubber Publishing Co.

49. Markowitz, M. M., and D. A. Boryta. "Some Aspects of the Crystallographic Transition Ammonium Perchlorate," ARS J, Vol. 32 (1962). Pp. 1941-2.

50. Goldsmid, H. J. The Thermal Properties of Solids. Dover Publications, Inc., New York, N. Y. (1965)

51. Rosser, Jr., W. A., S. H. Inami, and H. Wise. "Thermal Diffusivity of Ammonium Perchlorate," AIAA J, Vol. 4, No. 4 (April 1966), Pp. 663-6.

52. Powling, J. "Experiments Relating to the Combustion of Ammonium Perchlorate," in "Eleventh Symposium (International) on Combustion," Pittsburgh, Pa., Combustion Institute, 1967. Pp. 447-56.

53. Markowitz, M. M. and R. F. Harris. "The Differential Thermal Analysis of Perchlorates. III. The System $LiClO_4$," J PHYS CHEM, Vol. 63, (1959), p. 1519.

54. Crump, J. E. "Surface Characteristics of Quenched Samples of Composite Aluminum Propellants," in "1st Combustion Instability Conference, Interagency Chemical Rocket Propulsion Group," comp. and ed. by Chemical Propulsion Information Agency. Silver Spring, Md., CPIA, January 1965. CPIA Publ. No. 68, Vol. 1, Pp. 361-5.

55. Crump, J. E. "Photographic Survey of Aluminum Combustion in Solid Propellants," in "1st Combustion Instability Conference, Interagency Chemical Rocket Propulsion Group," comp. and ed. by Chemical Propulsion Information Agency. Silver Spring, Md., CPIA, January 1965. CPIA Publ. No. 68, Vol. 1, Pp. 367-70.

56. Crump, J. E. "Aluminum Combustion in Composite Propellants," in "2nd Combustion Instability Conference, Interagency Chemical Rocket Propulsion Group," comp. and ed. by Chemical Propulsion Information Agency. Silver Spring, Md., CPIA, May 1966. CPIA Publ. No. 105, Vol. 1, Pp. 321-9.

57. U. S. Naval Ordnance Test Station. Aluminum Combustion in Composite Propellants, a 12½ minute color/sound movie (16mm) produced by the Technical Information Department. China Lake, Calif.

58. Wood, William A. "Metal Combustion in Deflagrating Propellant," in Solid Propellant Rocket Research, Vol. 1, ed. by Martin Summerfield. New York, Academic Press, 1960. Pp. 287-91.

59. Miller, R. R. "Some Factors Affecting the Combustion of Aluminum in Solid Propellants," in "2nd Combustion Instability Conference, Interagency Chemical Rocket Propulsion Group," comp. and ed. by Chemical Propulsion Information Agency. Silver Spring, Md., CPIA, May 1966. CPIA Publ. No. 105, Vol. 1, Pp. 331-53.

60. Hart, R. W., and F. T. McClure. "Combustion Instability: Acoustic Interaction with a Burning Propellant Surface," J CHEM PHYS (June 1959), Pp. 1501-14.

61. Denison, M. R., and E. Baum. "A Simplified Model of Unstable Burning in Solid Propellants," ARS J, Vol. 31 (August 1961), Pp. 1112-22.

62. Friedly, J. C., and E. E. Peterson. "Influence of Combustion Parameters on Instability in Solid Propellant Motors," AIAA J, Vol. 4 (1966), Part I: Development of Model and Linear Analysis (pp. 1604-09); Part II: Nonlinear Analysis (pp. 1932-37).

63. Hart, R. W., R. A. Farrell, and R. H. Cantrell. "Theoretical Study of a Solid Propellant Having a Heterogeneous Surface Reaction. Part I: Acoustic Response, Low and Intermediate Frequencies," COMBUST AND FLAME, Vol. 10 (December 1966), Pp. 367-80.

64. Brown, R. S., R. J. Muzzy, and M. E. Steinle. "The Influence of Exothermic Surface Reactions on Pressure Coupled Combustion Instability of Composite Solid Propellants," in "3rd Combustion Conference, Interagency Chemical Rocket Propulsion Group," comp. and ed. by Chemical Propulsion Information Agency. Silver Spring, Md., CPIA, February 1967. CPIA Publ. No. 138, Vol. I, Pp. 231-5.

65. Culick, F. E. C. "A Review of Calculations of the Admittance Function for a Burning Surface," in ICRPG/AIAA 2nd Solid Propulsion Conference, Anaheim, Calif., American Institute of Aeronautics and Astronautics (June 1967), 26pp. (Also Appendix A)

66. Culick, F. E. C. "Calculation of the Admittance Function for a Burning Surface," ASTRONAUTICA ACTA, Vol. 13, No. 3 (1967).

67. Price, E. W. "Evidence for Velocity Coupling," in "1st Combustion Conference, Interagency Chemical Rocket Propulsion Group," comp. and ed. by Chemical Propulsion Information Agency. Silver Spring, Md., CPIA, January 1965. CPIA Publ. No. 68, Vol. 1, Pp. 403-8.

68. Eisel, J. L., and G. L. Dehority. "A Technique for Investigating Low Frequency Velocity-Coupled Combustion Instability," in "2nd Combustion Conference, Interagency Chemical Rocket Propulsion Group," comp. and ed. by Chemical Propulsion Information Agency. Silver Spring, Md., CPIA, May 1966. CPIA, May 1966. CPIA Publ. No. 105, Vol. 1, Pp. 703-12.

69. Price, E. W., and G. L. Dehority. "Velocity Coupled Axial Mode Combustion Instability in Solid Propellant Rocket Motors, in ICRPG/AIAA 2nd Solid Propulsion Conference, New York, N. Y., American Institute of Aeronautics and Astronautics, 1967. Pp. 213-27.

70. U. S. Naval Ordnance Test Station. Aluminum Particle Combustion Progress Report - 1 April 1964-30 June 1965, by The Metal Combustion Study Group. China Lake, Calif., NOTS, April 1966. 116 pp. (TPR 415, NOTS TP 3916).

71. Beckstead, M. W. "Non-Acoustic Combustion Instability of Solid Propellants," Univ. of Utah (June 1965). Unpublished Ph.D. Thesis.

72. Coates, R. L., N. S. Cohen, and L. R. Harvil. "An Interpretation of L* Combustion Instability in Terms of Acoustic Combustion Instability Theory," in "3rd Combustion Conference, Interagency Chemical Rocket Propulsion Group," comp. and ed. by Chemical Propulsion Information Agency. Silver Spring, Md., CPIA, February 1967. CPIA Publ. No. 138, Vol. 1, Pp. 291-302.

73. Rocketdyne. Effects of Aluminum on Solid-Propellant Combustion Instability, by C. L. Oberg and A. L. Huebner. Canoga Park, Calif., Report No. R-6654, Final Report No. AF49 (638)-1575 (July 1966).

74. Naval Weapons Center. Theory of Nonacoustic Combustor Instability, by E. W. Price. China Lake, Calif., NWC. (To be published)

75. Horton, M. D., and D. W. Rice. "The Effect of Compositional Variables Upon Oscillatory Combustion of Solid Rocket Propellants," COMBUST AND FLAME, Vol. 8, No. 1 (1964), Pp. 21-7.

76. Huggett, C., C. E. Bartley, and M. M. Mills. "Solid Propellant Rockets," Princeton, N. J., Princeton Universicy Press, 1960. (No. 2, Princeton Aeronautical Paperbacks, Coleman deP. Donaldson, General Editor), p. 88.

77. Anderson, F. A., R. A. Strehlow, and L. D. Strand. "Low Pressure Rocket Extinction," AIAA J, Vol. 1 (1963), Pp. 2669-71.

78. Price, E. W. Experimental Methods in Combustion Research, 2nd supplement. Oxford, London, New York and Paris, Pergamon Press, 1964. "Experimental Measurements in Solid Propellant Rocket Combustion Instability," pp. 53-74.

79. Horton, M. D. "One-Dimensional Solid-Propellant Oscillatory Burner," ARS J, Vol. 31 (November 1961), Pp. 1596-97.

80. -------. "Use of the One-Dimensional T-Burner to Study Oscillatory Combustion," AIAA J, Vol. 2 (June 1964), Pp. 1112-18.

81. Stepp, E. E. "Effect of Pressure and Velocity Coupling on Low Frequency Instability," AIAA J. Vol. 5, No. 5 (May 1967), Pp. 945-8.

82. U. S. Naval Ordnance Test Station. Low-Frequency Combustion Instability of Solid Rocket Propellants, 1 September 1962 - 1 May 1963, by M. D. Horton, J. L. Eisel, and E. W. Price. China Lake, Calif., NOTS, May 1963. (TPR 318, NOTS TP 3248).

83. Horton, M. D., J. L. Eisel, and E. W. Price. "Low-Frequency Acoustic Oscillatory Combustion," AIAA J, Vol. 1, No. 11 (November 1963), Pp. 2652-4.

84. Culick, F. E. C. Private communication at the U. S. Naval Ordnance Test Station, China Lake, Calif., August 1966.

85. Mathes, H. B. "Effect of Geometrical Variables on Losses in Motors as Determined by Cold-Flow Testing," in "1st Combustion Instability Conference, Interagency Chemical Rocket Propulsion Group," comp. and ed. by Chemical Propulsion Information Agency. Silver Spring, Md., CPIA, January 1965. CPIA Publ. No. 68, Vol. 1, Pp. 443-51.

86. U. S. Naval Ordnance Test Station. Acoustic Losses of a Subscale, Cold-Flow Rocket Motor for Various "J" Values, by F. G. Buffum, G. L. Dehority, R. O. Slates, and E. W. Price. China Lake, Calif., NOTS, February 1966. (NAVWEPS Report 8971, NOTS TP 3932).

87. Buffum, F. G., G. L. Dehority, R. O. Slates, and E. W. Price. "Acoustic Attenuation Experiments on Subscale, Cold-Flow Rocket Motors," AIAA J, Vol. 5, No. 2 (February 1967), Pp. 272-80.

88. Slates, R. O., and F. G. Buffum. "Nozzle Attenuation of Resonant Model-Rocket Motors," in "3rd Combustion Conference, Interagency Chemical Rocket Propulsion Group," comp. and ed. by Chemical Propulsion Information Agency. Silver Spring, Md., CPIA, February 1967. CPIA Publ. No. 138, Vol. 1, Pp. 429-40.

UNCLASSIFIED

Security Classification

DOCUMENT CONTROL DATA - R&D

(Security classification of title, body of abstract and indexing annotation must be entered when the overall report is classified)

1 ORIGINATING ACTIVITY *(Corporate author)* U. S. Naval Ordnance Test Station China Lake, California 93555	2a. REPORT SECURITY CLASSIFICATION UNCLASSIFIED 2b GROUP None

3 REPORT TITLE

COMBUSTION OF SOLID PROPELLANTS AND LOW FREQUENCY COMBUSTION INSTABILITY

4 DESCRIPTIVE NOTES *(Type of report and inclusive dates)*

Research Report

5 AUTHOR(S) *(Last name, first name, initial)*

Aerothermochemistry Division, Research Department

6. REPORT DATE	7a TOTAL NO. OF PAGES	7b. NO OF REFS
June 1967	244	88

8a CONTRACT OR GRANT NO. b. PROJECT NO. NASA Work Order No. 6030 c. d.	9a ORIGINATOR'S REPORT NUMBER(S) NOTS TP 4244 9b. OTHER REPORT NO(S) *(Any other numbers that may be assigned this report)*

10. AVAILABILITY/LIMITATION NOTICES

[redacted]

11. SUPPLEMENTARY NOTES	12. SPONSORING MILITARY ACTIVITY Naval Ordnance Systems Command Naval Material Command Washington, D.C. 20360

13. ABSTRACT

This report summarizes studies of ammonium perchlorate deflagration, combustion of sandwiches of ammonium perchlorate crystals and binders, behavior of aluminum in the combustion zone of propellants, oscillatory combustion of propellants in several experiments, and experimental measurement of attenuation of axial mode oscillations in models of rocket motors.

DD FORM 1 JAN 64 1473 0101-807-6800

UNCLASSIFIED

Security Classification

UNCLASSIFIED

Security Classification

14. KEY WORDS	LINK A		LINK B		LINK C	
	ROLE	WT	ROLE	WT	ROLE	WT
Combustion Propellant Instability Rocket						

INSTRUCTIONS

1. ORIGINATING ACTIVITY: Enter the name and address of the contractor, subcontractor, grantee, Department of Defense activity or other organization *(corporate author)* issuing the report.

2a. REPORT SECURITY CLASSIFICATION: Enter the overall security classification of the report. Indicate whether "Restricted Data" is included. Marking is to be in accordance with appropriate security regulations.

2b. GROUP: Automatic downgrading is specified in DoD Directive 5200.10 and Armed Forces Industrial Manual. Enter the group number. Also, when applicable, show that optional markings have been used for Group 3 and Group 4 as authorized.

3. REPORT TITLE: Enter the complete report title in all capital letters. Titles in all cases should be unclassified. If a meaningful title cannot be selected without classification, show title classification in all capitals in parenthesis immediately following the title.

4. DESCRIPTIVE NOTES: If appropriate, enter the type of report, e.g., interim, progress, summary, annual, or final. Give the inclusive dates when a specific reporting period is covered.

5. AUTHOR(S): Enter the name(s) of author(s) as shown on or in the report. Enter last name, first name, middle initial. If military, show rank and branch of service. The name of the principal author is an absolute minimum requirement.

6. REPORT DATE: Enter the date of the report as day, month, year; or month, year. If more than one date appears on the report, use date of publication.

7a. TOTAL NUMBER OF PAGES: The total page count should follow normal pagination procedures, i.e., enter the number of pages containing information.

7b. NUMBER OF REFERENCES: Enter the total number of references cited in the report.

8a. CONTRACT OR GRANT NUMBER: If appropriate, enter the applicable number of the contract or grant under which the report was written.

8b, 8c, & 8d. PROJECT NUMBER: Enter the appropriate military department identification, such as project number, subproject number, system numbers, task number, etc.

9a. ORIGINATOR'S REPORT NUMBER(S): Enter the official report number by which the document will be identified and controlled by the originating activity. This number must be unique to this report.

9b. OTHER REPORT NUMBER(S): If the report has been assigned any other report numbers *(either by the originator or by the sponsor)*, also enter this number(s).

10. AVAILABILITY/LIMITATION NOTICES: Enter any limitations on further dissemination of the report, other than those imposed by security classification, using standard statements such as:

(1) "Qualified requesters may obtain copies of this report from DDC."

(2) "Foreign announcement and dissemination of this report by DDC is not authorized."

(3) "U. S. Government agencies may obtain copies of this report directly from DDC. Other qualified DDC users shall request through _____."

(4) "U. S. military agencies may obtain copies of this report directly from DDC. Other qualified users shall request through _____."

(5) "All distribution of this report is controlled. Qualified DDC users shall request through _____."

If the report has been furnished to the Office of Technical Services, Department of Commerce, for sale to the public, indicate this fact and enter the price, if known.

11. SUPPLEMENTARY NOTES: Use for additional explanatory notes.

12. SPONSORING MILITARY ACTIVITY: Enter the name of the departmental project office or laboratory sponsoring *(paying for)* the research and development. Include address.

13. ABSTRACT: Enter an abstract giving a brief and factual summary of the document indicative of the report, even though it may also appear elsewhere in the body of the technical report. If additional space is required, a continuation sheet shall be attached.

It is highly desirable that the abstract of classified reports be unclassified. Each paragraph of the abstract shall end with an indication of the military security classification of the information in the paragraph, represented as *(TS), (S), (C), or (U)*.

There is no limitation on the length of the abstract. However, the suggested length is from 150 to 225 words.

14. KEY WORDS: Key words are technically meaningful terms or short phrases that characterize a report and may be used as index entries for cataloging the report. Key words must be selected so that no security classification is required. Identifiers, such as equipment model designation, trade name, military project code name, geographic location, may be used as key words but will be followed by an indication of technical context. The assignment of links, roles, and weights is optional.

UNCLASSIFIED

Security Classification